

IMPROVEMENT OF ZnO BY TEXTURAL MODIFICATION AND METAL
DOPING FOR ATRAZINE PHOTOCATALYSIS

Miss Pummarin Khamdahsag

A Dissertation Submitted in Partial Fulfillment of the Requirements
for the Degree of Doctor of Philosophy Program in Environmental Management
(Interdisciplinary Program)
Graduate School
Chulalongkorn University
Academic Year 2011
Copyright of Chulalongkorn University

บทคัดย่อและแฟ้มข้อมูลฉบับเต็มของวิทยานิพนธ์ตั้งแต่ปีการศึกษา 2554 ที่ให้บริการในคลังปัญญาจุฬาฯ (CUIR)
เป็นแฟ้มข้อมูลของนิสิตเจ้าของวิทยานิพนธ์ที่ส่งผ่านทางบัณฑิตวิทยาลัย

The abstract and full text of theses from the academic year 2011 in Chulalongkorn University Intellectual Repository(CUIR)
are the thesis authors' files submitted through the Graduate School.

การปรับปรุงเชิงค้ออกไซด์โดยการเปลี่ยนลักษณะพื้นผิวและการเติมด้วยโลหะเพื่อใช้สำหรับ
กระบวนการโฟโตคะตะไลซิสของอาหารขึ้น

นางสาวภุมรินทร์ คำเดชศักดิ์

วิทยานิพนธ์นี้เป็นส่วนหนึ่งของการศึกษาตามหลักสูตรปริญญาวิทยาศาสตรดุษฎีบัณฑิต
สาขาวิชาการจัดการสิ่งแวดล้อม (สหสาขาวิชา)
บัณฑิตวิทยาลัย จุฬาลงกรณ์มหาวิทยาลัย
ปีการศึกษา 2554
ลิขสิทธิ์ของจุฬาลงกรณ์มหาวิทยาลัย

Thesis Title	IMPROVEMENT OF ZnO BY TEXTURAL MODIFICATION AND METAL DOPING FOR ATRAZINE PHOTOCATALYSIS
By	Miss Pummarin Khamdahsag
Field of Study	Environmental Management
Thesis Advisor	Associate Professor Nurak Grisdanurak, Ph.D.
Thesis Co-advisor	Professor Mark A. Nanny, Ph.D.

Accepted by the Graduate School, Chulalongkorn University in Partial
Fulfillment of the Requirements for the Doctoral Degree

.....Dean of the Graduate School
(Associate Professor Pornpote Piumsomboon, Ph.D.)

THESIS COMMITTEE

.....Chairman
(Assistant Professor Chantra Tongcumpou, Ph.D.)

.....Thesis Advisor
(Associate Professor Nurak Grisdanurak, Ph.D.)

.....Thesis Co-advisor
(Professor Mark A. Nanny, Ph.D.)

.....Examiner
(Associate Professor Jin Anotai, Ph.D.)

.....Examiner
(Assistant Professor Patiparn Punypalakul, Ph.D.)

.....Examiner
(Assistant Professor Sumana Siripattanakul, Ph.D.)

.....External Examiner
(Associate Professor Jatuporn Wittayakun, Ph.D.)

ภุมรินทร์ คำเดชศักดิ์ : การปรับปรุงซิงค์ออกไซด์โดยการเปลี่ยนแปลงพื้นผิวและการเติมด้วยโลหะเพื่อใช้สำหรับกระบวนการโฟโตคะตะไลซิสของอาทราซีน.
(IMPROVEMENT OF ZnO BY TEXTURAL MODIFICATION AND METAL DOPING FOR ATRAZINE PHOTOCATALYSIS) อ.ที่ปรึกษา
วิทยานิพนธ์หลัก : รศ.ดร.นุรักษ์ กฤษดานุรักษ์, อ.ที่ปรึกษาวิทยานิพนธ์ร่วม : Prof.
Mark A. Nanny, Ph.D., 215 หน้า.

อาทราซีนเป็นยากำจัดวัชพืชที่ใช้ควบคุมหญ้าใบกว้างและหญ้าคลุมดิน การปนเปื้อนของอาทราซีนพบในสิ่งแวดล้อมโดยเฉพาะพื้นที่การเกษตร อาทราซีนเป็นพิษต่อแบคทีเรียแพลงก์ตอน พืช สัตว์ และมนุษย์ วัตถุประสงค์ของการวิจัยนี้คือการพัฒนาตัวเร่ง ZnO Ce-ZnO และ Cu-ZnO ที่ยึดเกาะอยู่บนเม็ดอะลูมินาโดยเทคนิคการเคลือบเชิงกลเพื่อใช้ย่อยสลายอาทราซีนที่ปนเปื้อนในน้ำภายใต้สภาวะแสงขาว ZnO Ce-ZnO และ Cu-ZnO ถูกสังเคราะห์ขึ้นอย่างประสบความสำเร็จโดยวิธีเคมีอย่างง่ายซึ่งใช้แป้งข้าวเหนียว (S) และโพลีไวนิลไพโรลิไดน (P) เป็นแม่แบบ ตัวเร่ง 0.02Ce-ZnO (S) สามารถกำจัดอาทราซีนได้ที่พีเอชไออีพีภายใต้แสงขาว แป้งข้าวเหนียวที่ใช้เป็นแม่แบบในการสังเคราะห์ตัวเร่งนั้นเป็นทางเลือกที่เป็นมิตรต่อสิ่งแวดล้อมเมื่อเปรียบเทียบกับโพลีไวนิลไพโรลิไดน Ce-ZnO (S) ที่เติมด้วย 0.02 และ 0.1 อัตราส่วนโดยโมลสามารถกำจัดอาทราซีนได้ดีกว่า Cu-ZnO (S) 0.02Ce-ZnO (S) 5:1 และ ZnO ที่ใช้ทางการค้าถูกใช้ในการศึกษาปัจจัยที่มีผลต่อกระบวนการโฟโตคะตะไลซิสของอาทราซีน ปริมาณตัวเร่งที่เหมาะสมคือ 0.1 กรัมสำหรับตัวเร่งแบบผง 2.5 กรัมสำหรับตัวเร่ง ZnO_550 แบบเม็ด และ 5.0 กรัมสำหรับตัวเร่ง 0.02Ce-ZnO (S) 5:1 แบบเม็ด ต่อ 100 มิลลิลิตรของสารละลายอาทราซีน (5 mg/L) การชะของ Zn ในสารละลายอาทราซีนค่อนข้างไม่มีนัยสำคัญ SO_4^{2-} และ Cl^- ช่วยเพิ่มการกำจัดอาทราซีน ในขณะที่ CO_3^{2-} HCO_3^- และ HPO_4^{2-} นั้นขัดขวางการกำจัดอาทราซีน 0.005Ag-0.005Ce-ZnO ถูกสังเคราะห์ขึ้นอย่างประสบความสำเร็จและสามารถกำจัดอาทราซีนได้ดี (87% ที่ 180 นาที) จลศาสตร์ของการกำจัดอาทราซีนขึ้นกับแบบจำลอง Langmuir-Hinshelwood-Hougen and Watson (LHHW) อย่างไรก็ตาม ปริมาณคาร์บอนอินทรีย์ทั้งหมด (TOC) ลดลงเพียง 64–65% ที่ 180 นาที และไซยานูริกเอซิดไม่ถูกตรวจพบในผลิตภัณฑ์สุดท้ายของกระบวนการโฟโตคะตะไลซิสของอาทราซีน

สาขาวิชา การจัดการสิ่งแวดล้อม.....ลายมือชื่อ.....
ปีการศึกษา 2554.....ลายมือชื่อ อ.ที่ปรึกษาวิทยานิพนธ์หลัก.....
ลายมือชื่อ อ.ที่ปรึกษาวิทยานิพนธ์ร่วม.....

5187802920: MAJOR ENVIRONMENTAL MANAGEMENT

KEYWORDS: PHOTOCATALYSIS / ATRAZINE / ZnO / SIMPLE CHEMICAL METHOD / STICKY RICE STARCH / MECHANICAL COATING TECHNIQUE

PUMMARIN KHAMDAHSAG: IMPROVEMENT OF ZnO BY TEXTURAL MODIFICATION AND METAL DOPING FOR ATRAZINE PHOTOCATALYSIS. ADVISOR: ASSOC. PROF. NURAK GRISDANURAK, Ph.D., CO-ADVISOR: PROF. MARK A. NANNY, Ph.D., 215 pp.

Atrazine is the herbicide used for controlling broadleaf and grassy weeds. Contamination of atrazine has been found in environment particularly in cultivated area. Atrazine can cause hazard to bacteria, plankton, plants, animals, and human. The objective of this study is to develop ZnO, Ce-ZnO, and Cu-ZnO catalysts fabricated on Al₂O₃ by mechanical coating technique (MCT) applied for the degradation of atrazine contaminated water under visible light irradiation. ZnO, Ce-ZnO, and Cu-ZnO were successfully synthesized by the simple chemical method using sticky rice starch (S) and polyvinylpyrrolidone (P) as templates. Under visible light irradiation, the 0.02Ce-ZnO (S) showed efficient removal of atrazine at the pH of the isoelectric point. The S template could represent an environmental friendly alternative for the catalyst synthesis compared to the P template. Ce-ZnO (S) at both 0.02 and 0.1 molar ratios of doping showed the higher atrazine removal than Cu-ZnO (S). The 0.02Ce-ZnO (S) 5:1 and the commercial ZnO were used further in the study of photocatalytic degradation of atrazine. The optimal catalyst loadings were 0.1 g for catalyst powder, 2.5 g for ZnO₅₅₀, and 5.0 g for 0.02Ce-ZnO (S) 5:1 bead per 100 mL atrazine solution (5 mg/L). Discharge of Zn into atrazine solution was quite insignificant. The SO₄²⁻ and Cl⁻ anions enhanced the atrazine removal while CO₃²⁻, HCO₃⁻, and HPO₄²⁻ anions inhibited the atrazine removal. 0.005Ag-0.005Ce-ZnO was successfully prepared and presented superiority on atrazine degradation (87% at 180 min). The kinetics of the atrazine removal relied on Langmuir-Hinshelwood-Hougen and Watson (LHHW) model. However, the total organic carbon (TOC) decreased only 64–65% at 180 min, and cyanuric acid was not observed as the final product in atrazine photocatalytic degradation.

Field of Study: Environmental Management Student's Signature.....

Academic Year: 2011..... Advisor's Signature.....

Co-advisor's Signature.....

ACKNOWLEDGEMENTS

I would like to express my gratitude to Assoc. Prof. Dr. Nurak Grisdanurak, my advisor, for giving me the great support, guidance, and independence. I feel really lucky to work on my dissertation in his laboratory at Thammasat University under his supervision. I would like to thank Prof. Dr. Mark A. Nanny, my co-advisor, for the opportunity to be his student. His knowledgeable advice, scientific suggestion, and generous encouragement significantly contribute to my research.

The stimulating questions and valuable suggestions on my work from the committee members, Assist. Prof. Dr. Chantra Tongcumpou, Assoc. Prof. Dr. Jatuporn Wittayakun, Assoc. Prof. Dr. Jin Anotai, Assist. Prof. Dr. Patiparn Punypalakul, and Assist. Prof. Dr. Sumana Siripattanakul, are also acknowledged. I am grateful to NCE-EHWM and graduate school, Chulalongkorn University, for the scholarship and the financial support. My gratitude also goes to the Department of Chemical Engineering, Faculty of Engineering, Thammasat University, SLRI, STREC, and NANOTEC for their laboratory facility.

The assistance from my colleagues at Chula (P'Koh, P'Jew, P'Pop, P'Nam, P'Ton, Ball, Kung, P'Noy, P'Champ, Ploy, Puii, Donut, Yummyum, Nan, Pond, Kob, Mai, P'Joy, P'Nok, PuiSunny, Fah, Jub, and Mew) and at Thammasat (P'Jew, P'BoyYai, P'Ple, Job, Rat, Tum, P'BoyLek, Eak, Aoy, P'Tu, Eddy, A, Pat, P'Pong, Mooh, New, P'Puek, Cyril, Mau, Tin, Ying, Jew, Pong, Prai, OMaetee, M, Rute, Best, Jeejy, Gun, Palm, Toon, Mont, Golf, and Cat) are highly appreciated. The one page acknowledgement specification limits what I would like to thank on what they have done to support my research in times of happiness as well as troubles in each single day during those challenging research years. The obligation gives to my teachers and my friends at Thammasat University, SIIT, Chiangmai University, Teerakarnbanhong School, Chumchonbanmaetuen School, and Art-Lamkom School. I will never forget all their friendship and abundant support for my doctoral study life. My appreciation also gives to Jee, Nim, Khawn, and Biig who are my best friends.

My big thankfulness goes to my father, mother, and family for unlimited love, intensive understanding, and reasonable freedom encouraged in living my own life.

CONTENTS

	Page
ABSTRACT (IN THAI).....	iv
ABSTRACT (IN ENGLISH)	v
ACKNOWLEDGEMENTS.....	vi
CONTENTS.....	vii
LIST OF TABLES.....	xii
LIST OF FIGURES.....	xxii
CHAPTER I INTRODUCTION.....	1
1.1 Motivations.....	1
1.2 Objectives.....	5
1.3 Scope of Study.....	6
1.4 Expected Outcomes.....	6
CHAPTER II BACKGROUND AND LITERATURE REVIEW.....	7
2.1 Mechanism of heterogeneous photocatalysis.....	7
2.2 ZnO under UV and visible light irradiation.....	9
2.3 ZnO with dopants.....	14
2.4 Simple chemical method.....	15
2.5 Atrazine general information.....	17
CHAPTER III MATERIALS AND METHODS.....	21
3.1 Chemicals.....	22
3.2 Catalyst preparation.....	23
3.2.1 Mechanical coating technique for ZnO.....	23

	Page
3.2.2 Simple chemical method using sticky rice starch and poly-vinylpyrrolidone.....	23
3.2.3 Mechanical coating technique for prepared catalysts.....	24
3.3 Catalyst characterization.....	24
3.3.1 Thermogravimetric property.....	24
3.3.2 Organic and inorganic identities.....	25
3.3.3 Structure and crystalline size.....	25
3.3.4 Oxidation state.....	25
3.3.5 Light absorption capacity.....	26
3.3.6 Specific surface area.....	26
3.3.7 Morphology.....	27
3.3.8 Surface charge.....	27
3.4 Catalyst activity test.....	27
3.4.1 Immobilization concernment.....	27
3.4.2 Preparation route concernment.....	29
3.5 Photocatalytic degradation of atrazine.....	31
3.6 Analytical technique.....	33
3.6.1 High performance liquid chromatography (HPLC).....	33
3.6.2 Total organic carbon (TOC).....	34
3.6.3 Liquid chromatography-mass spectrometer (LC-MS).....	34
CHAPTER IV RESULTS AND DISCUSSION.....	35
4.1 Catalyst screening and preliminary study.....	36

	Page
4.1.1 Catalyst characteristics.....	36
4.1.1.1 Thermogravimetric property.....	36
4.1.1.2 Organic and inorganic identities.....	42
4.1.1.3 Structure and crystalline size.....	45
4.1.1.4 Oxidation state.....	50
4.1.1.5 Light absorption capacity.....	52
4.1.1.6 Specific surface area.....	56
4.1.1.7 Morphology.....	59
4.1.1.8 Surface charge.....	62
4.1.2 Catalyst activity test.....	64
4.1.2.1 Immobilization concernment.....	64
4.1.2.2 Preparation route concernment.....	67
4.2 Photocatalytic degradation of atrazine.....	70
4.2.1 Photolysis and adsorption.....	71
4.2.2 Effect of transition metal dopants and molar ratio of doping.....	75
4.2.3 Effect of catalyst loading.....	77
4.2.4 Effect of pH.....	82
4.2.5 Effect of atrazine initial concentration.....	85
4.2.6 Surface passivation.....	87
4.2.7 Effect of ionic strength.....	89

	Page
4.2.8 Effect of anions.....	97
4.2.9 Other metal dopants on ZnO.....	100
4.2.10 Competitive effects from natural organic matter.....	103
4.2.11 Langmuir-Hinshelwood-Hougen and Watson (LHHW) Kinetics.....	105
4.2.12 Catalyst reliability.....	110
4.3 Evaluation of photocatalytic degradation pathway of atrazine.....	111
CHAPTER V CONCLUSIONS AND RECOMMENDATIONS.....	126
5.1 Conclusions.....	126
5.2 Recommendations.....	127
REFERENCES.....	129
APPENDICES.....	146
APPENDIX A Catalyst preparation.....	147
A.1 Mechanical coating technique.....	147
A.2 Condition of catalyst preparation.....	148
APPENDIX B Characterization.....	150
B.1 Zeta potential data.....	150
APPENDIX C Calibration.....	151
C.1 RR120 calibration data.....	151
C.2 Atrazine calibration data.....	152
APPENDIX D Catalyst activity test.....	155
D.1 Reactor setup.....	155

	Page
D.2 Immobilization concernment.....	156
D.3 Preparation route concernment.....	159
APPENDIX E Photocatalytic degradation of atrazine.....	160
E.1 Reactor setup.....	160
E.2 Photolysis and adsorption.....	160
E.3 Effect of transition metal dopants and molar ratio of doping.....	163
E.4 Effect of catalyst loading.....	166
E.5 Effect of pH.....	173
E.6 Effect of atrazine initial concentration.....	176
E.7 Surface passivation.....	180
E.8 Effect of ionic strength.....	182
E.9 Effect of anions.....	187
E.10 Other metal dopants on ZnO.....	188
E.11 Competitive effects from natural organic matter.....	192
E.12 Langmuir-Hinshelwood-Hougen and Watson (LHHW) kinetics.	194
E.13 Catalyst reliability.....	195
E.14 Evaluation of photocatalytic degradation pathway of atrazine....	196
BIOGRAPHY.....	215

LIST OF TABLES

TABLE	Page
2.1 Band gap energies and corresponding radiation wavelength required for photocatalysts excitation (De Lasa et al, 2004).....	11
2.2 Organic compounds and percentage of photocatalytic degradation under UV irradiation.....	12
2.3 Organic compounds and percentage of photocatalytic degradation under visible light irradiation.....	13
2.4 Physical and chemical properties of atrazine (Chung, and Gu, 2009; McGlamery and Slife, 1966: online; U.S. EPA, 2003: online; U.S. EPA, 2007: online).....	18
3.1 Overall study procedure.....	21
3.2 Chemical structure and properties of RR120 (Cho and Zho, 2007).....	28
3.3 Studied parameters of atrazine photocatalytic degradation.....	32
4.1 Contents of the experimental results and discussion.....	35
4.2 Crystalline sizes of the catalysts calculated from (110) plane in the XRD pattern in Figure 4.11.....	47
4.3 Crystalline sizes of catalysts calculated from (110) plane.....	50
4.4 Zn K-edge energy position of catalysts with respect to Zn foil.....	51
4.5 Ce K-edge energy position of catalysts with respect to Ce foil.....	52
4.6 BET surface areas of standard samples.....	57
4.7 BET surface areas of catalysts prepared by sticky rice starch (S) and polyvinylpyrrolidone (P) templates.....	57
4.8 Average pore sizes of 0.02Ce-ZnO (P), 0.02Ce-ZnO (S), and ZnO commercial powders.....	58

TABLE	Page
4.9 Studied parameters of photocatalytic degradation of atrazine using various catalysts.....	70
4.10 BET surface areas of catalysts prepared with the weight ratio $Zn(NO_3)_2 \cdot 6H_2O$ to sticky rice starch (S) of 5:1.....	77
4.11 Percent removal of atrazine by using 0.02Ce-ZnO (S) 5:1 and 0.1Ce-ZnO (S) 5:1.....	77
4.12 Percent removal of atrazine per catalyst weight-time by using ZnO powder and ZnO_550 at initial time of irradiation (15 min).....	82
4.13 BET surface areas of 0.005Ag-0.005Ce-ZnO (S), 0.005Fe-0.005Ce-ZnO (S), and 0.005Cu-0.005Ce-ZnO (S).....	101
4.14 Comparison of k_r (mg/L-min) and K_{ads} (L/mg) in the LHHW kinetics for photocatalytic degrading of atrazine using the suitable catalysts in powder and bead forms.....	109
4.15 LC-MS identified intermediates of atrazine photocatalytic degradation by ZnO powder.....	121
4.16 LC-MS identified intermediates of atrazine photocatalytic degradation by 0.005Ag-0.005Ce-ZnO (S) powder.....	125
A.1 pH of precursor measured during catalyst preparation.....	148
B.1 Average zeta potential of catalysts.....	150
C.1 RR120 standard solution and absorbance from UV-vis spectrometer...	151
C.2 Atrazine standard solution and peak area from HPLC for 10 μ L injection.....	152
C.3 Atrazine standard solution and peak area from HPLC for 80 μ L injection.....	153

D.1	RR120 adsorption on ZnO_550.....	156
TABLE		Page
D.2	RR120 photolysis under UV light.....	157
D.3	RR120 photolysis under visible light.....	157
D.4	RR120 photocatalytic degradation under UV light irradiation using ZnO_550.....	158
D.5	RR120 photocatalytic degradation under visible light irradiation using ZnO_550.....	158
D.6	RR120 photocatalytic degradation under visible light irradiation with ZnO_550 and 0.1Ce-ZnO (P) 1:2 bead using different initial RR120 concentrations.....	159
D.7	Percent removal of varied pH atrazine solution under visible light irradiation using Ce-ZnO (P).....	159
D.8	Percent removal of varied pH atrazine solution under visible light irradiation using Ce-ZnO (S).....	159
E.1	Atrazine photolysis under visible light.....	160
E.2	Atrazine adsorption on ZnO powder.....	161
E.3	Atrazine adsorption on ZnO_550.....	161
E.4	Atrazine adsorption on 0.02Ce-ZnO (S) powder.....	161
E.5	Atrazine adsorption on 0.02Cu-ZnO (S) powder.....	162
E.6	Atrazine adsorption on 0.02Ce-ZnO (S) bead.....	162
E.7	Atrazine adsorption on 0.02Cu-ZnO (S) bead.....	163
E.8	Photocatalytic degradation of atrazine by 0.02Ce-ZnO (S) 10:1 powder.....	163
E.9	Photocatalytic degradation of atrazine by 0.1Ce-ZnO (S) 10:1	164

powder.....	
TABLE	Page
E.10 Photocatalytic degradation of atrazine by 0.02Ce-ZnO (S) 5:1 powder	164
E.11 Photocatalytic degradation of atrazine by 0.1Ce-ZnO (S) 5:1 powder	164
E.12 Photocatalytic degradation of atrazine by 0.02Cu-ZnO (S) 10:1 powder.....	165
E.13 Photocatalytic degradation of atrazine by 0.1Cu-ZnO (S) 10:1 powder.....	165
E.14 Photocatalytic degradation of atrazine by 0.02Cu-ZnO (S) 5:1 powder	165
E.15 Photocatalytic degradation of atrazine by 0.1Cu-ZnO (S) 5:1 powder	166
E.16 Photocatalytic degradation of atrazine by 0.10 g of ZnO powder.....	166
E.17 Photocatalytic degradation of atrazine by 0.30 g of ZnO powder.....	166
E.18 Photocatalytic degradation of atrazine by 0.50 g of ZnO powder.....	167
E.19 Photocatalytic degradation of atrazine by 0.70 g of ZnO powder.....	167
E.20 Photocatalytic degradation of atrazine by 0.90 g of ZnO powder.....	167
E.21 Photocatalytic degradation of atrazine by 1.00 g of ZnO_550.....	168
E.22 Photocatalytic degradation of atrazine by 2.50 g of ZnO_550.....	168
E.23 Photocatalytic degradation of atrazine by 5.00 g of ZnO_550.....	168
E.24 Photocatalytic degradation of atrazine by 7.50 g of ZnO_550.....	169
E.25 Photocatalytic degradation of atrazine by 0.10 g of 0.02Ce-ZnO (S) 5:1 powder.....	169
E.26 Photocatalytic degradation of atrazine by 0.30 g of 0.02Ce-ZnO (S) 5:1 powder.....	169
E.27 Photocatalytic degradation of atrazine by 0.50 g of 0.02Ce-ZnO (S) 5:1 powder.....	170

TABLE	Page
E.28 Photocatalytic degradation of atrazine by 1.00 g of 0.02Ce-ZnO (S) 5:1 bead.....	170
E.29 Photocatalytic degradation of atrazine by 2.50 g of 0.02Ce-ZnO (S) 5:1 bead.....	170
E.30 Photocatalytic degradation of atrazine by 5.00 g of 0.02Ce-ZnO (S) 5:1 bead.....	171
E.31 Photocatalytic degradation of atrazine by 0.10 g of 0.02Cu-ZnO (S) 5:1 powder.....	171
E.32 Photocatalytic degradation of atrazine by 0.30 g of 0.02Cu-ZnO (S) 5:1 powder.....	171
E.33 Photocatalytic degradation of atrazine by 0.50 g of 0.02Cu-ZnO (S) 5:1 powder.....	172
E.34 Photocatalytic degradation of atrazine by 1.00 g of 0.02Cu-ZnO (S) 5:1 bead.....	172
E.35 Photocatalytic degradation of atrazine by 2.50 g of 0.02Cu-ZnO (S) 5:1 bead.....	172
E.36 Photocatalytic degradation of atrazine by 5.00 g of 0.02Cu-ZnO (S) 5:1 bead.....	173
E.37 Photocatalytic degradation of atrazine by ZnO powder at pH 3.99.....	173
E.38 Photocatalytic degradation of atrazine by ZnO powder at pH 4.89.....	173
E.39 Photocatalytic degradation of atrazine by ZnO powder at pH 6.92.....	174
E.40 Photocatalytic degradation of atrazine by ZnO powder at pH 8.49.....	174
E.41 Photocatalytic degradation of atrazine by ZnO_550 at pH 3.90.....	174
E.42 Photocatalytic degradation of atrazine by ZnO_550 at pH 4.95.....	175

TABLE	Page
E.43 Photocatalytic degradation of atrazine by ZnO_550 at pH 7.00.....	175
E.44 Photocatalytic degradation of atrazine by ZnO_550 at pH 8.84.....	175
E.45 Photocatalytic degradation of atrazine by ZnO powder using 1.0 mg/L of atrazine solution.....	176
E.46 Photocatalytic degradation of atrazine by ZnO powder using 2.3 mg/L of atrazine solution.....	176
E.47 Photocatalytic degradation of atrazine by ZnO powder using 4.9 mg/L of atrazine solution.....	177
E.48 Photocatalytic degradation of atrazine by ZnO powder using 7.1 mg/L of atrazine solution.....	177
E.49 Photocatalytic degradation of atrazine by ZnO powder using 9.9 mg/L of atrazine solution.....	177
E.50 Photocatalytic degradation of atrazine by ZnO_550 using 1.0 mg/L of atrazine solution.....	178
E.51 Photocatalytic degradation of atrazine by ZnO_550 using 2.3 mg/L of atrazine solution.....	178
E.52 Photocatalytic degradation of atrazine by ZnO_550 using 4.8 mg/L of atrazine solution.....	178
E.53 Photocatalytic degradation of atrazine by ZnO_550 using 7.1 mg/L of atrazine solution.....	179
E.54 Photocatalytic degradation of atrazine by ZnO_550 using 9.9 mg/L of atrazine solution.....	179
E.55 Electrical conductivity of atrazine photocatalytic degradation by ZnO_550.....	180

TABLE	Page
E.56 Zn element concentration of atrazine photocatalytic degradation by ZnO_550.....	180
E.57 Electrical conductivity of atrazine photocatalytic degradation by 0.02Ce-ZnO (S) 5:1 bead.....	180
E.58 Zn element concentrations of atrazine photocatalytic degradation by 0.02Ce-ZnO (S) 5:1 bead.....	181
E.59 Electrical conductivity of atrazine photocatalytic degradation by 0.02Cu-ZnO (S) 5:1 bead.....	181
E.60 Zn element concentrations of atrazine photocatalytic degradation by 0.02Cu-ZnO (S) 5:1 bead.....	181
E.61 Ionic strength (I) of Na_2SO_4 in atrazine solution.....	182
E.62 Electrical conductivity (σ) change before and after running reaction in the presence of Na_2SO_4 in atrazine solution.....	182
E.63 Atrazine photocatalytic degradation in the presence of Na_2SO_4 at different ionic strength values.....	182
E.64 Ionic strength (I) of NaCl in atrazine solution.....	183
E.65 Electrical conductivity (σ) change before and after running reaction in the presence of NaCl in atrazine solution.....	183
E.66 Atrazine photocatalytic degradation in the presence of NaCl at different ionic strength values.....	183
E.67 Ionic strength (I) of Na_2CO_3 in atrazine solution.....	184
E.68 Electrical conductivity (σ) change before and after running reaction in the presence of Na_2CO_3 in atrazine	184

solution.....	
E.69 Atrazine photocatalytic degradation in the presence of Na ₂ CO ₃ at different ionic strength values.....	184
TABLE	Page
E.70 Ionic strength (<i>I</i>) of NaHCO ₃ in atrazine solution.....	185
E.71 Electrical conductivity (σ) change before and after running reaction in the presence of NaHCO ₃ in atrazine solution.....	185
E.72 Atrazine photocatalytic degradation in the presence of NaHCO ₃ at different ionic strength values.....	185
E.73 Ionic strength (<i>I</i>) of Na ₂ HPO ₄ in atrazine solution.....	186
E.74 Electrical conductivity (σ) change before and after running reaction in the presence of Na ₂ HPO ₄ in atrazine solution.....	186
E.75 Atrazine photocatalytic degradation in the presence of Na ₂ HPO ₄ at different ionic strength values.....	186
E.76 Photocatalytic degradation of atrazine using ZnO_550 and 0.02Ce-ZnO (S) 5:1 bead with free anions.....	187
E.77 Photocatalytic degradation of atrazine using ZnO_550 in the presence of anions from sodium salts.....	187
E.78 Photocatalytic degradation of atrazine using 0.02Ce-ZnO (S) 5:1 bead in the presence of anions from sodium salts.....	188
E.79 Photocatalytic degradation of atrazine using 0.005Cu-0.005Ce-ZnO (S) powder.....	188
E.80 Photocatalytic degradation of atrazine using 0.005Fe-0.005Ce-ZnO (S) powder.....	189
E.81 Photocatalytic degradation of atrazine using 0.005Ag-0.005Ce-ZnO	189

(S) powder.....	
E.82 Photocatalytic degradation of atrazine by 0.005Ag-0.005Ce-ZnO (S) powder using 0.9 mg/L of atrazine solution.....	190
TABLE	
	Page
E.83 Photocatalytic degradation of atrazine by 0.005Ag-0.005Ce-ZnO (S) powder using 2.8 mg/L of atrazine solution.....	190
E.84 Photocatalytic degradation of atrazine by 0.005Ag-0.005Ce-ZnO (S) powder using 4.4 mg/L of atrazine solution.....	191
E.85 Photocatalytic degradation of atrazine by 0.005Ag-0.005Ce-ZnO (S) powder using 6.0 mg/L of atrazine solution.....	191
E.86 Photocatalytic degradation of atrazine by 0.005Ag-0.005Ce-ZnO (S) powder using 9.5 mg/L of atrazine solution.....	192
E.87 Photocatalytic degradation of atrazine by 0.02Ce-ZnO (S) bead with free humic acid.....	192
E.88 Photocatalytic degradation of atrazine by 0.02Ce-ZnO (S) bead in the presence of 1.0 mg/L humic acid.....	193
E.89 Photocatalytic degradation of atrazine by 0.02Ce-ZnO (S) bead in the presence of 3.0 mg/L humic acid.....	193
E.90 Photocatalytic degradation of atrazine by 0.02Ce-ZnO (S) bead in the presence of 5.0 mg/L humic acid.....	193
E.91 Photocatalytic degradation of atrazine by 0.005Ag-0.005Ce-ZnO (S) powder with free humic acid.....	194
E.92 Photocatalytic degradation of atrazine by 0.005Ag-0.005Ce-ZnO (S) powder in the presence of 50.0 mg/L humic acid.....	194
E.93 Initial rate of atrazine photocatalytic degradation by catalyst powders	194

	and catalyst bead.....	
E.94	Atrazine photocatalytic degradation by catalyst powders and catalyst bead for LHHW linear plotting.....	195
TABLE		Page
E.95	Reliability test of atrazine photocatalytic degradation by ZnO_550 at 120 min.....	195
E.96	C/C ₀ and TOC/TOC ₀ of atrazine photocatalytic degradation using ZnO and 0.005Ag-0.005Ce-ZnO (S) powders.....	196

LIST OF FIGURES

FIGURE	Page
2.1 Schematic mechanism of photocatalytic reaction.....	9
2.2 Unit cell of ZnO hexagonal wurtzite structure. Zinc atoms are in small spheres, oxygen atoms are in large spheres, and the dashed lines show the unit cell (Barron and Smith, 2010: online).....	10
3.1 Photocatalytic batch reactor setup for the immobilization concernment study.....	29
3.2 Photocatalytic batch reactor for the preparation route concernment study in 3.4.2 and the photocatalytic degradation of atrazine in 3.5.....	30
3.3 Top view of photocatalytic batch reactor for the preparation route concernment study in 3.4.2 and the photocatalytic degradation of atrazine in 3.5.....	30
4.1 TG-DTA curves of the ZnO coated on Al ₂ O ₃ beads.....	39
4.2 TG-DTA curves of ZnO (S).....	39
4.3 TG-DTA curves of 0.1Ce-ZnO (S).....	40
4.4 TG-DTA curves of sticky rice starch.....	40
4.5 TG-DTA curves of ZnO (P).....	41
4.6 TG-DTA curves of 0.1Ce-ZnO (P).....	41
4.7 TG-DTA curves of polyvinylpyrrolidone.....	42

4.8	FT-IR spectra of sticky rice starch (S) and polyvinylpyrrolidone (P) templates.....	43
4.9	FT-IR spectra of catalysts prepared with starch (S) and polyvinylpyrrolidone (P) templates.....	44
4.10	Raman spectra of 0.1Ce-ZnO (S) and 0.1Ce-ZnO (P).....	44
FIGURE		Page
4.11	XRD patterns of the catalysts prepared by MCT with different calcination temperatures.....	47
4.12	XRD patterns of standard ZnO and CeO ₂	48
4.13	Normalized XRD spectra of catalysts with sticky rice starch (S) template.....	48
4.14	Normalized XRD spectra of catalysts with polyvinylpyrrolidone (P) template.....	49
4.15	Normalized XRD patterns of 0.1Cu-ZnO (S) compared with ZnO (S).	49
4.16	XANES spectra of Zn element and Zn compounds.....	51
4.17	XANES spectra of Ce element and Ce compounds.....	52
4.18	UV-vis diffuse reflectance spectra of the ZnO coated on Al ₂ O ₃ bead prepared with different calcination temperatures.....	54
4.19	UV-vis diffuse reflectance spectra of ZnO prepared by sticky rice starch (S) and polyvinylpyrrolidone (P) templates.....	54
4.20	UV-vis diffuse reflectance spectra of 0.02Ce-ZnO and 0.1Ce-ZnO prepared by different templates comparing to commercial ZnO.....	55
4.21	Transformed Kubelka-Munk plots of 0.02Ce-ZnO and 0.1Ce-ZnO prepared by different templates comparing to commercial ZnO.....	55
4.22	Pore size distributions of 0.02Ce-ZnO (P), 0.02Ce-ZnO (S), and ZnO commercial.....	58

4.23	SEM images of Al ₂ O ₃ (left) and ZnO ₅₅₀ (right).....	60
4.24	SEM images of catalysts.....	61
4.25	Dependencies of zeta-potential of catalysts suspended in water at different pH.....	63
FIGURE		Page
4.26	RR120 spectrum from UV-vis spectrometer.....	65
4.27	RR120 photolysis and RR120 adsorption on ZnO ₅₅₀	66
4.28	RR120 photocatalytic degradation using ZnO ₅₅₀ under UV and visible light irradiation.....	66
4.29	RR120 photocatalytic degradation with ZnO ₅₅₀ and 0.1Ce-ZnO (P) 1:2 bead under visible light irradiation using the initial concentration of 10 and 20 mg/L.....	67
4.30	Percent removal of varied pH atrazine solution under visible light irradiation using Ce-ZnO on (a) sticky rice starch (S) and (b) polyvinylpyrrolidone (P) templates.....	69
4.31	Atrazine concentrations as a function of time on (a) atrazine photolysis under visible light irradiation and atrazine adsorption on ZnO powder and ZnO ₅₅₀ under dark condition.....	72
4.31	Atrazine concentrations as a function of time on atrazine adsorption under dark condition by (b) the prepared catalyst powders and (c) the prepared catalyst beads.....	73
4.32	Absorption spectrum of atrazine over 190 to 700 nm measured by UV-vis spectrometer.....	74
4.33	Spectra from common sources of visible light focused on the tungsten lamp (Spring and Davidson, 2009: online).....	74

4.34	Photocatalytic degradation of atrazine by (a) Ce-ZnO and (b) Cu-ZnO in powder form at different molar ratios.....	76
4.35	Photocatalytic degradation of atrazine by (a) ZnO powder and (b) ZnO_550 at different catalyst weights.....	79

	FIGURE	Page
4.36	Photocatalytic degradation of atrazine by (a) 0.02Ce-ZnO (S) 5:1 powder and (b) 0.02Ce-ZnO (S) 5:1 beads at different catalyst weight	80
4.37	Photocatalytic degradation of atrazine by (a) 0.02Cu-ZnO (S) 5:1 powder and (b) 0.02Cu-ZnO (S) 5:1 beads at different catalyst weights.....	81
4.38	Photocatalytic degradation of atrazine by (a) ZnO powder and (b) ZnO_550 at different pH.....	84
4.39	Photocatalytic degradation of atrazine by (a) ZnO powder and (b) ZnO_550 using varied initial concentrations of atrazine.....	86
4.40	Electrical conductivity of photocatalytic degradation of atrazine solution as a function of irradiation time in the presence of ZnO_550, 0.02Ce-ZnO (S) 5:1, and 0.02Cu-ZnO (S) 5:1.....	88
4.41	Zn element concentrations of photocatalytic degradation of atrazine solution as a function of irradiation time in the presence of catalysts	89
4.42	Effect of Na ₂ SO ₄ ionic strength on (a) electrical conductivity of atrazine solution and (b) the photocatalytic degradation of atrazine using ZnO_550.....	92
4.43	Effect of NaCl ionic strength on (a) electrical conductivity of atrazine solution and (b) the photocatalytic degradation of atrazine using ZnO_550.....	93

4.44	Effect of Na ₂ CO ₃ ionic strength on (a) electrical conductivity of atrazine solution and (b) the photocatalytic degradation of atrazine using ZnO_550.....	94
4.45	Effect of NaHCO ₃ ionic strength on (a) electrical conductivity of atrazine solution and (b) the photocatalytic degradation of atrazine using ZnO_550.....	95
FIGURE		Page
4.46	Effect of Na ₂ HPO ₄ ionic strength on (a) electrical conductivity of atrazine solution and (b) the photocatalytic degradation of atrazine using ZnO_550.....	96
4.47	Effect of anions on the photocatalytic degradation of atrazine (a) using ZnO_550 and (b) 0.02Ce-ZnO (S) 5:1 bead.....	99
4.48	Effect of other metal dopants on Ce-ZnO on atrazine photocatalytic degradation.....	101
4.49	UV-vis diffuse reflectance spectra of the other metal doped Ce-ZnO prepared by using sticky rice starch (S) templates compared with 0.02Ce-ZnO (S) 5:1.....	102
4.50	Photocatalytic degradation by 0.005Ag-0.005Ce-ZnO using varied initial concentrations of atrazine.....	102
4.51	Effect of natural organic matter on atrazine photocatalytic degradation using 0.02Ce-ZnO (S) 5:1.....	104
4.52	Effect of natural organic matter on atrazine photocatalytic degradation using 0.005Ag-0.005Ce-ZnO (S).....	104
4.53	Initial rate of atrazine photocatalytic degradation as a function of its initial concentration.....	108
4.54	LHHW linear plots of atrazine photocatalytic degradation using ZnO, 0.005Ag-0.005Ce-ZnO (S), and ZnO_550.....	108

4.55	Five cycles of atrazine photocatalytic degradation at 120 min of irradiation time using ZnO_550.....	111
4.56	Atrazine photocatalytic degradation using commercial ZnO and 0.005Ag-0.005Ce-ZnO (S) powders as a function of irradiation time..	115

	FIGURE	Page
4.57	TOC decrease in atrazine photocatalytic degradation using commercial ZnO and 0.005Ag-0.005Ce-ZnO powders as a function of irradiation time.....	115
4.58	Reaction mechanism of atrazine photocatalytic degradation (Minero et al., 1996; Lackhoff and Niessner, 2002).....	117
4.59	LC-MS spectra of atrazine photocatalytic degradation using ZnO powder at (a) 0, (b) 15, and (c) 30 min of irradiation time.....	118
4.59	LC-MS spectra of atrazine photocatalytic degradation using ZnO powder at (d) 45, (e) 60, and (f) 90 min of irradiation time.....	119
4.59	LC-MS spectra of atrazine photocatalytic degradation using ZnO powder at (g) 120, (h) 150, and (i) 180 min of irradiation time.....	120
4.60	LC-MS spectra of atrazine photocatalytic degradation using 0.005Ag-0.005Ce-ZnO (S) powder at (a) 0, (b) 15, and (c) 30 min of irradiation time.....	122
4.60	LC-MS spectra of atrazine photocatalytic degradation using 0.005Ag-0.005Ce-ZnO (S) powder at (d) 45, (e) 60, and (f) 90 min of irradiation time.....	123
4.60	LC-MS spectra of atrazine photocatalytic degradation using 0.005Ag-0.005Ce-ZnO (S) powder at (g) 120, (h) 150, and (i) 180 min of irradiation time.....	124

A.1	Raw material images: (a) Al ₂ O ₃ beads and (b) commercial ZnO powder.....	147
A.2	Mechanical coating apparatuses: (a) milling pot and (b) milling machine.....	147
A.3	Appearance of (a) 0.02Ce-ZnO polyvinylpyrrolidone gel and (b) 0.02Ce-ZnO starch gel.....	148
FIGURE		Page
A.4	Appearance of (a) Ce-ZnO (P) 1:2 and (b) Ce-ZnO (S) 1:2 after calcination.....	148
A.5	Appearance of (a) Ce-ZnO (P) 1:2 and (b) Ce-ZnO (S) 1:2 beads.....	149
A.6	Appearance of (a) and (b) Ce-ZnO (S), and (c) and (d) Cu-ZnO (S)....	149
C.1	Appearance of RR120 standard solution at different concentrations....	151
C.2	Calibration curve of RR120 solution.....	152
C.3	Calibration curve of atrazine (10 µL injection).....	153
C.4	Calibration curve of atrazine (80 µL injection).....	154
D.1	Reactor for photocatalytic degradation of RR120: (a), (b) under UV light and (c), (d) under visible light irradiation as described the procedure in 3.4.1 and the experimental result in 4.1.2.1.....	155
D.2	Reactor for photocatalytic degradation of atrazine under visible light irradiation as described the procedure in 3.4.2 and the experimental result in 4.1.2.2.....	156
E.1	Reactor for photocatalytic degradation of atrazine under visible light irradiation as described the procedure in 3.5 and the experimental result in 4.2.....	160
E.2	LC-MS spectra of atrazine photocatalytic degradation using ZnO powder at 0 min.....	197

E.3	LC-MS spectra of atrazine photocatalytic degradation using ZnO powder at 15 min.....	198
E.4	LC-MS spectra of atrazine photocatalytic degradation using ZnO powder at 30 min.....	199
E.5	LC-MS spectra of atrazine photocatalytic degradation using ZnO powder at 45 min.....	200
FIGURE		Page
E.6	LC-MS spectra of atrazine photocatalytic degradation using ZnO powder at 60 min.....	201
E.7	LC-MS spectra of atrazine photocatalytic degradation using ZnO powder at 90 min.....	202
E.8	LC-MS spectra of atrazine photocatalytic degradation using ZnO powder at 120 min.....	203
E.9	LC-MS spectra of atrazine photocatalytic degradation using ZnO powder at 150 min.....	204
E.10	LC-MS spectra of atrazine photocatalytic degradation using ZnO powder at 180 min.....	205
E.11	LC-MS spectra of atrazine photocatalytic degradation using 0.005Ag-0.005Ce-ZnO powder at 0 min.....	206
E.12	LC-MS spectra of atrazine photocatalytic degradation using 0.005Ag-0.005Ce-ZnO powder at 15 min.....	207
E.13	LC-MS spectra of atrazine photocatalytic degradation using 0.005Ag-0.005Ce-ZnO powder at 30 min.....	208
E.14	LC-MS spectra of atrazine photocatalytic degradation using 0.005Ag-0.005Ce-ZnO powder at 45 min.....	209
E.15	LC-MS spectra of atrazine photocatalytic degradation using 0.005Ag-	210

0.005Ce-ZnO powder at 60 min.....	
E.16 LC-MS spectra of atrazine photocatalytic degradation using 0.005Ag- 0.005Ce-ZnO powder at 90 min.....	211
E.17 LC-MS spectra of atrazine photocatalytic degradation using 0.005Ag- 0.005Ce-ZnO powder at 120 min.....	212
FIGURE	Page
E.18 LC-MS spectra of atrazine photocatalytic degradation using 0.005Ag- 0.005Ce-ZnO powder at 150 min.....	213
E.19 LC-MS spectra of atrazine photocatalytic degradation using 0.005Ag- 0.005Ce-ZnO powder at 180 min.....	214

CHAPTER I

INTRODUCTION

1.1 Motivations

Atrazine, 2-chloro-4-ethylamino-6-isopropylamino-1,3,5-triazine, is a chlorotriazine herbicide used to control broadleaf and grassy weeds in a variety of crops such as sorghum, fruits, vegetables, corn, and sugarcane (Guse et al., 2009). Many studies depicted its contamination in environment including Nishnabotna River and Wolf Creek, Iowa (The Earth's Best Defense, 2007: online), Des Plaines Wetland, Illinois (Alvord and Kadlec, 1996), Danube River, Bulgaria (Vitanov, Lekova, and Dobрева, 2003), and other cultivated sites. The reports indicated that the concentration of atrazine was higher than the maximum contaminant level (MCL) from the United States federal drinking water standard (3 ppb).

In Thailand, one to two million kg of atrazine is imported each year (Department of Agriculture, 2006). Furthermore, atrazine was the fourth hazardous chemical imported to the country in years 2001 and 2003. Atrazine has been used at 180 to 670 g per 60 to 80 L for 0.16 hectare (1 rai) for Spinach grass control (Department of Agriculture, 2006) or 1.5 to 4.5 kg active ingredient per hectare for overall weed control (Sukjaroen and Prayoonrat, 2001: online). As a result from using large amount of atrazine in Thailand particularly in agricultural area, surface water and groundwater are both likely to be contaminated by atrazine (Heepngoen, Sajjaphan, and Boonkerd, 2008). This herbicide has been found in Choa Praya River, east raw water canal, and tap water produced from Bang Kean waterworks approximately 58 to 106 ppb (Kruawal et al., 2005).

Atrazine could raise impacts to bacteria, plankton, plants, animals, and human; for example, atrazine distribution in field likely has a significant impact on amphibian, American Leopard frog, populations (Hayes et al., 2003), low concentrations of

atrazine may have ecological consequences on freshwater mussel quantities (Flynn and Spellman, 2009) and dietary exposure data results oncogenic risk to human (Tomerlin, 1989).

TiO₂/UV, which is one of advanced oxidation processes (AOPs), is widely applied for destructing organic pollutants including atrazine (Krýsová et al., 2003; McMurray, Dunlop, and Byrne, 2006; Minero et al., 1996) since the photocatalyst is low cost, non-toxic, and has long-term structural stability, abundance, high oxidation rate, and pollutant mineralization (Ling et al., 2008). However, intensive and widespread use of TiO₂ is unsuitable for large-scale wastewater treatment due to the reason of price and abundance. ZnO appears to be appropriable since its photodegradation ability is quite similar to that of TiO₂ (Daneshvar, Salari, and Khataee, 2004).

Generally, ZnO has been used in the form of particles and nanoparticles (Hong et al., 2009; Kumbhakar et al., 2008; Riahi-Noori et al., 2008; Zhang et al., 2007). From this practical point of view, wastewater treatment is usually operated with ZnO suspension in slurry reactors. However, the limitation always occurs with the problem of filtration related to the very small sizes of the particles that have to be removed from treated water. In addition, reagents, time, and cost are expensive for separation processes. Thus, ZnO has been modified to adhere with supports such as ceramic tiles with screen-printing method (Marto et al., 2009; Rego et al., 2009) in order to reduce the step of separation resulting in less capital for the treatment process. With the same reason, mechanical coating technique (MCT), which is another immobilization technique, is applied to this work. This technique was developed by Yoshida and co-workers (Yoshida et al., 2009). With their procedure, metallic titanium coating on alumina balls was firstly prepared via a planetary ball mill followed by oxidation process. The TiO₂ film was then adhered on the surface of alumina balls.

MCT is the simple and economical immobilization process of photocatalyst comparing to other processes. Technically, ZnO has high photocatalytic activity under UV range but has rather low photocatalytic activity under visible light range due to its band gap energy of 3.2 eV (De Lasa, Serrano, and Salaices, 2004). From many

literatures, ZnO has been doped with some metals such as In (Wang et al., 2007), Mn (Ullah and Dutta, 2008), As, P, and N (Vaithianathan et al., 2006), Li (Ko et al., 2003), Au and Pt (Pawinrat, Mekasuwandumrong, and Panpranot, 2009), and La (Anandan et al., 2007a; Anandan et al., 2007b) to improve its activity under visible light irradiation. In this study, cerium and copper dopants are supposed to enhance the photocatalytic activity of visible sensitized ZnO through the simple chemical method assisted by polymeric templates.

Polyvinylpyrrolidone has been used as an organic template for effortless preparations of nanocrystalline photocatalyst powders such as CeO₂, TiO₂, and ZnO by simple chemical and sol-gel method (Eskandari, Ahmandi V., and Ahmandi S.H., 2009; Maensiri, Laokul, and Klinkaewnarong, 2006a; Maensiri, Laokul, and Phokha., 2006b; Maensiri, Laokul, and Promarak, 2006c; Phoka et al., 2009; Wang, Gu, and Jin, 2003; Wei, Lian, and Jiang, 2009; Zheng et al., 2001). In catalyst synthesis, polyvinylpyrrolidone provided mesopores in the structure and assisted the distribution of catalyst active sites. The polyvinylpyrrolidone template was finally removed through the calcination process either at 300°C for 24 hr (Eskandari et al., 2009), 500°C for 2 hr (Phoka et al., 2009; Wang et al., 2003; Zheng et al., 2001), 550°C for 3 hr (Maensiri et al., 2006a; Maensiri et al., 2006b), or 600°C for 1 hr (Maensiri et al., 2006c). This variation of temperature and time is dependent on the thermal decomposition determined by thermogravimetric analysis (TG) and the crystallization of each prepared catalyst determined by differential thermal analysis (DTA). However, the amount of polyvinylpyrrolidone used in the synthesis, which affects the catalyst formation, has been rarely investigated. An optimal 30 wt% in the synthesis recipe was found in providing the smallest crystalline size and rutile ratio of TiO₂ (Wang et al., 2003).

Highly dense ZnO rods with good crystalline quality were reported when 1.0 mM of polyvinylpyrrolidone was used (Wei et al., 2009). With polyvinylpyrrolidone, ZnO and metal doped ZnO synthesis have resulted in the formation of nanoparticles and nanorods (Eskandari et al., 2009; Maensiri et al., 2006b; Maensiri et al., 2006c; Wei et al., 2009). Although template polyvinylpyrrolidone possibly plays a good role in the

synthesis, it is a polymeric compound produced from petrochemicals, and has some drawbacks such as dissolution inconvenience, high price, and high calcination temperature requirement generating some toxic gases such as CO₂, CO, and NO_x (ACROS ORGANICS BVBA, 2008: online).

It is interesting to search for an alternative template through green chemistry. Starch, an agro-product, is available in large amount. It consists of two polysaccharides: amylose and amylopectin. Amylose has a mostly linear chain structure containing up to 3,000 glucose molecules while amylopectin is a large branched polymer. A few studies have reported that starch could be used for material preparations such as Fe₂O₃, TiO₂, and ZnO (Chunming, Jingwen, and Quinan, 2009; Iwasaki, Davis, and Mann, 2004; Janardhanan, Ramasamy, and Nair, 2008; Shen et al., 2008). By means of the starch gel dispersion and the sol-gel method, synthesized nanoparticles were easily achieved through heat treatment either at 450°C for 3 hr (Chunming et al., 2009), 600°C for 2 hr (Iwasaki et al., 2004), 800°C for 2 hr (Janardhanan et al., 2008), or 600°C for 4 hr (Shen et al., 2008). The synthesized Fe₂O₃ was composed of high crystallinity with hematite X-ray diffraction (XRD) pattern and micro/nano sizes in range of 130 nm (Janardhanan et al., 2008). Like polyvinylpyrrolidone, starch from different plant sources provided a similar mesoporous structure for the synthesis. Iwasaki et al. (2004) used potato starch as a sponge gel template to fabricate TiO₂. The meso/macropore and thickness of TiO₂ deposits were dependent on the ratio of TiO₂/potato starch in the recipe. A mesoporous structure was also obtained when corn starch was used as a template for TiO₂ manufacturing (Chunming et al., 2009). ZnO nanoparticles were prepared by using zinc nitrate and starch (Shen et al., 2008). After zinc hydrate was dispersed in the starch gel, and the mixture was dried, 60 nm ZnO nanoparticles were formed via calcination.

By using polymeric materials and heat treatment, a gel framework could be formed. A metal hydrate would disperse on the gel framework leading to an increase in the distribution and rearrangement of metal in the gel. This simple method allows dopants to be added to the catalyst during the synthesis process without adjusting pH as is necessary in precipitation methods. In this study, ZnO is prepared, and cerium and

copper are selected as dopants. To search for alternative template, bioorganic template such as sticky rice starch is applied to synthesize photocatalysts in this study. Their characteristics are compared with the polyvinylpyrrolidone template usage on the same photocatalyst. In addition, an application of prepared materials has been carried out on photocatalytic degradation of atrazine under visible light irradiation. Many parameters which influence the ability of catalysts on atrazine photocatalytic degradation in the experimental system have been investigated. Based on Ce-ZnO preparation, other metal dopants (Cu, Fe, and Ag) have been considered to increase the performance of Ce-ZnO via the simple chemical method using sticky rice starch template.

1.2 Objectives

Main objective

This study aims to develop ZnO, Ce-ZnO, and Cu-ZnO catalysts fabricated on Al₂O₃ by mechanical coating technique applied for the degradation of atrazine contaminated water under visible light irradiation.

Sub-objectives

- 1) To select template using in catalyst preparation via sol-gel method.
- 2) To understand the physico-chemical properties of fabricated ZnO, Ce-ZnO, and Cu-ZnO mechano-coated on Al₂O₃.
- 3) To evaluate a suitable catalyst for the degradation of atrazine contaminated in water. The study is based on the highest degradation rate under following considerations;
 - Studied parameters: transition metal dopants, molar ratio of doping, catalyst loading, pH, initial concentration of atrazine, surface passivation, anions (SO₄²⁻, Cl⁻, CO₃²⁻, HCO₃⁻, and HPO₄²⁻), ionic strength, and competitive effects from dissolved natural organic matter.
 - Kinetic mechanism based on Langmuir-Hinshelwood-Hougen and Watson (LHHW) kinetics.
- 4) To test the reliability of selected catalyst by studying the lifetime of catalyst.

- 5) To evaluate the reaction pathway of atrazine photocatalytic degradation from the previous studies and measure the total organic carbon (TOC) and liquid chromatography mass spectrum (LC-MS) in the atrazine photocatalytic degradation under the proper conditions.

1.3 Scope of the Study

- 1) All experiments are done in a laboratory scale and a batch reactor.
- 2) Simple chemical method is conducted in catalyst preparation. Templates for this method are focused on polyvinylpyrrolidone and sticky rice starch. Catalyst base is ZnO. Main dopants are cerium and copper. Doping is dominated by molar ratio.
- 3) Catalysts are involved in powder and bead comparative forms.
- 4) Atrazine as solute in water is the probe of photocatalyst capability under visible light condition.
- 5) Atrazine photodecomposition is concentrated at point source studied parameters and partially considered in non-point source studied parameters applying for further study in open water.

1.4 Expected Outcomes

- 1) The alternative template such the sticky rice starch for catalyst preparation via simple chemical method is found.
- 2) The suitable catalyst in the experimental batch system is obtained.
- 3) The mechanical coating technique for ZnO and metal doped ZnO is understood and applied.
- 4) The photocatalytic degradation of atrazine by using the prepared catalysts is understood.
- 5) The prepared catalysts could be applied for degrading other organic pollutants contaminated in water.

CHAPTER II

BACKGROUND AND LITERATURE REVIEW

2.1 Mechanism of heterogeneous photocatalysis

In heterogeneous photocatalysis, which is characterized by having a variation of phase in a system, the catalyst phase is frequently found as solid or a mixture of solid which promotes chemical reaction with no phase change while another phase can be gas, pure organic liquid, or aqueous solutions (Herrmann, 1999). To convert reactants to products, the overall heterogeneous process involves the several steps (Smith, 1981):

- 1) Transport of reactants from the bulk fluid to the fluid-solid interface (external surface of catalyst particle)
- 2) Intraparticle transport of reactants into the catalyst particle (if it is porous)
- 3) Adsorption of reactants at interior sites of the catalyst particle
- 4) Chemical reaction of adsorbed reactants to adsorbed products (surface reaction—the intrinsic chemical step)
- 5) Desorption of adsorbed products
- 6) Transport of product from the interior sites to the outer surface of the catalyst particle
- 7) Transport of products from the fluid-solid interface to the bulk-fluid stream.

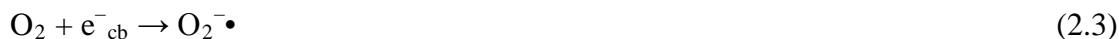
For wastewater treatment, organic compounds are the reactants in this heterogeneous process. These reactants are converted to products according to the steps 1) to 4). The products from the first four steps are CO_2 , H_2O , and other degraded organic compounds or intermediates are then transported back to the bulk solution via steps 5) to 7).

Focusing on chemical reaction, the reaction mechanism can be explained in terms of photochemistry. When the catalyst is irradiated by a certain level of light energy ($h\nu$),

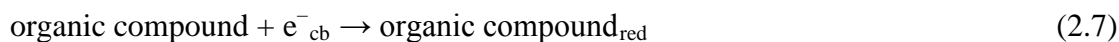
electron in valence band is activated to conduction band. This results in creation of an electron-hole pair. Electron presents at the conduction band (e^-_{cb}) while the hole or electron vacancy presents in the valence band (h^+_{vb}) (Rauf and Ashraf, 2009). The process is described by the following equation.



The e^-_{cb} and h^+_{vb} can both migrate to the catalyst surface. On the surface, reduction-oxidation reaction is relatively established when e^-_{cb} , h^+_{vb} and, other species are present. In wastewater treatment system, H_2O can react with to by h^+_{vb} to produce $\bullet OH$ radicals while O_2 can react with e^-_{cb} to develop oxygen superoxide radical anion. The radical anion then reacts with H_2O generating $\bullet OH$ radicals. Such reaction maintains no combination of e^-_{cb} and h^+_{vb} in the previous step.



$\bullet OH$ radicals can then react and oxidize organic compound. Moreover, the e^-_{cb} itself can react with an organic compound to become reducing organic compound. The overall possible mechanism of a photocatalytic reaction is shown in Figure 2.1.



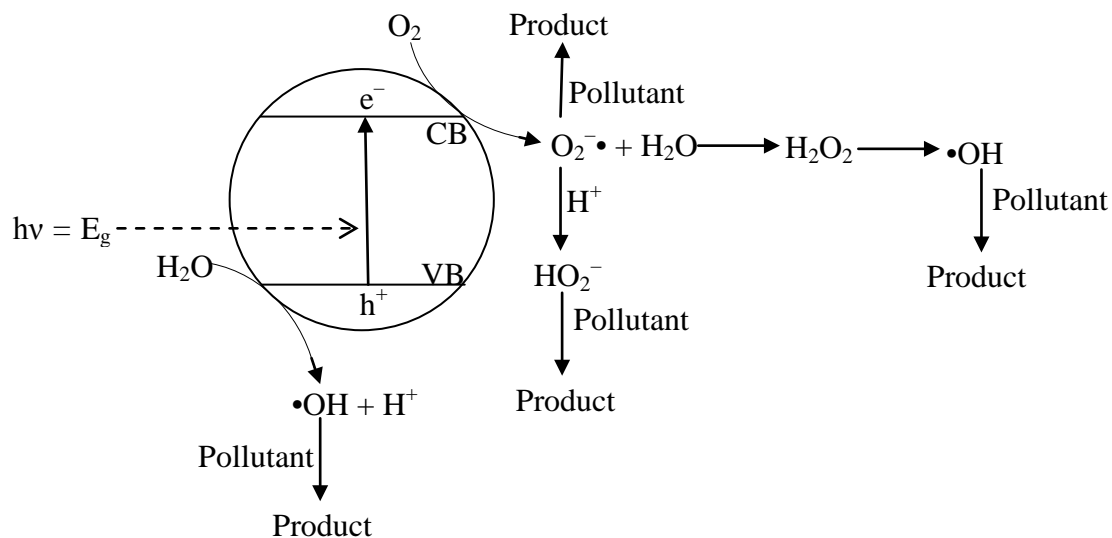


Figure 2.1 Schematic mechanism of photocatalytic reaction.

2.2 ZnO under UV and visible light irradiation

For the case of ZnO that favors the wurtzite structure as presented in Figure 2.2, its band gap energy (E_g), at room temperature, is 3.2 eV which requires a radiation of wavelength equal to 388 nm to promote excitation (De Lasa et al., 2004). For the radiation source of ZnO photocatalytic process, ultraviolet (UV) or more specifically near-ultraviolet radiation is very important. UV radiation is the wavelength range between 200 and 400 nm which can be divided into three regions. From 315 to 400 nm is UVA, 280 to 315 nm is UVB, and 200 to 280 nm is UVC. Thus, ZnO which has band gap energy of 3.2 eV can be excited in UV irradiation portion of below 388 nm covering specifically in UVA. Since 4 to 5% of sunlight reaching to the earth's surface are in near-UV range (300 to 400 nm), this portion of solar radiation can be used in ZnO photocatalysis (Pardeshi and Patil, 2009).

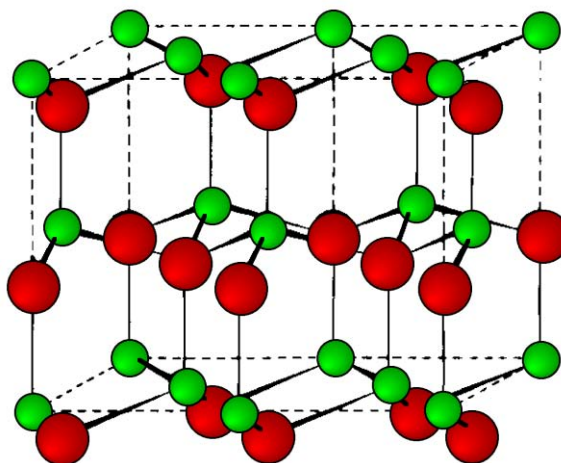


Figure 2.2 Unit cell of ZnO hexagonal wurtzite structure. Zinc atoms are in small spheres, oxygen atoms are in large spheres, and the dashed lines show the unit cell (Barron and Smith, 2010: online).

It is certain that TiO_2 is widely used in various applications particularly in environment cleanup (Fujishima, Zhang, and Tryk, 2007). Like TiO_2 photocatalyst, ZnO is accepted to be photoactive oxide because its band gap energy is close to that of TiO_2 as shown in Table 2.1. Photocatalytic performance of ZnO was proven to be similar to that of TiO_2 although it tended to exhibit little lower oxidation rate than TiO_2 (Dindar and Içli, 2001). ZnO was studied to compare organic compound degradation ability with TiO_2 in many literatures. As the study of photocatalytic degradation of dichlorvos, an organophosphorous insecticide, ZnO was more inferior to TiO_2 (Evgenidou, Fytianos, and Poullos, 2005). Dichlorvos disappeared in 20 min when treated with TiO_2 under UV wavelength range, Philips HPK 125W high pressure mercury lamp, while it took 120 minutes when treated with ZnO under the same condition. However, mineralization was unable to achieve on either TiO_2 or ZnO performance.

Table 2.1 Band gap energies and corresponding radiation wavelength required for photocatalysts excitation (De Lasa et al, 2004).

Semiconductor	Band gap energy (eV)	Wavelength (nm)
TiO ₂ (Rutile)	3.0	413
TiO ₂ (Anatase)	3.2	388
ZnO	3.2	388

Moreover, the degradation of phenol by TiO₂ was better than that of ZnO under sodium lamp and direct sunlight (Dindar and Içli, 2001). In contrast, under concentrated sunlight (40 to 50 suns) using Fix Focus FF 3.5-HTC GmbH (Germany) instrument, ZnO seemed to be as reactive as TiO₂ because phenol was completely degraded with TiO₂ and ZnO in less than 10 min. For more argument, this might relate to absorption characteristic of ZnO in 300 to 400 nm region that aluminum reflector of the light source instrument reflected the solar irradiation below 400 nm.

To give more support to potential of ZnO, photocatalytic degradation of acid brown 14 using ZnO and TiO₂ was evaluated under sunlight irradiation between 9 a.m. and 2 p.m. (Sakthivel et al., 2003). From absorption spectra of ZnO and TiO₂, the study was found that the absorbance of ZnO was more than that of TiO₂ in the range from 350 to 470 nm. As a result, ZnO could perform as photocatalyst to complete mineralization of the dye within 360 min while TiO₂ required more time which is 420 min. Thus, this experiment assures the great activity of ZnO over TiO₂ under sunlight. Since the photochemistry of ZnO is generally similar to that of other photocatalysts if the proper condition is provided in the system such as the level energy of light (hv), ZnO alone is now being investigated for environmental application.

From the affirmation from various studies, there is a strong possibility that organic compounds can be decomposed by ZnO photocatalyst. Under UV irradiation wavelength range, pollutants such as *p*-nitrophenol (Wang Y. et al., 2008), 4-chlorophenol (Gaya et al., 2009), diazinon (Daneshvar et al., 2007), kraft black liquor (Villaseñor and Mansilla, 1996), methyl orange (Hong et al., 2009), acid yellow 23 (Behnajadi, Modirshahla, and Hamzavi, 2006), remazol red F3B (Akyol and

Bayramoğlu, 2005), and acid red 14 (Daneshvar et al., 2004) had been degraded as summarized in Table 2.2.

Table 2.2 Organic compounds and percentage of photocatalytic degradation under UV irradiation.

Organic compound	Light source	ZnO Preparation	Reactor condition	% Degradation	Reference
Remazol red F3B	6Wx6U V lamps	ZnO, Merck	ZnO = 1.5 g/L and 150 mL/L remazol red F3B = 300 mL	90% in 60 min	Akyol and Bayramoglu, 2005
Acid yellow 23	30W UV-C lamp	ZnO, Merck	ZnO = 750 mg/L and 40 mg/L acid yellow 23	50% in 90 min	Behnajadi et al., 2006
Acid red 14	30W Hg lamp	ZnO, commercial	ZnO = 160 mg/L and 20 mg/L acid red 14 = 50 mL	100% in 60 min	Daneshvar et al., 2004
Diazinon	30W UV-C Hg lamp	ZnO nanocrystalline, precipitation method	ZnO = 150 mg/L and 20 mg/L diazinon = 50 mL	80% in 80 min	Daneshvar et al., 2007
4-chlorophenol	6W UV lamp	ZnO, Merck	ZnO = 2 g and 50 mg/L 4-chlorophenol = 1000 mL	100% in 300 min	Gaya et al., 2009
Methyl orange	UV light	ZnO, precipitation method	ZnO = 1.5 g/L and 20 mg/L methyl orange = 50 mL	100% in 5 hrs	Hong et al., 2009
Kraft black liquor	UV Hg lamp	ZnO, Merck	ZnO = 1 g and 120 mg/L kraft black liquor = 50 mL	> 95% in 15 min	Villaseñor and Mansilla, 1996
<i>p</i> -nitrophenol	200W high pressure Hg lamp	ZnO rod-like and chrysanthemum-like nanostructure, hydrothermal treatment method	ZnO = 0.05 g and 50 mg/L <i>p</i> -nitrophenol = 100 mL	70% in 120 min for rod-like and 100% in 120 min for chrysanthemum-like nanostructure	Wang Y. et al., 2008

Due to the fact that ZnO has the slight high absorbance from 350-470 nm, ZnO also shows the photocatalytic degradation performance under visible light range condition (Sakthivel et al., 2003). It was reported that ZnO could degrade the organic compounds such as resorcinol (Pardeshi and Patil, 2009), acridine orange (Pare et al., 2008), phenol and methyl orange (Qiu et al., 2008), and orange II (Marto et al., 2009)

under visible light irradiation. Table 2.3 presents the photocatalytic degradation details.

Table 2.3 Organic compounds and percentage of photocatalytic degradation under visible light irradiation.

Organic compound	Light source	ZnO Preparation	Reactor condition	% Degradation	Reference
Orange II	ML-160W lamp	ZnO, Merck, immobilized on screen-printed on 20 cm x10 cm ceramic tiles	ZnO = 50 g/m ² ×5 tiles and 40 mg/L and 20 mg/L orange II = 2 L	72% in 12 hrs	Marto et al., 2009
Resorcinol	Sunlight	ZnO, Merck	ZnO = 250 mg and 100 mg/L resorcinol = 100 mL	92–100% in 7 hrs	Pardeshi and Patil, 2009
Acridine orange	500W Halogen lamp	ZnO, commercial	ZnO = 250 mg and 2.0x10 ⁻⁵ M acridine orange = 50 mL	100% in 180 min	Pare et al., 2008
Phenol	1W LED (light-emitting diode)	ZnO, Shanghai Caiyu Nanometer-technology	ZnO = 1 g/L and 10 mg/L phenol	40% in 2 hrs	Qiu et al., 2008
Methyl orange			ZnO = 1 g/L and 20 mg/L methyl orange	41.3% in 2 hrs	
Rhodamine B			ZnO = 1.5 g/L and 10 mg/L rhodamine B	100% in 2 hrs	

From literatures, they indicated that the conditions of reactors could affect ZnO performance. Initial concentration of pollutant, amount of catalyst loading, type and intensity of light source, design of reactor, type of pollutant and catalyst, and even pH and additives of solution are wholly concerned. Thus, results in Tables 2.2 and 2.3 present different abilities of ZnO on the photocatalytic degradation.

ZnO characteristics including the relative amounts of different components which are active species, physical and/or chemical promoters and supports, shape, size, pore volume and distribution, and surface area are largely dependent on the chosen preparation method. On synthesis process optimization, requisite properties such as

activity, selectivity, lifetime, regeneration ease, and toxicity are involved (Campanati, Fornasari, and Vaccari, 2003). In addition, not only the agreeable cost but also environmental issues are now marked on the catalyst preparation. Therefore, route for photocatalyst fabrication needs to be carefully selected. ZnO synthesized via chemical method had been reported by many works such as precipitation (Aimable et al., 2010; Kumbhakar et al., 2008; Li and Haneda, 2003; Liqiang et al., 2005; Shokuhfar et al., 2008; Sui et al., 2009; Tong et al., 2009), simple method (Maensiri et al., 2006a), sol-gel method (Kwon et al., 2002; Siddheswaran R. et al., 2006), gel combustion (Riahi-Noori et al., 2008), mixture pyrolysis (Li and Haneda, 2003; Zhang et al., 2007), Zn metal burning (Nagao et al., 1974), hydrolysis (Li and Haneda, 2003), and hydrothermal method (Wang L. et al., 2009).

2.3 ZnO with dopants

Catalyst is generally classified into two types according to preparation procedure (Campanati et al., 2003). The first is bulk catalysts which include precipitation and gelation route (sol-gel method), and the second is supported catalysts consisting of impregnation, ion-exchange, adsorption, and deposition-precipitation. For hydrothermal treatment, it is defined as the treatment process of catalyst at rather low temperature, lower than 300°C, under ageing in the presence of the mother liquor.

Currently, ZnO has high expectation for increasing utilization of visible light on photocatalytic degradation. Doping ZnO by transition metals is the one of interesting process to achieve the expectation. The transition metals can help to narrow band gap energy of ZnO by providing the empty orbital for electron transfer at the lower energy level if appropriate transition metal is selected. There are many ways to prepare the transition metal doped ZnO. To incorporate the transition metal in ZnO, sol-gel method seems to be predominant over precipitation because it permits better control of texture, composition, homogeneity, and structure properties of final solids (Campanati et al., 2003). With sol-gel method, Zn^{2+} ion and the ion of dopant are mixed together and then formed the complex. If the ionic radius of dopant is smaller than Zn^{2+} ion, dopant is probably resided within the structure of ZnO after calcination.

The study of doped ZnO structure still has issued rather few publications; however, there are some reports available. $\text{Zn}_{0.95}\text{Co}_{0.05}\text{O}$ was prepared starting by mixing ZnO and CoO in a stainless steel mold (Liu et al., 2008). The study of the local structure of Co-doped ZnO film found that X-ray diffraction (XRD) patterns of fabricated $\text{Zn}_{0.95}\text{Co}_{0.05}\text{O}$ showed the peak of wurtzite ZnO. It could be concluded that there was no trace of impurity phases in the structure. The X-ray absorption spectroscopy (XAS) spectra confirmed that no Co ions were located at the octahedron center but the Co ions dissolved into ZnO and substituted for Zn^{2+} ions in the valence of +2 states assuring from the X-ray absorption near edge structure (XANES) spectra. In addition, the extended X-ray absorption fine structure (EXAFS) data indicated that Cu was substitutionally incorporated onto Zn site in the study of Cu-doped ZnO by molecular beam epitaxy (MBE) technique (Fons et al., 2003).

In most part of ZnO doping, the studies are interested in general characteristics. For example, the optical measurement of Cr-doped ZnO presented that Cr was in the ZnO lattice and the microstructural studies illustrated a network of petal-like structure of the samples (Singh, Senthil Kumar, and Ramachandra Rao, 2008), the band gap energy of Al-doped ZnO exponentially decreased comparing to pure ZnO (Shan and Yu, 2004), and the Ce^{3+} doped ZnO nanorods could enhance photoluminescence (Cheng, Jiang, and Liu, 2008). Moreover, several researchers have investigated ZnO doping with metal such as In (Wang B. et al., 2007), Mn (Han, Mantas, and Senos, 2002; Sun et al., 2009 Ullah and Dutta, 2008), As, P, and N (Vaithianathan et al., 2006), Li (Ko et al., 2003), Au and Pt (Pawinrat et al., 2009), and La (Anandan et al., 2007a; Anandan et al., 2007b).

2.4 Simple chemical method

Polyvinylpyrrolidone has been used as an organic template for effortless preparing crystalline photocatalyst powders such as TiO_2 and ZnO, (Eskandari et al., 2009; Maensiri et al., 2006a; Maensiri et al., 2006b; Maensiri et al., 2006c; Phoka et al., 2009; Wang et al., 2003; Wei et al., 2009; Zheng et al., 2001). This template assists

the distribution of catalyst active sites and provides mesopore in the structure. It is finally removed through the calcination process at 500°C (Zheng et al., 2001). The amount of polyvinylpyrrolidone in the synthesis recipe affecting on TiO₂ formation was investigated (Wang et al., 2003). Using 30 wt% in the synthesis recipe was optimally found. Difference of polyvinylpyrrolidone loading in ZnO and metal doped ZnO synthesis provided the catalysts in nanoparticles and nanorods (Eskandari et al., 2009; Maensiri et al., 2006b; Maensiri et al., 2006c; Wei et al., 2009). Polyvinylpyrrolidone template possibly plays a good role on the synthesis. However, it is a polymeric compound producing from petrochemical, which still has some drawbacks such as high price, difficulty of dissolution, high calcinations temperature requirement generating of some toxic gases such as CO₂, CO, and NO_x (ACROS ORGANICS BVBA, 2008: online).

It is interesting to search for an alternative template through green chemistry. Starch, an agro-product, is available in large amount. It consists of two polysaccharides: amylose and amylopectin. Amylose has a mostly linear chain structure containing up to 3,000 glucose molecules while amylopectin is a large branched polymer. A few studies have reported that starch could be used on material preparation such as Fe₂O₃, and TiO₂ (Chunming et al., 2009; Iwasaki et al., 2004; Janardhanan et al., 2008; Shen et al., 2008). Like polyvinylpyrrolidone, some starch could provide the similar mesoporous structure. Janardhanan et al. (2008) found that synthesized Fe₂O₃ nanoparticles by starch template were easily achieved through heat treatment. The obtained particles contained high crystallinity assuring hematite XRD pattern. Iwasaki et al. (2004) used potato starch as sponge gel template to fabricate TiO₂. It was also found that the meso/macropore of TiO₂ was obtained depending on the ratio of TiO₂/potato starch in recipe. Chunming et al. (2009) used corn starch to prepare TiO₂ which also provided mesopore structure in the catalyst.

Using polymers and heat treatment, metal ions dissolved in solution can be then adhered on the polymer network leading to increase distribution and rearrange of the ions in the gel. It is a simple method that dopants can be added on catalyst during synthesis process. In this study, cerium and copper are selected as dopants. As known,

cerium presents defect of oxygen vacancies which allows oxygen to move around in the crystal. As a result, cerium oxide can reduce and oxidize molecules or be co-catalyst at catalyst surface. Ling et al. (2008) reported that the Ce^{3+} on TiO_2 showed good photocatalytic activity. One main reason was the destruction of charge balance in the structure when titanium ions were replaced by cerium ions into the lattice. Hydroxyl ions would adsorb on the surface in order to maintain charge equilibrium which eventually contributed to generate electron hole pairs and increased the photocatalytic activity by 50-60%. Copper (II) oxide is used as a dopant because it has narrow band gap of 1.2 eV. The copper was considered to prevent the electron-hole recombination (Xin et al., 2008) and lower the band gap energy of catalyst (Navas et al., 2011; Roguska et al., 2010; Vidyasagar et al., 2011).

To search for alternative template, sticky rice starch bioorganic template is applied to synthesize ZnO, Ce-ZnO, and Cu-ZnO photocatalysts. Their characteristics are compared with polyvinylpyrrolidone template usage on the same basis. In addition, an application of prepared materials has been tested over photocatalytic degradation of atrazine under visible light irradiation.

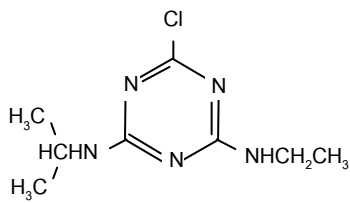
2.5 Atrazine general information

Atrazine is a synthetic herbicide that is used to kill broadleaf weeds in agricultural and roadway application (United States Environmental Protection Agency [U.S. EPA.], 2007: online). It was firstly introduced in 1958 (Rector et al., 2003). For release patterns, atrazine may be released to environment through effluents from manufacturing facilities and through its use as herbicide. Atrazine is the second most frequently detected pesticide in EPA's National Survey of Pesticides in Drinking Water Well. The database from survey indicated numerous detections of atrazine at concentration above 3 ppb of the maximum contaminant level (MCL) in groundwater in several states including Delaware, Illinois, Indiana, Iowa, Kansas, Michigan, Minnesota, Missouri, Nebraska, and New York (U.S. EPA., 2003: online). Atrazine was applied more than 60 million pounds active ingredient over the country (Thelin

and Gianessi, 2000: online). The highest amount of use was 0.26 to 2.11 pounds per hectare.

For environmental fate, atrazine is not very water soluble but it is expected to have a high potential for groundwater contamination. It persists in surface and groundwater with a half-life of longer than 6 months. Atrazine has a slight tendency to bioaccumulate in some aquatic organism, including invertebrates and fish. In soil, atrazine generally persists in the range of 14 to 109 days. It is expected to maintain a high to medium mobility class in soil and more readily adsorbed on muck or clay soils with high organic matter content. No atrazine is normally found below the first foot of soil even after years of continuous use. The leaching potential of atrazine is rated as large (highest rating). For volatilization, atrazine is not environment significant. However, it can be found in the particulate and vapor phases of air following application, and can be transported up to 186 miles from site of application. Properties of atrazine are presented in Table 2.4.

Table 2.4 Physical and chemical properties of atrazine (Chung and Gu, 2009; McGlamery and Slife, 1966: online; U.S. EPA., 2003: online; U.S. EPA., 2007: online).

Chemical name	Atrazine
IUPAC name	2-chloro-4-ethylamino-6-isopropylamino-1,3,5-triazine
Chemical structure	
Chemical formula	$C_8H_{14}ClN_5$
Appearance	White crystalline solid
Odor	Odorless
Molecular weight	215.7 g/mol
Density at 20°C	1.187 g/cm ³

Melting point	171–174°C
Solubility at 20°C in water	30 mg/L
Vapor pressure at 20°C	2.78×10^{-7} mm-Hg
Henry's constant	2.63×10^{-9} atm-m ³ /mol
Log Kow at 25°C	2.5
Koc	122 µg/g
Log BCF	0.3–2.0
pKa at 22°C in water	1.68
U.S. EPA chronic dietary reference dose (RfD)	0.018 mg/kg/day
U.S. EPA acute dietary reference dose (RfD) for females 13-50 years old	0.1 mg/kg/day

Several techniques on atrazine removal have been reported such as biodegradation adding organic fertilizer, activated carbon adsorption (Heepngoan et al., 2008), polycation-clay composites adsorption (Zadaka et al., 2009), radiolytic degradation (Basfar et al., 2009), electrochemical reduction (Guse et al., 2009), and other removal techniques. They were considered to eliminate atrazine in the environment.

However, some techniques still have limitations which are as follows: biodegradation; it takes a long time, and very high concentration of pollutants may be non-degraded by microorganisms since they might be unable to survive in that condition, adsorption; this technique only moves pollutants from one phase to another phase which incomplete mineralization of atrazine, radiolytic degradation; high concentration of atrazine is unable to be degraded, this technique is likely expensive, and ⁶⁰Co is used as a source of irradiation which may hazard to human and environment, and electrochemical reduction; it seems to depend on electricity for operation which obstructs the reduction of energy consuming.

Because of these technical and economic limitations, advanced oxidation processes (AOPs); for example, O₃/UV, H₂O₂/UV, O₃/H₂O₂, TiO₂/UV, and others, are more interesting to investigate. Photocatalytic reaction such as TiO₂/UV is widely applied for destruction of organic pollutants since photocatalyst is low cost, non-toxic, and

has long-term structural stability, abundance, high oxidation rate, and pollutant mineralization (Ling et al., 2008).

Atrazine has been reported to be degraded by photocatalytic reaction in many studies. Using TiO_2 , 98% of atrazine was rapidly removed in a large modular flow through system under sunlight (Minero et al., 1996). Alkyl substituted group in atrazine was incompletely mineralized, and intermediate concentration was increased. With the presence of $\text{Na}_2\text{S}_2\text{O}_8$, the cyanuric acid was found as the stable final product for further treatment. For other studies, photocatalytic degradation of atrazine has been investigated using a variety of catalysts (Krýsová et al., 2003; Lackhoff and Niessner, 2002; Liu et al., 2009; McMurray et al., 2006; Parra et al., 2004). Under artificial sunlight, a metal halide high-pressure lamp, TiO_2 and ZnO provided the fast photocatalytic degradation of atrazine with first-order kinetics (Lackhoff and Niessner, 2002). Cyanuric acid was the last product when reaction mechanism had been examined (Krýsová et al., 2003; Lackhoff and Niessner, 2002; McMurray et al., 2006; Parra et al., 2004). Under solar irradiation for 30 min, 60% of atrazine was removed by using S-doped TiO_2 corresponding to pseudo first order model (Liu et al., 2009).

CHAPTER III

MATERIALS AND METHODS

There are 4 main experimental steps on this study consisting of catalyst preparation, catalyst characterization, atrazine photocatalytic degradation, and atrazine photocatalytic degradation pathway evaluation as shown in Table 3.1. On catalyst preparation part, simple chemical method and MCT were carried out. Then, the catalyst was characterized by several techniques which are TG-DTA, FT-IR, XRD, XANES, UV-vis-DR, BET, SEM, and zeta-potentiometry. On atrazine photocatalytic degradation section, HPLC was used to analyze atrazine concentration with respect to operational parameter study and kinetics. Finally, atrazine photocatalytic degradation pathway evaluation was conducted using TOC and LC-MS.

Table 3.1 Overall study procedure.

Catalyst preparation	Catalyst characterization	Atrazine photocatalytic degradation	Atrazine photocatalytic degradation pathway evaluation
1) Simple chemical method 2) MCT - ZnO - Ce-ZnO - Cu-ZnO - Ag-Ce-ZnO - Fe-Ce-ZnO - Cu-Ce-ZnO	1) TG-DTA 2) FT-IR 3) XRD 4) XANES 5) UV-vis-DR 6) BET 7) SEM 8) Zeta potentiometry	1) HPLC - Parameter study - Kinetics	1) TOC 2) LC-MS

3.1 Chemicals

Chemical products in this study were used as received.

- 1) Zinc oxide, ZnO (Carlo Erba Reagents, 99.0%)
- 2) Zinc(II) nitrate hexahydrate, $\text{Zn}(\text{NO}_3)_2 \cdot 6\text{H}_2\text{O}$ (Acros Organics, 98%)
- 3) Cerium(III) nitrate hexahydrate, $\text{Ce}(\text{NO}_3)_3 \cdot 6\text{H}_2\text{O}$ (Acros Organics, 99.5%)
- 4) Copper(II) sulphate pentahydrate, $\text{CuSO}_4 \cdot 5\text{H}_2\text{O}$ (Carlo Erba Reagents, 98–102%)
- 5) Polyvinylpyrrolidone, $(\text{C}_6\text{H}_9\text{NO})_n$ (Acros Organics, K85–95, M.W. = 1,300.000)
- 6) Sticky rice starch (Erawan Brand, Thailand)
- 7) Activated alumina defluoridizer, Al_2O_3 (Pingxiang Huihua Packing, size = 0.5–1.2 mm of diameter)
- 8) Atrazine, $\text{C}_8\text{H}_{14}\text{ClN}_5$ (Fluka Analytical, 97.2%)
- 9) Reactive Red 120, RR120 (Ever Light Chemical Industry)
- 10) Sodium sulphate anhydrous, Na_2SO_4 (Analyticals Carlo Erba, 99.5%)
- 11) Sodium chloride, NaCl (Merck, 99.5%)
- 12) Sodium carbonate, Na_2CO_3 (Carlo Erba Reagents, 99.5%)
- 13) Sodium hydrogen carbonate, NaHCO_3 (Carlo Erba Reagents, 99.7%)
- 14) Disodium hydrogen phosphate, Na_2HPO_4 (Carlo Erba Reagents, 99%)
- 15) Silver nitrate, AgNO_3 (Carlo Erba Reagents, 99.8%)
- 16) Iron(III) nitrate nonahydrate, $\text{Fe}(\text{NO}_3)_3 \cdot 9\text{H}_2\text{O}$ (Merck, 99.0–101.0%)
- 17) Humic acid (Sigma Aldrich Chemistry)
- 18) Methanol HPLC, CH_3OH (RCI Labscan Limited, 99.99%)
- 19) Distilled water and deionized water
- 20) Sodium hydroxide, NaOH (Carlo Erba Reagents, 97.0%)
- 21) Nitric acid, HNO_3 (Carlo Erba Reagents, 65%)
- 22) Hydrochloric acid, HCl (Carlo Erba Reagents, 37%)

And additional chemicals for operational parameter study.

3.2 Catalyst preparation

3.2.1 Mechanical coating technique for ZnO

ZnO coated on Al_2O_3 bead was prepared using MCT for catalyst immobilized aspect. In the procedure, 40 g of commercial ZnO powder and 60 g of Al_2O_3 bead were introduced in a stainless steel pot and milled for 15 hr at 300 rpm using a planetary ball mill. After mechanical coating, catalyst bead was separated from the remained powder by sieving. Using a heating rate of $2^\circ\text{C}/\text{min}$, the catalyst bead was then calcined for 24 hr at 400, 450, 500, 550, 600, 650, 700°C , named as ZnO_400, ZnO_450, ZnO_500, ZnO_550, ZnO_600, ZnO_650, ZnO_700, respectively. The as-synthesized catalyst was denoted as ZnO_room temp.

3.2.2 Simple chemical method using sticky rice starch and polyvinylpyrrolidone

Throughout the research, sticky rice starch and polyvinylpyrrolidone were used as templates. ZnO with sticky rice starch template and ZnO with polyvinylpyrrolidone template were designated as ZnO (S) and ZnO (P), respectively. The effect of cerium doped ZnO on both templates was studied with cerium molar ratios of 0.02 and 0.1 which were denoted as 0.02Ce-ZnO (S), 0.02Ce-ZnO (P), 0.1Ce-ZnO (S), and 0.1Ce-ZnO (P), respectively. The effect of copper doped ZnO on only sticky rice starch template with copper molar ratios of 0.02 and 0.1 was also denoted as 0.02Cu-ZnO (S) and 0.1Ce-ZnO (S), respectively.

Zinc(II) nitrate hexahydrate, cerium(III) nitrate hexahydrate, sticky rice starch, polyvinylpyrrolidone, and distilled water were used as starting materials. Mostly, catalysts used in catalyst screening and preliminary study in 4.1, the weight ratio of zinc(II) nitrate hexahydrate to the template was fixed at 1: 2. This ratio was consistent with the studies of Maensiri et al. (2006a) and Maensiri et al. (2006b). In the part of photocatalytic degradation of atrazine in 4.2, the template was only focused on the sticky rice starch, and the weight ratios of zinc(II) nitrate hexahydrate to the template were 5:1 and 10:1.

The template was first added into 500 mL of water and blended under vigorous stirring on a hot plate stirrer at 80°C for 30 min to obtain a well dissolved solution until resulting in gel formation. Zinc(II) nitrate hexahydrate was dissolved separately in 50 mL of water and was eventually added into the gel. The mixture was stirred at 80°C for 30 min and subsequently dried in an oven at 100°C for approximately 48 hr. Based on a literature review and our TG-DTA results, the dried precursor was calcined at 550°C for 3 hr at a heating rate of 2°C/min. The calcined precursor was ground and then passed through a sieve in order to separate large agglomerates. White powder was obtained.

For Ce-ZnO powder synthesis, 0.02 and 0.1 molar ratios of cerium(III) nitrate and zinc(II) nitrate solutions were prepared. The process was then followed by the ZnO (S) and ZnO (P) preparation procedure. The Ce-ZnO catalysts prepared by both templates appeared in yellow powder. For Cu-ZnO powder synthesis, 0.02 and 0.1 molar ratios of copper(II) sulfate to zinc(II) nitrate were prepared by using only sticky rice starch as the template. The process was similar to ZnO (S) preparation procedure. The grey powder was the feature of Cu-ZnO (S) catalyst.

3.2.3 Mechanical coating technique for prepared catalysts

The obtained catalysts were immobilized via MCT. The catalyst powder (40 wt%) and Al₂O₃ bead (60 wt%) were measured. The mixture was introduced to the stainless steel pot. Then, under the similar operational condition, the procedure of MCT for ZnO in 3.2.1 was applied for immobilizing the prepared catalyst.

3.3 Catalyst characterization

3.3.1 Thermogravimetric property

The decomposition temperature along with the material preparation was determined by thermogravimetry and differential thermal analysis (TG-DTA) (SHIMADZU TGA-50 and DTA-50). The dried precursor was placed in a platinum pan, and the test was carried out under air atmosphere with the flow rate of 20

mL/min at a constant ramping rate of 5°C/min from 30 to 800°C for ZnO_room temp and 30 to 600°C for the as-synthesized Ce-ZnO. The weight change and the thermal of the sample were plotted as a function of temperature.

3.3.2 Organic and inorganic identities

To measure chemical functional groups of powders, Mid-IR Spectra with a spectral resolution of 4 cm⁻¹ were collected on a Fourier transform infrared (FT-IR) spectrometer (Bruker Tensor 27) using mirror single reflection with germanium on ATR (Attenuated Total Reflectance) crystal. The IR spectrometer was equipped with the global source, a KBr beam splitter, and a liquid nitrogen cooled mercury cadmium telluride (MCT) detector.

3.3.3 Structure and crystalline size

The crystal phases of the samples were analyzed by X-ray diffractometer (XRD) (Bruker D8 powder) with a Cu K α radiation source ($\lambda = 1.5406 \text{ \AA}$). Scan range of 2θ , angle range of 20 to 80°, step size of 0.04°, and time step of 1.0 sec were set to assess structures of the matrix. The peak of ZnO was selected to evaluate the crystalline size with Debye-Scherrer equation (Wang et al., 2008; Wang et al., 2009).

$$D = k\lambda/\beta\cos\theta \quad (3.1)$$

where D = the crystalline size (nm)

k = the Scherrer constant (0.89)

λ = the X-ray wavelength (0.15406 nm)

β = the full width at half maximum of diffraction peak

θ = the half diffraction angle (radian)

3.3.4 Oxidation state

X-ray absorption near edge structure (XANES) was performed at Beamline-8 of Synchrotron Light Research Institute (SLRI), Thailand. This technique was employed to determine the oxidation states by indentifying a sample as a fingerprint.

Catalyst powder was pressed into a frame covered by polyimide tape and mounted onto the sample holder. A double Ge (220) crystal monochromator was employed for selection of photon energy. The data were obtained at room temperature in fluorescent mode (Lytle). The photon energy was scanned from -30 eV below the edge to 80 eV above the edge with scan step 0.2 eV. The XANES spectra were analyzed using the conventional procedure by using Athena program. After background correction, the XANES spectra were normalized by the edge height and compared with standard references. Standard materials were Zn foil, commercial ZnO, Ce metal, $\text{Ce}(\text{NO}_3)_3 \cdot 6\text{H}_2\text{O}$, and CeO_2 .

3.3.5 Light absorption capacity

The UV-vis diffusive reflectance absorption spectra (UV-vis-DR) of catalysts were measured by UV-vis spectrophotometer (HITACHI U-3501) with dry-pressed disk samples attached to an integrating sphere assembly. The light sources used were deuterium lamp and halogen lamp. The spectra were recorded from 300 to 800 nm, and pure powder BaSO_4 was used as a reference. The indirect band gap energy (E_g) of each sample was calculated by fitting the absorption data to the direct transition equation (Wang et al., 2005).

$$\alpha = B_d(h\nu - E_g)^{1/2}/h\nu \quad (3.2)$$

where α = the optical absorption coefficient

$h\nu$ = the photon energy (eV)

B_d = the absorption constant for direct transition

E_g = the band gap energy (eV)

3.3.6 Specific surface area

Brunauer-Emmett-Teller (BET) surface area and pore size distribution of catalysts were determined by nitrogen adsorption (Quantachrome instruments Autosorb-1) with common adsorbate N_2 at -196°C . Prior to the measurement, sample was degassed at 150°C for several hours to remove humidity, gasses, and volatile

adsorbents adsorbed on the surface. Surface area of samples was calculated from adsorption data using the standard BET method.

3.3.7 Morphology

Morphology of the catalysts was examined by scanning electron microscopes (SEM) (INCA and JEOL JSM-6400) with magnification power between 50 and 10000 times. Catalysts were scattered on an adhesive tape on a brass bar and then coated with gold and finally transferred into the chamber of microscope for inspecting. The accelerating voltage was operated at 15 kV. The SEM images were print out using the video graphic printer (Sony UP-897MD).

3.3.8 Surface charge

Zeta-potential (Zeta-Meter 3.0+ and Zeta microscope module) was investigated in order to determine electrophoretic properties and isoelectric point (IEP) of catalysts. Before measurement, catalyst (5.0 mg) was suspended in 20 mL of distilled water that had been adjusted pH from pH 2 to pH 12 by 0.1 M HCl and 0.1 M NaOH. An average zeta-potential of 10-time-measurement of sample at each pH value was reported.

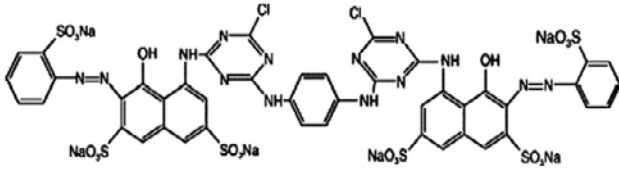
3.4 Catalyst activity test

3.4.1 Immobilization concernment

Photocatalytic degradation of RR120, azo dye, in batch reactor was investigated to study the effect of immobilization. The RR120 properties are shown in Table 3.2. The procedure of this experiment conformed to the studies of Bajamundi et al. (2011) and Yoshida et al. (2009). The RR120 solution (20 mg/L, 7.0 mL) was added to each cylindrical glass cell (diameter = 3.00 cm and height = 6.00 cm). The ZnO₅₅₀ or 0.1Ce-ZnO (P) 1:2 bead (0.3000 g) was then introduced to each cell and uniformly expanded at the bottom of the cell. The cells were closed with rubber stoppers to prevent evaporation of water and punctured with hypodermic syringe to allow the flow of air.

Without stirring the solution, the cells were immediately irradiated under two black light fluorescent lamps (Toshiba 18W) as UV light and one day light lamp (Philips E27 100W) as visible light. The intensity of light source was checked by solarimeter, 380 to 740 nm, (Kimo SL100, France) and UV-meter, 280 to 400 nm, (UV-meter model 5.0 digital, USA). The intensity of the UV light source measured by using UV-meter was 1.5 mW/cm^2 and measured by using solarimeter was 0 W/m^2 . Conversely, the intensity of the visible light source measured by using UV-meter was 0 mW/cm^2 and measured by using solarimeter was 177 W/m^2 . The orientation of the lamps was set under the cells with respect to the RR120 solution and the ZnO_550. The distance between the light source and the cells was 25 cm. The schematic of the reactor is represented in Figure 3.1. When timing approached, the samples were immediately collected by decantation to separate the RR120 and ZnO_550. The RR120 concentration was analyzed by UV-vis spectrometer (JASCO V-630). The experimental runs were performed in two replicates.

Table 3.2 Chemical structure and properties of RR120 (Cho and Zho, 2007).

Chemical structure	
Molecular formula	$\text{C}_{44}\text{H}_{24}\text{Cl}_2\text{N}_{14}\text{Na}_6\text{O}_{20}\text{S}_6$
Molecular weight	1470 g/mol
Water solubility	70 g/L
λ_{max} (nm)	536
Class	Diazo (–N=N– bond)

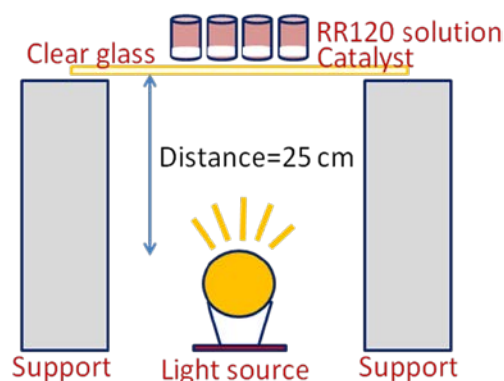


Figure 3.1 Photocatalytic batch reactor setup for the immobilization concernment study.

3.4.2 Preparation route concernment

Atrazine was used as an organic pollutant probe. Distilled water was used to prepare atrazine solution. Both HNO_3 and NaOH with the same concentration of 0.1 M were used for adjusting the pH of the solution. Photocatalytic reactions were carried out in batch reactors with the cooling water bath maintained at a temperature of $25 \pm 1^\circ\text{C}$. The catalyst bead (2.1428 g) was uniformly distributed at the bottom of beaker. Atrazine solution (150 mL) was then added to the container. After adsorption for 30 min, the reaction was immediately performed with five tungsten lamps (Philips E27 100W) under a constant paddle speed in the solution above the photocatalyst layer 2 cm. The orientation of the lamp was set perpendicular to the bottle. The distance between the light source and the bottle was 10 cm.

The intensity of the light source was periodically checked by solarimeter (Kimo SL100, France) and UV-meter (UV-meter model 5.0 digital, USA). The average light intensity in this experiment was 445.12 W/m^2 measured by using solarimeter and 0 mW/cm^2 measured by using UV-meter. The samples were collected by using pipettes at the second hour of the irradiation time. The experimental runs were performed in two replicates. The photocatalytic activity of this experiment was monitored by HPLC (Agilent Technologies) using Hypersil C18 ODS ($4.0 \times 125 \text{ mm}$, $5 \mu\text{m}$) column at 40°C and a wavelength of 254 nm (Fu, 2009). The mobile phases

were 55% methanol and 45% water with a flow rate of 1.0 mL/min. The injection volume was 10 μ L. The schematic of the reactor is represented in Figures 3.2 and 3.3.

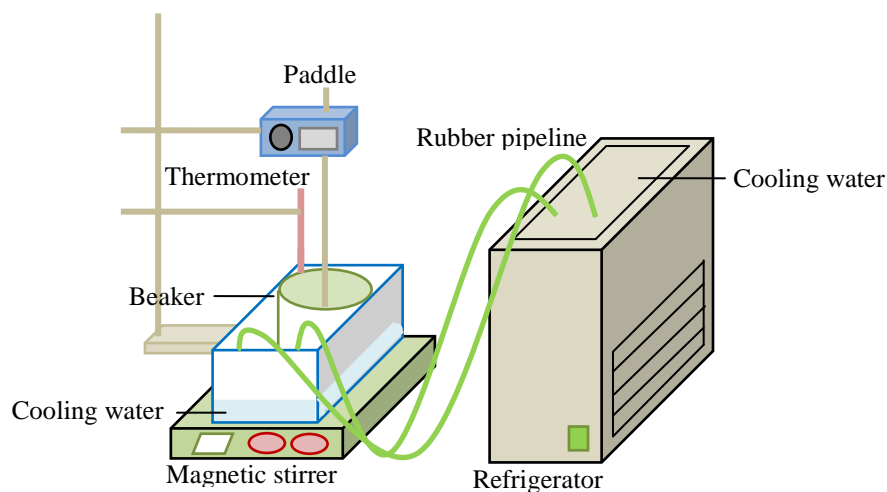


Figure 3.2 Photocatalytic batch reactor for the preparation route concernment study in 3.4.2 and the photocatalytic degradation of atrazine in 3.5.

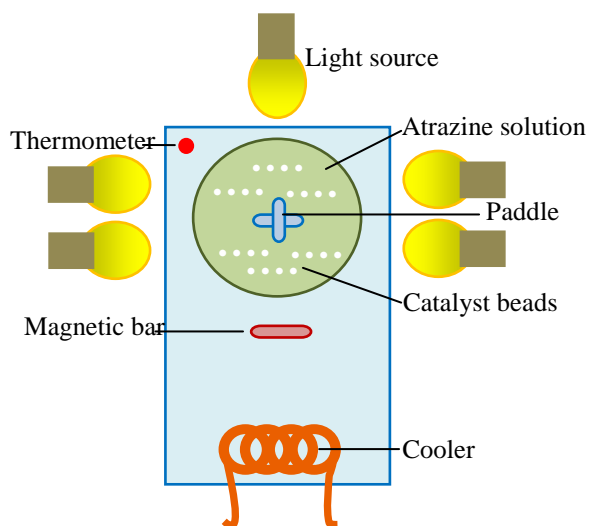


Figure 3.3 Top view of photocatalytic batch reactor for the preparation route concernment study in 3.4.2 and the photocatalytic degradation of atrazine in 3.5.

3.5 Photocatalytic degradation of atrazine

Deionized water was taken to prepare atrazine solution. Photocatalytic reaction was carried out in a batch reactor with cooling water bath control at temperature of $25\pm 1^\circ\text{C}$. In case of catalyst bead, certain amount of catalyst was uniformly expanded at the bottom of beaker. For catalyst powder case, the powder was stirred in slurry form. The atrazine solution (100 mL) was then added to beaker (1000 mL). After 30 min of adsorption, the reaction was immediately performed with five tungsten lamps (Philips E27 100W) under constant speed of paddle in the solution above the photocatalyst layer 1 cm. The orientation of the lamp was set perpendicular to the beaker. The distance between the light source and the beaker was 5 cm.

The intensity of light source was periodically checked using solarimeter (Kimo SL100, France) and UV-meter (UV-meter model 5.0 digital, USA). The average light intensity in this experiment was 607.12 W/m^2 measured by using solarimeter and 0 mW/cm^2 measured by using UV-meter. The samples were collected using syringe and syringe filter (in case of catalyst powder). The experimental runs were performed in three replicates. The studied parameters investigated in this study are shown in Table 3.3. The schematic of the reactor is represented in Figures 3.2 and 3.3.

Table 3.3 Studied parameters of atrazine photocatalytic degradation.

Studied parameter	Independent variable	Control variable
Transition metal dopants and mole ratio of doping	Dopants = cerium and copper Mole ratio = 0.02 and 0.1	Catalyst weight = 0.3 g (powder) Atrazine concentration = 5 mg/L pH = no adjusted
Catalyst loading	Catalyst weight = 0.1 – 0.9 g (powder) and 1.0 – 7.5 g (bead)	Catalyst = ZnO Atrazine concentration = 5 mg/L pH = no adjusted
pH	pH = 4.0, 5.6 (no adjusted pH), 7.0, and 8.5	Catalyst = ZnO Catalyst weight = 0.1 g (powder) and 2.5 g (bead) Atrazine concentration = 5 mg/L
Initial concentration of atrazine	Atrazine concentration = 1.0 – 10.0 mg/L	Catalyst = ZnO Catalyst weight = 0.1 g (powder) and 2.5 g (bead) pH = no adjusted
surface passivation	Catalyst = ZnO_550, 0.02Ce-ZnO (S) 5:1, and 0.02Cu-ZnO (S) 5:1	Catalyst weight = 2.50 g (bead) Atrazine concentration = 5 mg/L pH = no adjusted
anions	Additives = Na ₂ SO ₄ , NaCl, Na ₂ CO ₃ , NaHCO ₃ , and Na ₂ HPO ₄ Concentration of additive = 0.002, 0.006, and 0.01 M	Catalyst = ZnO_550 (bead) Catalysts weight = 2.50 g Atrazine concentration = 5 mg/L pH = no adjusted

Studied parameter	Independent variable	Control variable
Other metal dopants on ZnO	Catalyst = 0.005Cu-0.005Ce-ZnO, 0.005Fe-0.005Ce-ZnO, and 0.005Ag-0.005Ce-ZnO	Catalyst weight = 0.1000 g (powder) Atrazine concentration = 5 mg/L pH = no adjusted
Natural organic matter	Humic acid = 0.0, 1.0, 3.0, 5.0 and 50.0 mg/L	Catalyst = 0.02Ce-ZnO (S) 5:1 and 0.005Ag-0.005Ce-ZnO Catalyst weight = 2.50 g (bead) Atrazine concentration = 5 mg/L pH = no adjusted
Catalyst reliability	Catalyst reuse (without regeneration) = 5 times	Catalyst = ZnO_550 Catalyst weight = 2.50 g (bead) Atrazine concentration = 5 mg/L pH = no adjusted

3.6 Analytical technique

3.6.1 High performance liquid chromatography (HPLC)

The concentration of atrazine from the experiment in 3.5 was analyzed by high performance liquid chromatography (HPLC) (Agilent Technologies) using Hypersil C18 ODS (4.0 × 125 mm, 5 μm) column. In the case of catalyst powders, the sample was filtered with 0.45 μm syringe filter PTFE to remove all solid particles before analysis. The diode-array detector (HPLC-DAD 1200 series detector) and pump and controller (1100 series) were used. The HPLC conditions for atrazine analysis reported by Fu (2009) were used. The UV detector was set at 254 nm for the maximum absorption of atrazine. The mobile phases were 55% methanol and 45%

water with flow rate of 1.0 mL/min. The mobile phases were filtered and degassed for 60 min before loading to HPLC. The column temperature was 40°C. The injection volume was 80 µL. The retention time was kept at 10 min. The atrazine concentration was calculated using the standard calibration curve.

3.6.2 Total organic carbon (TOC)

Total organic carbon (TOC) was determined by TOC Analyzer (Shimadzu TOC-V CPH) with autosampler (Shimadzu ASI-V) based on high temperature catalytic combustion by CO₂ quantification by a non-dispersive IR detector. Injection volume was 50 µL, and the retention time was 2 min.

3.6.3 Liquid chromatography-mass spectrometer (LC-MS)

The intermediates products formed during the photocatalytic degradation of atrazine was analyzed by Liquid chromatography mass spectrometer (LC-MS) (Waters 3100 mass detector equipped with Waters 2695 separation module). The samples were infused into the mass spectrometer at a flow rate of 0.4 mL/min with injection volume of 5.00 µL. The run time was 15 min. The heated capillary temperature was 120°C, and the spray voltage set to 3.7 kV. The electrospray was in positive mode. The chromatographic conditions were the same as those described for atrazine concentration analysis.

CHAPTER IV

RESULTS AND DISCUSSION

All lab-scale experimental results and their discussion are divided into three main parts: 1) catalyst screening and preliminary study; 2) photocatalytic degradation of atrazine; and 3) evaluation of photocatalytic degradation pathway of atrazine. Before investigating further, the content in each part is shown in Table 4.1 for the ease in tracking the steps of the study.

Table 4.1 Contents of the experimental results and discussion.

1) Catalyst screening and preliminary study	
Catalyst characteristics	<ul style="list-style-type: none"> - Thermogravimetric property - Organic and inorganic identities - Structure and crystalline size - Oxidation state - Light absorption capacity - Specific surface area - Morphology - Surface charge
Catalyst activity test	<ul style="list-style-type: none"> - Immobilization concernment - Preparation route concernment
2) Photocatalytic degradation of atrazine	
Photolysis and adsorption Effect of transition metal dopants and molar ratio of doping Effect of catalyst loading Effect of pH Effect of atrazine initial concentration Surface passivation Effect of ionic strength Effect of anions Other metal dopants on ZnO Competitive effect from natural organic matter Langmuir-Hinshelwood-Hougen and Watson (LHHW) kinetics Catalyst reliability	
3) Evaluation of photocatalytic degradation pathway of atrazine	

4.1 Catalyst screening and preliminary study

There are two parts involved in this topic. The first is catalyst characteristics, and the second is catalyst activity test. The catalysts used in these two parts are divided into two forms. One is the bead form which was prepared by using MCT. Another one is the powder form which was prepared by using simple chemical method.

4.1.1 Catalyst characteristics

In catalyst characterization, the instruments including TG-DTA, FT-IR, FT-Raman, XRD, XANES, UV-vis-DR, BET surface area analyzer, SEM, and zeta-potentiometer were used to be the key to understand the properties and find the optimal conditions of the catalysts. There are many parameters which influence the catalyst's properties such as type of catalyst, the method of catalyst preparation, modification of catalyst, pressure and temperature of catalyst treatment, and other parameters (Campanati et al., 2003). The temperature of calcination can affect the catalyst transformation. Before calcination, the as-synthesized precursors were analyzed with the TG-DTA. The temperature range from the TG-DTA analysis could be the information for the further step of catalyst preparation and characterization. The measurement was focused on two types of samples in this study. The first was the commercial ZnO coated on Al₂O₃ beads varied by the calcination temperature. The second was the prepared ZnO and metal doped ZnO via the simple chemical method using polyvinylpyrrolidone and sticky rice starch as the templates in the weight ratio of 1 g Zn(NO₃)₂•6H₂O: 2 g template. Both were presented as follows.

4.1.1.1 Thermogravimetric property

Thermogravimetric analysis is widely used for determining the organic and inorganic content of various materials. The high precision measurement of weight loss or gain with increasing temperature under inert or reactive atmospheres is its fundamental. The weight change of the material together with energy released to the system by increasing temperature mean to the existence of physical (crystallization and phase transformation) and/or chemical (oxidation, reduction, and reaction) processes (Soulтанidis and Barron, 2009: online). With the thermogravimetric property analysis using TG-DTA, the ZnO coated on Al₂O₃ beads fabricated by using

MCT, noted as ZnO_room temp, was analyzed in order to find the range of the calcination temperature. In Figure 4.1, the TG showed the weight loss of ZnO_room temp when temperature was increased from 30 to 800°C. The TG curve exhibited two weight loss steps. Since the raw materials are the commercial ZnO powder and Al₂O₃ beads which maintain their stabilities in this temperature range (Carlo Erba Reagents, 2011: online; DESICCA CHEMICALS, 2012: online), the first step between 30 and 120°C had weight loss of only 9.00%. This step probably related to the loss of moisture. The weight loss of 9.16% between 120 and 800°C presented at the second step due to combustion of materials assembling in ZnO and Al₂O₃. In the DTA curve, the endothermic peaks showed at 119.1 and 455.4°C. This evidence could estimate the appropriate calcination temperature that had to be higher than 455.4°C. Thus, the temperature range of 400 to 700°C was considered. Similarly, the calcination temperature in air was varied at 300 to 700°C (573, 623, 673, 723, 773, 823, and 973 K) for 20 hr by Yoshida et al. (2009) who firstly fabricated the composite film of TiO₂ on Al₂O₃ ball via MCT.

Furthermore, the thermal property of the as-synthesized precursors of the prepared ZnO powders and metal doped ZnO powders was measured. By calcination, the organic templates, polyvinylpyrrolidone or sticky rice starch, used in catalyst preparation would be removed through oxidation, and the metal oxide could be formed through crystallization (Iwasaki et al., 2004; Janardhanan et al., 2008; Maensiri et al., 2006b; Maensiri et al., 2006c; Phoka et al, 2009; Wang et al., 2003).

In Figures 4.2 and 4.3, the TG curves presented two weight loss steps. The first step was observed from 30 to 100°C and contributed weight losses of 12.7 and 2.7% for ZnO (S) and 0.1Ce-ZnO (S), respectively, corresponding to the portion of the water content in the synthesis recipe. The second part was observed from 100 to 400°C and contributed 71.3 and 79.8% major weight losses attributing to the decomposition of nitrate and starch which associated with pure starch as shown in Figure 4.4. Under air atmosphere, the major weight loss of the pure sticky rice starch was 60% at 300°C which associated with the TG results of the corn starch (Aggarwal, Dollimore, and Heon, 1997; Beninca et al., 2008). After the initial mass loss, the

sticky rice starch was completely burnt at around 500°C. On the other hand, material synthesized through polyvinylpyrrolidone template contributed major weight losses of 83.8 and 84.2% as shown in Figures 4.5 and 4.6, respectively, around 100 to 500°C. This part was mainly assigned to the combustion of polyvinylpyrrolidone which related to the pure polyvinylpyrrolidone in Figure 4.7. The major weight loss of the pure polyvinylpyrrolidone was 80% at 430°C. The polyvinylpyrrolidone was completely combusted at 550°C which was slight higher than the temperature required for the sticky rice starch. The losses of templates were exothermic due to gaseous combustion. Only 7.3 and 3.4% as shown in Figures 4.2 and 4.3, respectively, of the weight losses were found in the low temperature region of 30 to 100°C for water evaporation. However, the materials were eventually obtained in a similar weight from using both templates.

Considering the DTA curves of ZnO (S) and Ce-ZnO (S), the exothermic peak (160 to 170°C) was observed through the steep decrease of weight due to the evaporation of water and the combustion of starch. These DTA curves were moved ahead against temperature, suggesting that the drying of water content was accompanied by a carbonization and combustion of starch causing the release of energy which assisted in calcination process (Bicudo et al., 2009). In addition, the small exothermic peaks of ZnO formation and CeO₂ crystallization were at 390 and 420°C. The DTA curves of ZnO (P) and Ce-ZnO (P) were different from those of ZnO (S) and Ce-ZnO (S). They exhibited three exothermic peaks at 260, 450, and 510°C. The results in this study were in agreement with the previous report by Maensiri et al. (2006c) for ZnO formation at 500°C and Phoka et al. (2009) for CeO₂ crystallization at 460°C via the simple chemical method using polyvinylpyrrolidone template. It was almost certain to conclude that Ce-ZnO could be completely formed at a lower temperature with sticky rice starch template, compared to using polyvinylpyrrolidone template. However, the calcination temperature in this study was set at 550°C to completely remove the template and control the identical phase formation of ZnO.

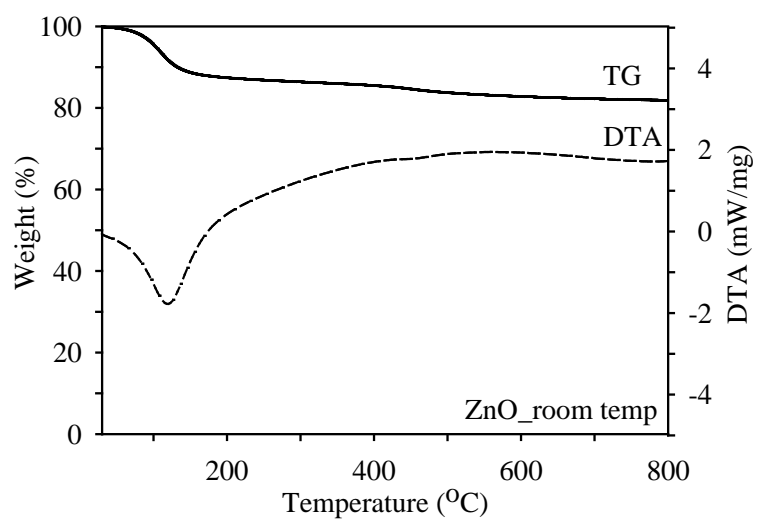


Figure 4.1 TG-DTA curves of the ZnO coated on Al_2O_3 beads.

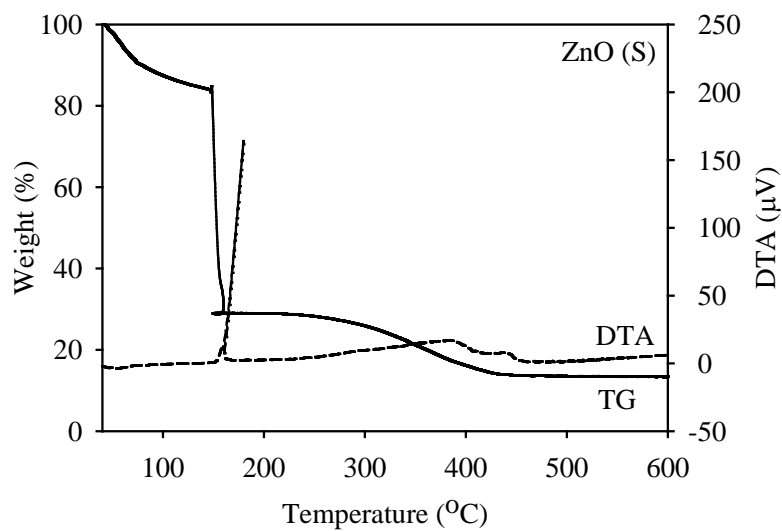


Figure 4.2 TG-DTA curves of ZnO (S).

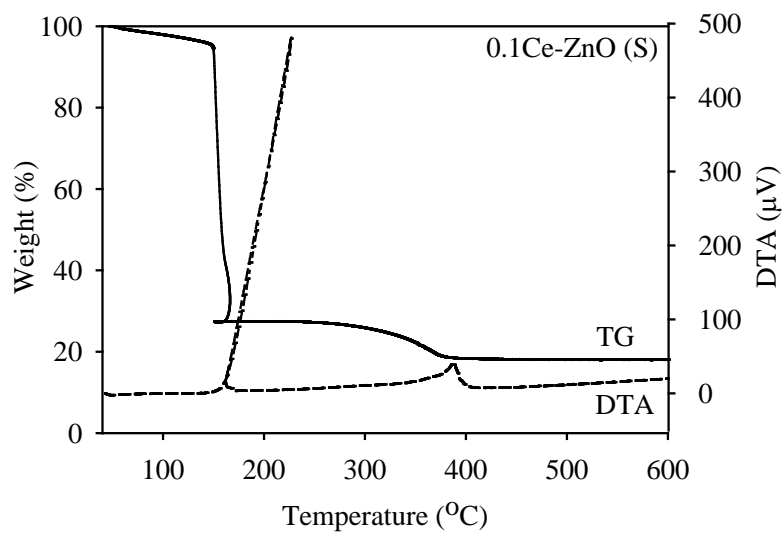


Figure 4.3 TG-DTA curves of 0.1Ce-ZnO (S).

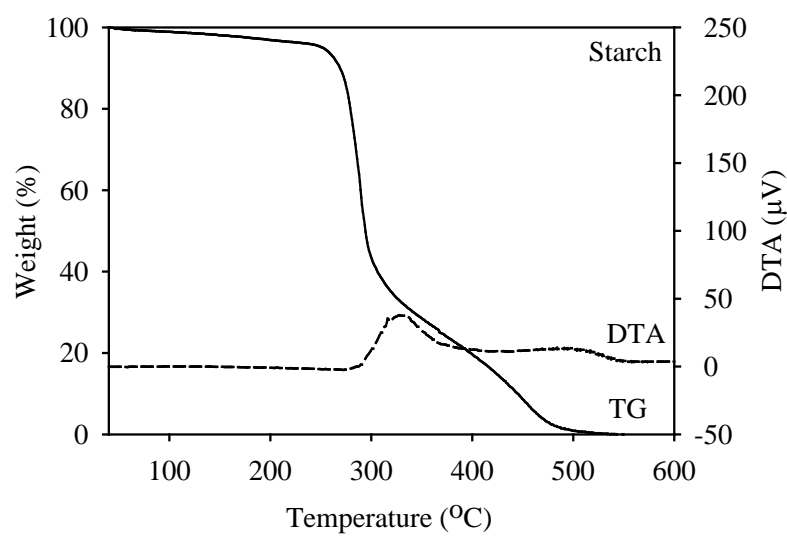


Figure 4.4 TG-DTA curves of sticky rice starch.

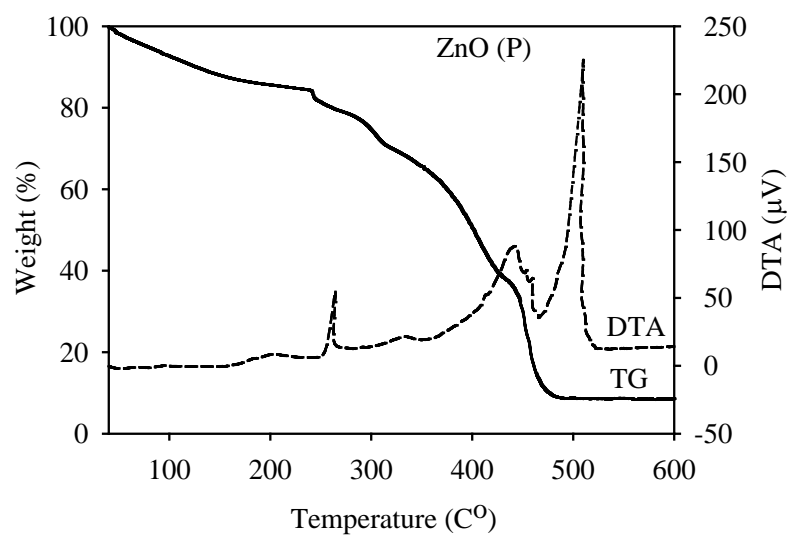


Figure 4.5 TG-DTA curves of ZnO (P).

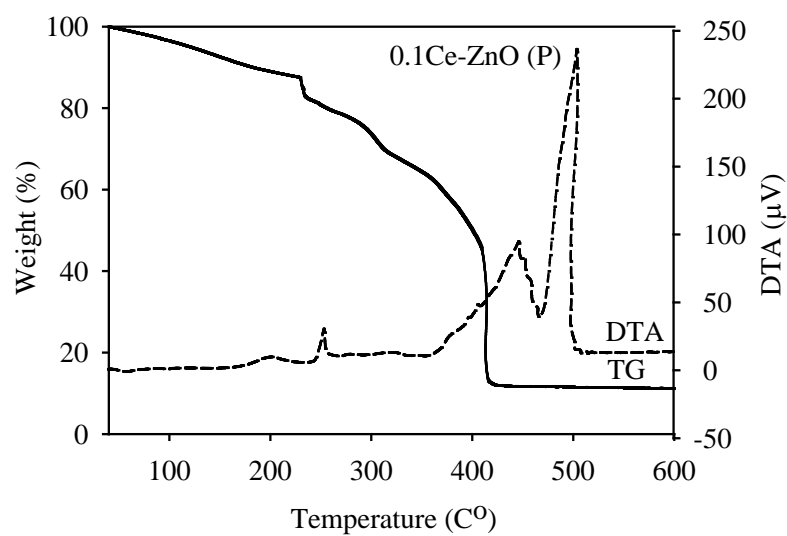


Figure 4.6 TG-DTA curves of 0.1Ce-ZnO (P).

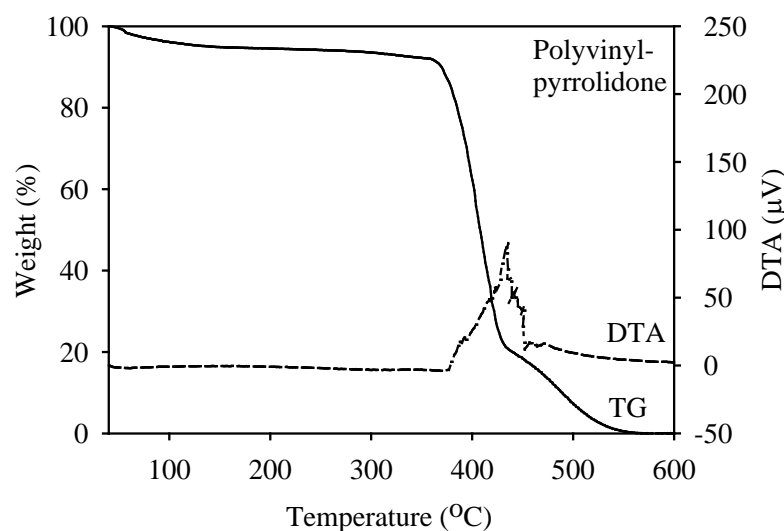


Figure 4.7 TG-DTA curves of polyvinylpyrrolidone.

4.1.1.2 Organic and inorganic identities

In order to confirm the availability of Ce and Zn composed on the prepared material, FT-IR spectra of ZnO and 0.1Ce-ZnO (both by polyvinylpyrrolidone and sticky rice starch types) were inspected compared to the reference spectral features of commercial ZnO, polyvinylpyrrolidone, and sticky rice starch as shown in Figures 4.8 and 4.9. The spectra were measured in the 4000 to 500 cm^{-1} region. The band at 3000 to 2800 cm^{-1} of polyvinylpyrrolidone and sticky rice starch in Figure 4.8 attributed to the C-H bonds of the organic compound. These bands disappeared from the catalysts prepared with both templates as shown in Figure 4.9. For the prepared catalysts, the intense IR absorption band at 3456 cm^{-1} corresponded to $\delta(\text{OH})$ mode of H-bond for water molecules. The IR peak at 1589 cm^{-1} presented the absorption of atmospheric CO_2 on the metallic cations (Zn and Ce), which was generated during the calcination. The three main peaks identified O-H, CO_2 , and C-O in the prepared catalysts associated with the studies of Maensiri et al. (2006b), Maensiri et al. (2006c), and Phoka et al. (2009). The IR absorption band from 1150 to 1000 cm^{-1} attributed to the C-O bond stretching. The IR peak at 1148 cm^{-1} indicated the saccharide structure (C-C) on ZnO (S) because of incomplete calcination from enlargement of the catalyst preparation. ZnO could be identified by a

strong band below wavenumber of 550 cm^{-1} (Kong et al., 2009; Maensiri et al., 2006c). The FT-IR spectrum of ceria exhibited a strong broad band peak below 400 cm^{-1} which was due to the Ce-O-Ce mode (Phoka et al., 2009). In Figure 4.10, FT-Raman spectrum appeared at 465 cm^{-1} to confirm the existence of ceria. This result was in agreement with the previous results presented by Grisdanurak et al. (2009).

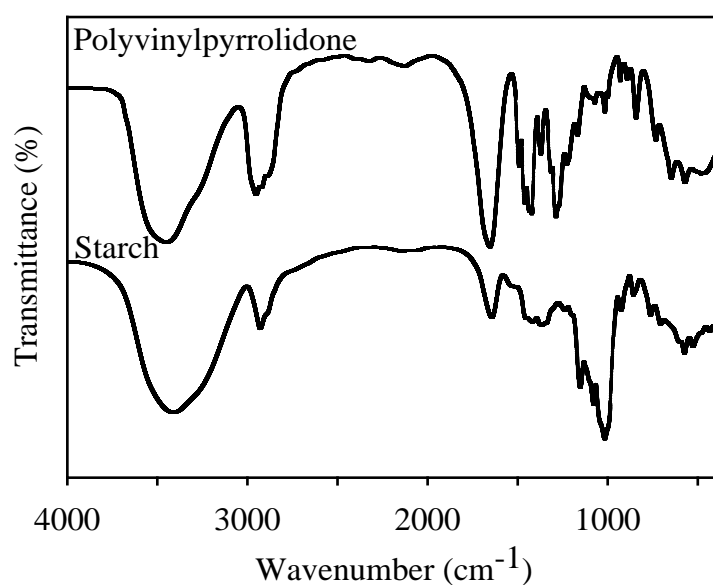


Figure 4.8 FT-IR spectra of sticky rice starch (S) and polyvinylpyrrolidone (P) templates.

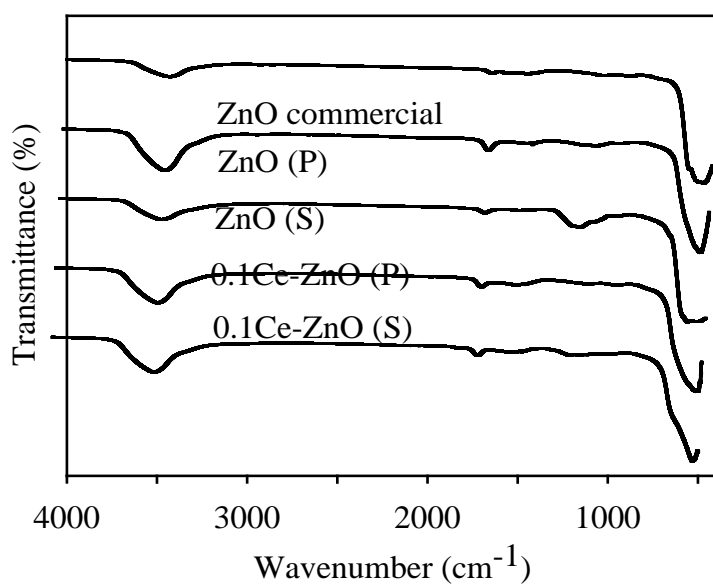


Figure 4.9 FT-IR spectra of catalysts prepared with starch (S) and polyvinylpyrrolidone (P) templates.

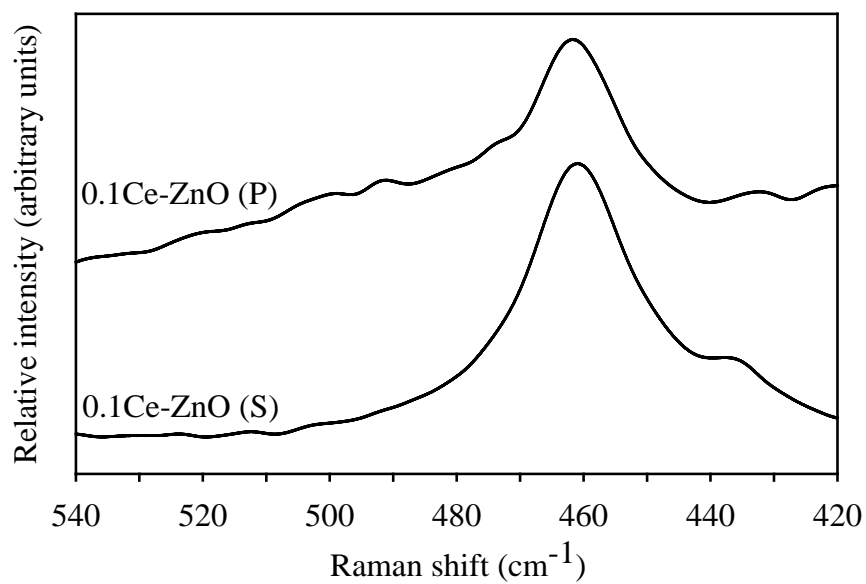


Figure 4.10 Raman spectra of 0.1Ce-ZnO (S) and 0.1Ce-ZnO (P).

4.1.1.3 Structure and crystalline size

XRD is one of the most important techniques for characterizing catalyst (Haber, Block, and Delmon, 1995). XRD is used to identify crystalline phases in powder form for most catalysts. It also gives valuable information on the size of individual crystallites from line-broadening peaks.

The XRD spectra of the ZnO coated on Al₂O₃ at different calcination temperatures are shown in Figure 4.11. The XRD patterns revealed the formation of crystalline wurtzite structure, hexagonal close packing (JCPDS, 36-1451). Furthermore, the same phase appeared on all samples since no shifts in each spectrum were observed confirmed by Bragg angle in Table 4.2. The diffraction peaks of catalysts calcined at 550 and 600°C, ZnO_550 and ZnO_600, were obviously seen due to sufficient long-range order of the catalysts. The observed diffraction lines were quite narrow leading ZnO_550 and ZnO_600 to be perfect crystals (Niemantsverdriet, 2007). This suggested that the optimum calcining temperature should be optimized at 550°C or 600°C. Although the high peak sharpness indicated that particles had crystallographically better defined, the crystalline size of ZnO_550 and ZnO_600 presented in similar range with other catalysts. The calculated crystalline size using the XRD pattern at (110) reflex (Comparelli et al, 2005) is provided in Table 4.2. The large crystalline size corresponding with lowering of surface area might cause the low reaction rate on photocatalysis. Nevertheless, the crystalline size of all samples in Table 4.2 was quite insignificantly different.

In addition, the presence of key phases in the synthesized ZnO and metal doped ZnO catalysts using sticky rice starch (S) and polyvinylpyrrolidone (P) templates was identified by the XRD pattern. In Figures 4.13 and 4.14, the diffraction peaks of all synthesized catalysts were similar to the ZnO reference peak (Figure 4.12) indexed as a wurtzite structure in the standard data (JCPDS, 36-1451). The appearance of a CeO₂ phase, at (111) plane, was also observed in all ZnO doped Ce samples. However, the intensity was quite low because the Ce loading is quite small. Via simple chemical method, polyvinylpyrrolidone was applied as the template in semiconductor and photocatalyst syntheses in many studies (Maensiri et al., 2006b;

Maensiri et al., 2006c; Phoka et al., 2009; Wang et al., 2003). The metal oxides were obtained with satisfied characteristics. Likewise, ZnO (P), 0.02Ce-ZnO (P), and 0.1Ce-ZnO (P) could be prepared from this study. In addition, ZnO (S), 0.02Ce-ZnO (S), and 0.1Ce-ZnO (S) were successfully synthesized by using the sticky rice starch as a template. This is due to the fact that starch, containing abundant hydroxyl groups, can be easily dispersed into the synthesis solution and can aid in the construction of the gel framework. In Figure 4.15, the XRD pattern of 0.1Cu-ZnO (S) is presented. The peak identified ZnO showed the similar trend with ZnO (S). The intensity of the 0.1Cu-ZnO (S) peaks was higher than 0.1Ce-ZnO (S). The peaks of CuO revealed at 2θ of 32.5, 35, 38.5, and 58°.

By means of simple chemical route using both templates, the molar ratios of doping were certainly maintained at 0.02 and 0.1 without loss of the metal dopant quantity since the as-synthesized solid precursors were not washed during the preparation process. In addition, there were no shifts on XRD patterns in Figures 4.13, 4.14, and 4.15 which established the same phase of ZnO base in all synthesized catalysts. The dopant probably formed oxide on the ZnO because of the XRD peaks indicating the CeO₂ and CuO. It is likely that the simple chemical method using templates contributed most dopants on the surface of catalyst base. The incorporation of dopants into the structure of catalyst base was unlikely clarified by XRD results from this study.

The crystalline sizes of the prepared catalysts are shown in Table 4.3. The similar size presented on commercial ZnO and ZnO (S) while the smaller size showed on ZnO (P). For the metal doped ZnO using both templates, their crystalline sizes were in range of 13.46–22.65 nm. The decrease of the size was probably caused by the formation of CeO₂ and CuO which obstructed the crystallization of catalysts during the increase of calcination temperature. However, the sticky rice starch usage seemed to lower the crystalline size comparing to polyvinylpyrrolidone usage. As a result of lowering crystalline size, the surface area was likely to be manifolded. The smaller crystalline size of ZnO doped with Ce, 0.1Ce-ZnO (S), was presented

comparing to ZnO doped with Cu, 0.1Cu-ZnO (S), which probably associated with the sizes of Ce and Cu ions.

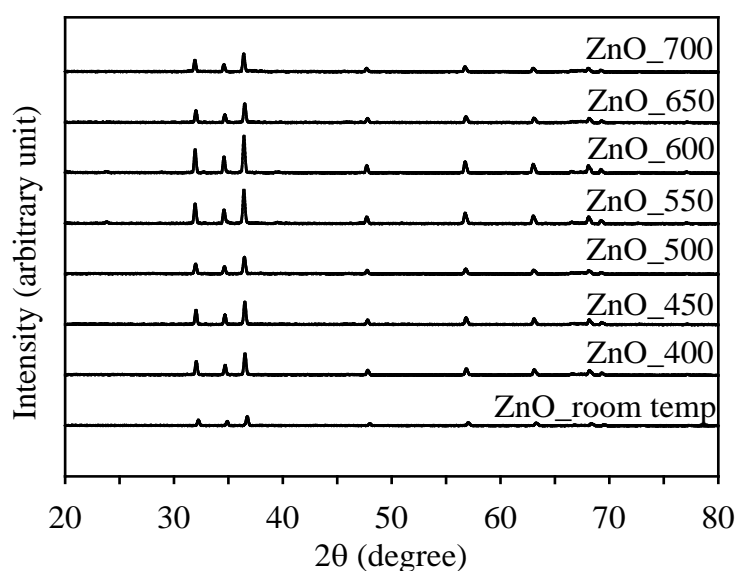


Figure 4.11 XRD patterns of the catalysts prepared by MCT with different calcination temperatures.

Table 4.2 Crystalline sizes of the catalysts calculated from (110) plane in the XRD pattern in Figure 4.11.

Catalyst	Bragg angle (degree)	Crystalline size (nm)
ZnO_700	56.72	27.98
ZnO_650	56.80	28.47
ZnO_600	56.74	29.96
ZnO_550	56.76	30.08
ZnO_500	56.78	30.22
ZnO_450	56.82	30.53
ZnO_400	56.68	30.90
ZnO_room temp	57.04	35.74

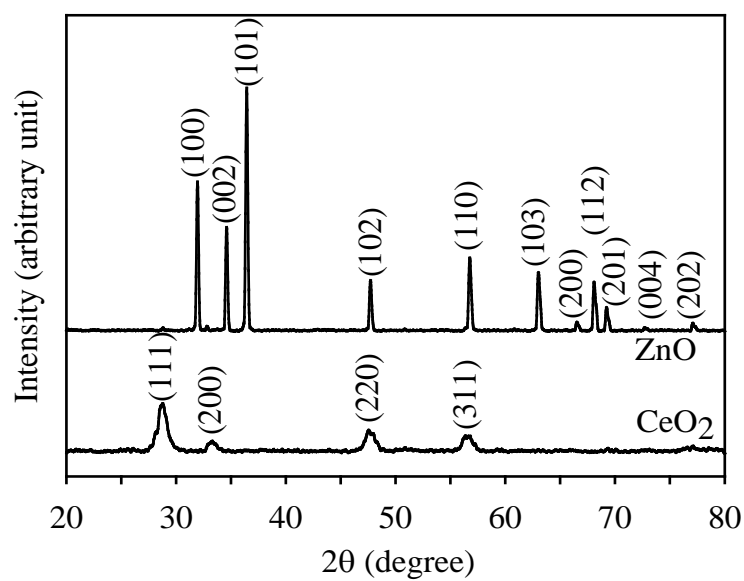


Figure 4.12 XRD patterns of standard ZnO and CeO₂.

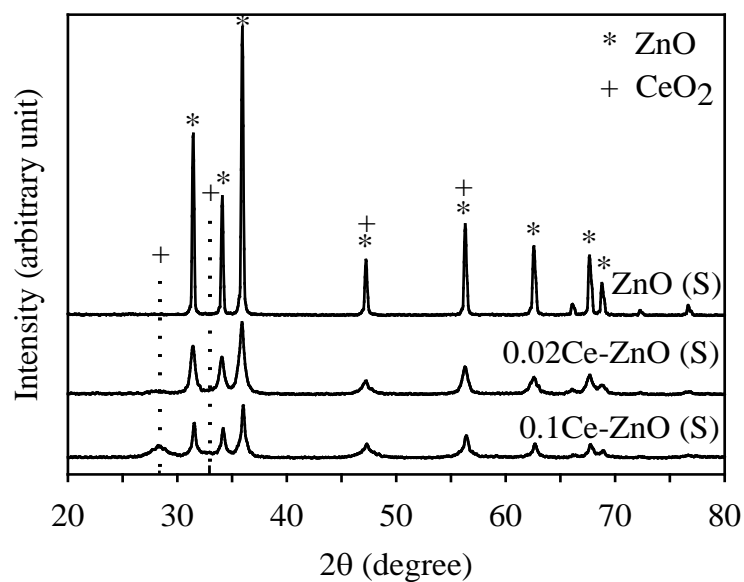


Figure 4.13 Normalized XRD spectra of catalysts with sticky rice starch (S) template.

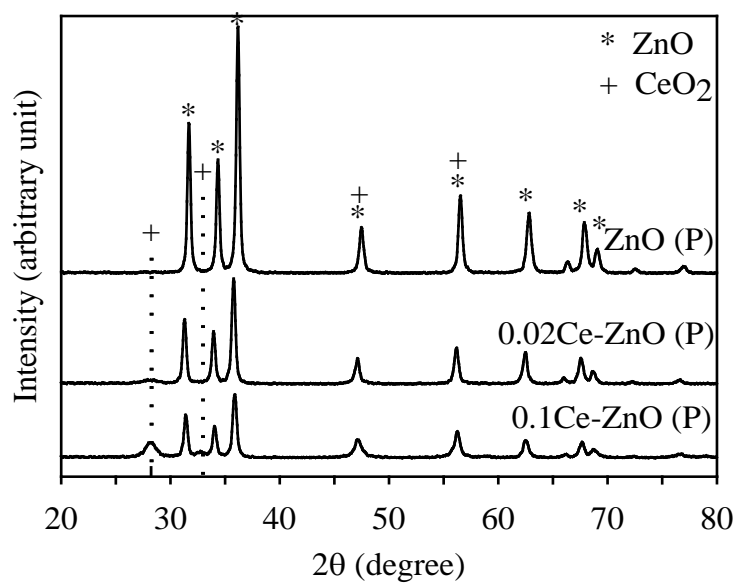


Figure 4.14 Normalized XRD spectra of catalysts with polyvinylpyrrolidone (P) template.

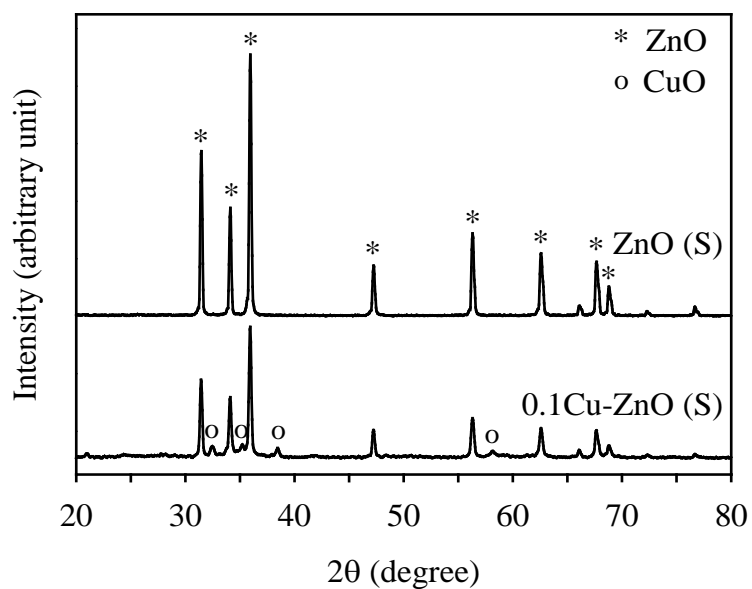


Figure 4.15 Normalized XRD patterns of 0.1Cu-ZnO (S) compared with ZnO (S).

Table 4.3 Crystalline sizes of catalysts calculated from (110) plane.

Catalyst	Bragg angle (degree)	Crystalline size (nm)
ZnO commercial	56.28	28.60
ZnO (P)	56.52	20.06
0.02Ce-ZnO (P)	56.16	18.34
0.1Ce-ZnO (P)	56.24	15.43
ZnO (S)	56.32	28.31
0.02Ce-ZnO (S)	56.28	13.46
0.1Ce-ZnO (S)	56.40	15.93
0.1Cu-ZnO (S)	56.32	22.65

4.1.1.4 Oxidation state

XANES is the characterization technique used for determining the oxidation number of interested species which becomes more popular with availability of the synchrotron beam line. This technique offers the geometry and oxidation state of catalyst (Niemantsverdriet, 2007). With the reference spectra of known compounds, XANES spectra can usually be very well interpreted. In Figure 4.16 and Table 4.4, XANES spectra showed that the edge energy positions of the synthesized ZnO (P) and 0.3Ce-ZnO (P) were close to that of ZnO commercial which was used as the reference. This evidence revealed oxidation state +2 of Zn. The 0.3Ce-ZnO (P) presented another edge energy position at higher energy compared to the reference which might affect in the difference of oxidation state of Zn. In Figure 4.17 and Table 4.5, the edge energy positions from XANES spectra of CeO₂ (P) and 0.3Ce-ZnO (P) were similar to that of the CeO₂ reference. It could be interpreted that oxidation state of Ce doped on ZnO was +4. The oxidation number of Ce in 0.3Ce-ZnO (P) supported the formation of CeO₂ on the synthesized catalysts associating with the XRD results.

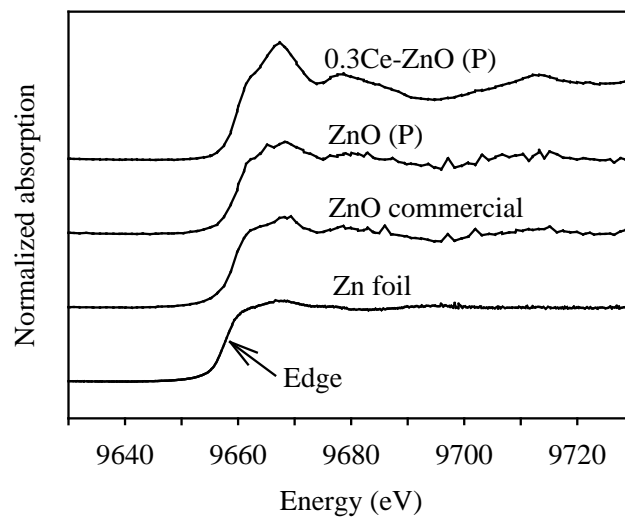


Figure 4.16 XANES spectra of Zn element and Zn compounds.

Table 4.4 Zn K-edge energy position of catalysts with respect to Zn foil.

catalyst	K-edge (eV)	ΔE (eV)
ZnO foil	9657.35	0.00
ZnO commercial	9659.84	2.49
ZnO (P)	9659.89	2.54
0.3Ce-ZnO (P)	9659.84	2.49

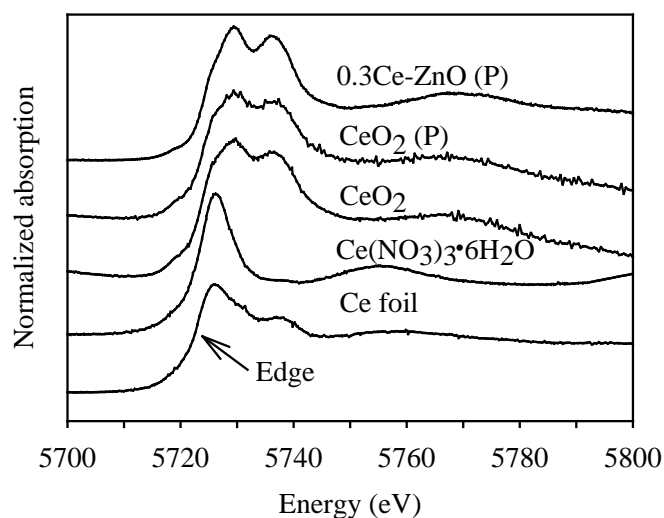


Figure 4.17 XANES spectra of Ce element and Ce compounds.

Table 4.5 Ce K-edge energy position of catalysts with respect to Ce foil.

catalyst	K-edge (eV)	ΔE (eV)
Ce foil	5722.99	0.00
$\text{Ce}(\text{NO}_3)_3 \cdot 6\text{H}_2\text{O}$	5723.38	0.39
CeO_2	5724.57	1.58
CeO_2 (P)	5724.56	1.57
0.3Ce-ZnO (P)	5724.57	1.58

4.1.1.5 Light absorption capacity

To determine the light absorption property of catalysts, the diffuse reflectance measurement from UV-visible spectrophotometer is a standard technique. Besides, the band gap energy can be calculated by using absorption data (Murphy, 2007; Escobedo Morales, Sánchez Mora, and Pal, 2007; Wang et al., 2005)

As shown in Figure 4.18, the UV-vis-DR spectra of ZnO and Al_2O_3 were used to compare with other samples. It was found that ultraviolet region was greatly absorbed by ZnO and poorly absorbed by Al_2O_3 . The samples of ZnO coated on Al_2O_3 varied by calcination temperature revealed the absorbance in ultraviolet

region, 250 to 380 nm. Therefore, the property of only ZnO would be the main determinant on the UV-vis-DR results of the samples. From the spectra, the ZnO coated on Al₂O₃ beads calcined at temperature of 550°C, ZnO_550, had the highest absorbance under UV light which relates to the XRD result. The ZnO_550 had the perfect crystal affecting to provide great absorbance in UV-vis-DR. Thus, it was interesting in applying to photocatalytic degradation experiment. Moreover, ZnO would have performance under visible light range condition since it showed little high absorbance at 380 to 470 nm (Sakthivel et al., 2003). This supported the ability of ZnO to degrade an organic pollutant under visible light.

The UV-vis-DR spectra of the synthesized metal doped ZnO compared with commercial ZnO are illustrated in Figures 4.19 and 4.20. The spectrum of the commercial ZnO displayed an adsorption peak in the UV range (<380 nm). When ZnO was doped with Ce or Cu, its absorbance in the visible light range (380 to 740 nm) increased. The yellow color of the Ce-ZnO or the gray color of Cu-ZnO as well as method of catalyst preparation would cause the adsorption in the visible light region. Therefore, transition metal doping such as Ce probably increased the effectiveness for visible light range absorption and played a role in enhancing photocatalytic activity under visible light irradiation. The UV-vis adsorption edge of the catalysts was used as data to find the exact band gap energy (Kong et al., 2009; Wang et al., 2005; Yoong, Chong, and Dutta, 2009). Transformed Kubelka-Munk plots of $Ah\nu^{1/2}$ versus $h\nu$ from the spectral data is depicted on Figure 4.21. The 0.1Cu-ZnO (S) presented the band gap energy of 2.88 eV while the commercial ZnO had the band gap energy of 3.12 eV. With cerium doping, 0.02Ce-ZnO (S) showed the band gap energy of 2.88 eV. Slight differences in band edge wavelength for all catalysts were seen. It could be hypothesized that the best molar ratio of doping for enhancing photocatalytic activity under visible light irradiation was 0.02, and a catalyst using sticky rice starch template was superior to one using polyvinylpyrrolidone template.

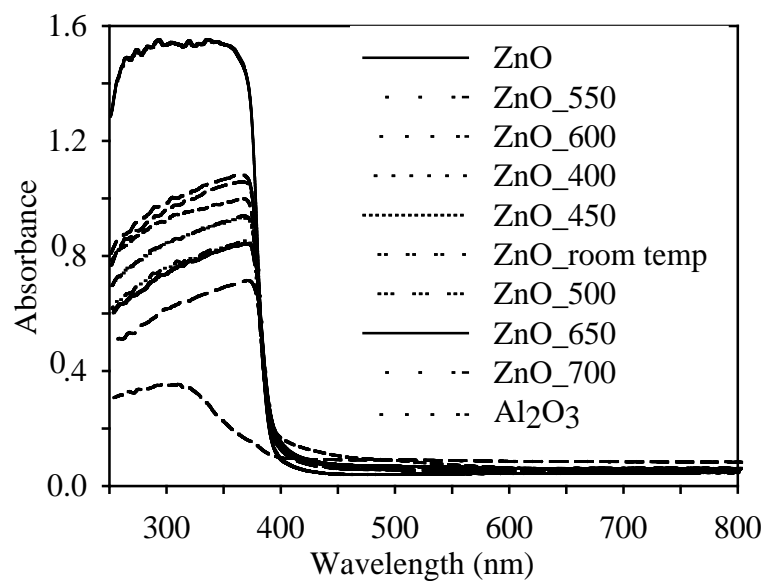


Figure 4.18 UV-vis diffuse reflectance spectra of the ZnO coated on Al_2O_3 bead prepared with different calcination temperatures.

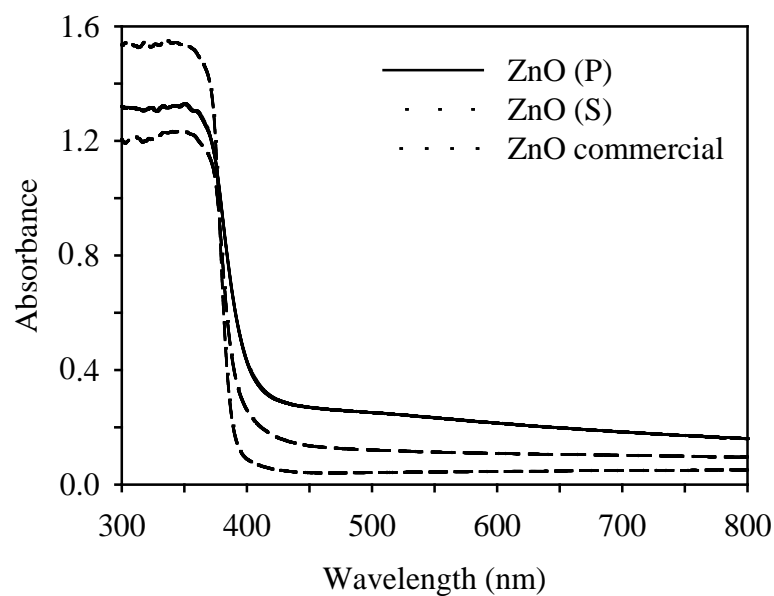


Figure 4.19 UV-vis diffuse reflectance spectra of ZnO prepared by sticky rice starch (S) and polyvinylpyrrolidone (P) templates.

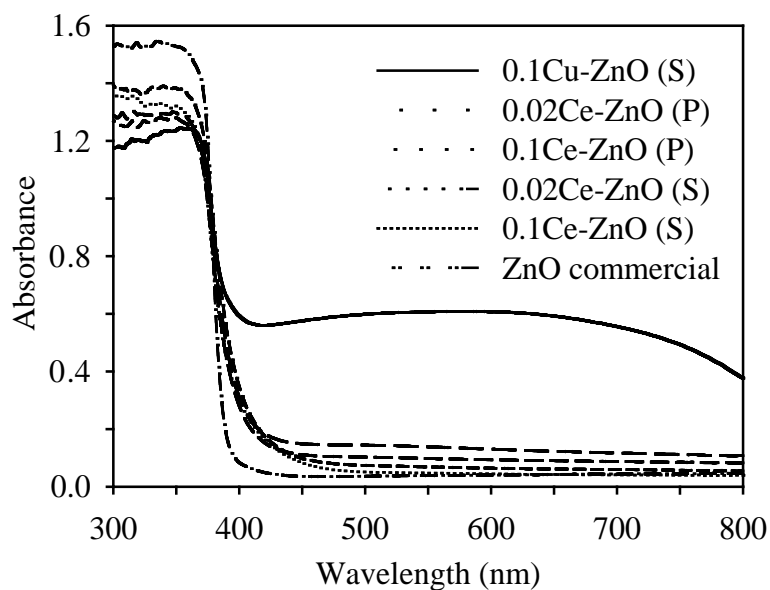


Figure 4.20 UV-vis diffuse reflectance spectra of 0.02Ce-ZnO and 0.1Ce-ZnO prepared by different templates comparing to commercial ZnO.

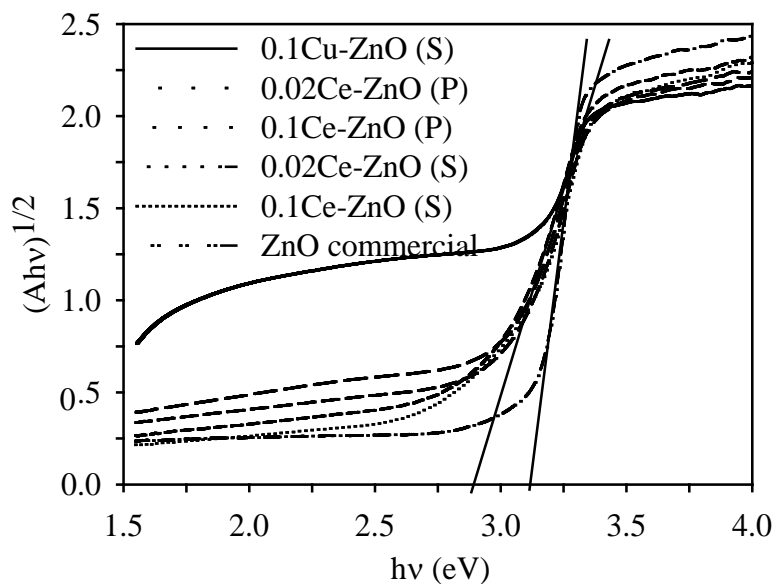


Figure 4.21 Transformed Kubelka-Munk plots of 0.02Ce-ZnO and 0.1Ce-ZnO prepared by different templates comparing to commercial ZnO.

4.1.1.6 Specific surface area

The surface area and pore size distribution of catalysts were measured by using Brunauer-Emmett-Teller method (BET). The surface area can be the data to assess the space of active sites for adsorption and reaction occurring on catalyst's surface. The pore size distribution is used for predicting whether the adsorbate, which is atrazine in this study, is adsorbed in the pores of catalyst's surface.

Table 4.6 illustrates the surface area of standard samples of ZnO and Al₂O₃ in powder and beads types. It was clearly seen that Al₂O₃ beads had a preferable surface area when were compared to others due to the amorphous structure forming the high porous material. This property caused the Al₂O₃ beads to be the choice as adsorbent for adsorption of arsenite, arsenate, and fluoride (Ghorai and Pant, 2005; Lin and Wu, 2001). However, the Al₂O₃ itself presented poor absorbance under UV and visible light resulting in inactivity in photocatalysis. The surface area of commercial ZnO is 5 m²/g. When the ZnO was coated on Al₂O₃ and calcined at 550°C, ZnO_550, its surface area became 166 m²/g and was lower than that of Al₂O₃. This was certain that the obtained surface area involved with the surface area of Al₂O₃, and the commercial ZnO powder partially concealed the pore of Al₂O₃. This explanation could be also devoted to the surface area of beads in Table 4.7.

The surface areas of the prepared catalysts are provided in Table 4.7. As powder form with sticky rice starch or polyvinylpyrrolidone, ZnO doping with Ce or Cu in different molar ratios showed a higher surface area than the commercial ZnO. The catalysts obtained through the starch gel preparation proposed higher surface areas than the ones through the polyvinylpyrrolidone gel preparation except ZnO (S). It could be summarized that the surface area of the prepared catalysts were enhanced with the template assistance. In addition, the surface area of the catalyst could be increased by sticky rice starch template and the increasing of molar ratio of cerium nitrate to zinc nitrate.

Table 4.8 and Figure 4.122 display the pore size distributions of prepared catalysts and commercial ZnO. All catalysts were in classified as

mesoporous structure ($0.2 \text{ nm} < \varnothing < 50 \text{ nm}$) ranging in the pore width of approximately 1.9 to 31.8 nm (Kaneko, 1994). The mesopore of the prepared catalysts in this study had relevance with the metal oxide syntheses used polyvinylpyrrolidone or starch as template in other studies (Chunming et al., 2009; Iwasaki et al., 2004; Shen et al., 2008; Wang et al., 2003; Zheng et al., 2001). The molecular size of atrazine is $0.96 \times 0.84 \times 0.3 \text{ nm}$ (Pelekani and Snoeyink, 2001). It could be predicted that the atrazine would be able to approach the surface in the pores of the prepared catalysts.

Table 4.6 BET surface areas of standard samples.

Type	Sample	BET surface area (m^2/g)
Powder	ZnO commercial	5
Beads	ZnO_550	166
	Al_2O_3	312

Table 4.7 BET surface areas of catalysts prepared by sticky rice starch (S) and polyvinylpyrrolidone (P) templates.

Type	Catalyst with S template	BET surface area (m^2/g)	Catalyst with P template	BET surface area (m^2/g)
Powder	ZnO (S)	7	ZnO (P)	13
	0.02Ce-ZnO (S)	25	0.02Ce-ZnO (P)	22
	0.1Ce-ZnO (S)	34	0.1Ce-ZnO (P)	32
	0.1Cu-ZnO (S)	13		
Beads	0.02Ce-ZnO (S)	128	0.02Ce-ZnO (P)	137
	0.1Ce-ZnO (S)	147	0.1Ce-ZnO (P)	130
	0.02Cu-ZnO (S)	171		

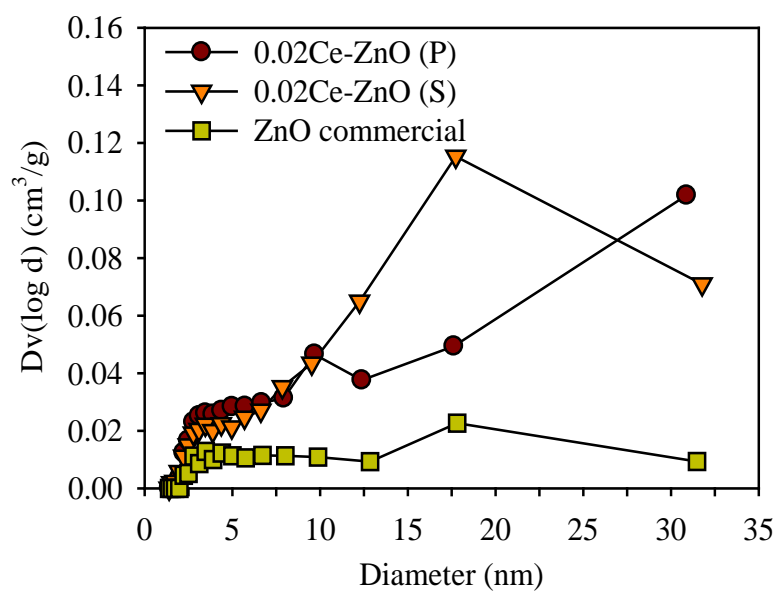


Figure 4.22 Pore size distributions of 0.02Ce-ZnO (P), 0.02Ce-ZnO (S), and ZnO commercial.

Table 4.8 Average pore sizes of 0.02Ce-ZnO (P), 0.02Ce-ZnO (S), and ZnO commercial powders.

Catalyst	Average pore size (nm)
0.02Ce-ZnO (P)	30.9
0.02Ce-ZnO (S)	17.7
ZnO commercial	17.8

4.1.1.7 Morphology

Scanning electron microscopy (SEM) is the useful technique for exploring the morphology of catalysts. Before using MCT, Al_2O_3 beads were milled without adding catalyst powder in order to inspect cracking surface of the Al_2O_3 beads. As a result, few amount of Al_2O_3 was lost leading to assumption that Al_2O_3 beads maintain the same amount after the coating process. This information used for estimating the amount of catalyst powder coating on Al_2O_3 beads.

To prepare the ZnO coated on Al_2O_3 beads, raw materials were used with the weight ratio of 60.0000 g Al_2O_3 : 40.0000 g ZnO. After 15-hour-coating, the catalyst beads were obtained with weight of 74.55 g. This meant 19.52% of ZnO powder was concealed on Al_2O_3 beads. In Figure 4.23 (right), the complexion of ZnO_550 revealed small particles of ZnO compared to that of Al_2O_3 in Figure 4.23 (left) which was rather smooth. The particles of ZnO presented in size of approximately 0.1 to 1 μm . The partial surface of Al_2O_3 on ZnO_550 indicated the imperfection of coating which related to the discussion of surface areas of ZnO_550. However, no cracked surface was observed.

The comparative morphologies of Al_2O_3 , ZnO_550, 0.02Ce-ZnO (P), 0.02Ce-ZnO (S), and 0.02Cu-ZnO (S) coated on Al_2O_3 beads were shown in Figure 4.24. By MCT, all synthesized catalysts coated to the Al_2O_3 bead supporter. The size of the coated beads was varied from 0.5 to 1.2 mm.

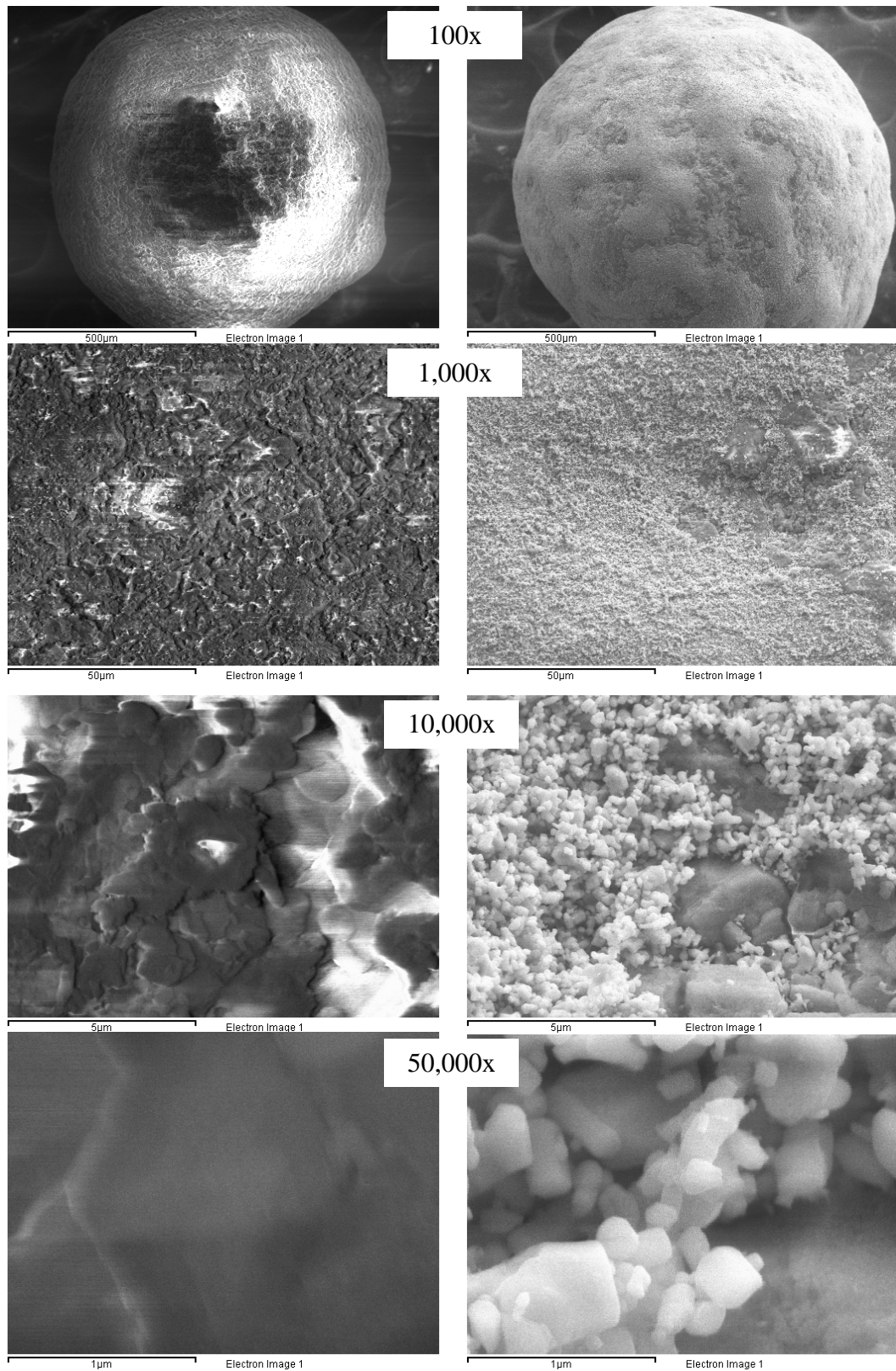


Figure 4.23 SEM images of Al_2O_3 (left) and ZnO_{550} (right).

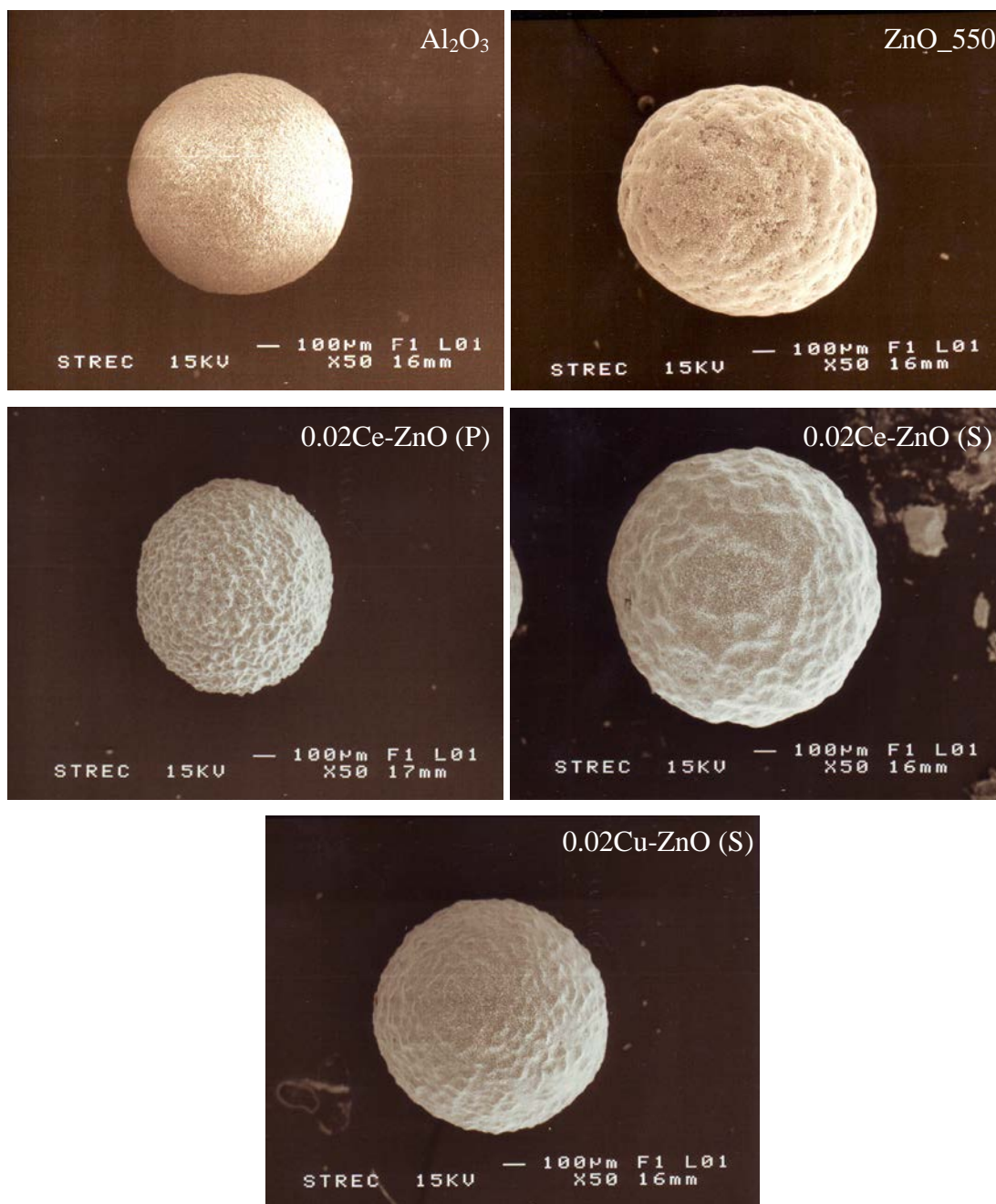


Figure 4.24 SEM images of catalysts.

4.1.1.8 Surface charge

The surface charge is very important in adsorption mechanism study. It provides the understanding in type of interaction between the adsorbent and adsorbate which are catalyst's surface and atrazine molecule, respectively. The charge on the catalyst surface was measured by zeta potentiometer (Dmitrieva et al., 2007; Lee et al., 2009). In Figure 4.25, the electrophoretic properties at the surface of the 0.1Ce-ZnO (P) and 0.1Ce-ZnO (S) catalysts were identified. When pH of water was varied from 4.00 to 12.00, the 0.1Ce-ZnO (P) showed a positive charge on its surface at pH 4.00 and then a negative charge at pH 6.00. With steep falling line, the isoelectric point (IEP) of 0.1Ce-ZnO (P) presented at pH 4.60. On the other hand, the 0.1Ce-ZnO (S) gave a positive charge at pH 4.00 to 8.00 and negative charge at pH 10.00 to 12.00. The IEP of 0.1Ce-ZnO (S) was at pH 8.50 to be similar to that of ZnO (S). This feature showed that the type of template probably influences the IEP of catalyst. However, the IEP of 0.1Cu-ZnO (S) presented at pH 10.30 which might be influenced by the type of dopant.

The IEP of commercial ZnO accurately presented at pH 9.00 according to other study (Akyol, Yatmaz, and Bayramoglu, 2004).

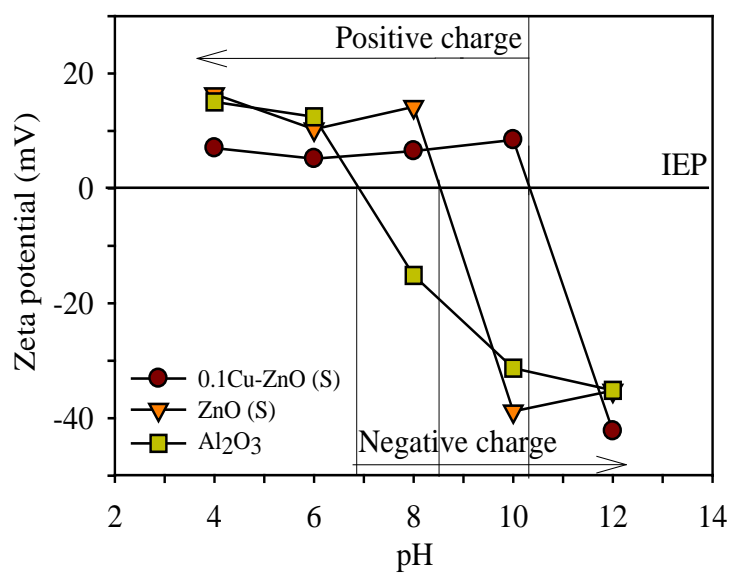
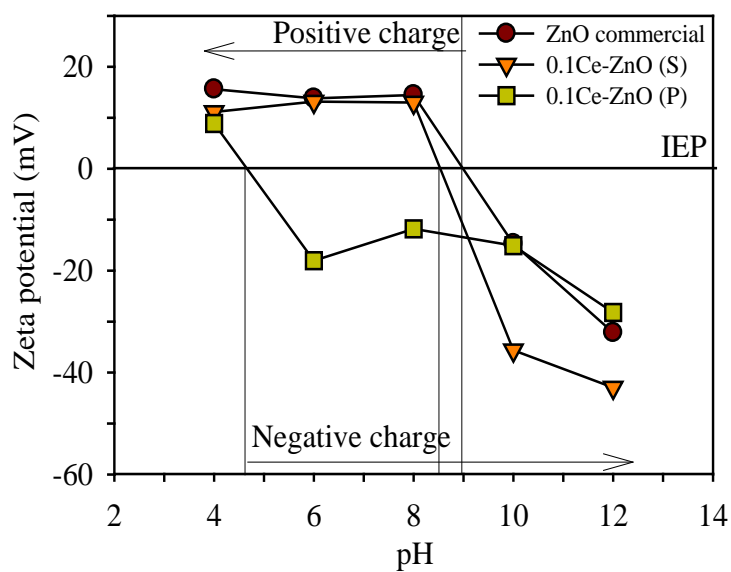


Figure 4.25 Dependencies of zeta-potential of catalysts suspended in water at different pH.

4.1.2 Catalyst activity test

After the characteristics of the catalysts were examined and understood, each catalyst was tested in preliminary photocatalytic reactor. The factors involved in the activity of catalyst were concentrated in two points which were the immobilization via MCT and the preparation route via simple chemical method.

4.1.2.1 Immobilization concernment

RR120 photocatalytic degradation by the catalyst beads of ZnO_550 was set for testing immobilization. Using ZnO_550 beads in the setup batch reactor that allowed ZnO_550 to settled in RR120 solution at the bottom of container without agitation, it was concerned whether the ZnO powder concealed at the bead surface are able to peel and suspend in the RR120 solution. This was possibly proved by monitoring of RR120 concentration trend. Without filtration, if particles were suspended in the RR120 solution, it would greatly affect to RR120 absorbance in UV-vis spectrometer resulting in the fluctuation of RR120 concentration as a function of time. Figure 4.26 shows the spectrum of RR120 solution measured by UV-vis spectrometer. The RR120 removal (%) can be calculated by using the following equation (Kosin, 2009).

$$\text{Removal (\%)} = ((C_0 - C)/C_0) \times 100 \quad (4.1)$$

where C_0 = Initial concentration (mg/L)

C = Concentration at time t (mg/L)

In Figure 4.27, in the presence of UV and visible light, the low percent removals of RR120 revealed at 60 min and were likely to be steady through 540 min of irradiations. The removal of RR120 was 36.2% when adsorption was performed for 600 min. The RR120 concentration was quite greatly reduced by adsorption on ZnO_550 in darkness. In Figure 4.28, within 600 min, 96.3 and 76.3% of RR120 were removed under UV and visible light, respectively. Since ZnO has higher absorbance in UV region, electrons in the valence band is easily excited to the conduction band when UV light is applied generating $\cdot\text{OH}$ radicals to destruct RR120. Thus, the

percent removal of RR120 under UV was superior to that under visible light irradiation. It could be noted that the Al_2O_3 had no effects on the photocatalytic degradation of RR120. However, RR120 removal depended on not only the reaction under UV and visible light irradiation but also the adsorption. The immobilization of the catalyst through MCT was pay attention by observation of the RR120 photocatalytic degradation with ready reactor setup. It was very probable that this immobilization technique had suitability for the next step of study.

In addition, 0.1Ce-ZnO (P) 1:2 was synthesized via simple chemical method using polyvinylpyrrolidone as the template. This catalyst was immobilized with MCT and then tested in the RR120 photocatalytic degradation under the conditions that were stated in 3.4.1. As illustrated in Figure 4.29, 0.1Ce-ZnO (P) 1:2 bead tended to enhance the photocatalytic activity to degrade RR120 comparing to ZnO_550 at the same experimental condition (both 10 and 20 mg/L of RR120) especially at initial irradiation time. Therefore, the ZnO catalyst being doped by Ce^{3+} using simple chemical method probably has efficiency for atrazine photocatalytic degradation.

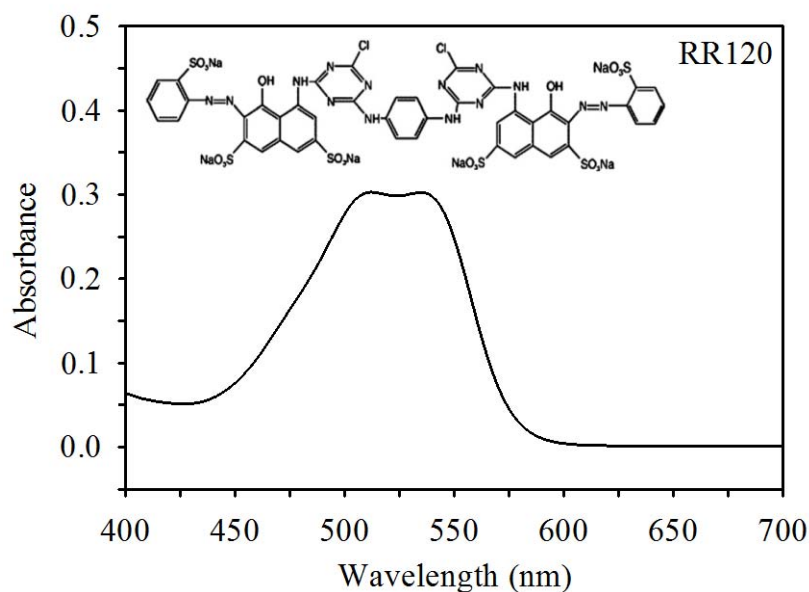


Figure 4.26 RR120 spectrum from UV-vis spectrometer.

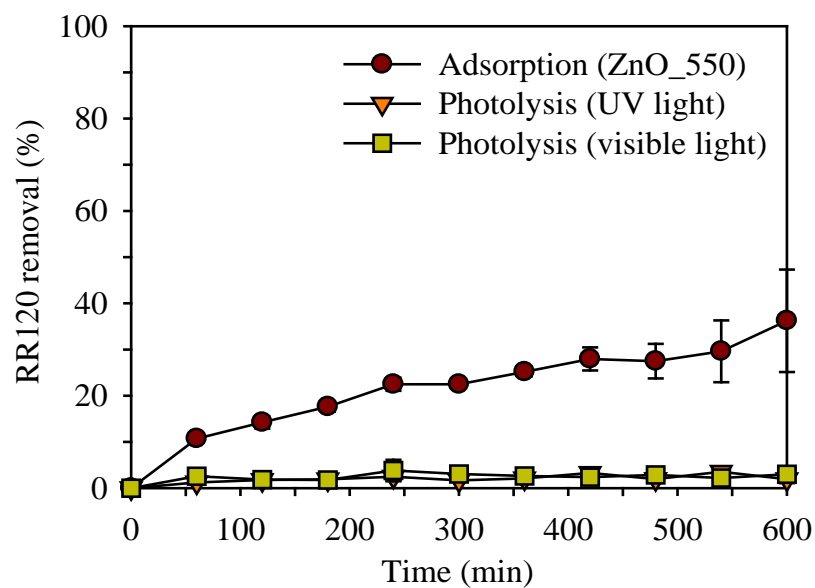


Figure 4.27 RR120 photolysis and RR120 adsorption on ZnO_550.

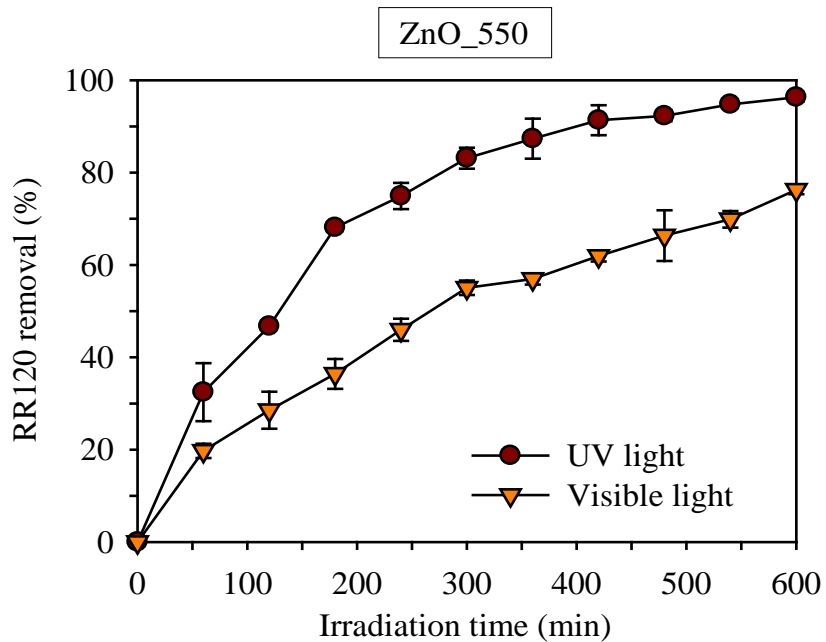


Figure 4.28 RR120 photocatalytic degradation using ZnO_550 under UV and visible light irradiation.

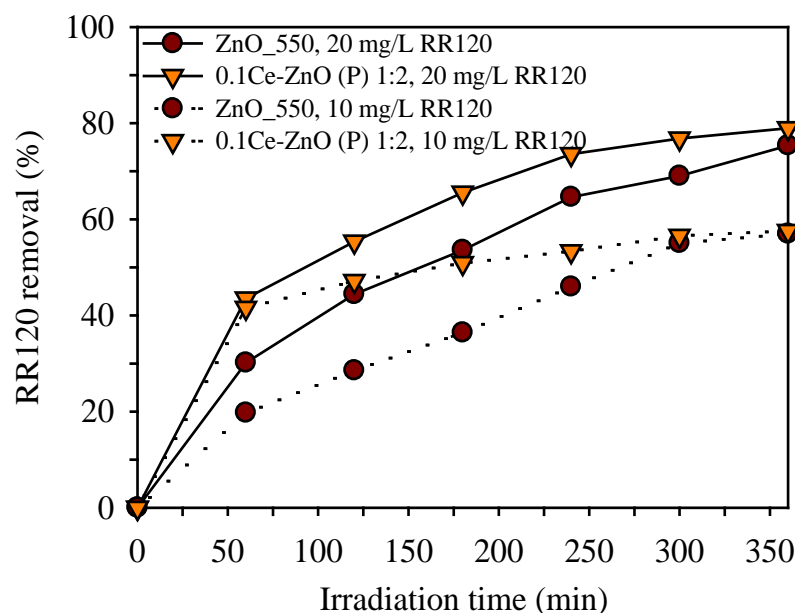


Figure 4.29 RR120 photocatalytic degradation with ZnO_550 and 0.1Ce-ZnO (P) 1:2 bead under visible light irradiation using the initial concentration of 10 and 20 mg/L.

4.1.2.2 Preparation route concernment

Atrazine photocatalytic degradation by Ce-ZnO (S) and Ce-ZnO (P) was investigated in order to confirm the activity of catalyst prepared through simple chemical method. The prepared catalysts were tested for their photocatalytic performance over atrazine contaminated in water under visible light irradiation. The study was carried out within 120 min in a batch test and at different value of pH. Since pK_a of atrazine is 1.68 in water (McGlamery and Slife, 1996; Plust et al., 1981), atrazine would present itself as a neutral charge at $pH > 1.68$. The degradation performance was studied in the neutral behavior of atrazine.

From duplicated work, it was clearly seen that 0.02Ce-ZnO showed a higher performance than one with 0.1Ce-ZnO for both polyvinylpyrrolidone and sticky rice starch templates as shown in Figure 4.30. This was probably due to the smaller surface area of the catalyst exposed to the light irradiation. In Figure 4.30 (a),

the experimental was carried out at pH 3.00, 4.50, and 7.00, which encouraged the charge on the catalyst surface to be positive, neutral, and negative charge, respectively. The highest percent removal of atrazine was observed with 0.02Ce-ZnO (P) at pH 4.50. This was the pH at the IEP or neutral charge of the catalyst.

In Figure 4.30 (b), 0.02Ce-ZnO (S) was tested at pH 4.50, 7.00, and 8.50, which caused a negative, negative, and neutral charge, respectively, on the catalyst surface. The atrazine degradation increased with increasing pH of solution. This was probably due to the van der Waals force of attracting between the atrazine molecules and the catalyst's surface when the surface of the catalyst was at IEP. At the IEP of Figures 4.30 (a) and (b) which presents the highest atrazine removal, the catalyst with sticky rice starch template enhanced the atrazine removal more than the one with polyvinylpyrrolidone template. This could be explained by their specific surface areas and surface charge; therefore, atrazine molecules would be adsorbed, reacted with the catalyst, and eventually degraded.

Considering the highest atrazine removals for both catalysts, it was found that the degradation rate of atrazine was approximately 9.8596×10^{-4} and 1.2268×10^{-3} mg/cm²-hr for 0.2Ce-ZnO (P) at pH 4.50 and 0.2Ce-ZnO (S) at pH 8.50, respectively. Using catalyst prepared through simple chemical method particularly with assistance of sticky rice starch assured the activity of catalyst.

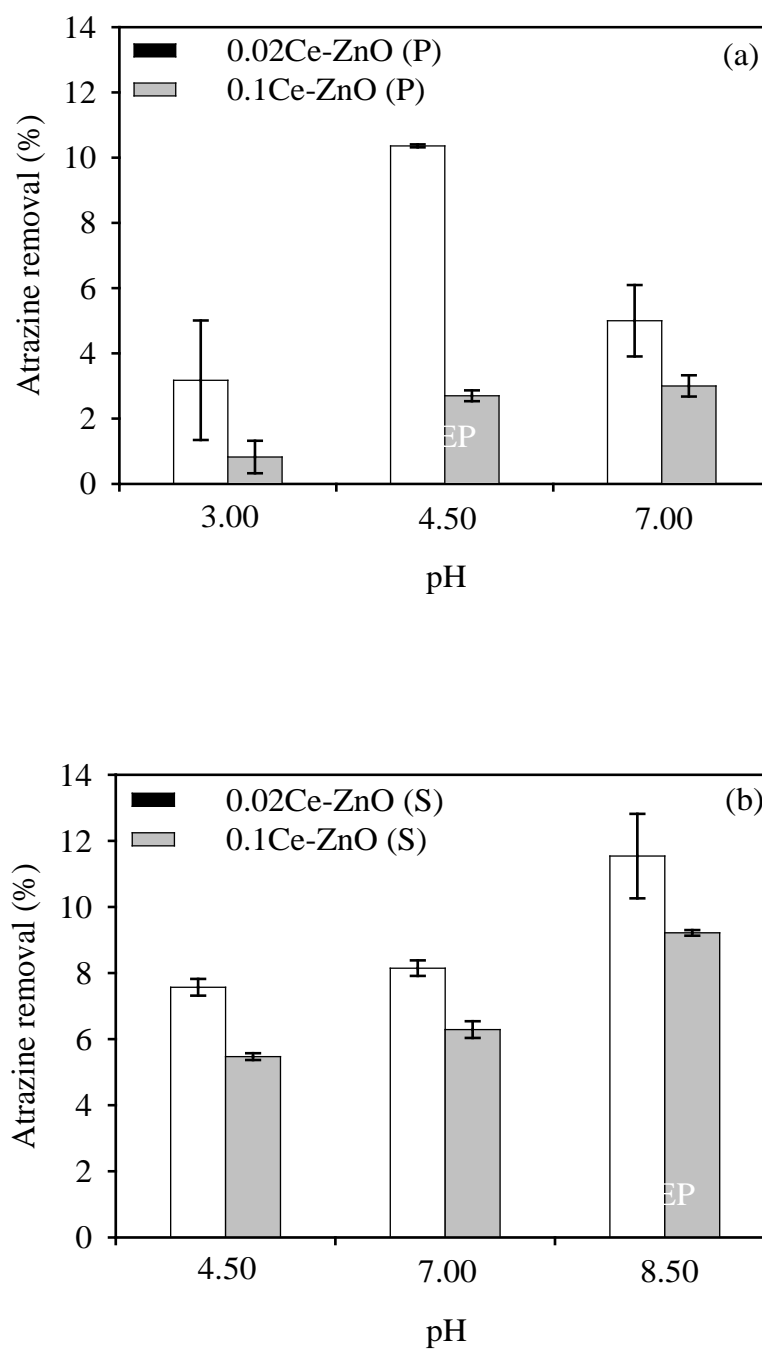


Figure 4.30 Percent removal of varied pH atrazine solution under visible light irradiation using Ce-ZnO on (a) sticky rice starch (S) and (b) polyvinylpyrrolidone (P) templates.

4.2 Photocatalytic degradation of atrazine

This section is the photocatalytic degradation of atrazine study that focuses on the factors involved in the atrazine treatment system. The catalysts used in this part were the ones prepared by simple chemical method with only sticky rice starch template. The catalysts used in this part were summarized in Table 4.9.

Table 4.9 Studied parameters of photocatalytic degradation of atrazine using various catalysts.

Studied parameter	Catalyst	Figure no.	
		Powder	Bead
Photolysis	–	4.31 (a)	
Adsorption	ZnO commercial	4.31 (a)	4.31 (a)
	0.02Ce-ZnO (S) 5:1	4.31 (b)	4.31 (c)
	0.02Cu-ZnO (S) 5:1	4.31 (b)	4.31 (c)
Dopant and molar ratio of doping	Ce-ZnO	4.34 (a)	–
	Cu-ZnO	4.34 (b)	–
Catalyst loading	ZnO commercial	4.35 (a)	4.35 (b)
	0.02Ce-ZnO (S) 5:1	4.36 (a)	4.36 (b)
	0.02Cu-ZnO (S) 5:1	4.37 (a)	4.37 (b)
pH	ZnO commercial	4.38 (a)	4.38 (b)
Initial concentration	ZnO commercial	4.39 (a)	4.39 (b)
Surface passivation	ZnO commercial	–	4.40, 4.41
	0.02Ce-ZnO (S) 5:1	–	4.40, 4.41
	0.02Cu-ZnO (S) 5:1	–	4.40, 4.41
Ionic strength	ZnO commercial	–	4.42, 4.43, 4.44, 4.45, 4.46
Anions	ZnO commercial	–	4.47 (a)
	0.02Ce-ZnO (S) 5:1	–	4.47 (b)
Other metal dopants	0.005Cu-0.005Ce-ZnO	4.48	–
	0.005Fe-0.005Ce-ZnO	4.48	–
	0.005Ag-0.005Ce-ZnO	4.48, 4.50	–
Natural organic matter	0.02Ce-ZnO (S) 5:1	–	4.51
	0.005Ag-0.005Ce-ZnO	4.52	–
Kinetics	ZnO commercial	4.53, 4.54	4.53, 4.54
	0.005Ag-0.005Ce-ZnO	4.53, 4.54	–
Reliability	ZnO commercial	–	4.55

4.2.1 Photolysis and adsorption

Photolysis was tested to measure how much atrazine could be decomposed if only the visible light irradiated with the absence of the catalyst. It is certain that photolysis is the natural major route to destruct atrazine contaminated in surface water. At wavelengths greater than or equal to 290 nm, the photolysis half-life of atrazine at a concentration of 10 mg/L in aqueous solution at 15°C is 25 hr (U.S. EPA., 2003: online). The absence of atrazine by direct photolysis testing caused by pH could be considerable (Lackhoff and Niessner, 2002). From the report, in distilled water, atrazine acidic solution (pH 4) presented a faster photolysis than atrazine neutral solution (pH 7). The photolysis in the acidic solution of atrazine (pH 5.5) was also faster than in the buffer solution (pH 7.6). The improvement of atrazine photolysis caused by pH values or ionic strengths is unclear until now. Nevertheless, photolysis of atrazine is inexistent in water at wavelengths greater than 300 nm (U.S. EPA., 2003: online). In this study, the atrazine solution was prepared by using deionized water as a solvent, and the pH of the solution was its natural pH, approximately 4.7 to 5.6, which had no adjustment with HCl and NaOH. From Figure 4.31 (a), no atrazine concentration tended to decrease from the initial concentration. The concentration seemed to remain steady throughout 60 min of irradiation. The direct atrazine photodegradation was probably not observed since the atrazine absorptivity presented in only the UV range from 195 to 290 nm, as shown in Figure 4.32. The absorption spectrum of atrazine from this study also associated with other reports (McMurray et al., 2006; Parra et al., 2004). In addition, it was nonequivalent to the wavelength range of the tungsten lamps ($\lambda > 400$ nm), in Figure 4.33, used in the experiment.

The Figures 4.31 (a), (b), and (c) also showed the adsorption of atrazine over catalyst powder and catalyst beads. It was likely that atrazine was hardly removed under dark condition with catalysts. Atrazine still remained in the bulk solution upon the accomplishment of adsorption/desorption through 60 min for ZnO and 360 min for 0.02Ce-ZnO (S) and 0.02Cu-ZnO (S). In terms of the interaction between catalyst's surface and atrazine molecules, the functional groups of the atrazine could involve in H-bonding, van der Waals interaction, and ligand exchange (Spark and

Swift, 2002). However, overall polarity of atrazine structure was quite low which caused retrogression of H-bonding potential. In addition, the low polar molecule was more unlikely to move closer to the charged surface of catalysts decreasing the occurrence of van der Waals interactions. Therefore, the atrazine adsorption over catalyst powders and beads was probably negligible in this study. The result was consistent with Parra et al. (2004) who found the relatively weak adsorption of atrazine in AFM images although the atrazine adsorption over TiO_2 presented the sharp rise under the initial concentration 0.08 mmol/L. The rising of adsorption corresponded to the transition behavior from a monolayer to a multilayer adsorption. Furthermore, from their AFM images, atrazine was rarely adsorbed or chemisorbed. The molecules already adsorbed seemed to move around and were localized in certain regions for possible crystallization.

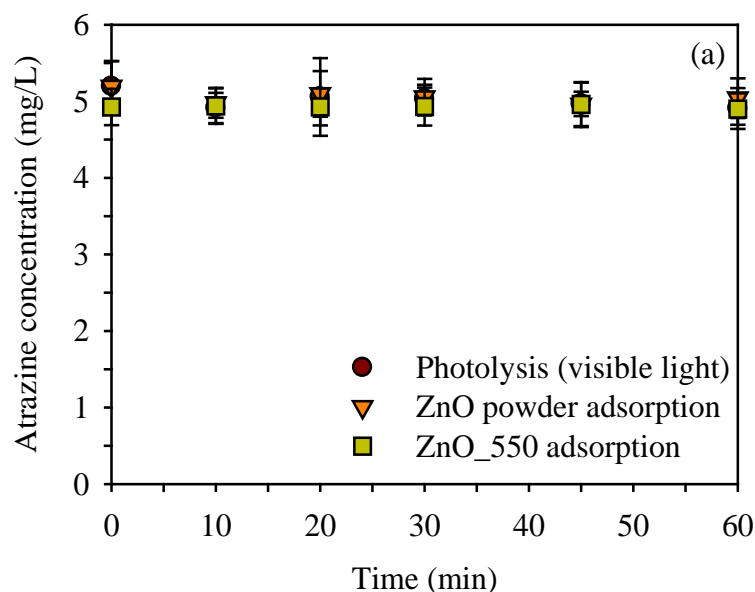


Figure 4.31 Atrazine concentrations as a function of time on (a) atrazine photolysis under visible light irradiation and atrazine adsorption on ZnO powder and ZnO_550 under dark condition.

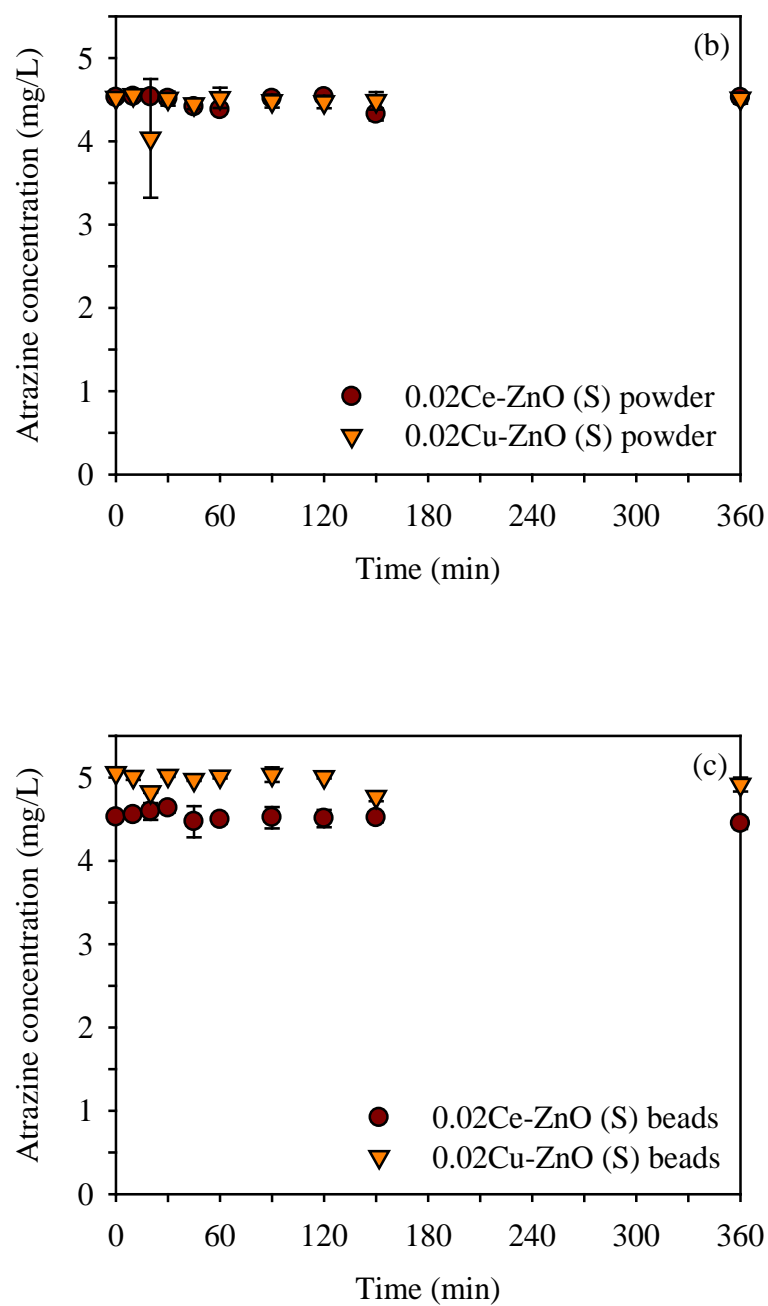


Figure 4.31 Atrazine concentrations as a function of time on atrazine adsorption under dark condition by (b) the prepared catalyst powders and (c) the prepared catalyst beads.

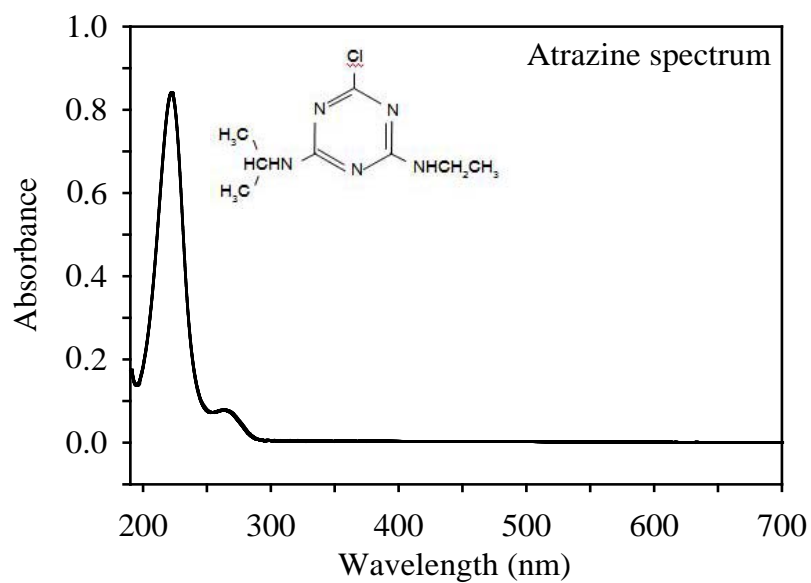


Figure 4.32 Absorption spectrum of atrazine over 190 to 700 nm measured by UV-vis spectrometer.

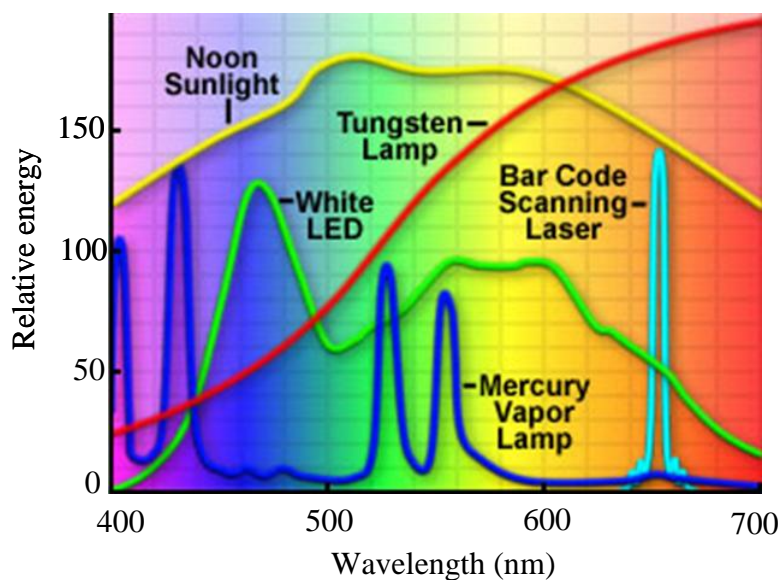


Figure 4.33 Spectra from common sources of visible light focused on the tungsten lamp (Spring and Davidson, 2009: online).

4.2.2 Effect of transition metal dopants and molar ratio of doping

Previously in 4.1.2.2, photocatalytic activity of Ce-ZnO prepared via the simple chemical method using different templates; sticky rice starch (S), and polyvinylpyrrolidone (P), was studied. The portion of metal and template used for catalyst preparing was 1: 2. It was found that Ce-ZnO (S) presented the higher percent removal, at 2 hr and IEP, than Ce-ZnO (P). Besides, the molar ratio of cerium nitrate and zinc nitrate significantly indicated that the percent removal of Ce-ZnO with the molar ratio of 0.02 was superior to that of 0.1. It was very probable that the route of catalyst preparation, type and amount of templates, and amount of cerium dopant affect the characteristics of catalysts and consequently improve or discard the activity of the catalysts.

To investigate further, cerium and copper were selected as dopants for ZnO. With cerium, it was supposed to help in providing of oxygen vacancies and stability (Mohammadi and Fray, 2010; Xu et al., 2008). The copper was considered to prevent the electron-hole recombination (Xin et al., 2008) and lower the band gap energy of catalyst (Navas et al., 2011; Roguska et al., 2010; Vidyasagar et al., 2011). On effect of dopants, it was likely that Ce-ZnO had higher ability to degrade atrazine than Cu-ZnO as illustrated in Figures 4.34 (a) and (b). For Cu-ZnO in Figure 4.34 (b), at any molar ratio of copper nitrate and zinc nitrate, there was no greatly difference between four catalysts at any irradiation time. Although the light absorption capacity in the range of visible was quite high, the low activity and selectivity of Cu-ZnO in atrazine degradation might be the reasons of this result. In Figure 4.34 (a), the ratio of zinc nitrate to sticky rice starch of 5:1 influenced better activity of catalyst than that of 10:1 which was probably due to the distribution of cerium and zinc ions on the sticky rice starch template, and the crystallization of Ce-ZnO while the metal oxide was formed. The distribution of the ions and crystallization of the catalyst consequently provided the dissimilarity of crystalline size and specific surface area of the catalysts. By molar ratio of doping, the surface area of 0.02Ce-ZnO (S) 5:1 and 0.1Ce-ZnO (S) 5:1 were quite different as shown in Table 4.10. The percent removal of atrazine throughout 120 min with 0.02Ce-ZnO (S) 5:1 was superior as presented in Table 4.11. This result was also relative to the former result in Figure 4.30.

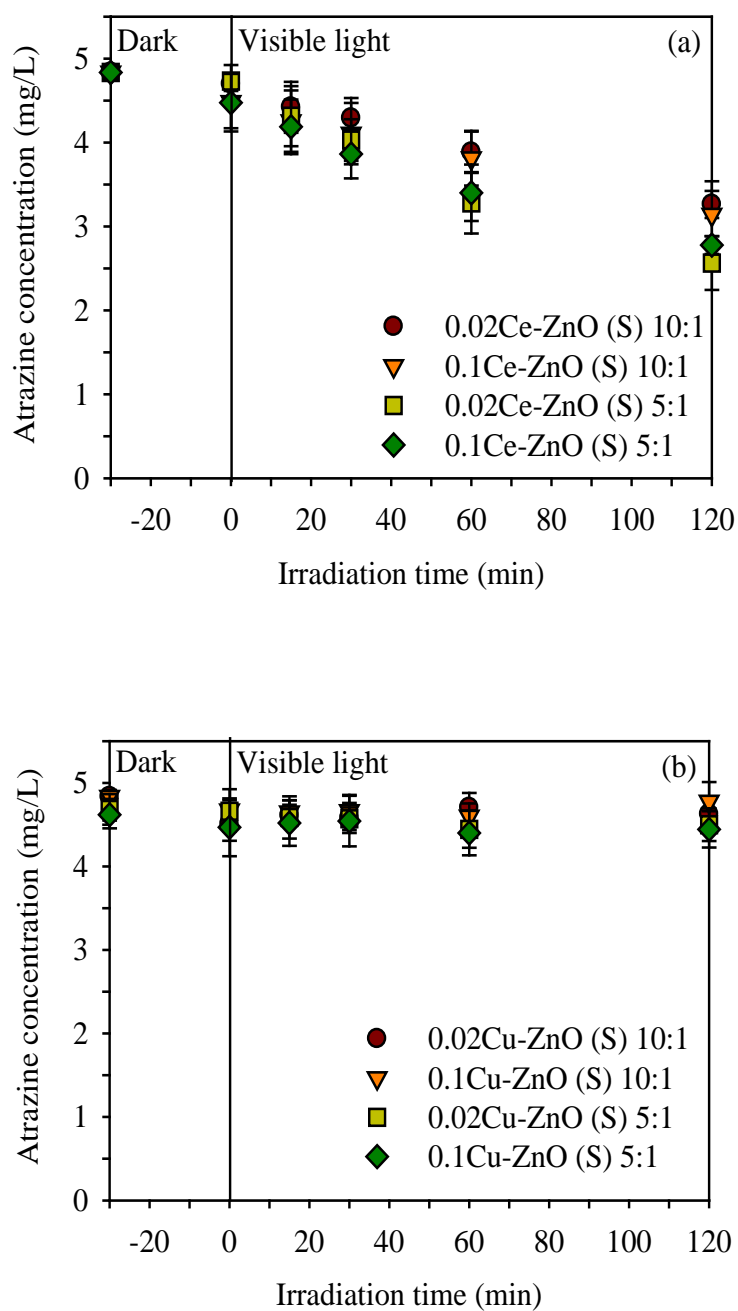


Figure 4.34 Photocatalytic degradation of atrazine by (a) Ce-ZnO and (b) Cu-ZnO in powder form at different molar ratios.

Table 4.10 BET surface areas of catalysts prepared with the weight ratio $\text{Zn}(\text{NO}_3)_2 \cdot 6\text{H}_2\text{O}$ to sticky rice starch (S) of 5:1.

Catalyst	BET surface area (m^2/g)
0.02Ce-ZnO (S) 5:1	15
0.1Ce-ZnO (S) 5:1	19

Table 4.11 Percent removal of atrazine by using 0.02Ce-ZnO (S) 5:1 and 0.1Ce-ZnO (S) 5:1.

Irradiation time (min)	Removal (%)	
	0.02Ce-ZnO (S) 5:1	0.1Ce-ZnO (S) 5:1
0	0.000	0.000
15	8.742	6.420
30	14.825	13.640
60	30.706	24.015
120	45.916	37.742

4.2.3 Effect of catalyst loading

The reactor geometry is the important determinant which influences the condition in the system. Not only the particularities of reactor setup but also the nature of the compounds and the characteristic of the catalysts largely cause the differences in the optimum of studied parameters. The amount of catalyst is the parameter that has often been firstly studied by many works (Behnajady et al., 2006; Evgenidou et al., 2005; McMurray et al., 2006; Pare et al., 2008; Parra et al., 2004). Generally, for TiO_2 Degussa P25 in slurry photocatalytic process, the optimal amount was 0.10 to 5.00 g/L (Parra et al., 2004).

In this work, ZnO and metal doped ZnO catalysts were studied. The catalyst loading was varied from 0.10 to 0.90 g and 2.50 to 7.50 g per 100 mL of the atrazine solution in case of ZnO powder and ZnO_550 bead, respectively. The detection limit of atrazine under the HPLC condition in this study being 0.1 mg/L was marked. As shown in Figure 4.35 (a), almost 100 percent of atrazine removal at 120 min of irradiation appeared for all ZnO powder loadings. However, the highest percent

removal per catalyst weight-time at initial radiation time (15 min) was given to the loading of 0.1 g ZnO powder (26.397%/g-min) as illustrated in Table 4.12. Therefore, the catalyst loading for ZnO powder was optimized at 0.10 g per 100 mL of the atrazine solution. The optimal amount of ZnO powder was as same as the one of TiO₂ powder (1.00 g/L) for atrazine degrading studied by Parra et al., 2004. As the ZnO powder amount increased, the number of active sites on the ZnO surface would be increased due to the enlargement of the surface area. This incident raised the number of hydroxyl and superoxide radicals generating by light penetration for destruction of atrazine molecules. However, the percent removal decreased due to an increase in the turbidity of the suspension and a decrease in the light penetration resulting in an increase of scattering effect (Behnajady et al., 2006).

In Figure 4.35 (b), at initial irradiation time, little higher atrazine removal presented when the amount of catalyst bead, ZnO_550, increased. From Table 4.12, the optimal catalyst loading of ZnO_550 was 2.50 g per 100 mL of atrazine solution since it granted the highest percent removal per catalyst weight-time (0.133%/g-min). In the case of the catalyst bead, the scattering effect was highly likely to be unimportant because ZnO was immobilized. However, when the amount of ZnO increased until it reached the balance between the numbers of catalyst's active site and the numbers of atrazine molecule, the increase of catalyst might be unable to urge the photocatalytic reaction resulting in the atrazine removal. Moreover, the immobilization became the factor reducing the interactive opportunities of ZnO and atrazine.

The effect of change in the amount of the 0.02Ce-ZnO (S) 5:1 and 0.02Cu-ZnO (S) 5:1 were performed in the range of 0.10 to 0.50 g in the powder form and 1.00 to 5.00 g in the bead form per 100 mL of the atrazine solution. In Figures 4.36 (a) and (b), the 0.02Ce-ZnO (S) 5:1 powder loading of 0.10 g (4.344%/g-min) and its bead loading of 5.00 g (0.020%/g-min) were the optimal amount. Although the absorbance capacity in visible light range from UV-vis-DR and the surface area of 0.02Ce-ZnO (S) 5:1 were higher, the efficiency of the 0.02Ce-ZnO (S) 5:1 for degrading atrazine was inferior compared to that of commercial ZnO. It is very

interesting to unveil this doubt, and more work is needed in this regard. In Figures 4.37 (a) and (b), the powder and the bead of 0.02Cu-ZnO (S) 5:1 presented incapacity in all loadings due to the reason as introduced in 4.2.2.

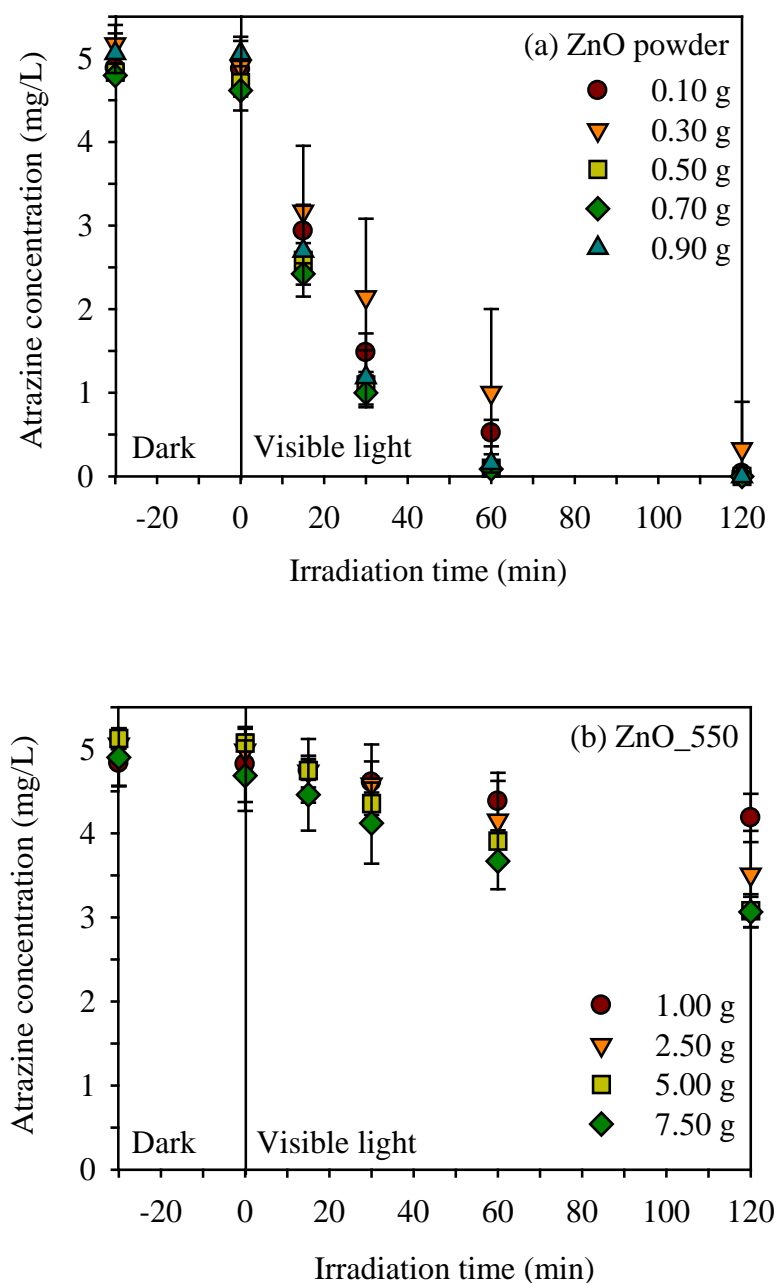


Figure 4.35 Photocatalytic degradation of atrazine by (a) ZnO powder and (b) ZnO_550 at different catalyst weights.

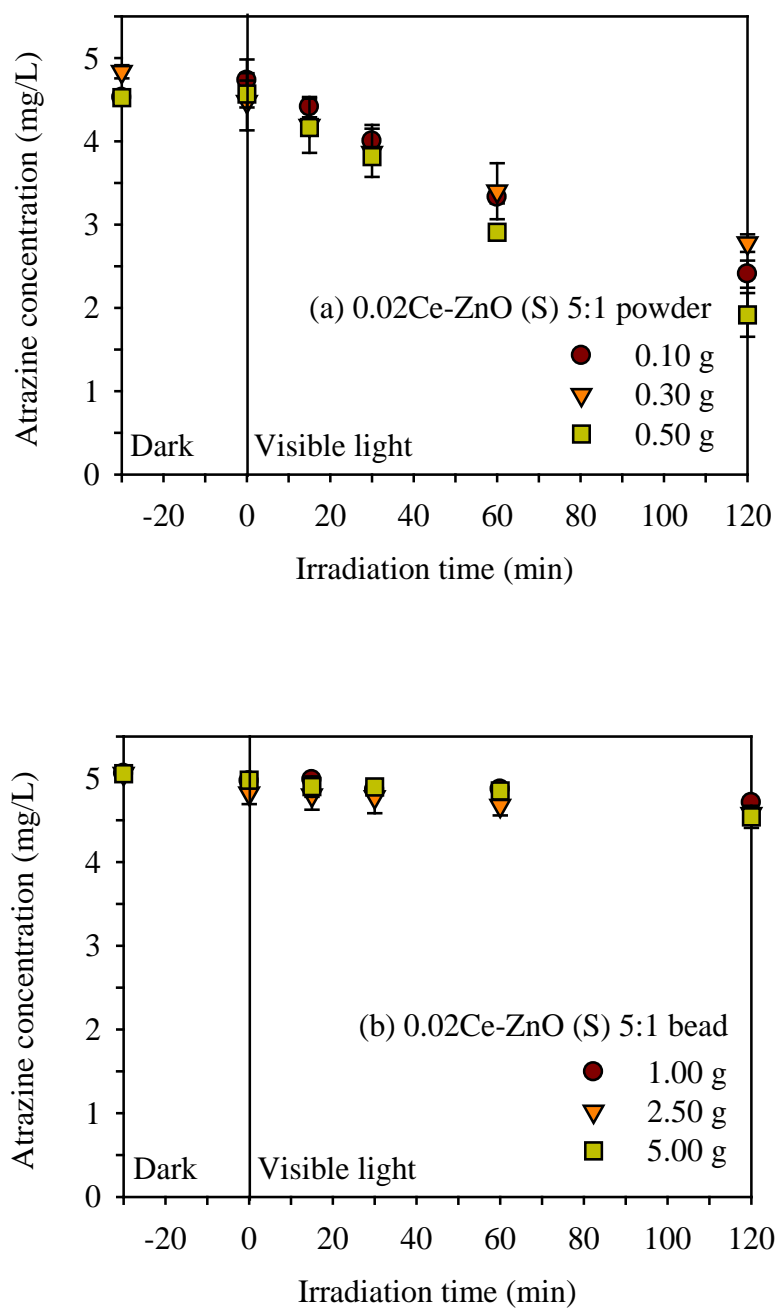


Figure 4.36 Photocatalytic degradation of atrazine by (a) 0.02Ce-ZnO (S) 5:1 powder and (b) 0.02Ce-ZnO (S) 5:1 beads at different catalyst weights.

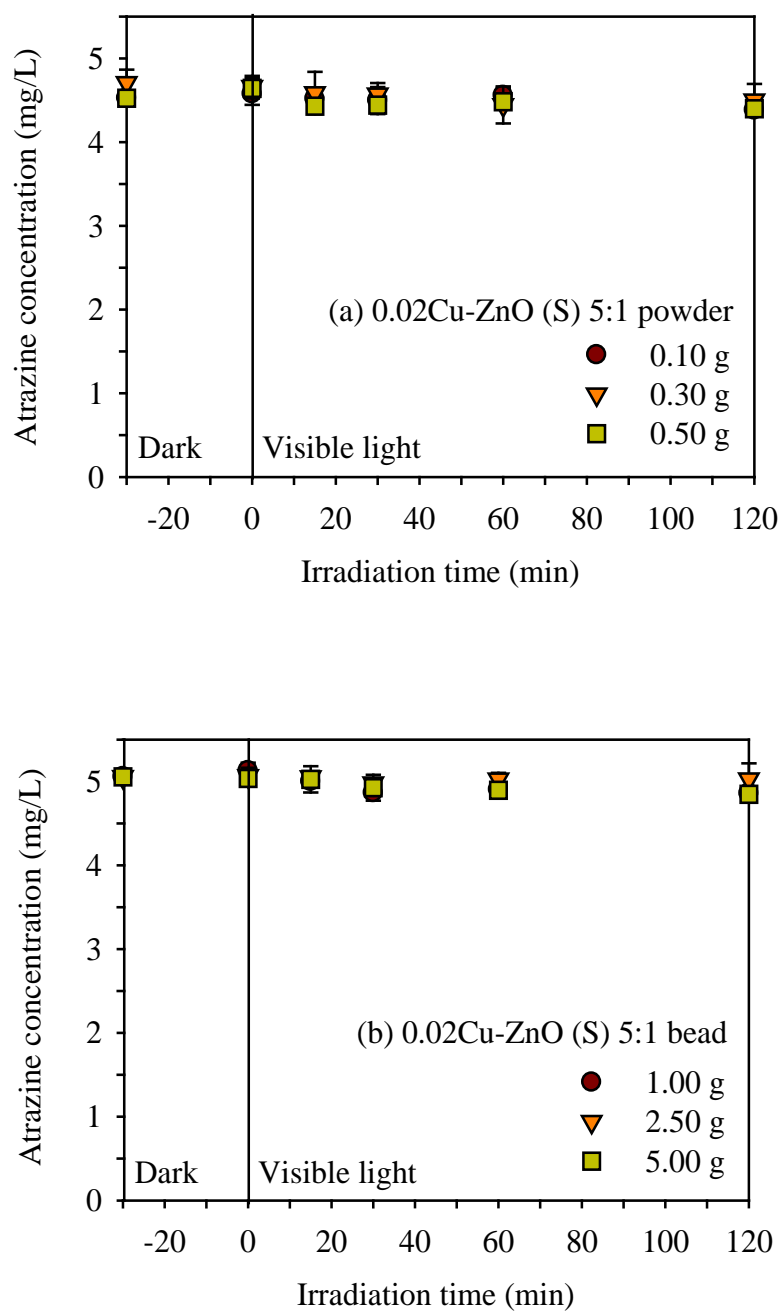


Figure 4.37 Photocatalytic degradation of atrazine by (a) 0.02Cu-ZnO (S) 5:1 powder and (b) 0.02Cu-ZnO (S) 5:1 beads at different catalyst weights.

Table 4.12 Percent removal of atrazine per catalyst weight-time by using ZnO powder and ZnO_550 at initial time of irradiation (15 min).

ZnO powder		ZnO_550	
Catalyst loading (g/100 mL of atrazine)	Removal of atrazine/catalyst weight-time (%/g-min)	Catalyst loading (g/100 mL of atrazine)	Removal of atrazine/catalyst weight-time (%/g-min)
0.10	26.397	1.00	0.099
0.30	7.630	2.50	0.133
0.50	6.013	5.00	0.086
0.70	4.523	7.50	0.043
0.90	3.465		

4.2.4 Effect of pH

Efficiency of the photocatalytic degradation of atrazine depended on initial pH of the solution in the system (Parra et al., 2004). The pH influenced the surface charge of catalyst particles comprising the catalyst's supporter and ionization state of ionizable organic compounds (Liu et al., 2009). Based on the surface charge of ZnO analyzed by zeta-potentiometer, the IEP for ZnO, the pH at which the surface of ZnO was uncharged, was 9.00. Above and below this value, ZnO was negatively and positively charged, respectively. The pK_a 1.68 of atrazine expressed the unionization of its molecule at pH above the pK_a .

In Figure 4.38 (a), pH of the atrazine solution was varied in pH 3.99, 4.89 (no adjusted pH), 6.92, and 8.49. Four pH values encouraged the negative charge on the ZnO powder surface and the uncharged atrazine molecule. Thus, there was no electrostatic attraction or repulsion occurred between ZnO and atrazine resulting in similarity of atrazine degradation trend at all pH. It also happened in the ZnO bead, ZnO_550, as presented in Figure 4.38 (b). However, the atrazine degradation by ZnO_550 increased at pH 8.84 (39.97% at 120 min) due to van der Waals force at pH which was close to the IEP of ZnO.

Likewise, the atrazine degradation by 0.02Ce-ZnO (S) in 4.1.2.2 resulted the higher percentage at IEP (11.54% at 120 min). Despite the fact, it should be noted that the low degradation of atrazine at acidic pH was due to dissolution of ZnO (Ali, Bakar, and Teck, 2010; Wang H. et al., 2007) since it was amphoteric in nature. At below pH 4, ZnO could react with acid to produce the Zn^{2+} (Behnajady et al., 2006; Gaya et al., 2009) and the corresponding salt (Evgenidou et al., 2005; Parra et al., 2008).



At alkaline pH, ZnO could react with base to form complexes like $[Zn(OH)_4]^{2-}$ (Evgenidou et al., 2005; Pare et al., 2008) and was possible to be $[Zn(OH)_2]^{2+}$ from alkalinedissolution (Gaya et al., 2009).



The photocatalysis might be carried on in alkaline condition due to the excess of OH^- which facilitated photogeneration of $\bullet OH$ (Behnajady et al., 2006). Further experiments were performed at the natural pH of atrazine aqueous solution which was around 4.59 to 5.61.

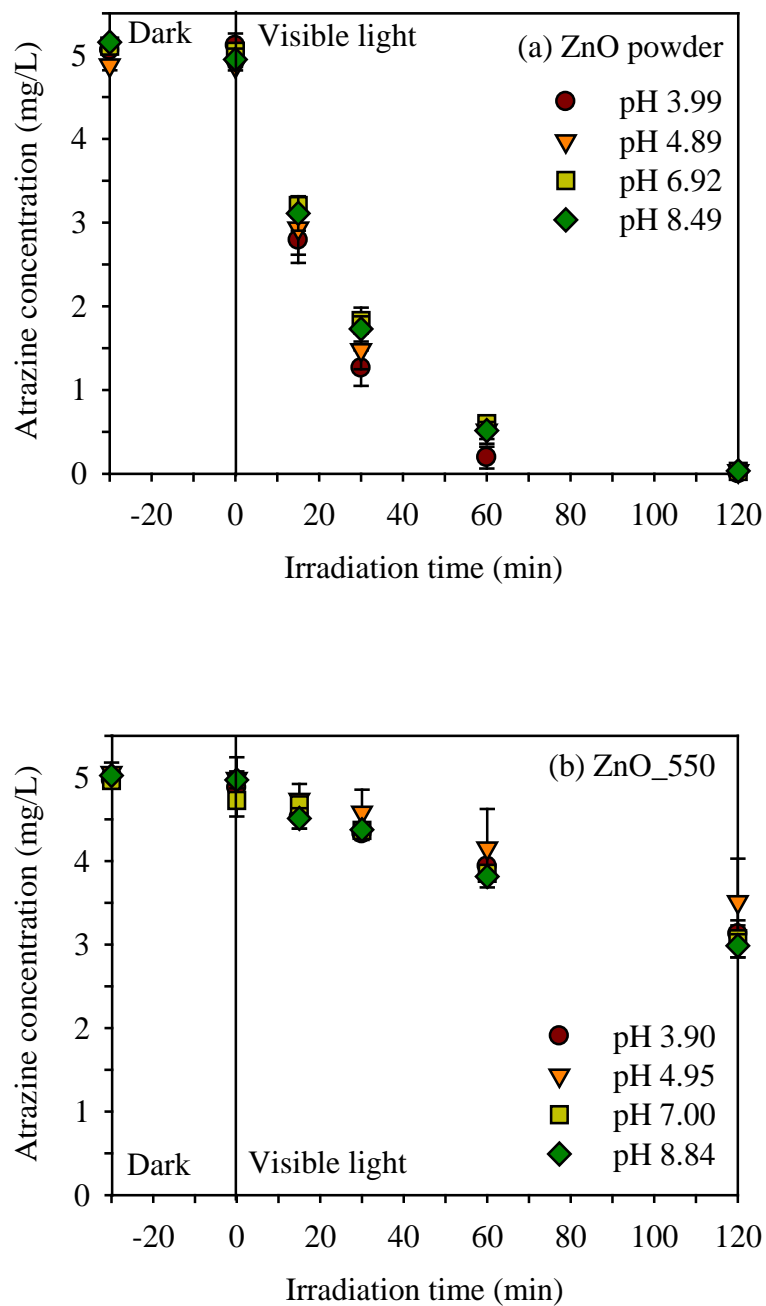


Figure 4.38 Photocatalytic degradation of atrazine by (a) ZnO powder and (b) ZnO_550 at different pH.

4.2.5 Effect of atrazine initial concentration

Atrazine concentration is regulated at extremely low level in water for example ppb class with the maximum contaminant level allowed by the United States Federal Drinking Water Standard for atrazine is 3 $\mu\text{g/L}$ (U.S. EPA., 2003: online). To study the photocatalytic degradation at such low level requires extremely sensitive analytical method. The HPLC method for atrazine detection was incapable to measure atrazine at such low level without pre-concentration (McMurray et al., 2006). Therefore, the concentrations of 1.0 to 10.0 mg/L atrazine were used at their natural pH in this experiment. The detection limit of the HPLC was 0.1 mg/L.

The initial concentration of atrazine solution on photocatalytic degradation is the important effect. In Figures 4.39 (a) and (b), the percent photodegradation decreased with increasing of atrazine initial concentration. From Figure 4.39 (a) in case of ZnO powder, atrazine removal proceeded in a shorter time at lower concentration since there were more available active sites on ZnO surface comparing to the number of atrazine molecules. Conversely, the high atrazine concentrations were rapidly removed at initial irradiation time. As the initial concentration was high, many atrazine molecules were adsorbed on the ZnO surface under darkness. When the reaction was immediately progressed after the lights were turn on, the adsorbed atrazine would be attacked by $\text{O}_2\bullet$ and $\bullet\text{OH}$. Because the atrazine solution was transparent, the $\text{O}_2\bullet$ and $\bullet\text{OH}$ radicals could be normally generated at the ZnO surface under high concentration of atrazine without the problem of light penetration as happened in the high concentrations of dyes (Behnajady et al., 2006; Pare et al., 2008). In case of ZnO_550 bead as shown in Figure 4.39 (b), atrazine was hardly removed and unable to be totally degraded at all initial concentrations which were probably caused by smaller surface area comparing to ZnO powder.

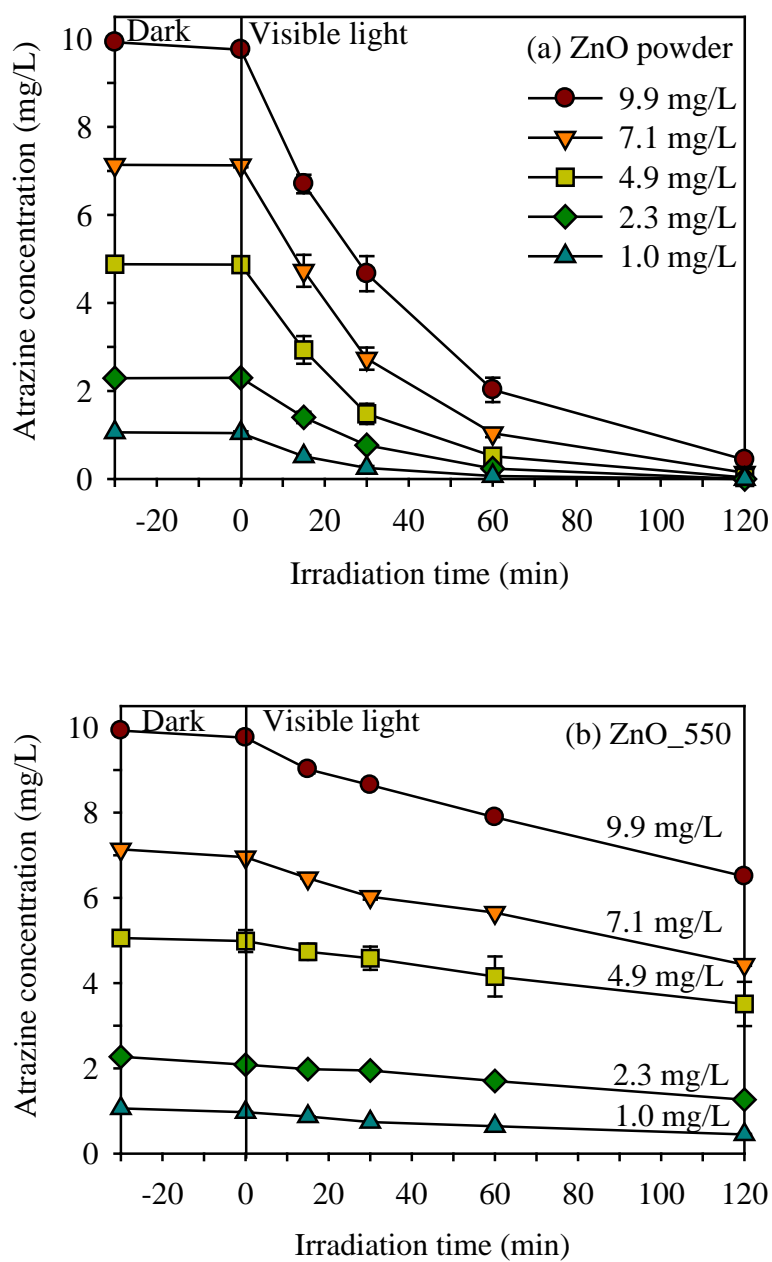


Figure 4.39 Photocatalytic degradation of atrazine by (a) ZnO powder and (b) ZnO_550 using varied initial concentrations of atrazine.

4.2.6 Surface passivation

Surface passivation was studied to assure if catalyst coated on the bead support could be eroded into atrazine solution while the photocatalytic reaction was performed under its natural pH. When catalyst underwent the passivation, the photocatalytic reaction may be interrupted, and the dissolved ions could harm the organisms living in water after the treatment process. The protection provided against passivation mainly depends on the thickness, the structure, the electronic properties, the porosity, and the adhesion of the coating (Spathis and Poullos, 1995).

With preliminary measurement, Figure 4.40 presents the electrical conductivity (σ) of the atrazine in the presence of catalyst beads. Electrical conductivity is a measure of the ability to conduct an electric current depending on concentration of ions, specific nature of the ions, and temperature of solution. Under regular condition, without adding additives or pH adjustment, σ of atrazine solution was 0 $\mu\text{S}/\text{cm}$ before running reaction. After 30 min of adding the catalyst beads for under darkness, σ of atrazine solution rose to 73, 126, and 182 $\mu\text{S}/\text{cm}$ for ZnO_550, 0.02Ce-ZnO (S) 5:1, and 0.02Cu-ZnO (S) 5:1, respectively. When photocatalytic reaction was proceeding, σ of atrazine solution slightly increased through 120 min. It indicated that ions from the beads would discharge into atrazine solution.

To study further, Zn element in atrazine solution were measured by flame atomic absorption spectrometry (AAS) (Varian AA 280 FS) at 60 and 120 min of irradiation time compared with initial time. As a result, Zn is found in all runs as shown by Figure 4.41. Zn concentrations are low, little higher, and much higher for ZnO_550, 0.02Ce-ZnO (S) 5:1, and 0.02Cu-ZnO (S) 5:1, respectively. It was obvious that Zn concentration trend related to electrical conductivity of each catalyst.

However, the discharged Zn might be acceptable since it was still lower than 5 mg/L of Zn amount in National Secondary Drinking Water Regulations (NSDWRs or secondary standards) (U.S. EPA, 2011: online). The little loss of ZnO under irradiation collected by ICP-OES for ZnO dissolution was reported in other study (Gaya et al., 2009). In addition, it was noted that none of Ce and Cu elements was

measured because the Ce and the Cu were filled in very small amount in the catalyst preparation. Reported by Wang, Wick, and Xing (2009), the Al_2O_3 also had the lower dissolution with solubility of 0.39 and 0.38 mg/L at 96 hr for 407.8 mg/L nanoparticulate and bulk Al_2O_3 , respectively. Therefore, it was generally considered to have low solubility.

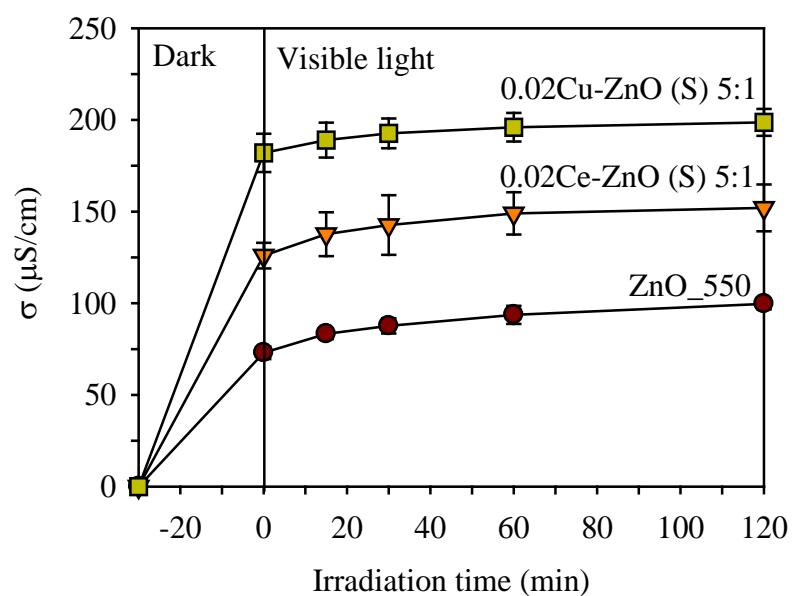


Figure 4.40 Electrical conductivity of photocatalytic degradation of atrazine solution as a function of irradiation time in the presence of ZnO_550, 0.02Ce-ZnO (S) 5:1, and 0.02Cu-ZnO (S) 5:1.

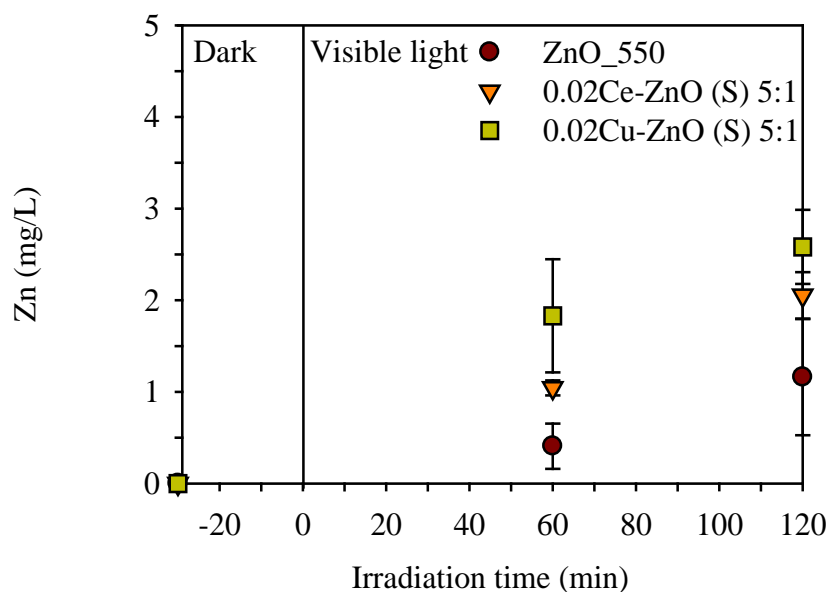


Figure 4.41 Zn element concentrations of photocatalytic degradation of atrazine solution as a function of irradiation time in the presence of catalysts.

4.2.7 Effect of ionic strength

Organic pollutant and inorganic ions existing together in real water could affect the photocatalytic reaction performance. The type and concentration of ion contained in the water provide various ionic strength values. The effect of ionic strength in photocatalytic degradation of atrazine using ZnO_550 was investigated. Each sodium salt being Na₂SO₄, NaCl, Na₂CO₃, NaHCO₃, or Na₂HPO₄ with concentrations of 0.000, 0.002, 0.006, and 0.010 mol/kg was added into the atrazine solution to gain different ionic strengths. It was noted that the atrazine solution was prepared by using deionized water. The ionic strength was calculated by using the following equation (Mortimer, 1993).

$$I = \frac{1}{2} \sum_{i=1}^s m_i z_i^2 \quad (4.4)$$

where I = the ionic strength

m_i = the molality of species i (kg/mol)

z_i = its valence (number of proton charge per ion)

s = the different charged species

The electrical conductivity (σ) of the mixture was conducted to confirm the ionic strength. The adsorption and the photocatalytic reaction involved in atrazine photocatalytic degradation were determined by atrazine concentration measurement. The σ of atrazine solution in presence of Na_2SO_4 is provided in Figure 4.42 (a). Before running reaction, the σ of the mixture without ZnO_550 increased with the increasing of the ionic strength from Na_2SO_4 . After running reaction, the σ of the mixture was slightly higher than that before running reaction. The change was approximately 55 to 81 $\mu\text{S}/\text{cm}$. This would respond to surface passivation of ZnO_550 occurring in the mixture. In Figure 4.43 (a), the σ of NaCl in atrazine solution also presented the similar trend with that of Na_2SO_4 . It was interesting that the σ change of atrazine solution with NaCl between before and after running reaction (60 to 169 $\mu\text{S}/\text{cm}$) was rather higher than that of atrazine solution with Na_2SO_4 and much higher than that of atrazine solution in the surface passivation test.

It was reported that the ionic strength affected the adsorption capacity and adsorption mechanism of TiO_2 in photocatalytic degradation of 4-chlorobenzoic acid in water (Doinysiou et al., 2000). Increasing of ionic strength by KNO_3 in the solution decreased the 4-chlorobenzoic acid adsorption capacity on the TiO_2 surface. As a result, higher initial concentration of 4-chlorobenzoic acid at the end of dark phase was obtained. This possibly produced at different reaction rates. The photocatalytic degradation of atrazine with the ionic strength from Na_2SO_4 is shown in Figure 4.42 (b). In contrast to the result of Doinysiou et al. (2000), the presence of ionic strength from Na_2SO_4 improved the atrazine adsorption on ZnO_550 and eventually enhanced the photocatalytic reaction of ZnO_550. At the end of dark adsorption phase, atrazine was more adsorbed at the lower concentration of Na_2SO_4 but less adsorbed at the higher concentration of Na_2SO_4 . These were due to the attraction between Zn^{2+} and SO_4^{2-} at high ionic strength of the solution resulting to lower adsorption ability of atrazine onto ZnO_550. However, the higher ionic strength from Na_2SO_4 largely

enhanced the photocatalytic reaction of ZnO_550 in the light phase. Atrazine removal in free ion condition after 120 min of irradiation time is 30.72% which was lower than adding Na₂SO₄ (41.19 to 50.33%). Obviously, the higher ionic strength of Na₂SO₄ finally presents the much higher of atrazine photocatalytic degradation. This trend also happened in the presence of NaCl (41.48 to 46.30%) as revealed in Figure 4.43 (b). Therefore, the increasing of ionic strength could enhance the photocatalytic performance in these two cases due to the type and concentration of ion leading to influence or change the adsorption and photocatalytic reaction mechanism.

In the other hand, the results in Figures 4.44 (b), 4.45 (b), and 4.45 (b) confirmed that the increasing of ionic strength by some ions could retard the photocatalytic degradation of atrazine. The adsorption ability of ZnO_550 was improved by Na₂CO₃ while that was dropped by NaHCO₃, and Na₂HPO₄. With the presence of Na₂CO₃, NaHCO₃, or Na₂HPO₄, atrazine removal was gradually inhibited with the increasing of ionic strength from the sodium salt through 120 min of irradiation time. In Figure 4.44 (a), it was suspicious that the σ of atrazine solution with Na₂CO₃ at all ionic strength values decreased after running reaction as similar as that with Na₂HPO₄ at 0.006 and 0.010 mol/kg as shown in Figure 4.46 (a). Although the σ was supposedly increased by ZnO_550 surface passivation, it was likely that there was a strong interaction between Zn²⁺ and CO₃²⁻ or Zn²⁺ and HPO₄²⁻ at the surface of ZnO_550. This might be the reason of decreasing of the σ after running reaction. The fluctuation of the σ changing under different ionic strength before and after running reaction remains the serious explanation that requires extensive effort in future work.

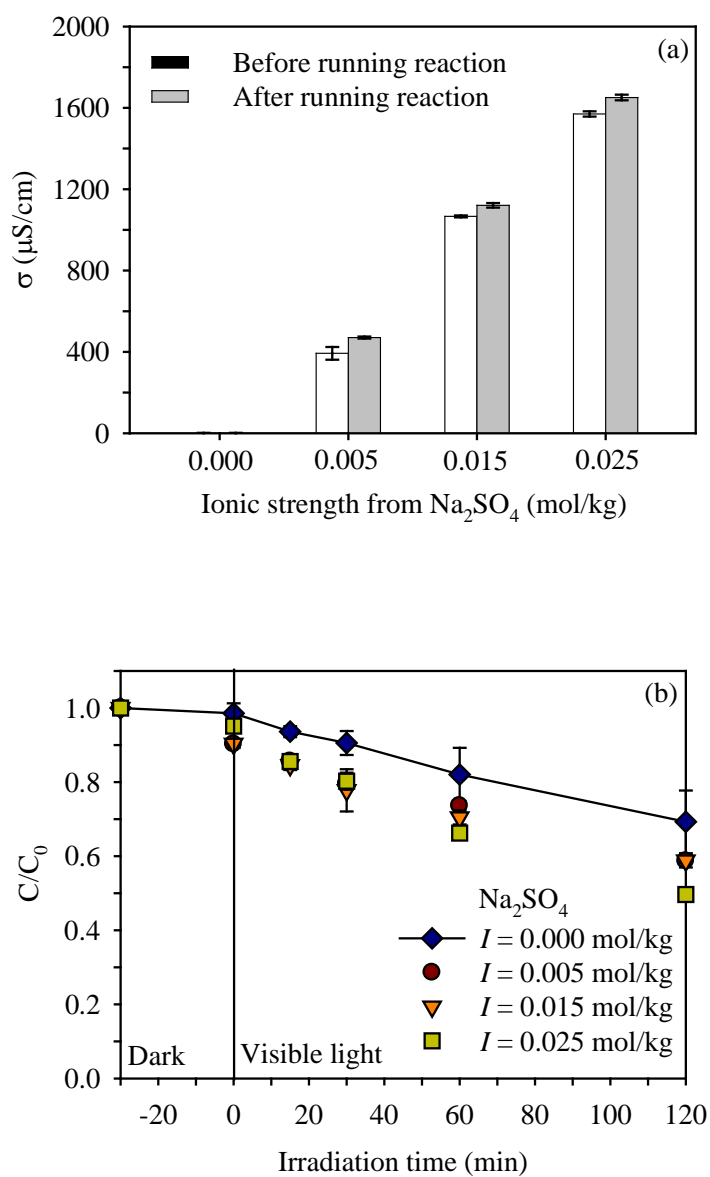
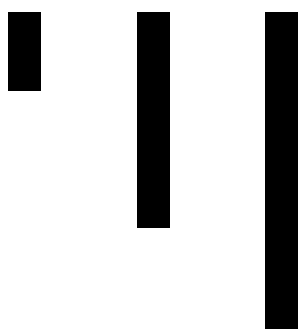


Figure 4.42 Effect of Na_2SO_4 ionic strength on (a) electrical conductivity of atrazine solution and (b) the photocatalytic degradation of atrazine using ZnO_{550} .



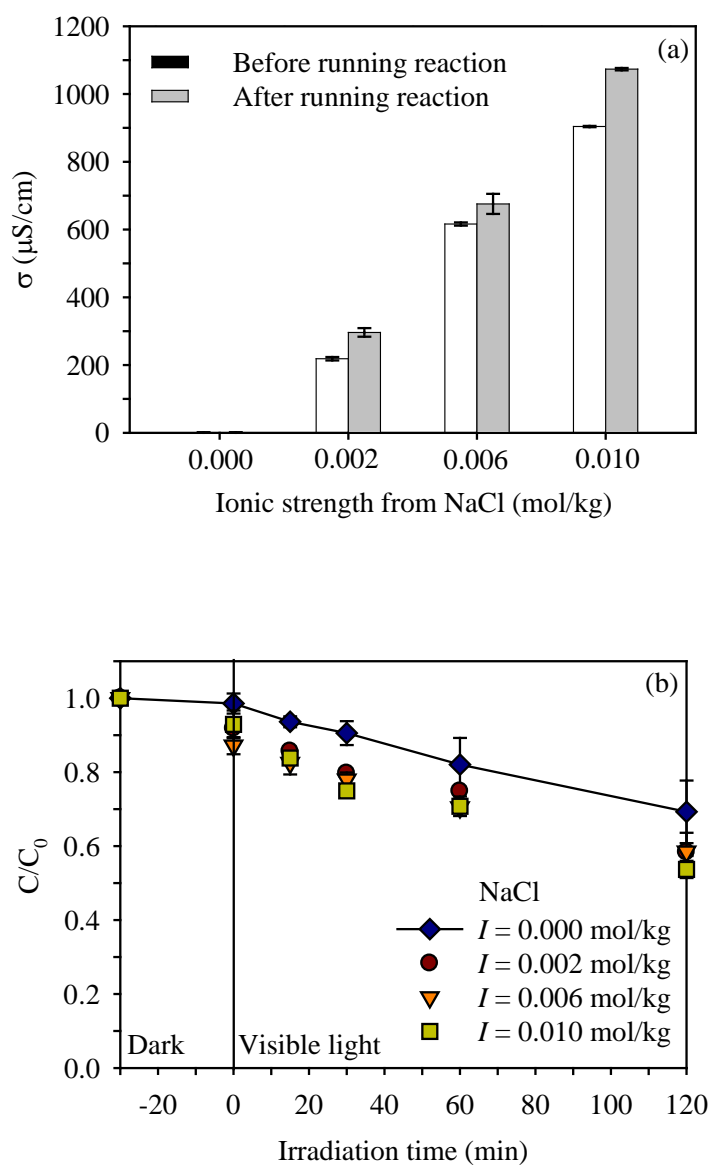
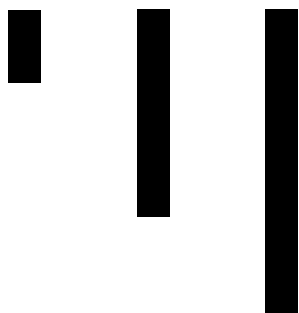


Figure 4.43 Effect of NaCl ionic strength on (a) electrical conductivity of atrazine solution and (b) the photocatalytic degradation of atrazine using ZnO₅₅₀.



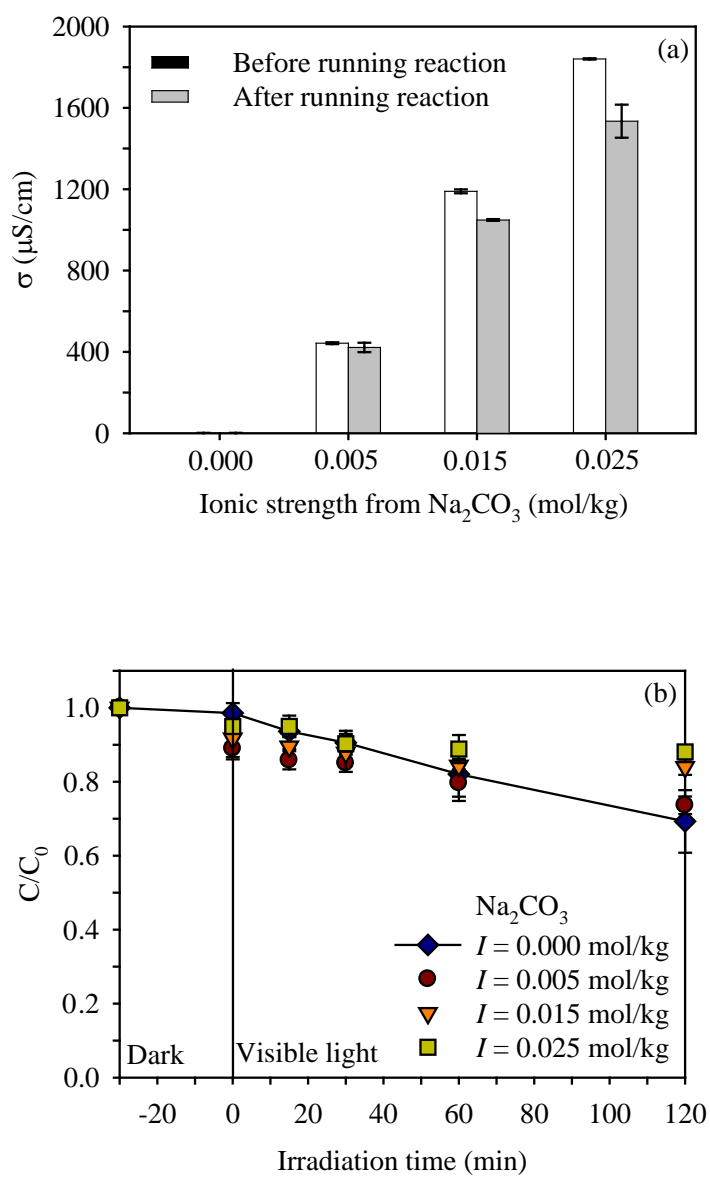
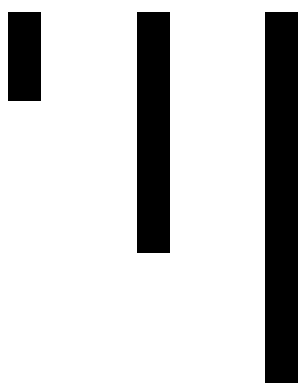


Figure 4.44 Effect of Na_2CO_3 ionic strength on (a) electrical conductivity of atrazine solution and (b) the photocatalytic degradation of atrazine using ZnO_{550} .



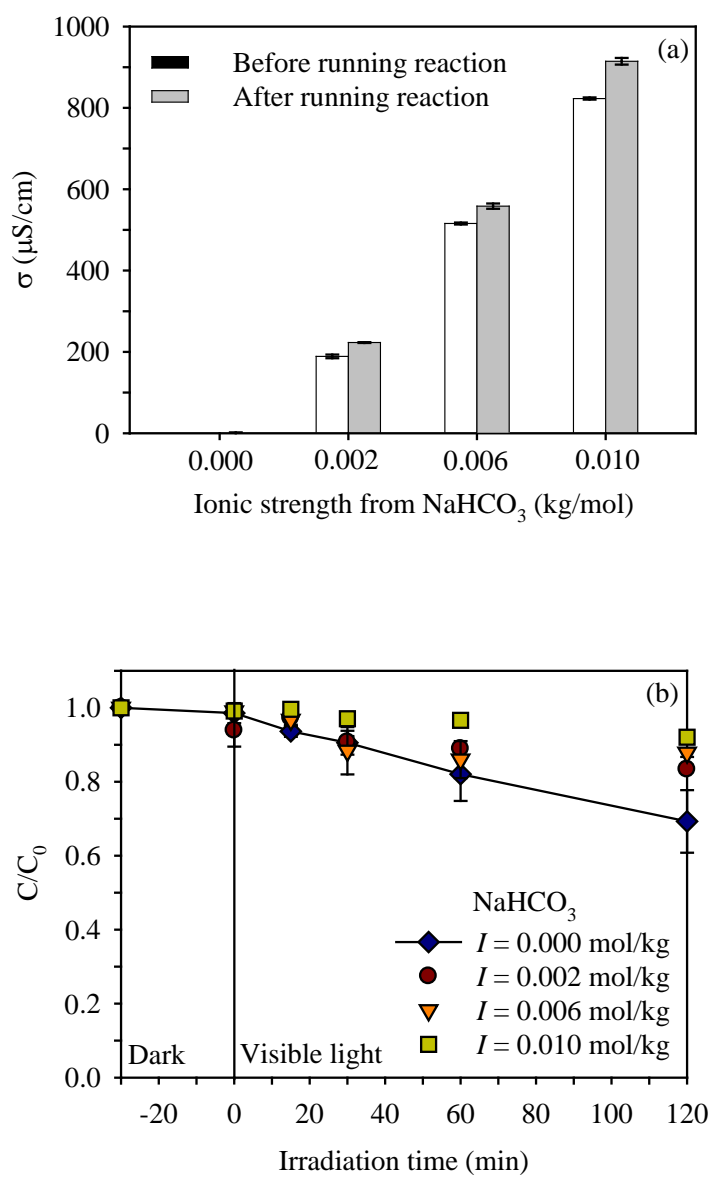


Figure 4.45 Effect of NaHCO_3 ionic strength on (a) electrical conductivity of atrazine solution and (b) the photocatalytic degradation of atrazine using ZnO_{550} .

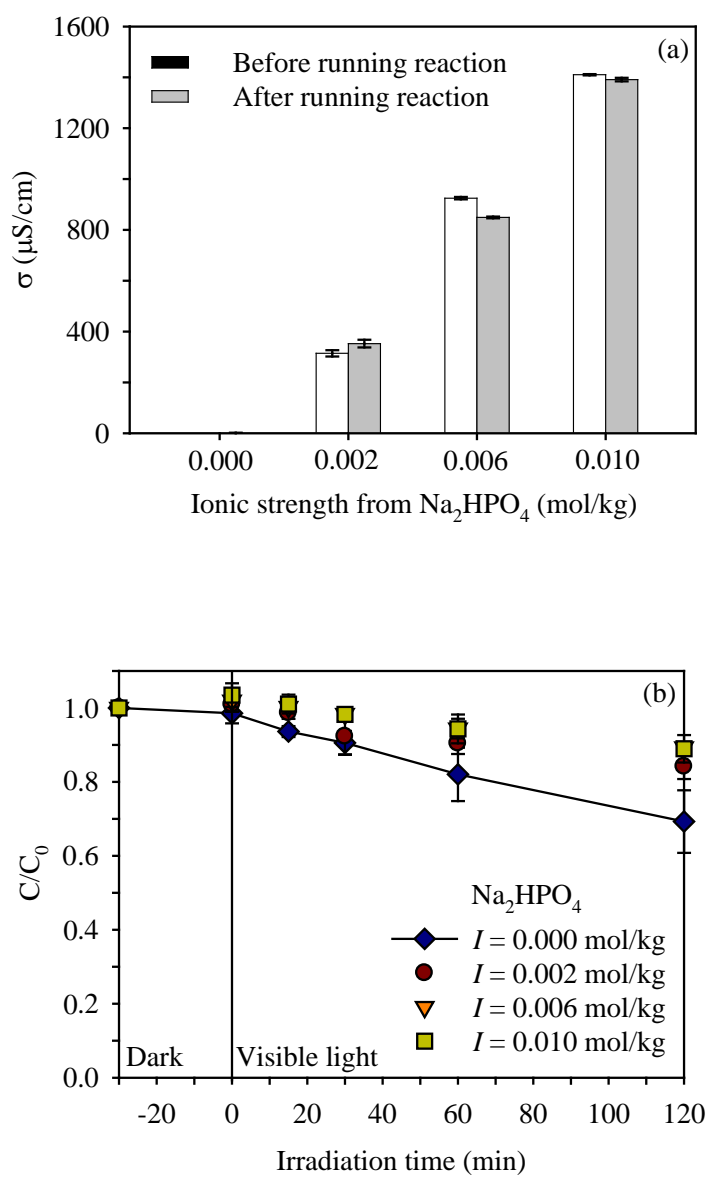
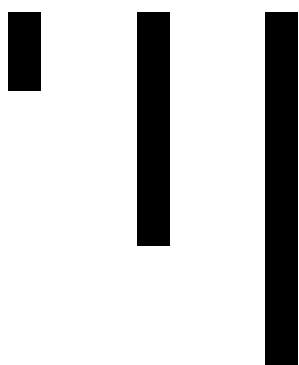


Figure 4.46 Effect of Na_2HPO_4 ionic strength on (a) electrical conductivity of atrazine solution and (b) the photocatalytic degradation of atrazine using ZnO_{550} .



4.2.8 Effect of anions

From the effect of ionic strength study, it was clear that the photocatalytic degradation efficiency considerably depended on the addition of inert salts like Na_2SO_4 , NaCl , Na_2CO_3 , NaHCO_3 , and Na_2HPO_4 . Based on the same concentration of the sodium salt (0.010 mol/kg), the effect of anions on the photocatalytic degradation of atrazine using ZnO_550 and 0.02Ce-ZnO (S) 5:1 bead were discussed. In Figures 4.47 (a) and (b), the photocatalytic degradation of atrazine was enhanced by the presence of SO_4^{2-} and Cl^- ions but inhibited by CO_3^{2-} , HCO_3^- , and HPO_4^{2-} ions.

The improvement of atrazine removal by adding SO_4^{2-} possibly related to the formation of $\text{SO}_4^{\bullet-}$ (Gaya et al., 2009). The $\text{SO}_4^{\bullet-}$ was a sufficiently strong oxidizing agent ($E^0 = 2.6 \text{ eV}$) to degrade the atrazine molecule at a faster rate or initiated the formation of $\bullet\text{OH}$ (Pare et al., 2008).



Usually, Cl^- retarded photocatalytic degradation rate. Since it was favored by acidic pH which would adsorb strongly on the surface of catalyst, it consequently hindered organic pollutant to adsorb on the surface of catalyst. The decreasing in dye photocatalytic degradation rate with the increasing of Cl^- was due to the hole scavenging property of this ion as shown in the following equation (Pare et al., 2008). However, there was no inhibition of Cl^- in the photocatalytic degradation of 4-chlorophenol using ZnO from the study of Gaya et al. (2009). In addition, the increasing in photocatalytic degradation of naphthalene with the presence of Cl^- was reported which attributed to substrate loss through volatilization of naphthalene caused by rise in ionic strength (Lair et al., 2008). The enhancement of the atrazine removal under its natural pH by SO_4^{2-} and Cl^- ions is welcome as they are among the common anions in open water.



Conversely, the result in this study showed a slight decrease in atrazine removal with the presence of CO_3^{2-} and HCO_3^- . The inhibition by CO_3^{2-} and HCO_3^- was due to its ability to act as hydroxyl radical's scavengers and to block the active sites on ZnO surface (Behnajady et al., 2006). Although the generation of $\text{CO}_3^{\bullet-}$ (as well as $\text{Cl}^{\bullet-}$ and $\text{Cl}_2^{\bullet-}$ originated from Cl^-) was an oxidizing agent itself, its oxidation potential was less than that of $\bullet\text{OH}$.



The photocatalytic degradation of atrazine was prohibited by HPO_4^{2-} due to the strong binding of HPO_4^{2-} to the active sites of ZnO. Thus, the adsorption of atrazine on the ZnO surface was prevented (Gaya et al., 2009).

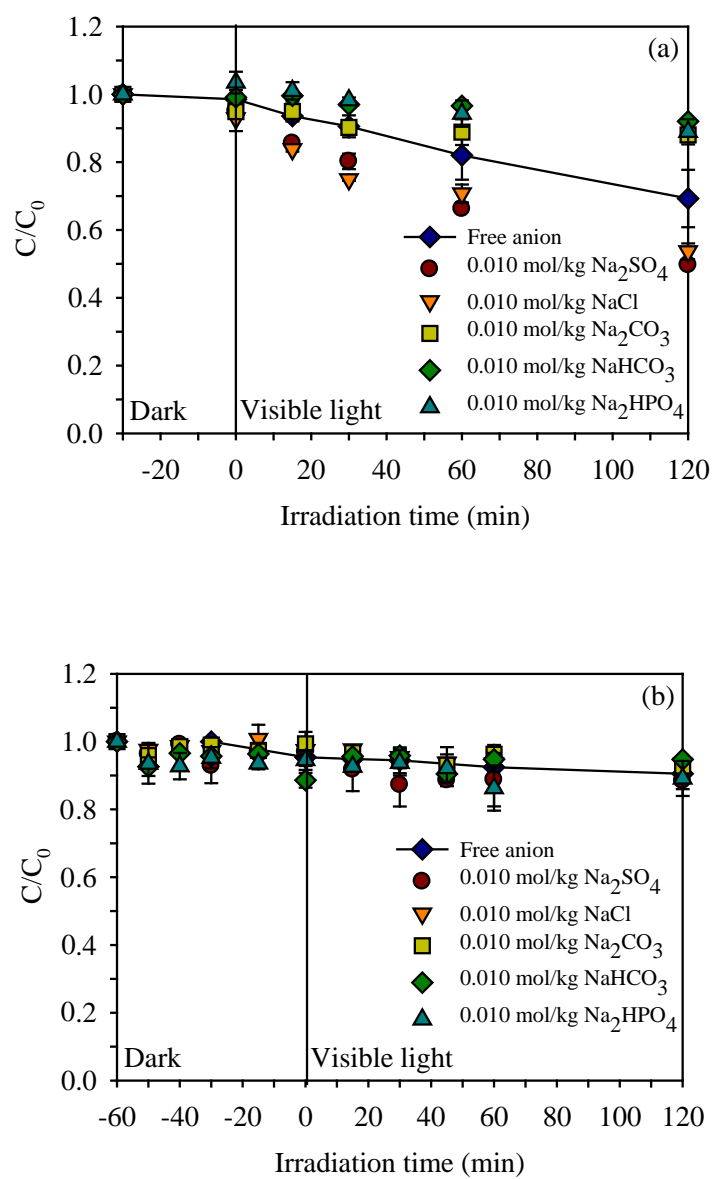


Figure 4.47 Effect of anions on the photocatalytic degradation of atrazine (a) using ZnO_{550} and (b) 0.02Ce-ZnO (S) 5:1 bead.

4.2.9 Other metal dopants on ZnO

Previously with 0.02Ce-ZnO (S) 5:1 powder, its activity on atrazine degradation was higher than other prepared catalysts. This might be due to its photocatalytic property from the differences in terms of type of metal, molar ratio of doping, and amount and type of template. Practically, 0.02Ce-ZnO (S) 5:1 in the bead form presented rather unsatisfactory results for applying to atrazine photodecomposition. The catalyst preparation was investigated further by producing other metal dopants on Ce-ZnO. In Figure 4.48, 0.005Ag-0.005Ce-ZnO powder presented superiority on atrazine photocatalytic degradation corresponding to the high absorbance in visible light range in UV-vis-DR (Figure 4.49.). The specific surface areas of the three new catalysts as summarized in Table 4.13 were insignificantly different (14.60 to 23.04 m²/g). Comparing to 0.02Ce-ZnO (S) 5:1, 0.005Fe-0.005Ce-ZnO and 0.005Cu-0.005Ce-ZnO still presented the lower activity than 0.02Ce-ZnO (S) 5:1 which is the original catalyst.

In Figure 4.50, the effect of initial concentration on photocatalytic degradation of atrazine using 0.005Ag-0.005Ce-ZnO was examined. The percent photocatalytic degradation of atrazine at 120 min of irradiation time increased with the decreasing of atrazine initial concentration (67.39 to 84.07%). Unfortunately, the 100% atrazine removal was unapproachable with 0.005Ag-0.005Ce-ZnO powder but with the commercial ZnO powder. The high atrazine concentrations were rapidly removed at initial irradiation time by 0.005Ag-0.005Ce-ZnO due to the same reason for the commercial ZnO powder stated in 4.2.5.

The 0.005Ag-0.005Ce-ZnO was used in the further studies on 4.2.10 competitive effects from natural organic matter, 4.2.11 kinetics, and 4.3 evaluation of photocatalytic degradation pathway of atrazine.

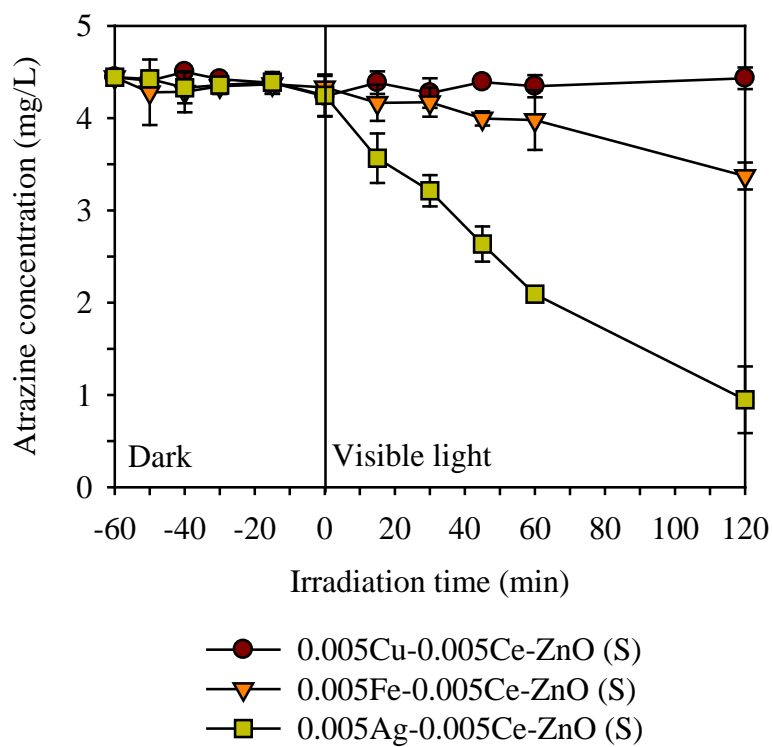


Figure 4.48 Effect of other metal dopants on Ce-ZnO on atrazine photocatalytic degradation.

Table 4.13 BET surface areas of 0.005Ag-0.005Ce-ZnO (S), 0.005Fe-0.005Ce-ZnO (S), and 0.005Cu-0.005Ce-ZnO (S).

Catalyst	BET surface area (m ² /g)
0.005Cu-0.005Ce-ZnO (S)	23
0.005Fe-0.005Ce-ZnO (S)	15
0.005Ag-0.005Ce-ZnO (S)	17

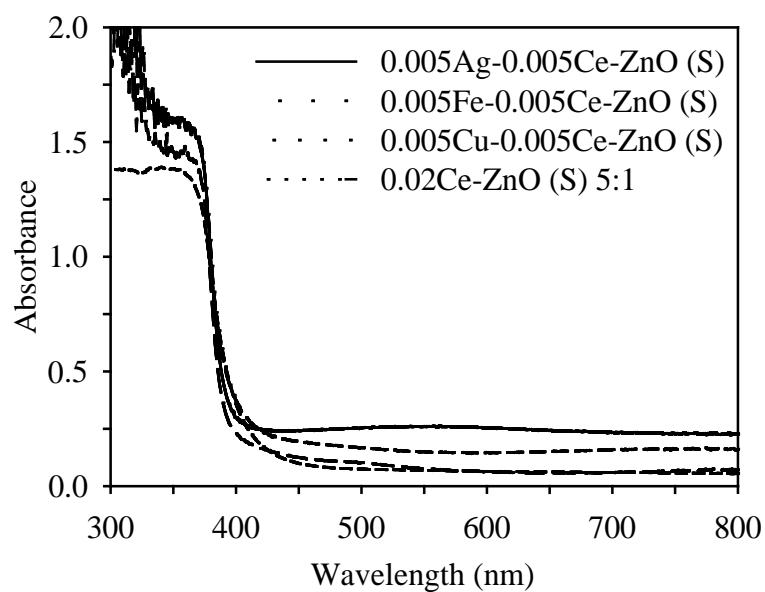


Figure 4.49 UV-vis diffuse reflectance spectra of the other metal doped Ce-ZnO prepared by using sticky rice starch (S) templates compared with 0.02Ce-ZnO (S) 5:1.

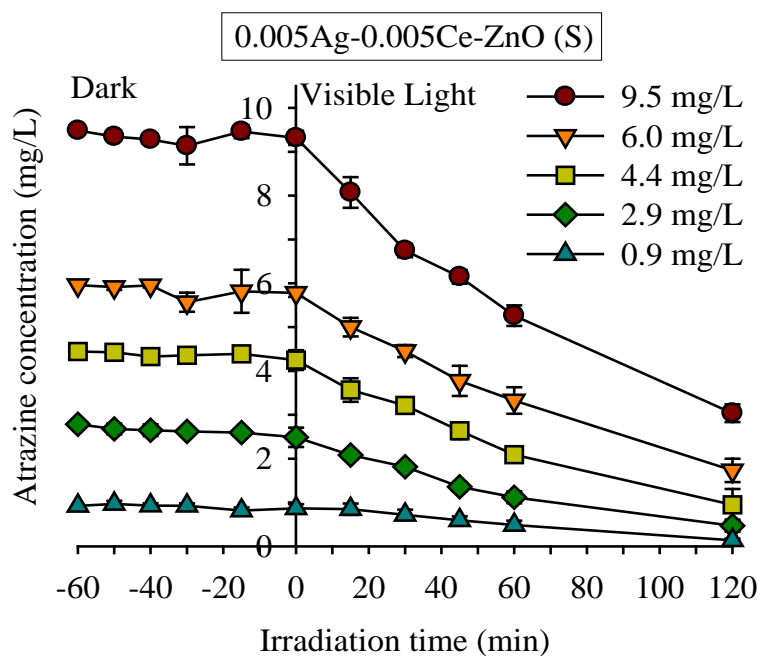


Figure 4.50 Photocatalytic degradation by 0.005Ag-0.005Ce-ZnO using varied initial concentrations of atrazine.

4.2.10 Competitive effects from natural organic matter

Generally, atrazine is considered as non-point source pollutant. In nature, atrazine presents with other natural organic matter (NOM) (Liu et al., 2009). Humic acid (HA) was used by adding to the atrazine solution to examine whether the atrazine photocatalytic degradation by using 0.02Ce-ZnO (S) 5:1 bead and 0.005Ag-0.005Ce-ZnO (S) powder could be affected by existing of other common organic in natural water. In Figure 4.51, the photocatalytic degradation of atrazine using 0.02Ce-ZnO (S) 5:1 bead with the presence of the humic acid was unable to be clearly seen. The variation of the humic acid amount (0.0 to 5.0 mg/L) influenced the atrazine removal was likely to be indifferent due to the low activity of 0.02Ce-ZnO (S) 5:1 in the bead form and the low concentration of the humic acid. In Figure 4.52, the humic acid added on the atrazine solution was increased to be 50.0 mg/L. Obviously, the atrazine removal by 0.005Ag-0.005Ce-ZnO (S) powder was considerably hindered as the humic acid exists. The atrazine removal at 120 min of irradiation time with the absence of the humic acid was 77.41% while that with the presence of the humic acid was 50.56%. The humic acid, as a kind of organic, could be promptly attacked by oxidative species (Liu et al., 2009). Furthermore, the quantity of photon that could irradiate the catalyst was possibly reduced since the humic acid severely absorbed the light. These correlatively caused the directive competitive effect for the radicals to react with the atrazine molecules and the diminution of the radical yield.

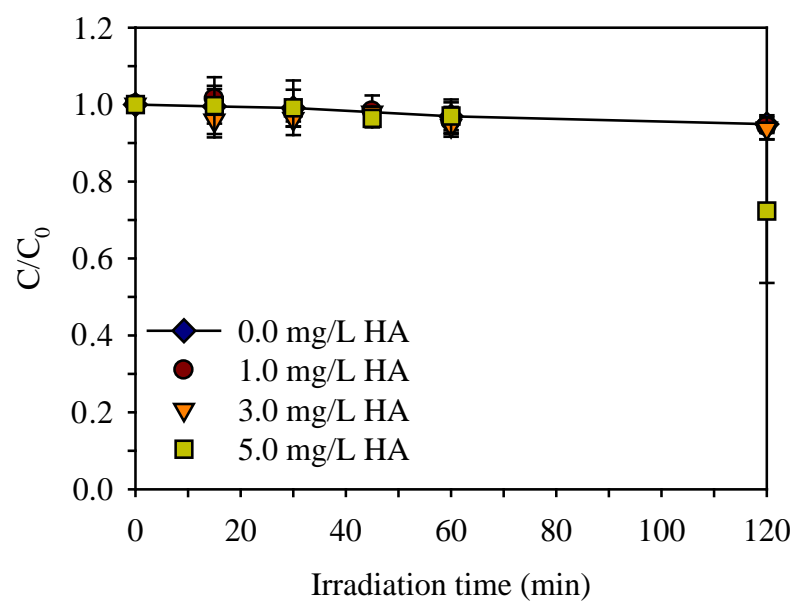


Figure 4.51 Effect of natural organic matter on atrazine photocatalytic degradation using 0.02Ce-ZnO (S) 5:1.

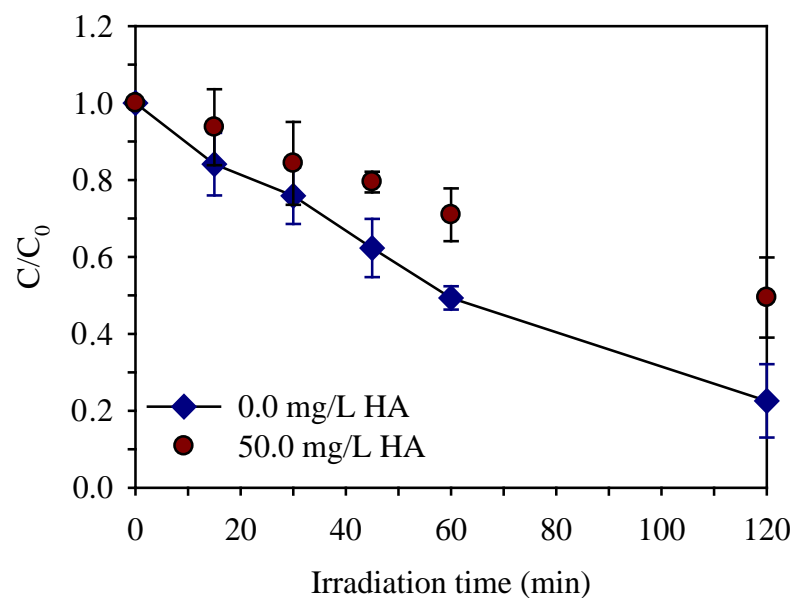


Figure 4.52 Effect of natural organic matter on atrazine photocatalytic degradation using 0.005Ag-0.005Ce-ZnO (S).

4.2.11 Langmuir-Hinshelwood-Hougen and Watson (LHHW) kinetics

The photocatalytic oxidation kinetics of many organic compounds has been validated with the Langmuir-Hinshelwood-Hougen and Watson (LHHW) model (Behnajady et al., 2006; Evgenidou et al., 2005; Lackhoff and Niessner, 2002; Parra et al., 2004). This model covers the adsorption property of pollutant on the catalyst surface coupled with the reaction occurring at the solid-liquid interface. The results from the studies of the effect of initial concentration in 4.2.5 and the other metal dopants on ZnO in 4.2.9 were used to calculate the reaction rate constants (k_r) and equilibrium adsorption constants (K_{ads}) of atrazine on catalysts based on the Langmuir-Hinshelwood-Hougen and Watson (LHHW) model in Equation 4.14. The catalysts that were studied in those topics consist of ZnO powder, 0.005Ag-0.005Ce-ZnO (S) powder, and ZnO_550 bead.

$$r_0 = \frac{k_r K_{ads} C_0}{1 + K_{ads} C_0} \quad (4.14)$$

where k_r = reaction rate constant (mg/L-min)

K_{ads} = adsorption equilibrium constant (L/mg)

C_0 = initial equilibrium concentration of atrazine (mg/L)

With the numerical method, the three-point differentiation formula was applied to estimate the initial photocatalytic degradation rate (r_0) for each initial concentration of atrazine (Fogler, 2006). The r_0 calculation concerns only the experimental data obtained during the first minutes of irradiation time in order to minimize variation as a result of competitive effect of intermediates, pH changes, and other parameters.

$$r_0 = \frac{(-3C_0 + 4C_1 - C_2)}{2\Delta t} \quad (4.15)$$

where r_0 = initial photocatalytic degradation rate (mg/L-min)

C = concentration of atrazine at reaction time t (mg/L)

$$\Delta t = t_2 - t_1 \text{ (min)}$$

In Figure 4.53, the initial photocatalytic degradation rates (r_0) by ZnO and 0.005Ag-0.005Ce-ZnO (S) powders presented the sharp rise at the beginning run until they reach plateaus when the concentration of atrazine was around 5 mg/L. Then, the rates (r_0) continually increased with the sharp rise for ZnO and the slight inclined for 0.005Ag-0.005Ce-ZnO (S). These behaviors indicated the saturation-type Langmuir kinetics (Parra et al., 2004). In contrast, the initial photocatalytic degradation rates (r_0) by ZnO_550 slowly increased without plateau. This evidence seemed to be unmatched with saturation-type Langmuir kinetics. The assumption could be in two points 1) the kinetics possibly obeyed through other models being involved by many factors in the system and/or 2) the study further by increasing the initial concentration on the photocatalytic degradation of atrazine might be necessary to confirm the trend of the rate.

The initial photocatalytic degradation rates (r_0) by the three catalysts were used in the linear LHHW model plots of the inverse initial photocatalytic degradation rates ($1/r_0$) versus the inverse initial equilibrium atrazine concentrations ($1/C_0$) as shown in Figure 4.54.

$$\frac{1}{r_0} = \frac{1}{k_r K_{ads} C_0} + \frac{1}{k_r} \quad (4.16)$$

The reaction rate constants (k_r) and the equilibrium adsorption constants (K_{ads}) were determined from the linear equation obtaining from the plots as summarized in Table 4.14. The reaction rate constant (k_r) of atrazine photocatalytic degradation were in the order ZnO_550 < 0.005Ag-0.005Ce-ZnO (S) < ZnO whereas the equilibrium adsorption constants (K_{ads}) were in order ZnO < 0.005Ag-0.005Ce-ZnO (S) < ZnO_550. For ZnO and 0.005Ag-0.005Ce-ZnO (S), the k_r values were greater than the K_{ads} values (10^4 to 10^5 -fold greatness). It implied that the reaction was the most important factor in the elimination of atrazine. The K_{ads} of ZnO_550 was quite high comparing to its k_r . It was likely that the adsorption became the significant one of all

determinants in the system since the ZnO_550 was in the bead form which was different from the two former catalysts. The total rate constant (k_{tot}), which was $k_r \times K_{ads}$, were found in the order ZnO (0.0938 /min) < 0.005Ag-0.005Ce-ZnO (S) (0.2913 /min) < ZnO_550 (0.7530 /min). It suggested that the adsorption played a key role in photocatalytic degradation mechanism and eventually enhances the k_{tot} of ZnO_550.

The photocatalytic degradation of atrazine under the experimental conditions of the study agreed with the kinetics of LHHW model corresponding to other atrazine photocatalytic degradation studies (Parra et al., 2004; Lackhoff and Niessner, 2002) as demonstrated in Table 4.14. Unlike the study of Lackhoff and Niessner (2002) and this study, the K_{ads} was great higher than the k_r explored by Parre et al. (2004). It was certain that this deviation was governed by atrazine concentration level, catalyst loading, catalyst type, light source type, pH, temperature, and other conditions in the reactor. The proportion of K_{ads} and k_r was also revealed when using ZnO to destruct other organic compounds such as Acid Yellow 23 (Behnajady et al., 2006) and dichlorvos (Evgenidou et al., 2005).

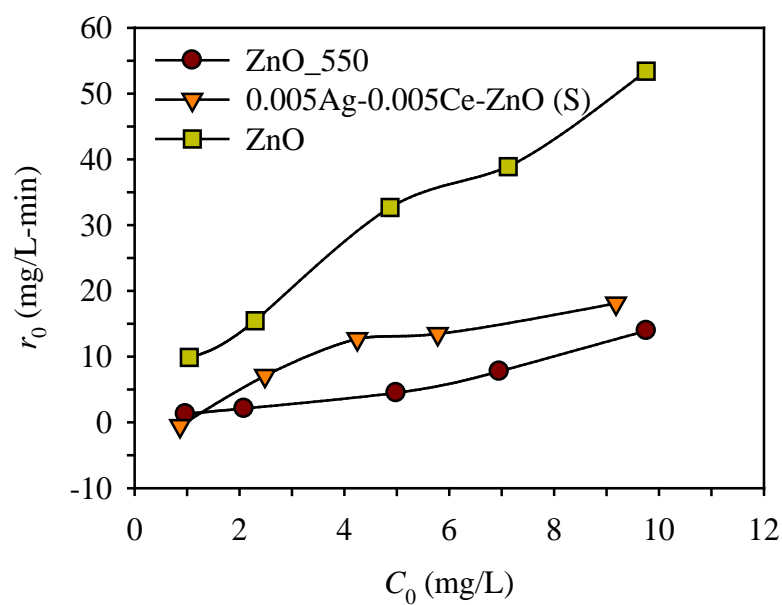


Figure 4.53 Initial rate of atrazine photocatalytic degradation as a function of its initial concentration.

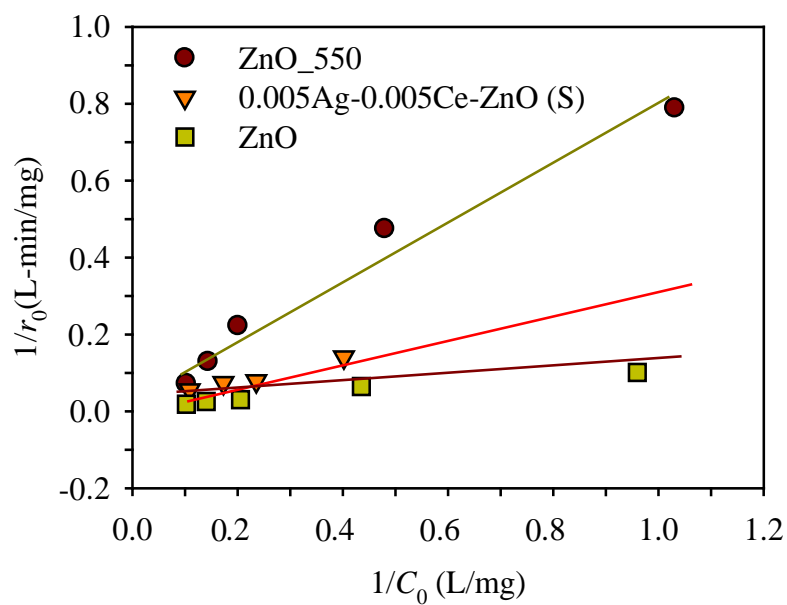


Figure 4.54 LHHW linear plots of atrazine photocatalytic degradation using ZnO, 0.005Ag-0.005Ce-ZnO (S), and ZnO_550.

Table 4.14 Comparison of k_r (mg/L-min) and K_{ads} (L/mg) in the LHHW kinetics for photocatalytic degrading of atrazine using the suitable catalysts in powder and bead forms.

Catalyst	$\frac{1}{r_0} = \frac{1}{k_r K_{ads} C_0} + \frac{1}{k_r}$	R^2	k_r	K_{ads}
<u>Powder</u>				
ZnO commercial	$y = 0.0959x + 0.0128$	0.9716	78.12	0.0012
0.005Ag-0.005Ce-ZnO (S)	$y = 0.2902x + 0.0206$	0.9668	48.54	0.0060
<u>Bead</u>				
ZnO_550	$y = 0.7541x + 0.0421$	0.9726	23.75	0.0317
<u>Other atrazine study</u>				
TiO ₂	–	–	0.0013	0.0150
Conditions: 1 g/L, atrazine = 2–25 ppm, metal halide lamp (Parra et al., 2004)				
TiO ₂	–	0.9850	416.0	0.0019
Conditions: 5 g/L, atrazine = 500 ppb, xenon lamp ($\lambda > 300$ nm (Lackhoff and Niessner, 2002)				
<u>Other ZnO study</u>				
ZnO (Behnajady et al., 2006)	–	–	1.796	113.0
ZnO (Evgenidou et al., 2005)	–	–	7.34	0.03

4.2.12 Catalyst reliability

The catalyst immobilization, which was coating on Al_2O_3 bead via MCT in this study, is expected for the continuous use of the catalyst, elimination of the post-process filtration and particle recovery, catalyst regeneration, and improvement of organic compound removal when using a support with adsorption property (De Lasa et al., 2004). However, the immobilized catalyst probably displays a number of drawbacks such as low surface area to volume ratio, catalyst fouling or catalyst wash out, light scattering by immobilized media, and significant pressure drop in continuous reactor.

In order to evaluate the stability and long-term use of catalyst bead (ZnO_550), a five-cycle atrazine degradation was carried out. At every 120 min of reaction time, the remained atrazine in the batch reactor was removed, and the same initial concentration of atrazine solution was introduced into the reactor without regeneration of catalyst. As shown in Figure 4.55, the removal efficiency of atrazine was 29.82 in the first cycle and decreased after that to be 26.31, 21.86, 16.94, and 15.84% in the last four cycles. The ZnO_550 presented the decrease of activity every time of reuse which might be due to the erosion of ZnO powder during drainage the rest of atrazine solution after finishing each cycle. This implied that it significantly lost in activity and extremely needs to be developed to be active, stable, and durable in further study.

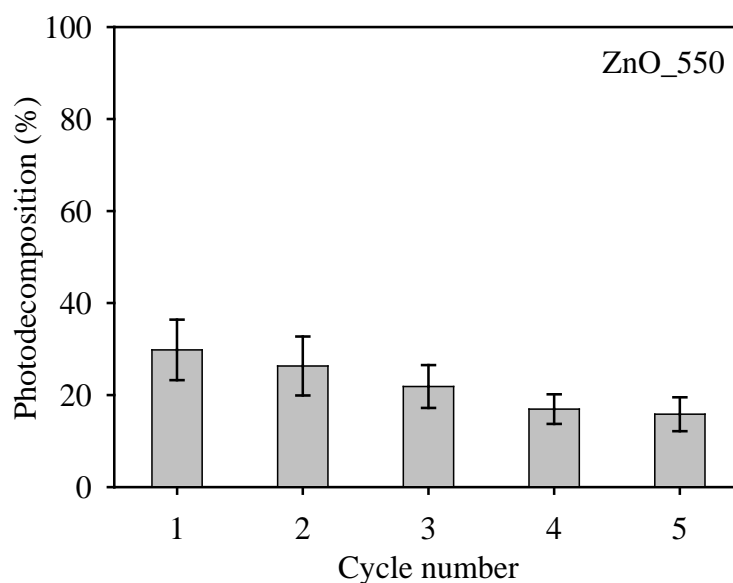


Figure 4.55 Five cycles of atrazine photocatalytic degradation at 120 min of irradiation time using ZnO_550.

4.3 Evaluation of photocatalytic degradation pathway of atrazine

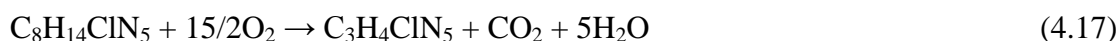
Photocatalytic degradation of atrazine has been studied by many researchers but the degrading reaction mechanisms were rarely investigated. The intermediates produced during the photocatalytic degradation of atrazine with TiO₂ under UV irradiation were reported (McMurray et al., 2006). It was found that a number of intermediate compounds were formed when the atrazine concentration and total organic carbon (TOC) decreased. Eventually, the cyanuric acid was observed as a final stable product. The concentrations of significant intermediates such as ammelide and ammeline were also trailed in the photocatalytic degradation of atrazine with TiO₂ (Minero et al., 1996).

The atrazine concentration along with TOC as a function of irradiation time was examined in this study. The C/C₀ of atrazine photocatalytic degradation using commercial ZnO and 0.005Ag-0.005Ce-ZnO (S) powders is presented in Figure 4.56. Through 120 and 180 min of irradiated ZnO, the atrazine was removed for almost 100% but the TOC was still slightly eliminated. This attributed to the oxidation of

lateral alkyl chains in atrazine structure (Konstantinou and Albanis, 2002) leading to completely reduce atrazine concentration and incompletely reduce TOC.

Atrazine was completely eliminated at 180 min of irradiation with ZnO powder while it was mainly removed around 87% with 0.005Ag-0.005Ce-ZnO (S). At 180 min, the TOC removal of atrazine reached 64 and 65% for its degradation by 0.005Ag-0.005Ce-ZnO (S) and ZnO powders, respectively, as shown in Figure 4.57. From the TOC trends, they were unlikely to be further removed after 180 min. The incomplete decrease of TOC corresponded to partial removal of carbon within the atrazine side chains. The TOC of atrazine photocatalytic degradation using TiO₂ in supercritical water or hydrothermal water reported by Horikoshi and Hidaka (2003) also never totally disappeared.

When the 60% of TOC decrease, the lateral alkyl chains in atrazine structure would be reduced from eight carbons to three carbons (McMurray et al., 2006), as demonstrated in Equation 4.17. The three carbons meant to those carbons consisting in triazine ring. This incident was possible to obtain the cyanuric acid as a final product. However, the cyanuric acid was seldom reached as well as the complete mineralization particularly in the presence of catalyst alone (Huster, Moza, and Pouyet, 1991; Minero et al., 1996; Pelizzetti et al., 1990). The atrazine photocatalytic degradation using catalyst with the presence of fluoride ions or sodiumpersulfate had occurred by several steps and finally provided the cyanuric acid (Minero et al., 1996; Oh and Jenks, 2004). This appearance was encouraged by additives.



The reaction mechanism of atrazine photocatalytic degradation is shown in Figure 4.58 (Lackhoff and Niessner, 2002; Minero et al., 1996). It revealed only the main and more stable intermediates. The numbers were compounds, namely

- (1) 2-chloro-4-acetamido-6-isopropylamino-1,3,5-triazine,
- (2) 2-hydroxy-4-ethylamino-6-isopropylamino-1,3,5-triazine or hydroxyatrazine,
- (3) 2-chloro-4-amino-6-isopropylamino-1,3,5-triazine or desethylatrazine,

- (4) 2-chloro-4-ethylamino-6-amino-1,3,5-triazine or desisopropylatrazine,
- (5) 2-isopropylamino-1,3,5-triazine,
- (6) 2-hydroxy-4-amino-6-isopropylamino-1,3,5-triazine or hydroxydesethylatrazine,
- (7) 2-hydroxy-4-ethylamino-6-amino-1,3,5-triazine or hydroxydesisopropylatrazine,
- (8) 2-hydroxy-4,6-diamino-1,3,5-triazine or ammeline,
- (9) 2-chloro-4,6-diamino-1,3,5-triazine or desethyl-desisopropylatrazine,
- (10) 2,4-dihydroxy-6-amino-1,3,5-triazine or ammelide,
- (11) 2-chloro-4-amino-6-hydroxy-1,3,5-triazine,
- (12) 2-chloro-4,6-dihydroxy-1,3,5-triazine, and
- (13) 2,4,6-trihydroxy-1,3,5-triazine or cyanuric acid (Héquet, Gonzales, and Le Cloirec, 2001).

The dash line represented as 3/8 TOC limit. The transformation of each step was the only one of the following three processes; 1) lateral alkyl chain oxidation or dealkylation, 2) dechlorination, and 3) deamination. The transformation process above the dash line could be only 1) and 2) while that after the dash line could be 1), 2), and 3) (Carlin, Minero, and Pelizzetti, 1990).

In this work, intermediates produced from the parent atrazine compound in photocatalytic oxidation were analyzed by LC-MS to ensure what compounds remain in the system and whether cyanuric acid was found as a final product. The appearance of the intermediates was pursued by using the LC-MS spectra of atrazine photocatalytic degradation using ZnO (Figure 4.59) and 0.005Ag-0.005Ce-ZnO (S) powders (Figure 4.60). In Figure 4.59 (a) at starting point, atrazine peak, which was confirmed by the atrazine standard, was presented. After 15 min, in Figure 4.59 (b), the appearance of two unknown peaks was noticed. The area of the two peaks increased throughout 150 min. Finally at 180 min, in Figure 4.59 (i), four unknown peaks with the one largest peak area were observed, and the atrazine peak area was reduced. The intermediates obtained from LC-MS based on mass spectrum values, which were added in Appendix E.14, were proposed in Table 4.15. The photocatalytic reaction could transform atrazine to the product number (6) 2-hydroxy-4-amino-6-isopropylamino-1,3,5-triazine, which appeared at 180 min. The atrazine was detected

by LC-MS although no atrazine remained at 180 min from HPLC analysis. It was due to the detection limit of HPLC under the experimental conditions which were remarked previously.

Figure 4.60 presents the photocatalytic degradation of atrazine with 0.005Ag-0.005Ce-ZnO (S) powder. The trend of LC-MS spectra was as similar as shown in Figures 4.59 (a) to (e) but (f). The atrazine peak decreased, and the small unknown peaks appeared through 180 min. It was strengthened that the potential of ZnO powder for destructing atrazine was superior to that of 0.005Ag-0.005Ce-ZnO (S) powder. The identified intermediates were also proposed as contained in Table 4.16. The atrazine photocatalytic degradation could reach number (5) 2-isopropylamino-1,3,5-triazine starting to be seen at 120 min. It was implied that the reaction mechanisms of atrazine photocatalytic degradation using ZnO and 0.005Ag-0.005Ce-ZnO (S) powders were rather different.

Starting from atrazine, the parent compound was transformed to compound number (1), (2), (3), (4), and (6) with ZnO powder use and (1), (2), (3), (4), and (5) with 0.005Ag-0.005Ce-ZnO (S) powder use. These happened through lateral alkyl chain oxidation and dechlorination. Within 180 min, the reaction of atrazine degrading was unable to go further and still far from transforming to cyanuric acid which was the final stable product. However, this verification was consistent with the TOC results, which reached to 60% without triazine ring mineralization, and the 3/8 TOC limit, which was unable to progress to the other step with the catalyst alone in the system.

The photocatalytic reaction normally degraded and mineralized organic compounds to CO₂ and inorganic ions, but it hardly took place with cyanuric acid. The resistance of cyanuric acid to photocatalysis including band gap exited TiO₂ was reported (Minero, Maurino, and Pelizzetti, 1997). Although the cyanuric acid is very low toxic and biodegradable, the photocatalytic processes used in water purification must be concerned if the water is contaminated by compounds having 1,3,5-triazine ring in their structure.

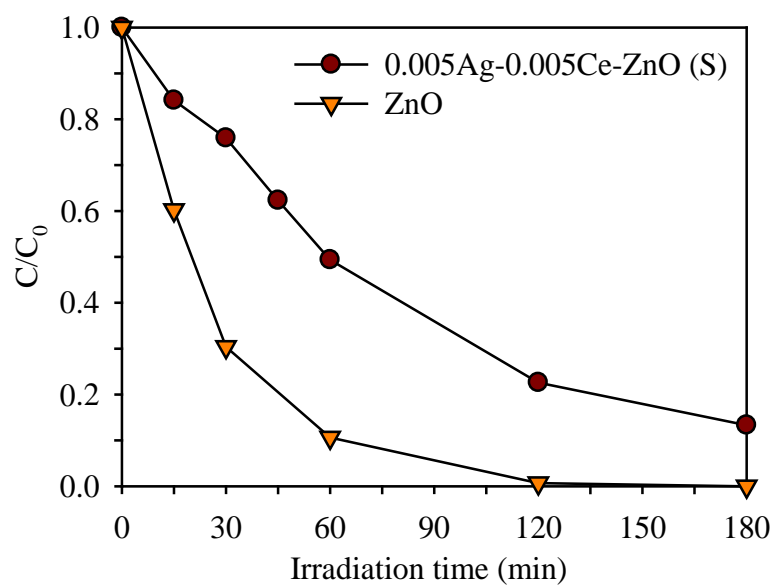


Figure 4.56 Atrazine photocatalytic degradation using commercial ZnO and 0.005Ag-0.005Ce-ZnO (S) powders as a function of irradiation time.

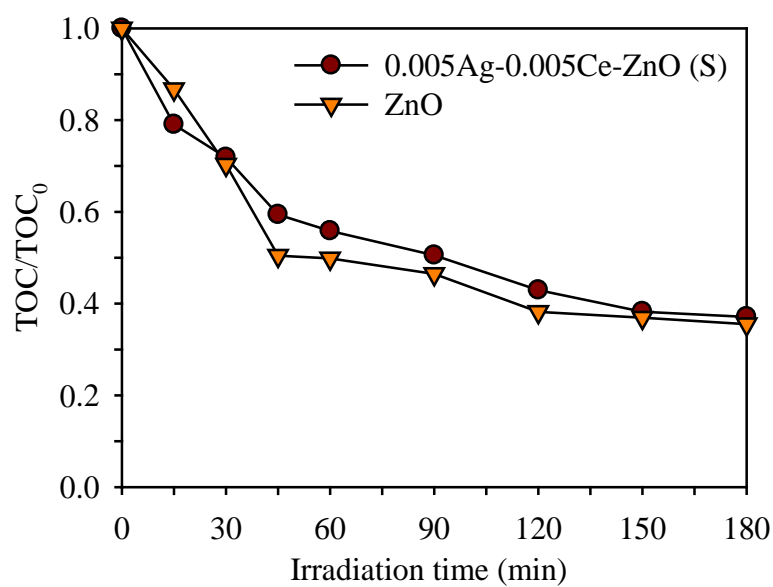
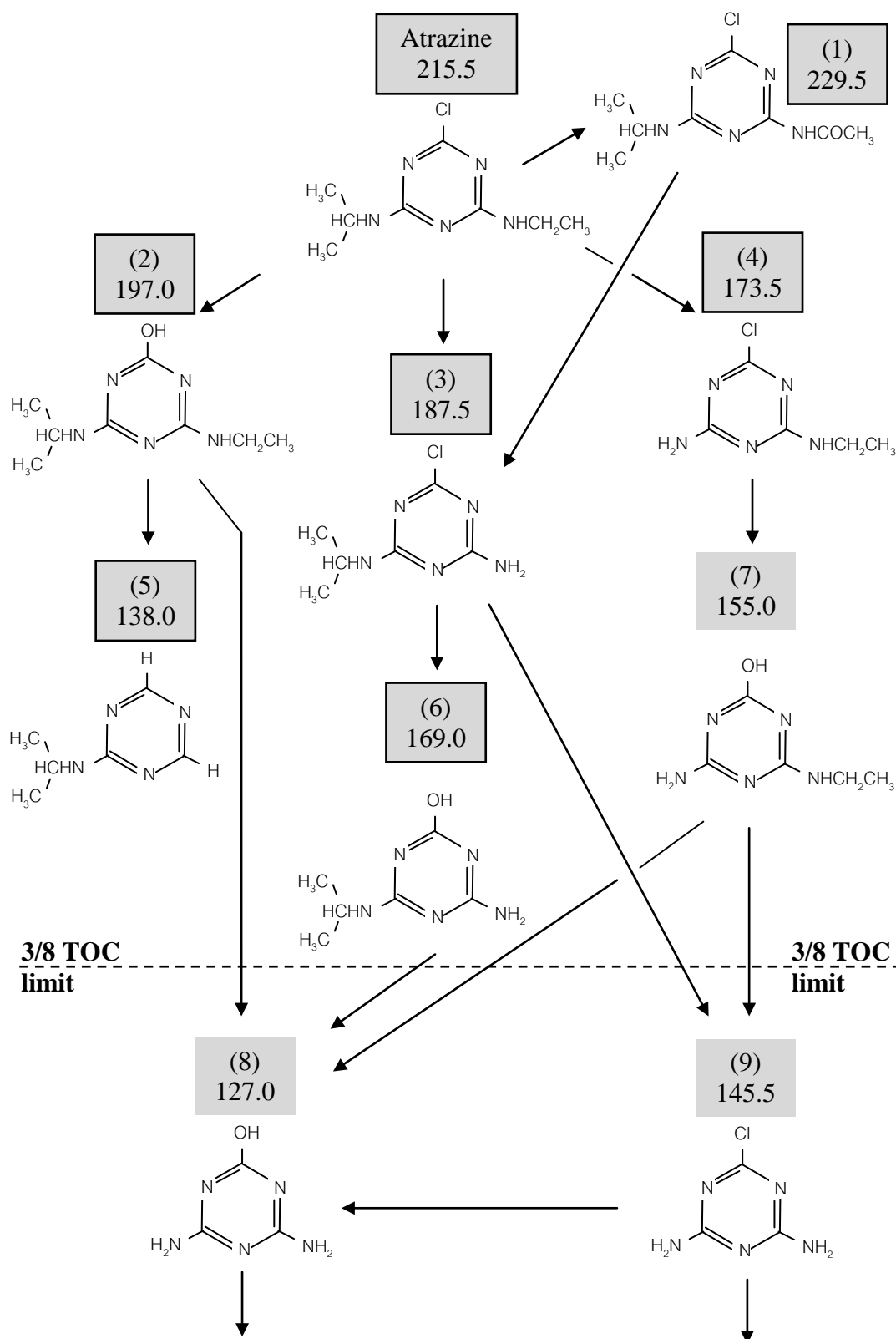


Figure 4.57 TOC decrease in atrazine photocatalytic degradation using commercial ZnO and 0.005Ag-0.005Ce-ZnO powders as a function of irradiation time.



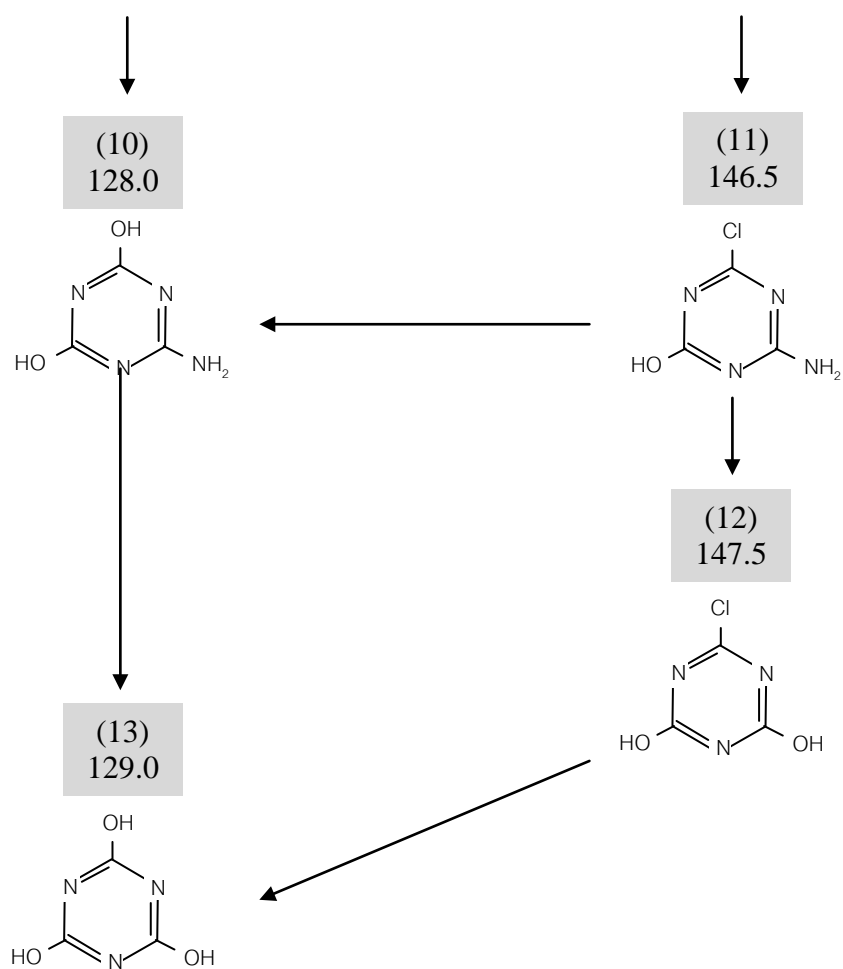


Figure 4.58 Reaction mechanism of atrazine photocatalytic degradation (Minero et al., 1996; Lackhoff and Niessner, 2002).

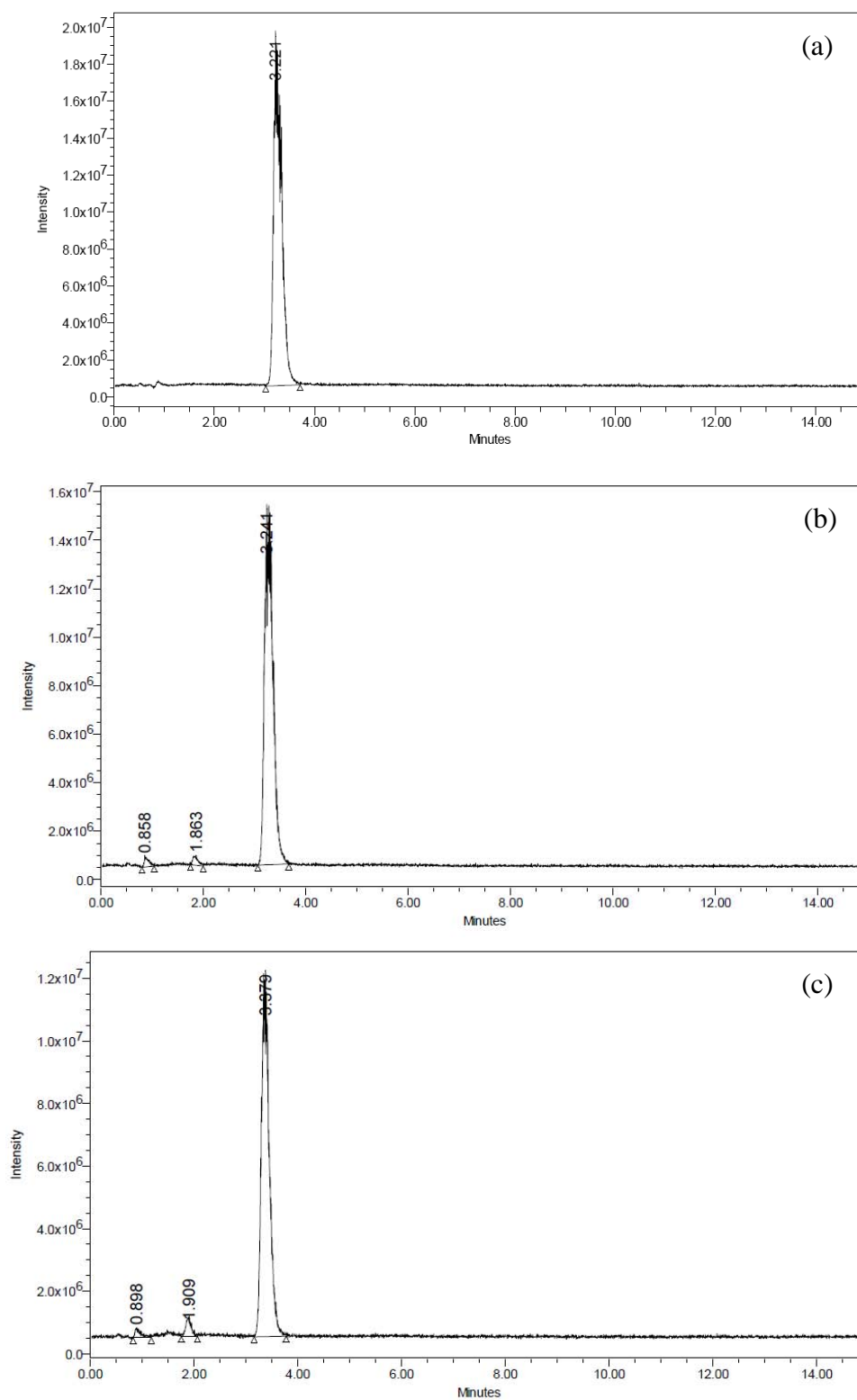


Figure 4.59 LC-MS spectra of atrazine photocatalytic degradation using ZnO powder at (a) 0, (b) 15, and (c) 30 min of irradiation time.

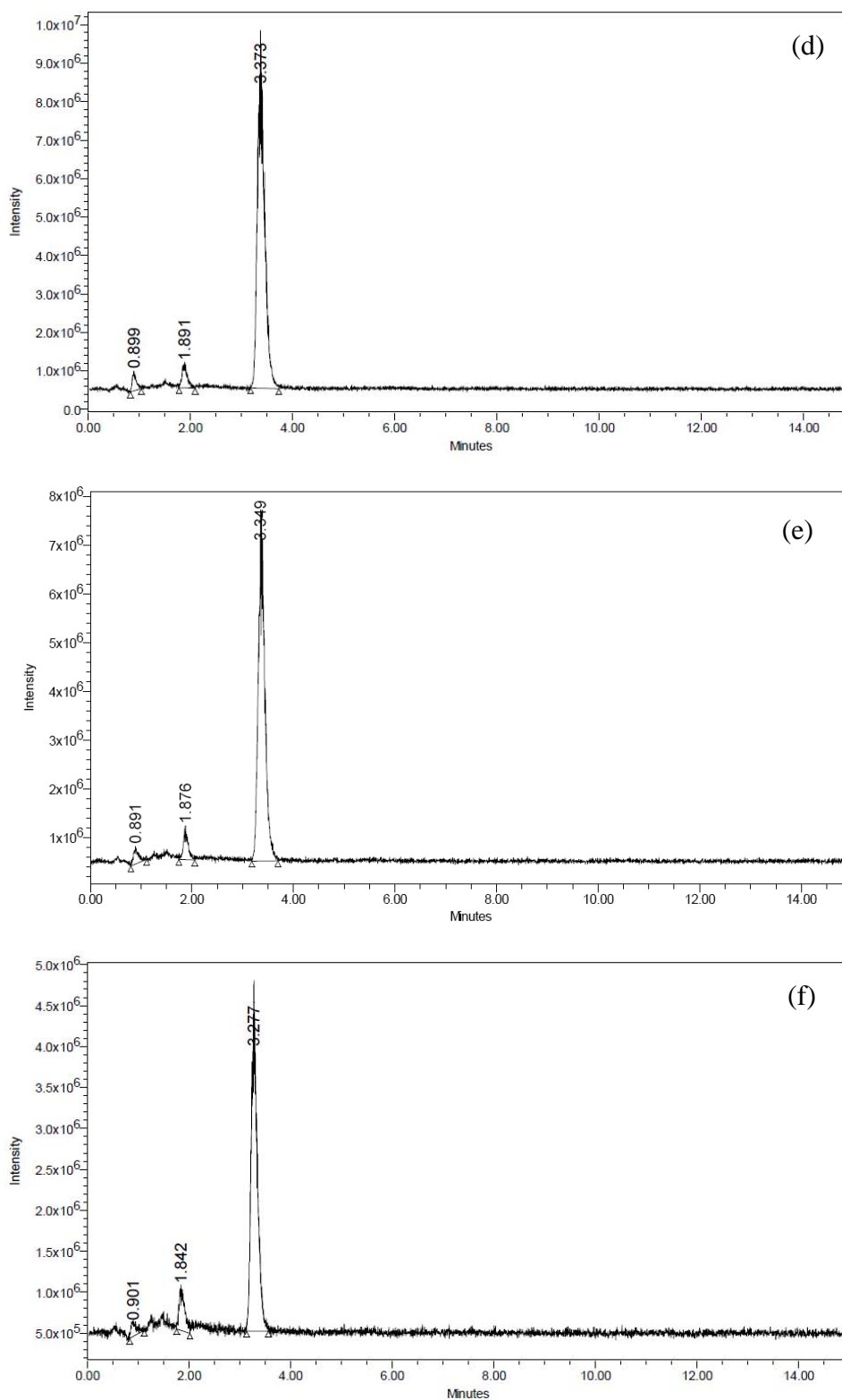


Figure 4.59 LC-MS spectra of atrazine photocatalytic degradation using ZnO powder at (d) 45, (e) 60, and (f) 90 min of irradiation time.

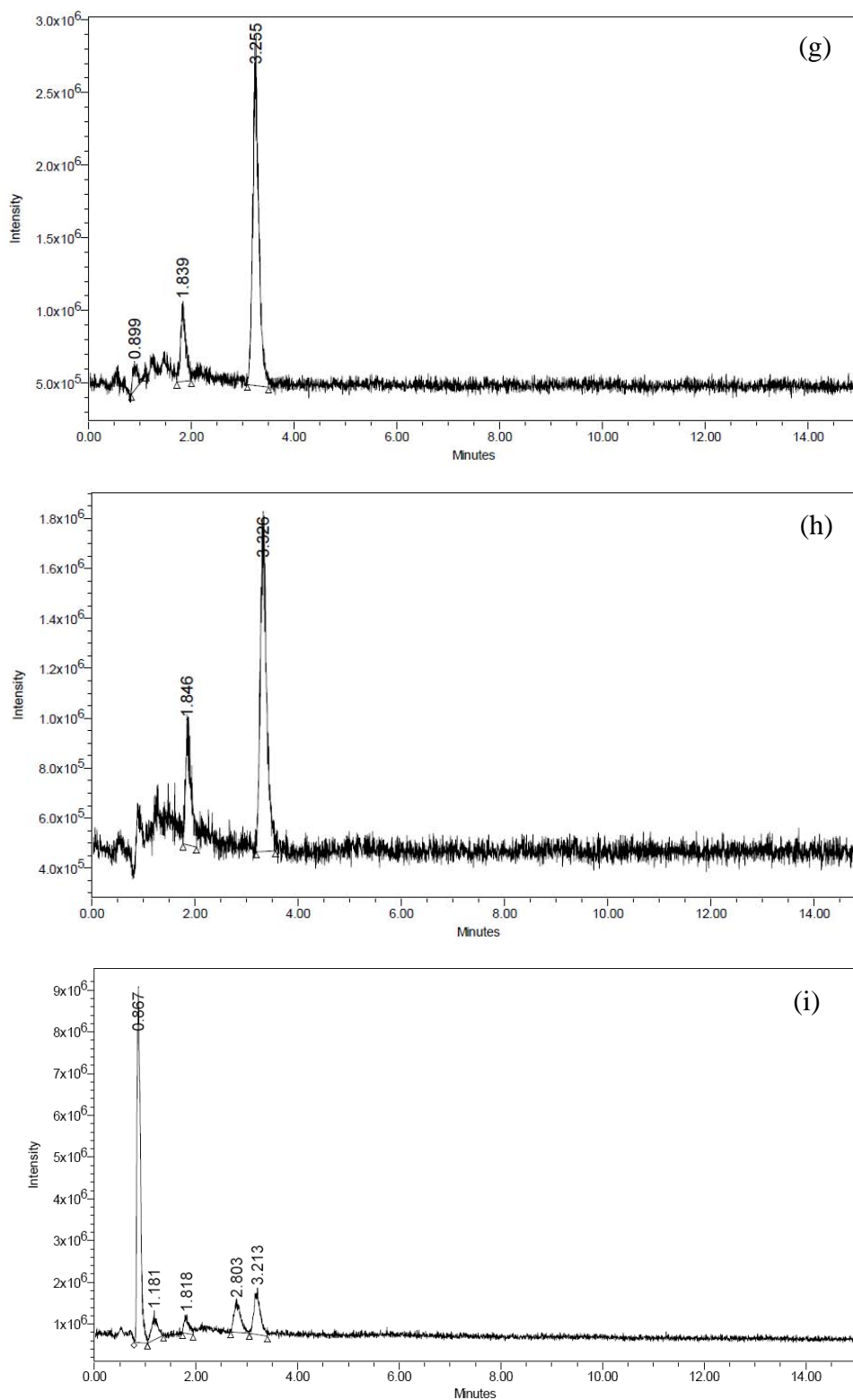


Figure 4.59 LC-MS spectra of atrazine photocatalytic degradation using ZnO powder at (g) 120, (h) 150, and (i) 180 min of irradiation time.

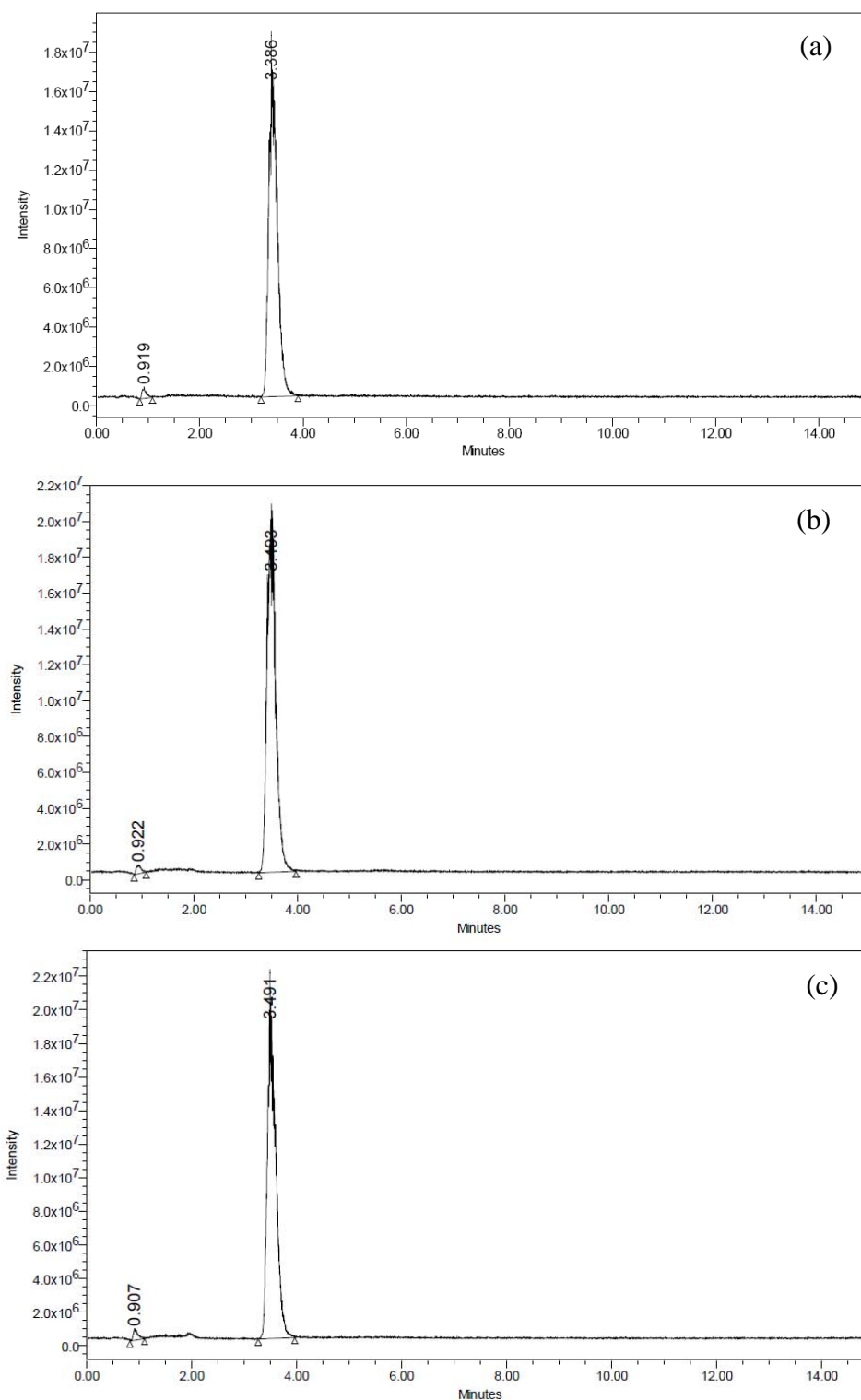


Figure 4.60 LC-MS spectra of atrazine photocatalytic degradation using 0.005Ag-0.005Ce-ZnO (S) powder at (a) 0, (b) 15, and (c) 30 min of irradiation time.

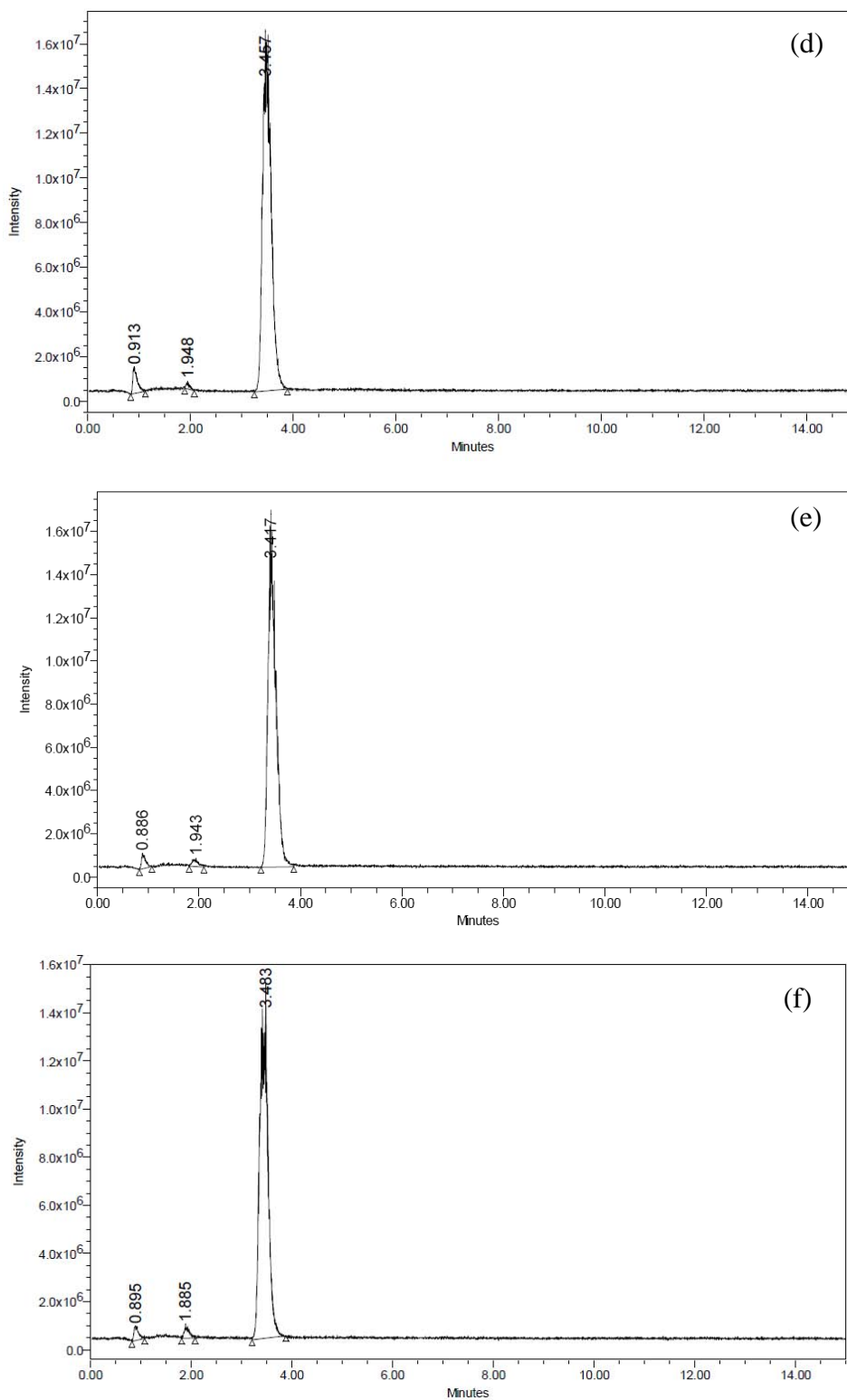


Figure 4.60 LC-MS spectra of atrazine photocatalytic degradation using 0.005Ag-0.005Ce-ZnO (S) powder at (d) 45, (e) 60, and (f) 90 min of irradiation time.

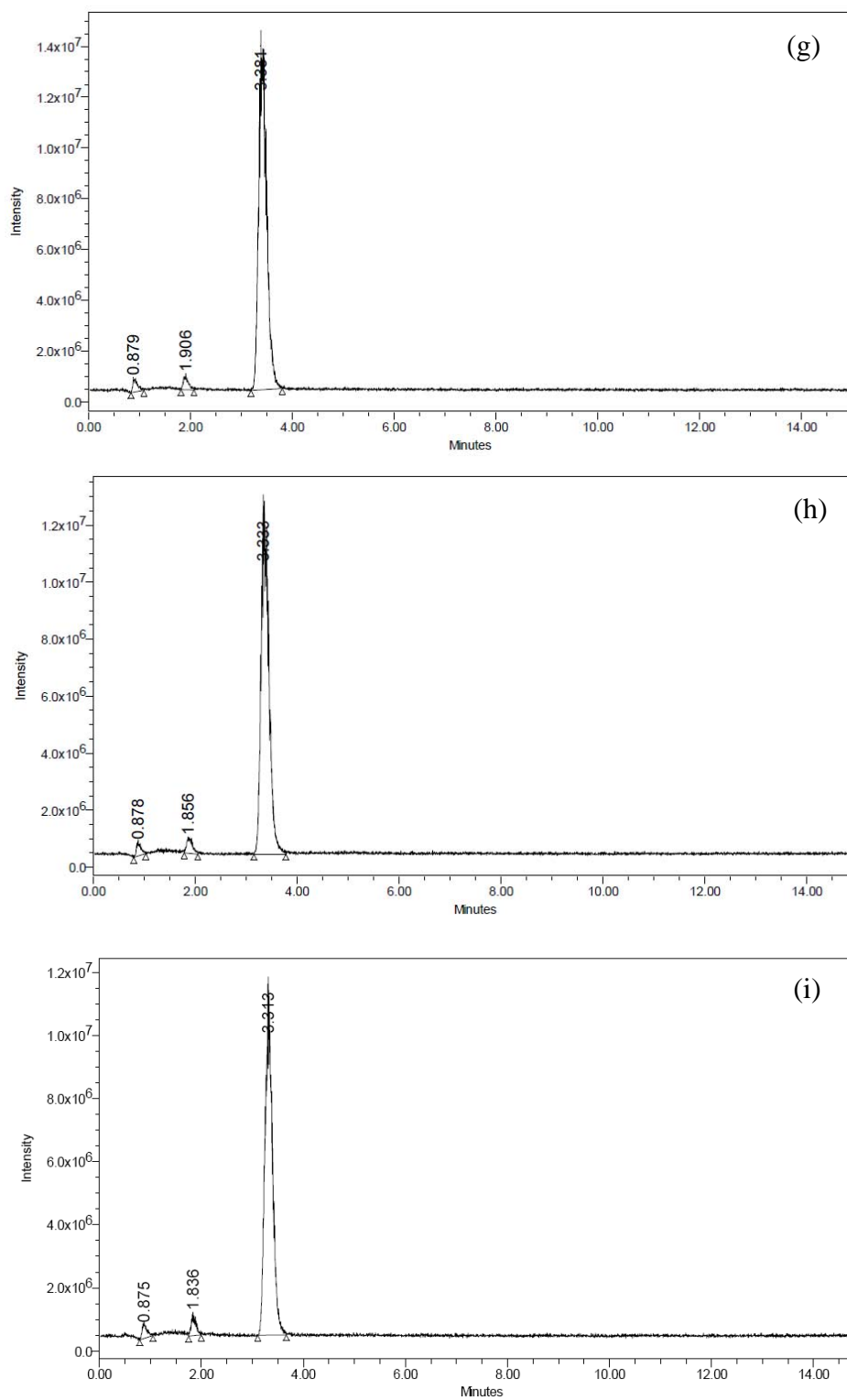


Figure 4.60 LC-MS spectra of atrazine photocatalytic degradation using 0.005Ag-0.005Ce-ZnO (S) powder at (g) 120, (h) 150, and (i) 180 min of irradiation time.

CHAPTER V

CONCLUSIONS AND RECOMMENDATIONS

5.1 Conclusions

Mechanical coating technique (MCT) was used for catalyst immobilization. XRD and UV-vis-DR results indicated that ZnO_550 had good crystallinity and absorbance. The ZnO_550 could perform photocatalytic degradation of RR120 without cracking. The RR120 removal efficiency of 0.1Ce-ZnO (P) 1:2 bead was higher than that of ZnO_550. ZnO, Ce-ZnO, and Cu-ZnO were successfully synthesized by the simple chemical method using sticky rice starch and polyvinylpyrrolidone as templates.

The characteristics of the catalysts with sticky rice starch and polyvinylpyrrolidone template were quite similar, as demonstrated by TG-DTA, FT-IR, XRD, BET surface area analyzer, and SEM studies. Under visible light irradiation, the 0.02Ce-ZnO (S) showed efficient removal of atrazine at the pH of the isoelectric point. The sticky rice starch template could represent an environmental friendly alternative for ZnO and Ce-ZnO photocatalyst synthesis.

Ce-ZnO at both 0.02 and 0.1 molar ratios of doping showed the higher atrazine removal than Cu-ZnO. The proper weight ratio of zinc(II) nitrate hexahydrate and sticky rice starch template was 5:1. The optimal catalyst loadings were 0.1 g for catalyst powder, 2.5 g for ZnO_550, and 5.0 g for 0.02Ce-ZnO (S) 5:1 bead per 100 mL of atrazine solution (5 mg/L). Changing of pH in atrazine solution was quite unaffected on atrazine removal. Discharge of Zn into atrazine solution in the system was quite insignificant. The SO_4^{2-} and Cl^- anions enhanced the atrazine photocatalytic degradation while CO_3^{2-} , HCO_3^- , and HPO_4^{2-} inhibited the atrazine photocatalytic degradation at all concentrations of the sodium salt.

0.005Ag-0.005Ce-ZnO (S) was successfully prepared and presented superiority on atrazine degradation. The photocatalytic degradation of atrazine under the experimental conditions of this study agreed with the kinetics of LHHW model. Atrazine was completely eliminated at 180 min of irradiation with ZnO powder while it was mainly removed around 87% with 0.005Ag-0.005Ce-ZnO (S). The TOC decrease reached 64 and 65% for atrazine photocatalytic degradation by 0.005Ag-0.005Ce-ZnO (S) and ZnO powders, respectively. The cyanuric acid was not observed as the final product in atrazine photocatalytic degradation.

5.2 Recommendations

- 1) The ability of catalyst to absorb a specific wavelength of light depends upon the band gap. However, the commercial ZnO, which properly absorbs the UV light due to its band gap, had high potential to remove atrazine under visible light irradiation in this study although the prepared catalysts such as 0.02Ce-ZnO (S) 5:1 and 0.05Ag-0.05Ce-ZnO (S) presented the good characteristics to have better activity under visible light compared to the commercial ZnO. Therefore, it needs the intensive works to explain this phenomenon. The molecular structure of the catalyst and the computational chemistry may help to identify what is controlling the band gap.
- 2) The non-point source study requires the method for measuring at the very low concentration of atrazine. The more proper conditions of HPLC and/or the other analytical techniques lead to obtain the higher detection limit of atrazine concentration measurement that can meet the non-point source goal.
- 3) The pH of atrazine solution should be measured after running the photocatalytic reaction in the presence of anions particularly in the presence of CO_3^{2-} and HCO_3^{2-} .
- 4) TOC measurement or humic acid absorbance over irradiation time is the possible way to confirm that atrazine photocatalytic degradation rate was slow because the humic acid competed for hydroxyl radicals.
- 5) Adsorption mechanism and other unidentifiable factors taken place in the ZnO_550 are important to be understood.

- 6) The ZnO₅₅₀ activity decrease during the five-cycle reuse which may be due to the erosion of ZnO powder during drainage the rest of atrazine solution after finishing each cycle. Development of MCT is necessary in further study.
- 7) The IEP is controlled by the number of acidic functional groups such as terminal oxygen groups that can bind with a proton. Possibly, the starch, having more oxygen atom, adds oxygen to the inorganic matrix that then acts as an acid/base functional group. The reason why the IEPs of the same catalyst prepared from polyvinylpyrrolidone and sticky rice starch were different although the templates were finally removed by calcination should be answered. The oxygen content measurement via elemental analysis is recommended. The second possibility is that the two templates are different enough in size and shape such that the inorganic catalyst has a different molecular structure depending upon the type of template employed. Having a different molecular structure could allow for different numbers of acid/base groups, or even just controlling the pK_a of those acid/base groups. This could be tested by examining the crystal structure for the catalysts.
- 8) How Zn²⁺ and template accompany during the catalyst synthesis needs to be understood and studied further.

REFERENCES

- ACROS ORGANICS BVBA. Safety data sheet: polyvinylpyrrolidone. [online]. 2008. Available from: www.acros.com/DesktopModules. [2011, July 27]
- Aggarwal, P., Dollimore, D., and Heon, K. Comparative thermal analysis study of two biopolymers, starch and cellulose. Journal of Thermal Analysis 50 (1997): 7-17.
- Aimable, A., Buscaglia, M.T., Buscaglia, V., and Bowen, P. Polymer-assisted preparation of ZnO nanoparticles with narrow particle size distribution. Journal of the European Ceramic Society 30 (2010): 591-598.
- Akyol, A., and Bayramoğlu, M. Photocatalytic degradation of Remazol Red F3B using ZnO catalyst. Journal of Hazardous Materials B 124 (2005): 241-246.
- Akyol, A., and Bayramoglu, M. The degradation of an azo dye in a batch slurry photocatalytic reactor. Chemical Engineering and Processing 47 (2008): 2150-2156.
- Akyol, A., Yatmaz, H.C., and Bayramoglu, M. Photocatalytic decolorization of remazol red RR in aqueous ZnO suspensions. Environmental 54 (2004): 19-24.
- Ali, R., Bakar, W.A.W.A, and Teck, L.K. Zn/ZnO/TiO₂ and Al/Al₂O₃/TiO₂ photocatalysts for the degradation of cypermethrin. Modern Applied Science 4 (2010): 59-65.
- Alvord, H.H., and Kadlec, R.H. Atrazine fate and transport in the Des Plaines Wetlands. Ecological Modelling 90 (1996): 97-107.
- Anandan, S., Vinu, A., Mori, T., Gokulakrishnan, N., Srinivasu, P., Murugesan, V., and Ariga, K. Photocatalytic degradation of 2,4,6-trichlorophenol using lanthanum doped ZnO in aqueous suspension. Catalysis Communications 8 (2007): 1377-1382.

- Anandan, S., Vinu, A., Sheeja Lovely, K.L.P., Gokulakrishnan, N., Srinivasu, P., Mori, T., Murugesan, V., Sivamurugan V., and Ariga, K. Photocatalytic activity of La-doped ZnO for the degradation of monocrotophos in aqueous suspension. Journal of Molecular Catalysis A: Chemical 266 (2007): 149-157.
- Bajamundi, C.J.E., Dalida, M.L.P., Wantala, K., Khemthong, P., and Girsdanurak, N. Effect of Fe³⁺ doping in the performance of TiO₂ mechanocoated alumina bead photocatalysts. Korean Journal of Chemical Engineering 28 (2011): 1688-1692.
- Barron, A.R., and Smith, C. Crystal structure. [online]. 2010. Available from: <http://cnx.org/content/m16927/latest/>. [2012, May 27]
- Basfar, A.A., Mohamed, K.A., Al-Abduly, A.J., and Al-Shahrani, A.A. Radiolytic degradation of atrazine aqueous solution containing humic substances. Ecotoxicology and Environmental Safety 72 (2009): 984-953.
- Behnajady, M.A., Modirshahla, N., and Hamzavi, R. Kinetic study on photocatalytic degradation of C.I. Acid Yellow 23 by ZnO photocatalyst. Journal of Hazardous Materials B 133 (2006): 226-232.
- Beninca, C., Demiate, I.M., Lacerda, L.G., Carvalho Filho, M.A.S., Ionashiro, M., and Schnitzler, E. Thermal behavior of corn starch granules modified by acid treatment at 30 and 50°C. Ecletica Quimica 33 (2008): 13-18.
- Bicudo, S.C.W., Demiate, I.M., Bannach, G., Lacerda, L.G., Carvalho Filho, M.A.S., Ionashiro, M., and Schnitzler, E. Thermoanalytical study and characterization of native starches of Paraná pine seeds (*Araucaria angustifolia*, Bert O. Ktze) and European chesnut seeds (*Castanea sativa*, Mill). Ecletica Quimica 34 (2009): 7-12.
- Campanati, M., Fornasari, G., and Vaccari, A. Fundamental in the preparation of heterogeneous catalyst. Catalysis Today 77 (2003): 299-314.

- Carlin, V., Minero, C., and Pelizzetti, E. Effect of chlorine on photocatalytic degradation of organic contaminants. Environmental Technology 11 (1990): 919-926.
- Carlo Erba Reagents. Safety data sheet: zincoxide. [online]. 2011. Available from: www.carloerbareagenti.com/repository/DIR199/CH0565_GB.pdf. [2012, March 1]
- Cheng, C., Jiang, Z.J., and Liu, C.Y. Plus green emission of ZnO nanorods induced by Ce^{3+} doping and concentration. Journal of Photochemistry and Photobiology A: Chemistry 195 (2008): 151-155.
- Cho, I.H., and Zho, K.D. Photocatalytic degradation of azo dye (Reactive Red 120) in TiO_2/UV system: optimization and modeling using a response surface methodology (RSM) based on the central composite design, Dyes and Pigments 75 (2007): 533-543.
- Chung, S.W., and Gu, R.R. Prediction of the fate and transport processes of atrazine in a reservoir. Environment Management 44 (2009): 46-61.
- Chunming, C., Jingwen, R., and Qiunan, Y. Preparation of mesoporous titania particles using ionic liquid dissolving starch as templates. Rare Metals 28 (2009): 434-438.
- Comparelli, R., Fanizza, E., Curri, M.L., Cozzoli, P.D., Mascolo, G., Agostiano, A. UV-induced photocatalytic degradation of azo dyes by organic-capped ZnO nanocrystals immobilized onto substrates. Applied Catalysis B: Environmental 60 (2005): 1-11.
- Daneshvar, N., Aber, S., Seyed Dorraji, M.S., Khataee, A.R., and Rasoulifard, M.H. Photocatalytic degradation of the insecticide diazinon in the presence of prepared nanocrystalline ZnO powders under irradiation of UV-C light. Separation and Purification Technology 58 (2007): 91-98.

- Daneshvar, N., Salari, D., and Khataee, A.R. Photocatalytic degradation of azo dye Acid Red 14 in water on ZnO as an alternative catalyst to TiO₂. Journal of Photochemistry and Photobiology A: Chemistry 162 (2004): 317-322.
- De Lasa, H., Serrano, B., and Salaices M. Photocatalytic Reaction Engineering, United States of America: Springer, 2005.
- Department of Agriculture. Imported chemical data. Thailand: Ministry of Agriculture and Cooperative, 2006.
- DESICCA CHEMICALS. Material safety data sheet: activated alumina balls. [online]. 2012. Available from: www.desiccachemical.com/actialuminaballs.html. [2012, March 1]
- Dindar, B., and Içli, S. Unusual photoreactivity of zinc oxide irradiated by concentrated sunlight. Journal of Photochemistry and Photobiology A: Chemistry 140 (2001): 263-268.
- Dionysiou, D.D., Suidan, M.T., Bekou, E., Baudin, I., and Laîné, J.M. Effect of ionic strength and hydrogen peroxide on the photocatalytic degradation of 4-chlorobenzoic acid in water. Applied Catalysis B: Environmental 26 (2000): 153-171.
- Dmitrieva, I.B., Tikhomolova, K.P., Chukhno, A.S., Prokopovich, P.P., and Starov, V.M. Investigation of the electrochemical properties of NiO and Fe₂O₃ in azole solution. Colloids and Surfaces A: Physicochemical and Engineering Aspects 300 (2007): 315-320.
- Escobedo Morales, A., Sánchez Mora, E., and Pal, U. Use of diffuse reflectance spectroscopy for optical characterization of un-supported nanostructures. Revista Mexicana de Física S 53 (2007): 18-22.
- Eskandari, M., Ahmadi, V., and Ahmadi, S.H. Low temperature synthesis of ZnO nanorods by using PVP and their characterization. Physica B 404 (2009): 1924-1928.

- Evgenidou, E., Fytianos, K., and Poullos, I. Semiconductor-sensitized photodegradation of dichlorvos in water using TiO₂ and ZnO as catalysts. Applied Catalysis B: Environmental 59 (2005): 81-89.
- Flynn, K., and Spellman, T. Environmental levels of atrazine decrease spatial aggregation in the freshwater mussel, *Elliptio complanata*. Ecotoxicology and Environment Safety 72 (2009): 1228-1233.
- Fogler, H.S. Elements of chemical reaction engineering, Fourth edition. United States of America: Person education, 2006.
- Fons, P., Yamada, A., Iwata, K., Matsubara, K., Niki, S., Nakahara, K., and Takasu, H. An EXAFS and XANES study of MBE grown Cu-doped ZnO. Nuclear Instruments and Methods in Physics Research B 199 (2003): 190-194.
- Fu, R. Analysis of atrazine in drinking water at the ppb level using new Agilent reversed phase LC columns. [Online]. 2009. Available from: www.labplus.co.kr/tech/.../5989-8328EN_Atrazine.pdf. [2009, November 25]
- Fujishima, A., Zhang, X., and Tryk, D.A. Heterogeneous photocatalysis: from water photolysis to applications in environmental cleanup. International Journal of Hydrogen Energy 32 (2007): 2664-2672.
- Gaya, U.I., Abdullah, A.H., Zainal, Z., Hussein, M.Z. Photocatalytic treatment of 4-chlorophenol in aqueous ZnO suspensions: intermediates, influence of dosage and inorganic anions. Journal of Hazardous Materials 168 (2009): 57-63.
- Ghorai, S., and Pant, K.K. Equilibrium, kinetics and breakthrough studies for adsorption of fluoride on activated alumina. Separation and Purification Technology 42 (2005): 265-271.
- Guse, D., Bruzek, M.J., DeVos, P., and Brown, J.H. Journal of Electroanalytical Chemistry 626 (2009): 171-173.

- Haber, J., Block, J.H., and Delmon, B. Manual of methods and procedures for catalyst characterization. Pure and Applied Chemistry 67 (1995): 1257-1306.
- Han, J., Mantas, P.Q., and Senos, A.M.R. Defect chemistry and electrical characteristics of undoped and Mn-doped ZnO. Journal of the European Ceramic Society 22 (2002): 49-59.
- Hayes, T., Haston, K., Tsui, M., Hoang, A., Haeffele, C., and Vonk, A. Atrazine – induced hermaphroditism at 0.1 ppb in American Leopard Frogs (*Rana pipiens*): laboratory and field evidence. Environment Health Perspectives 111: 4 (2003): 568-575.
- Heepngoan, P., Sajjaphan, K., and Boonkerd, N. Effect of organic fertilizer amendment on atrazine biodegradation in soil. Kamphaengsean Academic Journal 6: 3 (2008): 14-21.
- Héquet, V., Gonzalez, C., and Le Cloirec, P. Photochemical processes for atrazine degradation: methodological approach. Water Research 35 (2001): 4253-4260.
- Herrmann, J.M. Heterogeneous photocatalysis: fundamentals and applications to the removal of various types of aqueous pollutants. Catalysis Today 53 (1999): 115-129.
- Hong, R.Y., Li, J.H., Chen, L.L., Liu, D.Q., Li, H.Z., Zheng, Y., and Ding, J. Synthesis, surface modification and photocatalytic property of ZnO nanoparticles. Powder Technology 189 (2009): 426-432.
- Horikoshi, S., and Hidaka, H. Non-degradable triazine substrate of atrazine and cyanuric acid hydrothermally and in supercritical water under the UV-illuminated photocatalytic cooperation. Chemosphere 51 (2003): 139-142.
- Hustert, K., Moza, P.N., and Pouyet, B. Photocatalytic degradation of s-triazine herbicides. Toxicological and Environmental Chemistry 31 (1991): 97-102.

- Iwasaki, M., Davis, S.A., and Mann, S. Spongelike macroporous TiO₂ monoliths prepared from starch gel template. Journal of Sol-Gel Science and Technology 32 (2004): 99-105.
- Janardhanan, S.K., Ramasamy, I., and Nair, B.U. Synthesis of iron oxide nanoparticles using chitosan and starch template. Transition Metal Chemistry 33 (2008): 127-131.
- Kaneko, K. Determination of pore size and pore size distribution 1. Adsorbents and catalysts. Journal of Membrane Science 96 (1994): 59-89.
- Ko, H.J., Chen, Y., Hong, S.K., and Yao, T. Doping effects in ZnO layers using Li₃N as a doping source. Journal of Crystal Growth 251 (2003): 628-632.
- Kong, J.Z., Li, A.D., Zhai, H.F., Gong, Y.P., Li, H., and Wu, D. Preparation, characterization of the Ta-doped ZnO nanoparticles and their photocatalytic activity under visible-light illumination. Journal of Solid State Chemistry 182 (2009): 2061-2067.
- Konstantinou, I.K., and Albanis, T.A. Photocatalytic transformation of pesticides in aqueous titanium dioxide suspensions using artificial and solar light: intermediates and degradation pathways. Applied Catalysis B: Environmental 1310 (2002): 1-17.
- Kosin, P. Visible light photodegradation of 2,4-dichlorophenol in aqueous solution on Fe(III)/N Co-doped TiO₂: effect of amine template. Master's Thesis, Graduate School, Chulalongkorn University, 2009.
- Kruawal, K., Sacher, F., Werner, A., Muller, J., and Knepper, T.P. Chemical water quality in Thailand and its impacts on the drinking water production in Thailand. Science of the Total Environment 340 (2005): 57-70.
- Krýsová, H., Jirkovský, J., Krýsa, J., Mailhot, G., and Bolte, M. Comparative kinetic study of atrazine photodegradation in aqueous Fe(ClO₄)₃ solutions and TiO₂ suspensions. Applied Catalysis B: Environmental 40 (2003): 1-12.

- Kumbhakar, P., Singh, D., Tiwary, C.S., and Mitra, A.K. Chemical synthesis and visible photoluminescence emission from monodispersed ZnO nanoparticles. Chalcogenide Letters 5: 12 (2008): 387-394.
- Kwon, Y.J., Kim, K.H., Lim, C.S., and Shim, K.B. Characterization of ZnO nanopowders synthesized by the polymerized complex method via an organochemical route. Journal of Ceramic Processing Research 3: 3 (2002): 146-149.
- Lackhoff, M., and Niessner, R. Photocatalytic atrazine degradation by synthetic minerals, atmospheric aerosols, and soil particles. Environmental Science and Technology 36 (2002): 5342-5347.
- Lair, A., Ferronato, C., Chovelon, J.-M., and Herrmann, J.-M. Naphthalene degradation in water by heterogeneous photocatalysis: an investigation of the influence of inorganic anions. Journal of Photochemistry and Photobiology A: Chemistry 193 (2008): 193-203.
- Lee, M.A., Park, B.J., Chin I.J., and Choi H.J. Polymer modified hematite nanoparticles for electrophoretic display. Journal of Electroceramics 23 (2009): 474-477.
- Li, D., and Haneda, H. Morphologies of zinc oxide particles and their effects on photocatalysis. Chemosphere 51 (2003): 129-137.
- Lin, T.F., and Wu, J.K. Adsorption of arsenite and arsenate within activated alumina grains: equilibrium and kinetics. Water Research 35 (2001): 2049-2057.
- Ling, Q., Sun, J., Zhou, Q., Zhao, Q., Ren, H. Visible-light-driven boron/ferrous/cerium/titania photocatalyst. Journal of Photochemistry and Photobiology A: Chemistry 200 (2008): 141-147.
- Liqiang J., Fulong Y., Haige H, Baifu, X., Weimin, C., and Honggang F. Relationship of surface oxygen vacancies with photoluminescence and photocatalytic

performance of ZnO nanoparticles. Science in China, Series B: Chemistry 48: 1 (2005): 25-30.

Liu, C., Chen, W., Sheng, Y., and Li, L. Atrazine degradation in solar irradiation/ S-doped titanium dioxide treatment. [Online]. 2009. Available from: http://ieeexplore.ieee.org/xpls/abs_all.jsp?arnumber=5162423&tag=1. [2009, December 1]

Liu, X.C., Shi, E.W., Chen, Z.Z., Chen, B.Y., Huang, W., Song, L.X., Zhou, K.J., Cui, M.Q., Xie, Z., He, B., and Wei, S.Q. The local structure of Co-doped ZnO films studied by X-ray absorption spectroscopy. Journal of Alloys and Compounds 463 (2008): 435-439.

Maensiri, S., Laokul, P., and Klinkaewnarong, J. A simple synthesis and room-temperature magnetic behavior of Co-doped anatase TiO₂ nanoparticles. Journal of Magnetism and Magnetic Materials 302 (2006): 448-453.

Maensiri, S., Laokul, P., and Phokha, S. A simple synthesis and magnetic behavior of nanocrystalline Zn_{0.9}Co_{0.1}O powders by using Zn and Co acetates and polyvinylpyrrolidone as precursors. Journal of Magnetism and Magnetic Materials 305 (2006): 381-387.

Maensiri, S., Laokul, P., and Promarak, V. Synthesis and optical properties of nanocrystalline ZnO powders by a simple method using zinc acetate dihydrate and poly(vinyl pyrrolidone). Journal of Crystal Growth 289 (2006): 102-106.

Marto, J., São Marcos, P., Trindade, T., and Labrincha, J.A. Photocatalytic decolouration of Orange II by ZnO active layers screen-printed on ceramic tiles. Journal of Hazardous Materials 163 (2009): 36-42.

McGlamery, M.D., and Slife F.W. The adsorption and desorption of atrazine as affected by pH, temperature, and concentration. [Online]. 1966. Available from: <http://www.jstor.org/stable/4040921>. [2009, December 1]

- McMurray, T.A., Dunlop, P.S.M., and Byrne, J.A. The photocatalytic degradation of atrazine on nanoparticulate TiO₂ films. Journal of Photochemistry and Photobiology A: Chemistry 182 (2006): 43-51.
- Minero, C., Maurino, V., and Pelizzetti, E. Heterogeneous photocatalytic transformations of s-triazine derivatives. Research on Chemical Intermediates 23 (1997): 291-310.
- Minero, C., Pelizzetti, E., Malato, S., and Blanco, J. Large solar plant photocatalytic water decontamination: degradation of atrazine. Solar Energy 56 (1996): 411-419.
- Mohammadi, M.R., and Fray, D.J. Nanostructured TiO₂-CeO₂ mixed oxides by an aqueous sol-gel process: effect of Ce:Ti molar ratio on physical and sensing properties. Sensors and Actuators B Chemical 150 (2010) 613-640.
- Mortimer, R.G. Physical chemistry. The United States of America: The Benjamin/Cummings Publishing Company, Inc., 1993.
- Murphy, A.B. Band-gap determination from diffuse reflectance measurements of semiconductor films, and application to photoelectrochemical water-splitting. Solar Energy Materials and Solar Cells 91 (2007): 1326-1337.
- Nagao, M., Morishige, K., Takeshta, T., and Morimoto, T. Porous Structure Formed by the Decomposition of the Surface Product in ZnO Preserved in the Atmosphere. Bulletin of the Chemical Society of Japan 47: 9 (1974): 2107-2110.
- Navas, J., Fernández-Lorenzo, C., Aguilar, T., Alcántara, R., and Martín-Calleja, J. Improving open-circuit voltage in DSSCs using Cu-doped TiO₂ as a semiconductor. Physica Status Solidi A (2011): 1-8.
- Niemantsverdriet, J.W. Spectroscopy in catalysis: an introduction, Third, completely revised and enlarged edition. Federal Republic of Germany: Wiley-VCH, 2007.

- Oh, Y.C., and Jenks, W.S. Photocatalytic degradation of a cyanuric acid, a recalcitrant species. Journal of Photochemistry and Photobiology A: Chemistry 162 (2004): 323-328.
- Pardeshi, S.K., and Patil A.B. Solar photocatalytic degradation of resocinol a model endocrine disrupter in water using zinc oxide. Journal of Hazardous Materials 163 (2009): 403-409.
- Pare, B., Jonnalagadda, S.B., Tomar, H., Singh, P., and Bhagwat, V.W. ZnO assisted photocatalytic degradation of acridine orange in aqueous solution using visible irradiation. Desalination 232 (2008): 80-90.
- Parra, S., Stanca, S.E., Guasaquillo, I., and Thampi, K.R. Photocatalytic degradation of atrazine using suspended and supported TiO₂. Applied Catalysis B: Environmental 51(2004): 107-116.
- Pawinrat, P., Mekasuwandumrong, O., and Panpranot, J. Synthesis of Au-ZnO and Pt-ZnO nanocomposites by one-step flame spray pyrolysis and its application for photocatalytic degradation of dyes. Catalysis Communications 10 (2009): 1380-1385.
- Pelekani, C., and Snoeyink, V.L. A kinetic and equilibrium study of competitive adsorption between atrazine and Congo red dye on activated carbon: the importance of pore size distribution. Carbon 39 (2001): 25-37.
- Pelizzetti, E., Maurino, V., Minero, C., Carlin, V., Pramauro, E., Zerbinati, O., and Tosato, M.L. Photocatalytic Degradation of Atrazine and Other s-Triazine Herbicides. Environmental Science and Technology 24 (1990): 1559-1565.
- Phoka, S., Laokul, P., Swatsitang, E., Promarak, V., Seraphin, S., and Maensiri, S. Synthesis, structural and optical properties of CeO₂ nanoparticles synthesized by a simple polyvinyl pyrrolidone (PVP) solution route. Material Chemistry and Physics 115 (2009): 423-428.

- Plust, S.J., Loehe, J.R., Feher, F.J., Benedict, J.H., and Herbrandson, H.F. Kinetics and mechanism of hydrolysis of chloro-1,3,5-triazines. Atrazine. Journal of Organic Chemistry 46 (1981): 3661-3665.
- Qiu, R., Zhang, D., Mo, Y., Song, L., Brewer, E., Huang, X., and Xiong, Y. Photocatalytic activity of polymer-modified ZnO under visible light irradiation. Journal of Hazardous Materials 156 (2008): 80-85.
- Rauf, M.A., and Ashraf, S.S. Fundamental principles and application of heterogeneous photocatalytic degradation of dyes in solution. Chemical Engineering Journal 151 (2009): 10–18.
- Rector, R.J., Regehr, D.L., Barnes, P.I., and Loughin, T.M. Atrazine, S-metolachlor, and isoxaflutole loss in runn off as affected by rainfall and management. Weed Science 51 (2003): 810-816.
- Rego, E., Marto, J., São Marcos, P., and Labrincha, J.A. Decolouration of Orange II solutions by TiO₂ and ZnO active layers screen-printed on ceramic tiles under sunlight irradiation. Applied Catalyst A: General 355 (2009): 109-114.
- Riahi-Noori, N., Sarraf-Mamoory, R., Alizadeh, P., and Mehdikhani, A. Synthesis of ZnO nano powder by a gel combustion method. Journal of Ceramic Processing Research 9: 3 (2008): 246-249.
- Roguska, A., Kudelski, A., Pisarek, M., Opara, M., and Janik-Czachor, M. Surface-enhanced Raman scattering (SERS) activity of Ag, Au and Cu nanoclusters on TiO₂-nanotubes/Ti substrate. Applied Surface Science 257 (2011): 8182-8189.
- Sakthivel, S., Neppolian, B., Shankar, M.V., Arabindoo, B., Palanichamy, M., and Murugesan, V. Solar photocatalytic degradation of azo dye: comparison of photocatalytic efficiency of ZnO and TiO₂. Solar Energy Materials & Solar Cells 77 (2003): 65-82.

- Shan, F.K., and Yu, Y.S. Band gap energy of pure and Al-doped ZnO thin films. Journal of the European Ceramic Society 24 (2004): 1869-1872.
- Shen, W., Li, Z., Wang, H., Liu, Y., Guo, Q., and Zhang, Y. Photocatalytic degradation for methylene blue using zinc oxide prepared by codeposition and sol-gel methods. Journal of Hazardous Materials 152 (2008): 172-175.
- Shokuhfar, T., Vaezi, M.R., Sadrnezhad, S.K., and Shokuhfar, A. Synthesis of zinc oxide nanopowder and nanolayer via chemical processing. International Journal of Nanomanufacturing 2: 1/2 (2008): 149-161.
- Siddheswaran, R., Sankar, R., Ramesh Babu, M., Rathnakumari, M., Jayavel, R., Murugakoothan, P., and Sureshkumar, P. Preparation and characterization of ZnO nanofibers by electrospinning. Crystal Research and Technology 41: 5 (2006): 446-449.
- Singh, S., Kumar, E.S., and Rao, M.S.R. Microstructural, optical and electrical properties of Cr-doped ZnO. Scripta Materialia 58 (2008): 866-869.
- Smith, J.M. Chemical Engineering Kinetics, Third edition. Singapore: McGRAW-HILL, 1981.
- Soultanidis, N., and Barron, A.R. TGA/DSC-FTIR characterization of oxide nanoparticles. [online]. 2009. Available from: <http://creativecommons.org/licenses/by/3.0/>. [2011, January 8]
- Spark, K.M., and Swift, R.S. Effect of soil composition and dissolved organic matter on pesticide sorption. The Science of the Total Environment 298 (2002): 147-161.
- Spathis, P., and Poulios, I. The corrosion and photocorrosion of zinc and zinc oxide coatings. Corrosion Science 37 (1995): 673-680.
- Spring, K.R., and Davidson, M.W. Sources of visible light. [Online]. 2011. Available from: www.olympusmicro.com/primer/lightandcolor/lightsourcesintro.html. [2011, July 27]

- Sui, Y., Yang, H., Fu, W., Xu, J., Chang L., Zhu, H., Yu, Q., Li, M., and Zou, G. Preparation and characterization of hollow glass microspheres/ZnO composites. Journal of Alloys and Compounds 469 (2009): L1-L5.
- Sukjaroen, K., and Prayoonrat, P. Effect of certain herbicides on Mungbean. [Online]. (2001) Available from: <http://plantpro.doae.go.th/weed-research/P-44.pdf> . [2009, December 1]
- Sun, L., Rippon, J.A., Cookson, P.G., Koulaeva, O., and Wang, X. Effects of undoped and manganese-doped zinc oxide nanoparticles on the colour fading of dyed polyester fabrics. Chemical Engineering Journal 147 (2009): 391-398.
- The Earth's Best Defense. Atrazine contamination in Iowa. [Online]. 2007. Available from: http://docs.nrdc.org/health/files/hea_07091201c.pdf. [2009, March 2]
- Thelin, G.P., and Gianessi, L.P. Method for estimating pesticide use for county areas of the conterminous United States. [Online]. 2000. Available from: <http://water.usgs.gov/nawqa/pnsp/pubs/ofr00250/ofr00250.pdf>. [2009, December 1]
- Tomerlin, J.R. 1989. Dietary exposure and oncogenic risk assessment for atrazine. United States Environmental Protection Agency Washington, D.C. 20460: 1-10.
- Tong, Y., Cheng, J., Liu Y., and Sui, G.G. Enhanced photocatalytic performance of ZnO hierarchical nanostructures synthesized via a two-temperature aqueous solution route. Scripta Materialia 60 (2009): 1093-1096.
- Ullah, R., and Dutta, J. Photocatalytic degradation of organic dyes with manganese-doped ZnO nanoparticles. Journal of Hazardous Materials 156 (2008): 194-200.
- United States Environmental Protection Agency (U.S. EPA.). Atrazine chemical summary U.S.EPA toxicity and exposure assessment for children's health

atrazine. [Online]. 2007. Available from: www.epa.gov/teach/chem_summ/Atrazine_summary.pdf. [2009, March 2]

United States Environmental Protection Agency (U.S. EPA.). National Secondary Drinking Water Regulations. [Online]. 2007. Available from: <http://water.epa.gov/drink/contaminants/index.cfm>. [2011, July 27]

United States Environmental Protection Agency (U.S. EPA.). Technical Factsheet on: Atrazine. [Online]. 2003. Available from: www.epa.gov/safewater/pdfs/factsheets/soc/tech/altrazine.pdf. [2009, March 2]

Vaithianathan, V., Lee, Y.H., Lee, B.T., Hishita, S., and Kim, S.S. Doping of As, P and N in laser deposited ZnO films. Journal of Crystal Growth 287 (2006): 85-88.

Vidyasagar, C.C., Arthoba Naik, Y., Venkatesh, T.G., and Viswanatha, R. Solid-state synthesis and effect of temperature on optical properties of Cu-ZnO, Cu-Cdo and CuO nanoparticles. Powder Technology 214 (2011): 337-343.

Villaseñor, J., and Mansilla, H.D. Effect of temperature on kraft black liquor degradation by ZnO-photoassisted catalysis. Journal of Photochemistry and Photobiology A: Chemistry 93 (1996): 205-209.

Vitanov, N.K., Lekova, K.I., and Dobрева, N.I. Monitoring river water in the lower Danube for atrazine contamination. ACTA Chromatographica 13 (2003): 230-242.

Wang, B., Callahan, M.J., Xu, C., Bouthillette, L.O., Giles, N.C., Bliss, D.F. Hydrothermal growth and characterization of indium-doped-conducting ZnO crystals. Journal of Crystal Growth 304 (2007): 73-79.

Wang, H., Wick, R.L., and Xing, B. Toxicity of nanoparticulate and bulk ZnO, Al₂O₃ and TiO₂ to the nematode *Caenorhabditis elegans*. Environmental Pollution 157 (2009): 1171-1177.

- Wang, H., Xie, C., Zhang, W., Cai, S., Yang, Z., and Gui, Y. Comparison of dye degradation efficiency using ZnO powders with various size scales. Journal of Hazardous Materials 141 (2007): 645-652.
- Wang, J., Jiang, Z., Zhang, Z., Xie, Y., Lv, Y., Li, J., Deng, Y., and Zhang, X. Study on inorganic oxidants assisted sonocatalytic degradation of Acid Red B in presence of nano-sized ZnO powder. Separation and Purification Technology 67 (2009): 38-43.
- Wang, J., Jiang, Z., Zhang, Z., Xie, Y., Wang, X., Xing, Z., Xu, R., and Zhang, X. Sonocatalytic degradation of acid red B and rhodamine B catalyzed by nano-size ZnO powder under ultrasonic irradiation. Ultrasonics Sonochemistry 15 (2008): 768-774.
- Wang, L., Zhang, X., Shou, C., Hong, X., Qiao, Q., and Liu, Y. Hexamethylenediamine-assisted hydrothermal preparation of uniform ZnO particles and their morphology-dependent photoluminescent properties. Materials Chemistry and Physics 115 (2009): 547-550.
- Wang, W., Gu, M., and Jin, Y. Effect of PVP on the photocatalytic behavior of TiO₂ under sunlight. Materials Letters 57 (2003): 3276-3281.
- Wang, X.H., Li, J.-G., Kamiyama, H., Katada, M., Ohashi, N., Moriyoshi, Y., and Ishigaki, T. Pyrogenic iron(III)-doped TiO₂ nanopowders synthesized in RF thermal plasma: phase formation, defect structure, band gap, and magnetic properties. Journal of the American Chemical Society 127 (2005): 10982-10990.
- Wang, Y., Li, X., Lu, G., Chen, G., and Chen, Y. Synthesis and photo-catalytic degradation property of nanostructured-ZnO with different morphology. Materials Letters 62 (2008): 2359-2362.
- Wei, S.F., Lian, J.S., and Jiang, Q. Controlling growth of ZnO rods by polyvinylpyrrolidone (PVP) and their optical properties. Applied Surface Science 255 (2009): 6978-6984.

- Xin, B., Wang, P., Ding, D., Liu, J., Ren, Z., and Fu, H. Effect of surface species on Cu-TiO₂ photocatalytic activity. Applied Surface Science 254 (2008): 2569-2574.
- Xu, W., Yu, Y., Zhang, C., and He, H. Selective catalytic reduction of NO by NH₃ over a Ce/TiO₂ catalyst. Catalysis Communications 9 (2008): 1453-1457.
- Yoong, L.S., Chong, F.K., and Dutta, B.K. Development of copper-doped TiO₂ photocatalyst for hydrogen production under visible light. Energy 34 (2009): 1652-1661.
- Yoshida, H., Lu, Y., Nakayama, H., and Hirohashi, M. Fabrication of TiO₂ film by mechanical coating technique and its photocatalytic activity. Journal of Alloys and Compounds 475 (2009): 383-386.
- Zadaka, D., Nir, S., Radian, A., and Mishael, Y.G. Atrazine removal from water by polycation-clay composites: effect of dissolved organic matter and comparison to activated carbon. Water Research 43 (2009): 677-683.
- Zhang, H., Chen, G., Yang, G., Zhang, J., and Lu, X. Optical properties of amorphous/crystalline ZnO nano-powder prepared by solid state reaction. Journal of Material Science: Material in Electronics 18 (2007): 381-384.
- Zheng, M.P., Gu, M.Y., Jin, Y.P., Wang, H.H., Zu, P.F., Tao, P., and He, J.B. Effects of PVP on structure of TiO₂ prepared by the sol-gel process. Materials Science and Engineering B 87 (2001): 197-201.

APPENDICES

APPENDIX A

Catalyst preparation

A.1 Mechanical coating technique



Figure A.1 Raw material images: (a) Al_2O_3 beads and (b) commercial ZnO powder.

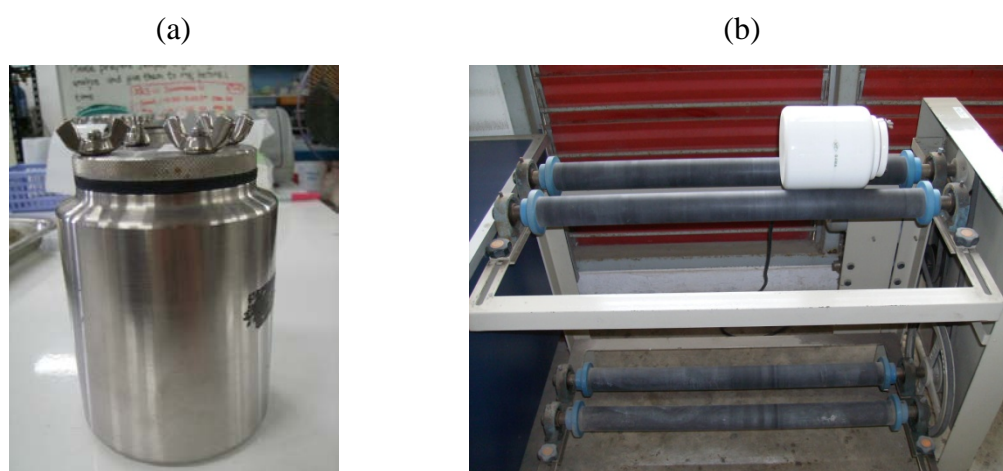


Figure A.2 Mechanical coating apparatuses: (a) milling pot and (b) milling machine.

A.2 Condition of catalyst preparation via simple chemical method

Table A.1 pH of precursor measured during catalyst preparation.

Catalyst	pH			
	Distilled water	After adding template	After adding $\text{Zn}(\text{NO}_3)_2 \cdot 6\text{H}_2\text{O}$ solution	After adding $\text{Ce}(\text{NO}_3)_3 \cdot 6\text{H}_2\text{O}$ solution
0.02Ce-ZnO (S) 1:2	6.91	5.56	3.75	4.74
0.02Ce-ZnO (P) 1:2	6.91	4.46	2.32	5.16



Figure A.3 Appearance of (a) 0.02Ce-ZnO polyvinylpyrrolidone gel and (b) 0.02Ce-ZnO starch gel.



Figure A.4 Appearance of (a) Ce-ZnO (P) 1:2 and (b) Ce-ZnO (S) 1:2 after calcination.



Figure A.5 Appearance of (a) Ce-ZnO (P) 1:2 and (b) Ce-ZnO (S) 1:2 beads.

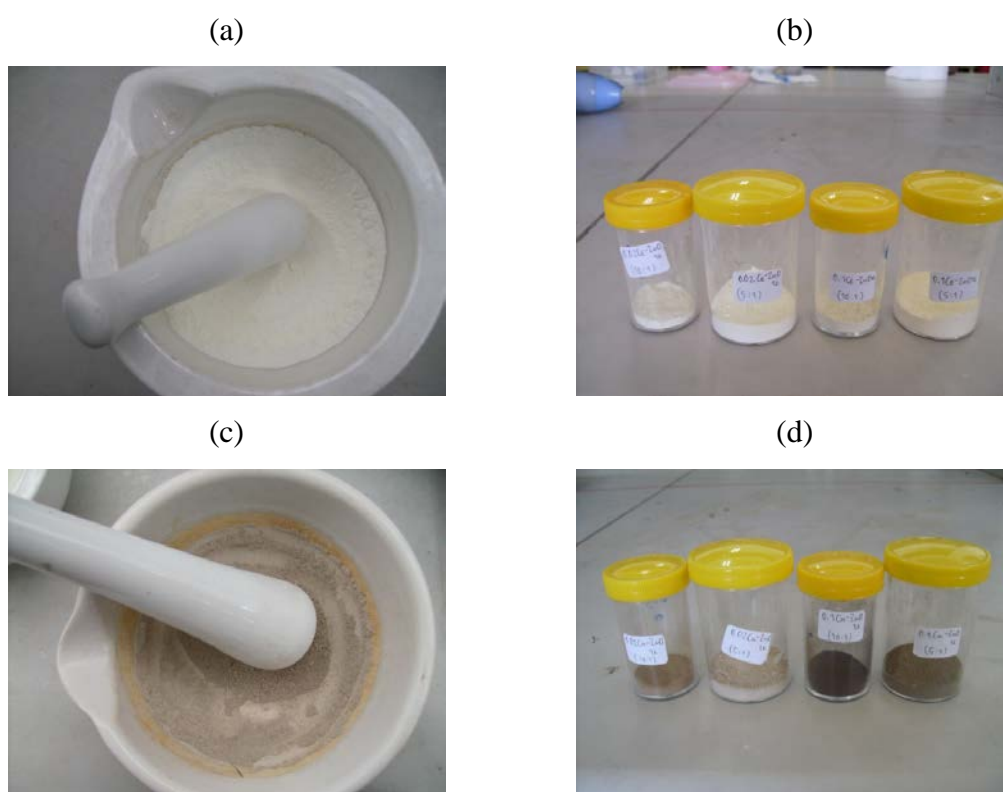


Figure A.6 Appearance of (a) and (b) Ce-ZnO (S), and (c) and (d) Cu-ZnO (S).

APPENDIX B

Characterization

B.1 Zeta potential data

Table B.1 Average zeta potential of catalysts.

Catalyst	Average zeta potential (mV) at pH				
	4	6	8	10	12
ZnO commercial	15.60	13.80	14.47	-14.74	-32.16
0.1Ce-ZnO (S)	11.13	13.17	12.99	-35.62	-42.93
0.1Ce-ZnO (P)	8.87	-18.05	-11.80	-15.10	-28.21
0.1Cu-ZnO (S)	7.03	5.16	6.51	8.46	-42.24
ZnO (S)	16.41	10.30	14.20	-38.82	-35.20
Al ₂ O ₃	15.06	12.47	-15.14	-31.30	-35.16

APPENDIX C

Calibration

C.1 RR120 calibration data

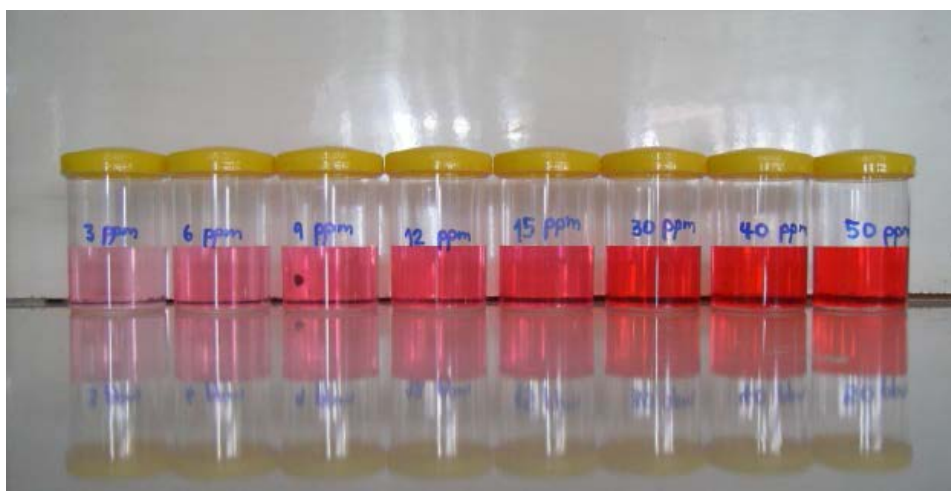


Figure C.1 Appearance of RR120 standard solution at different concentrations.

Table C.1 RR120 standard solution and absorbance from UV-vis spectrometer.

Standard no.	RR120 Concentration (mg/L)	Absorbance
1	3.0	0.0675
2	6.0	0.1447
3	9.0	0.2224
4	12.0	0.2943
5	15.0	0.3684
6	30.0	0.7375
7	40.0	0.9802
8	50.0	1.2283

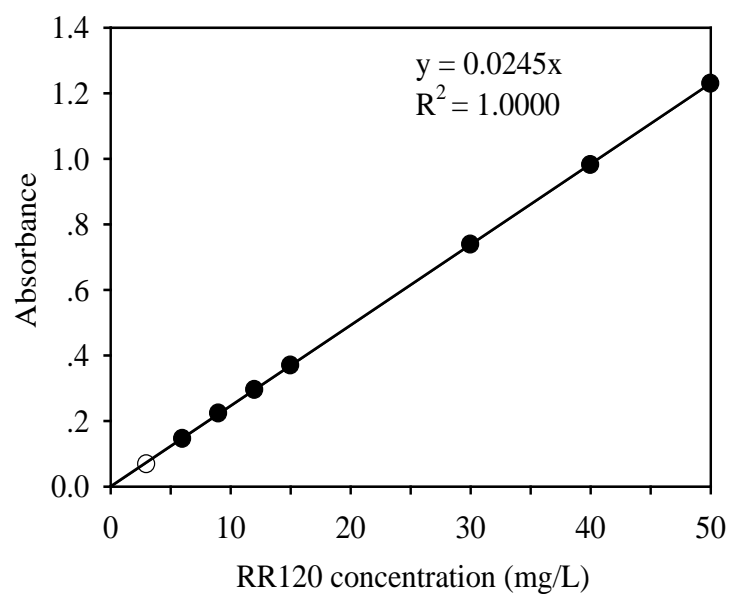


Figure C.2 Calibration curve of RR120 solution.

C.2 Atrazine calibration data

Table C.2 Atrazine standard solution and peak area from HPLC for 10 μ L injection.

Standard no.	Atrazine concentration (mg/L)	Peak area
1	0.5	5.0
2	1.0	8.2
3	5.0	45.5
4	10.0	86.5
5	15.0	129.1
6	18.5	157.1

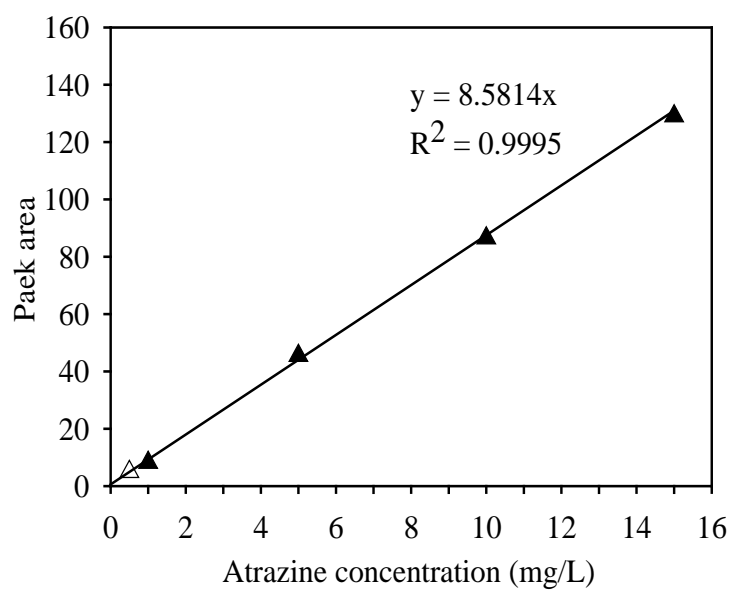


Figure C.3 Calibration curve of atrazine (10 μ L injection).

Table C.3 Atrazine standard solution and peak area from HPLC for 80 μ L injection

Standard no.	Atrazine concentration (mg/L)	Peak area
1	0.1	8.8
2	0.5	38.0
3	1.0	68.3
4	2.5	165.1
5	5.0	344.1
6	10.0	676.3
7	15.2	1040.0

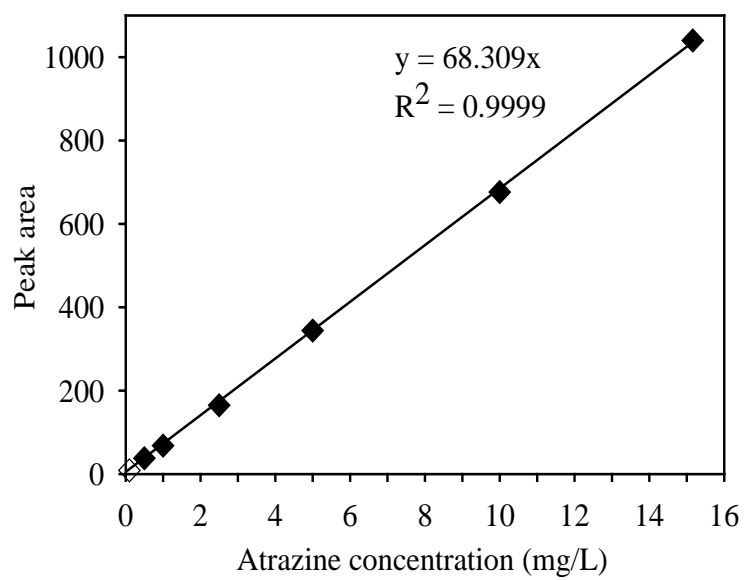


Figure C.4 Calibration curve of atrazine (80 μ L injection).

APPENDIX D

Catalyst activity test

D.1 Reactor setup

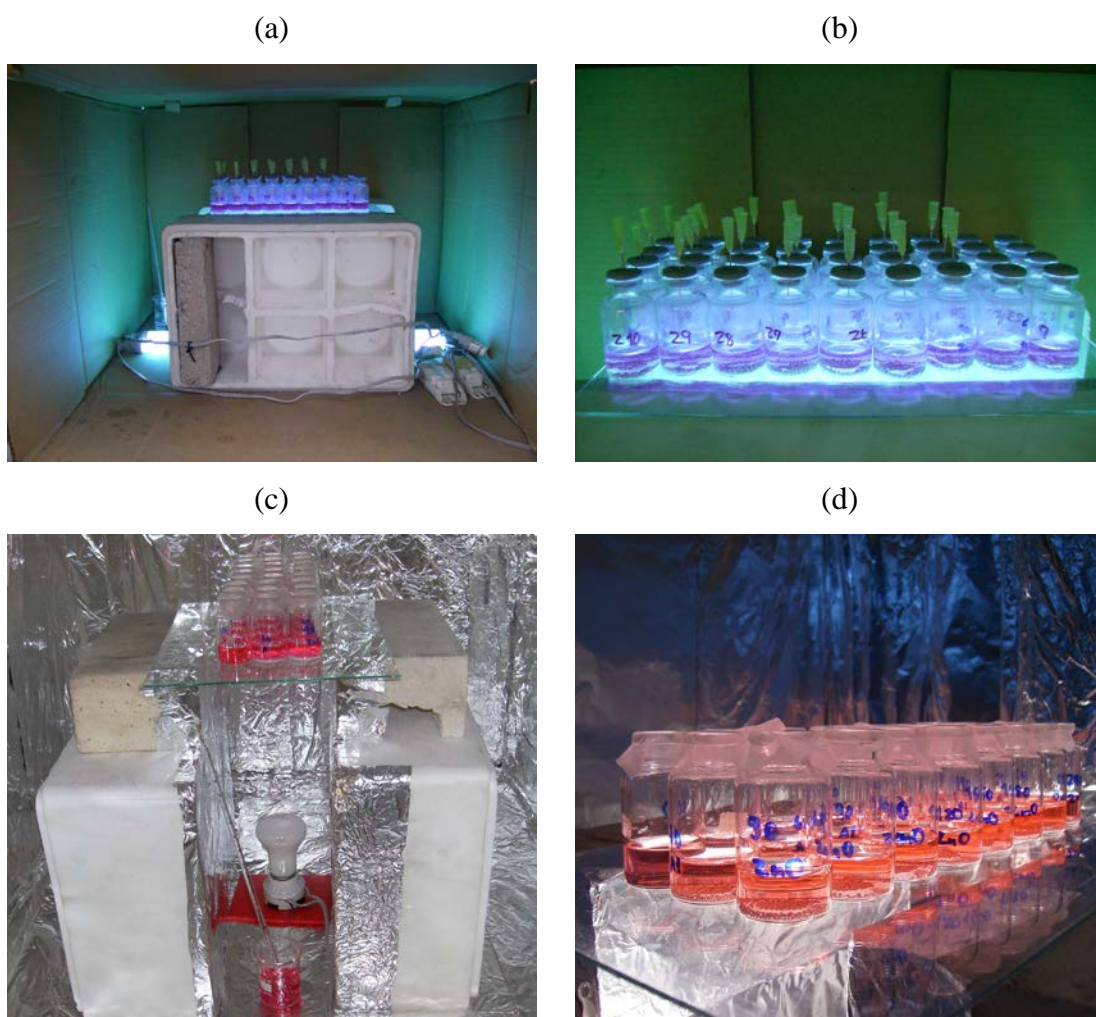


Figure D.1 Reactor for photocatalytic degradation of RR120: (a), (b) under UV light and (c), (d) under visible light irradiation as described the procedure in 3.4.1 and the experimental result in 4.1.2.1.



Figure D.2 Reactor for photocatalytic degradation of atrazine under visible light irradiation as described the procedure in 3.4.2 and the experimental result in 4.1.2.2.

D.2 Immobilization concernment

Table D.1 RR120 adsorption on ZnO_550.

Time (min)	Absorbance at 536 nm		Concentration (mg/L)		Average concentration (mg/L)
	1st	2nd	1st	2nd	
0	0.4614	0.4614	18.833	18.833	18.833
60	0.4118	0.4122	16.808	16.824	16.816
120	0.4001	0.3913	16.331	15.971	16.151
180	0.3836	0.3765	15.657	15.367	15.512
240	0.3623	0.3530	14.788	14.408	14.598
300	0.3563	0.3590	14.543	14.653	14.598
360	0.3486	0.3419	14.229	13.955	14.092
420	0.3405	0.3242	13.898	13.233	13.565
480	0.3468	0.3224	14.155	13.159	13.657
540	0.3466	0.3029	14.147	12.363	13.255
600	0.3304	0.2581	13.486	10.535	12.010

Table D.2 RR120 photolysis under UV light.

Time (min)	Absorbance at 536 nm		Concentration (mg/L)		Average concentration (mg/L)
	1st	2nd	1st	2nd	
0	0.5190	0.5190	21.184	21.184	21.184
60	0.5179	0.5075	21.139	20.714	20.927
120	0.5065	0.5132	20.673	20.947	20.810
180	0.5041	0.5141	20.576	20.984	20.780
240	0.5095	0.5030	20.796	20.531	20.663
300	0.5093	0.5113	20.788	20.869	20.829
360	0.5060	0.5103	20.653	20.829	20.741
420	0.5020	0.5019	20.490	20.486	20.488
480	0.5083	0.5093	20.747	20.788	20.767
540	0.5026	0.4985	20.514	20.347	20.431
600	0.5058	0.5121	20.645	20.902	20.773

Table D.3 RR120 photolysis under visible light.

Time (min)	Absorbance at 536 nm		Concentration (mg/L)		Average concentration (mg/L)
	1st	2nd	1st	2nd	
0	0.4880	0.5205	19.918	21.245	20.582
60	0.4778	0.5046	19.502	20.596	20.049
120	0.4781	0.5119	19.514	20.894	20.204
180	0.4780	0.5129	19.510	20.935	20.222
240	0.4773	0.4921	19.482	20.086	19.784
300	0.4730	0.5046	19.306	20.596	19.951
360	0.4718	0.5102	19.257	20.824	20.041
420	0.4769	0.5074	19.465	20.710	20.088
480	0.4750	0.5045	19.388	20.592	19.990
540	0.4767	0.5097	19.457	20.804	20.131
600	0.4756	0.5023	19.412	20.502	19.957

Table D.4 RR120 photocatalytic degradation under UV light irradiation using ZnO_550.

Time (min)	Absorbance at 536 nm		Concentration (mg/L)		Average concentration (mg/L)
	1st	2nd	1st	2nd	
0	0.5218	0.5218	21.298	21.298	21.298
60	0.3756	0.3293	15.331	13.441	14.386
120	0.2776	0.2785	11.331	11.367	11.349
180	0.1694	0.1637	6.914	6.682	6.798
240	0.1413	0.1203	5.767	4.910	5.339
300	0.0964	0.0797	3.935	3.253	3.594
360	0.0820	0.0500	3.347	2.041	2.694
420	0.0571	0.0332	2.331	1.355	1.843
480	0.0446	0.0360	1.820	1.469	1.645
540	0.0300	0.0245	1.224	1.000	1.112
600	0.0228	0.0155	0.931	0.633	0.782

Table D.5 RR120 photocatalytic degradation under visible light irradiation using ZnO_550.

Time (min)	Absorbance at 536 nm		Concentration (mg/L)		Average concentration (mg/L)
	1st	2nd	1st	2nd	
0	0.4880	0.5043	19.918	20.582	20.361
60	0.3994	0.4009	16.302	16.361	16.341
120	0.3617	0.3542	14.763	14.455	14.558
180	0.3061	0.3223	12.494	13.153	12.933
240	0.2587	0.2747	10.559	11.210	10.993
300	0.2270	0.2228	9.265	9.094	9.151
360	0.2097	0.2174	8.559	8.871	8.767
420	0.1794	0.1953	7.322	7.969	7.754
480	0.1404	0.1825	5.731	7.447	6.875
540	0.1369	0.1570	5.588	6.406	6.133
600	0.1115	0.1219	4.551	4.973	4.833

Table D.6 RR120 photocatalytic degradation under visible light irradiation with ZnO_550 and 0.1Ce-ZnO (P) 1:2 bead using different initial RR120 concentrations.

Time (min)	RR120 removal (%) at the initial concentration of			
	10 mg/L		20 mg/L	
	ZnO_550	0.1Ce-ZnO (P) 1:2 bead	ZnO_550	0.1Ce-ZnO (P) 1:2 bead
0	0.00	0.00	0.00	0.00
60	30.14	43.54	19.74	41.60
120	44.40	55.36	28.54	47.17
180	53.58	65.54	36.42	50.92
240	64.61	73.56	45.97	53.35
300	69.01	76.82	55.05	56.57
360	75.35	78.97	56.97	57.58

D.3 Preparation route concernment

Table D.7 Percent removal of varied pH atrazine solution under visible light irradiation using Ce-ZnO (P).

pH	Atrazine removal (%) with catalyst			
	0.02Ce-ZnO (P) 1:2	Standard deviation	0.1Ce-ZnO (P) 1:2	Standard deviation
3.00	3.18	1.83	0.82	0.50
4.50	10.36	0.05	2.70	0.17
7.00	5.00	1.09	3.00	0.33

Table D.8 Percent removal of varied pH atrazine solution under visible light irradiation using Ce-ZnO (S).

pH	Atrazine removal (%) with catalyst			
	0.02Ce-ZnO (S) 1:2	Standard deviation	0.1Ce-ZnO (S) 1:2	Standard deviation
4.50	7.57	0.25	5.47	0.10
7.00	8.15	0.24	6.29	0.25
8.50	11.54	1.28	9.22	0.09

APPENDIX E

Photocatalytic degradation of atrazine

E.1 Reactor setup

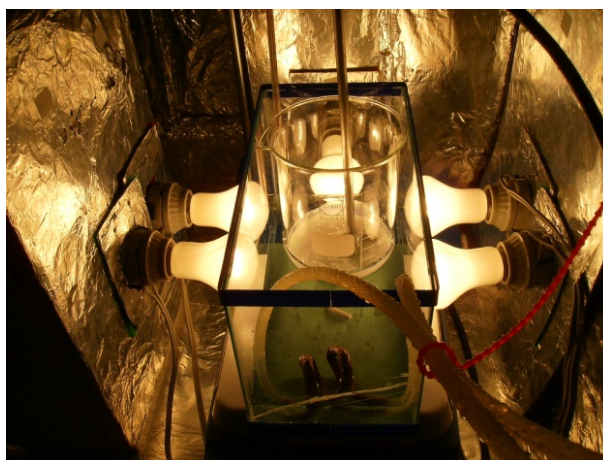


Figure E.1 Reactor for photocatalytic degradation of atrazine under visible light irradiation as described the procedure in 3.5 and the experimental result in 4.2.

E.2 Photolysis and adsorption

Table E.1 Atrazine photolysis under visible light.

Time (min)	Peak area			Concentration (mg/L)			Average concentration (mg/L)	Standard deviation
	1st	2nd	3rd	1st	2nd	3rd		
0	328.5	367.8	367.8	4.809	5.384	5.384	5.193	0.332
10	326.4	329.4	351.0	4.778	4.822	5.138	4.913	0.197
20	331.1	384.9	320.2	4.847	5.635	4.688	5.056	0.507
30	336.2	336.3	358.3	4.921	4.923	5.245	5.030	0.187
45	327.0	342.9	347.8	4.786	5.020	5.092	4.966	0.160
60	332.8	354.4	318.2	4.872	5.188	4.658	4.906	0.267

Table E.2 Atrazine adsorption on ZnO powder.

Time (min)	Peak area			Concentration (mg/L)			Average concentration (mg/L)	Standard deviation
	1st	2nd	3rd	1st	2nd	3rd		
0	328.5	367.8	367.8	4.809	5.384	5.384	5.193	0.332
10	326.2	352.4	341.2	4.775	5.158	4.996	4.976	0.192
20	325.7	365.4	353.2	4.768	5.350	5.170	5.096	0.298
30	328.8	345.5	361.4	4.813	5.058	5.291	5.054	0.239
45	315.6	348.1	352.2	4.619	5.096	5.155	4.957	0.294
60	324.4	358.0	350.6	4.748	5.242	5.132	5.041	0.259

Table E.3 Atrazine adsorption on ZnO_550.

Time (min)	Peak area			Concentration (mg/L)			Average concentration (mg/L)	Standard deviation
	1st	2nd	3rd	1st	2nd	3rd		
0	355.1	327.1	327.1	5.198	4.789	4.789	4.925	0.237
10	356.1	327.3	329.2	5.212	4.791	4.819	4.941	0.236
20	355.7	327.8	326.4	5.207	4.798	4.778	4.928	0.242
30	356.4	327.2	327.0	5.217	4.790	4.787	4.932	0.248
45	361.2	328.1	327.3	5.287	4.802	4.791	4.960	0.283
60	350.7	327.6	325.6	5.134	4.795	4.766	4.898	0.205

Table E.4 Atrazine adsorption on 0.02Ce-ZnO (S) powder.

Time (min)	Peak area			Concentration (mg/L)			Average concentration (mg/L)	Standard deviation
	1st	2nd	3rd	1st	2nd	3rd		
0	309.1	309.1	309.1	4.525	4.525	4.525	4.525	0.000
10	311.7	309.1	309.0	4.563	4.525	4.524	4.537	0.022
20	308.6	310.2	309.9	4.518	4.541	4.537	4.532	0.012
30	314.9	305.3	304.5	4.610	4.469	4.458	4.512	0.085
45	299.5	302.3	302.3	4.384	4.425	4.425	4.412	0.024
60	297.7	300.7	298.9	4.358	4.402	4.376	4.379	0.022
90	310.8	306.9	306.8	4.550	4.493	4.491	4.511	0.033
120	310.6	309.7	308.6	4.547	4.534	4.518	4.533	0.015
150	290.1	300.1	295.8	4.247	4.393	4.330	4.323	0.073
360	310.3	308.8	307.8	4.543	4.521	4.506	4.523	0.018

Table E.5 Atrazine adsorption on 0.02Cu-ZnO (S) powder.

Time (min)	Peak area			Concentration (mg/L)			Average concentration (mg/L)	Standard deviation
	1st	2nd	3rd	1st	2nd	3rd		
0	309.1	309.1	309.1	4.525	4.525	4.525	4.525	0.000
10	312.0	311.2	310.7	4.567	4.556	4.548	4.557	0.010
20	219.4	304.3	303.2	3.212	4.455	4.439	4.035	0.713
30	308.7	305.4	310.7	4.519	4.471	4.548	4.513	0.039
45	308.4	302.7	300.2	4.515	4.431	4.395	4.447	0.062
60	317.7	307.7	301.2	4.651	4.505	4.409	4.522	0.122
90	309.9	300.1	308.8	4.537	4.393	4.521	4.484	0.079
120	306.8	309.9	299.8	4.491	4.537	4.389	4.472	0.076
150	307.9	298.5	312.7	4.507	4.370	4.578	4.485	0.106
360	313.5	305.5	306.3	4.589	4.472	4.484	4.515	0.065

Table E.6 Atrazine adsorption on 0.02Ce-ZnO (S) bead.

Time (min)	Peak area			Concentration (mg/L)			Average concentration (mg/L)	Standard deviation
	1st	2nd	3rd	1st	2nd	3rd		
0	309.1	309.1	309.1	4.525	4.525	4.525	4.525	0.000
10	313.2	311.1	308.6	4.585	4.554	4.518	4.552	0.034
20	321.6	308.7	310.8	4.708	4.519	4.550	4.592	0.101
30	313.1	315.7	320.7	4.584	4.622	4.695	4.633	0.057
45	295.4	300.8	319.7	4.324	4.404	4.680	4.469	0.187
60	304.6	305.4	311.1	4.459	4.471	4.554	4.495	0.052
90	318.7	304.2	302.9	4.666	4.453	4.434	4.518	0.128
120	314.5	308.7	300.4	4.604	4.519	4.398	4.507	0.104
150	311.5	304.3	309.9	4.560	4.455	4.537	4.517	0.055
360	301.7	300.8	309.1	4.417	4.404	4.525	4.448	0.067

Table E.7 Atrazine adsorption on 0.02Cu-ZnO (S) bead.

Time (min)	Peak area			Concentration (mg/L)			Average concentration (mg/L)	Standard deviation
	1st	2nd	3rd	1st	2nd	3rd		
0	345.3	345.3	345.3	5.055	5.055	5.055	5.055	0.000
10	340.3	345.3	341.2	4.982	5.055	4.995	5.011	0.039
20	328.9	330.1	329.8	4.815	4.832	4.828	4.825	0.009
30	343.1	344.2	342.1	5.023	5.039	5.008	5.023	0.015
45	339.1	340.9	339.2	4.964	4.991	4.966	4.973	0.015
60	340.6	344.0	342.7	4.986	5.036	5.017	5.013	0.025
90	342.0	339.0	350.6	5.007	4.963	5.133	5.034	0.088
120	343.2	340.7	342.2	5.024	4.988	5.010	5.007	0.018
150	324.1	323.3	330.1	4.745	4.733	4.832	4.770	0.054
360	334.4	342.1	330.9	4.895	5.008	4.844	4.916	0.084

E.3 Effect of transition metal dopants and molar ratio of doping

Table E.8 Photocatalytic degradation of atrazine by 0.02Ce-ZnO (S) 10:1 powder.

Time (min)	Peak area			Concentration (mg/L)			Average concentration (mg/L)	Standard deviation
	1st	2nd	3rd	1st	2nd	3rd		
-30	336.5	327.1	327.1	4.926	4.789	4.789	4.834	0.079
0	327.2	317.0	318.2	4.790	4.640	4.658	4.696	0.082
15	324.5	297.6	283.7	4.750	4.356	4.153	4.420	0.303
30	306.0	274.7	298.6	4.479	4.021	4.371	4.290	0.240
60	283.9	251.2	260.8	4.155	3.677	3.818	3.883	0.246
120	231.5	210.5	226.7	3.389	3.081	3.318	3.263	0.161

Table E.9 Photocatalytic degradation of atrazine by 0.1Ce-ZnO (S) 10:1 powder.

Time (min)	Peak area			Concentration (mg/L)			Average concentration (mg/L)	Standard deviation
	1st	2nd	3rd	1st	2nd	3rd		
-30	336.5	327.1	327.1	4.926	4.789	4.789	4.834	0.079
0	329.9	301.4	287.8	4.829	4.412	4.213	4.485	0.314
15	319.1	280.6	272.3	4.671	4.108	3.986	4.255	0.365
30	309.3	267.8	264.4	4.528	3.920	3.871	4.106	0.366
60	285.3	253.9	242.3	4.177	3.716	3.547	3.813	0.326
120	246.0	199.4	198.5	3.601	2.918	2.906	3.142	0.398

Table E.10 Photocatalytic degradation of atrazine by 0.02Ce-ZnO (S) 5:1 powder.

Time (min)	Peak area			Concentration (mg/L)			Average concentration (mg/L)	Standard deviation
	1st	2nd	3rd	1st	2nd	3rd		
-30	336.5	327.1	327.1	4.926	4.789	4.789	4.834	0.079
0	333.4	327.9	308.5	4.881	4.800	4.516	4.732	0.191
15	316.0	268.1	300.1	4.625	3.924	4.393	4.314	0.357
30	294.1	261.1	270.6	4.305	3.822	3.961	4.029	0.248
60	252.9	207.1	212.6	3.702	3.031	3.112	3.281	0.366
120	199.0	170.7	155.9	2.913	2.498	2.282	2.564	0.320

Table E.11 Photocatalytic degradation of atrazine by 0.1Ce-ZnO (S) 5:1 powder.

Time (min)	Peak area			Concentration (mg/L)			Average concentration (mg/L)	Standard deviation
	1st	2nd	3rd	1st	2nd	3rd		
-30	336.5	327.1	327.1	4.926	4.789	4.789	4.834	0.079
0	331.6	286.0	299.4	4.854	4.187	4.382	4.474	0.343
15	311.5	270.9	275.6	4.560	3.966	4.035	4.187	0.325
30	286.5	254.6	250.4	4.194	3.727	3.666	3.862	0.289
60	258.3	224.2	214.5	3.781	3.282	3.140	3.401	0.337
120	196.9	190.1	182.4	2.882	2.783	2.670	2.778	0.106

Table E.12 Photocatalytic degradation of atrazine by 0.02Cu-ZnO (S) 10:1 powder.

Time (min)	Peak area			Concentration (mg/L)			Average concentration (mg/L)	Standard deviation
	1st	2nd	3rd	1st	2nd	3rd		
-30	336.5	327.1	327.1	4.926	4.789	4.789	4.834	0.079
0	322.3	295.0	306.5	4.718	4.319	4.486	4.508	0.201
15	324.7	307.8	312.2	4.753	4.505	4.570	4.609	0.129
30	327.0	304.1	307.6	4.786	4.452	4.503	4.580	0.180
60	321.0	309.5	333.6	4.699	4.530	4.883	4.704	0.176
120	326.3	301.6	320.0	4.777	4.414	4.684	4.625	0.188

Table E.13 Photocatalytic degradation of atrazine by 0.1Cu-ZnO (S) 10:1 powder.

Time (min)	Peak area			Concentration (mg/L)			Average concentration (mg/L)	Standard deviation
	1st	2nd	3rd	1st	2nd	3rd		
-30	336.5	327.1	327.1	4.926	4.789	4.789	4.834	0.079
0	331.0	299.3	327.0	4.846	4.382	4.787	4.671	0.253
15	328.5	309.6	314.7	4.808	4.532	4.606	4.649	0.143
30	331.0	320.0	304.8	4.846	4.684	4.462	4.664	0.193
60	324.8	303.6	314.3	4.754	4.444	4.600	4.599	0.155
120	326.2	342.4	310.6	4.775	5.012	4.547	4.778	0.232

Table E.14 Photocatalytic degradation of atrazine by 0.02Cu-ZnO (S) 5:1 powder.

Time (min)	Peak area			Concentration (mg/L)			Average concentration (mg/L)	Standard deviation
	1st	2nd	3rd	1st	2nd	3rd		
-30	328.5	327.1	309.1	4.809	4.789	4.525	4.708	0.158
0	323.2	324.0	308.1	4.731	4.742	4.510	4.661	0.131
15	322.3	324.4	293.4	4.718	4.748	4.295	4.587	0.253
30	319.4	315.5	301.8	4.675	4.619	4.417	4.570	0.135
60	320.5	299.0	291.3	4.691	4.377	4.264	4.444	0.221
120	321.4	306.1	294.7	4.704	4.481	4.313	4.500	0.196

Table E.15 Photocatalytic degradation of atrazine by 0.1Cu-ZnO (S) 5:1 powder.

Time (min)	Peak area			Concentration (mg/L)			Average concentration (mg/L)	Standard deviation
	1st	2nd	3rd	1st	2nd	3rd		
-30	328.5	309.1	309.1	4.809	4.525	4.525	4.620	0.164
0	331.1	284.9	299.8	4.847	4.170	4.388	4.468	0.346
15	330.1	295.5	300.7	4.832	4.326	4.401	4.520	0.273
30	333.0	305.7	292.4	4.874	4.475	4.280	4.543	0.303
60	321.5	287.7	292.6	4.706	4.212	4.283	4.400	0.267
120	320.7	295.2	294.8	4.695	4.322	4.315	4.444	0.217

E.4 Effect of catalyst loading

Table E.16 Photocatalytic degradation of atrazine by 0.10 g of ZnO powder.

Time (min)	Peak area			Concentration (mg/L)			Average concentration (mg/L)	Standard deviation
	1st	2nd	3rd	1st	2nd	3rd		
-30	328.5	335.8	335.8	4.809	4.916	4.916	4.880	0.062
0	331.8	333.3	332.9	4.857	4.879	4.873	4.870	0.012
15	176.0	216.9	208.1	2.576	3.175	3.046	2.932	0.315
30	85.5	117.0	100.8	1.251	1.712	1.475	1.479	0.231
60	23.8	45.3	37.1	0.348	0.662	0.542	0.518	0.158
120	0.0	7.0	0.0	0.000	0.102	0.000	0.034	0.059

Table E.17 Photocatalytic degradation of atrazine by 0.30 g of ZnO powder.

Time (min)	Peak area			Concentration (mg/L)			Average concentration (mg/L)	Standard deviation
	1st	2nd	3rd	1st	2nd	3rd		
-30	336.5	355.1	367.8	4.926	5.198	5.384	5.170	0.230
0	350.3	347.4	306.7	5.128	5.086	4.489	4.901	0.357
15	203.2	170.6	275.5	2.975	2.497	4.033	3.168	0.786
30	114.8	104.5	220.2	1.680	1.530	3.224	2.144	0.938
60	32.8	25.0	147.2	0.480	0.366	2.155	1.000	1.002
120	0.0	0.0	66.9	0.000	0.000	0.979	0.326	0.565

Table E.18 Photocatalytic degradation of atrazine by 0.50 g of ZnO powder.

Time (min)	Peak area			Concentration (mg/L)			Average concentration (mg/L)	Standard deviation
	1st	2nd	3rd	1st	2nd	3rd		
-30	336.5	327.1	327.1	4.926	4.789	4.789	4.834	0.079
0	333.0	295.5	336.5	4.874	4.326	4.925	4.709	0.332
15	170.1	192.7	166.8	2.490	2.821	2.442	2.584	0.206
30	79.9	77.4	67.0	1.170	1.132	0.981	1.094	0.100
60	10.8	9.2	0.0	0.158	0.134	0.000	0.097	0.085
120	0.0	0.0	0.0	0.000	0.000	0.000	0.000	0.000

Table E.19 Photocatalytic degradation of atrazine by 0.70 g of ZnO powder.

Time (min)	Peak area			Concentration (mg/L)			Average concentration (mg/L)	Standard deviation
	1st	2nd	3rd	1st	2nd	3rd		
-30	328.5	327.1	327.1	4.809	4.789	4.789	4.795	0.012
0	318.1	315.9	312.1	4.656	4.624	4.569	4.616	0.044
15	166.5	173.7	156.2	2.437	2.542	2.287	2.422	0.128
30	75.3	74.8	54.7	1.102	1.094	0.800	0.999	0.172
60	12.9	0.0	5.1	0.188	0.000	0.074	0.087	0.095
120	0.0	0.0	0.0	0.000	0.000	0.000	0.000	0.000

Table E.20 Photocatalytic degradation of atrazine by 0.90 g of ZnO powder.

Time (min)	Peak area			Concentration (mg/L)			Average concentration (mg/L)	Standard deviation
	1st	2nd	3rd	1st	2nd	3rd		
-30	355.1	355.1	327.1	5.198	5.198	4.789	5.062	0.237
0	350.2	352.7	333.7	5.126	5.163	4.884	5.058	0.151
15	168.9	226.9	157.1	2.472	3.321	2.299	2.697	0.547
30	64.3	106.1	72.3	0.941	1.553	1.058	1.184	0.325
60	17.7	11.4	2.8	0.259	0.167	0.041	0.156	0.109
120	0.0	0.0	0.0	0.000	0.000	0.000	0.000	0.000

Table E.21 Photocatalytic degradation of atrazine by 1.00 g of ZnO_550.

Time (min)	Peak area			Concentration (mg/L)			Average concentration (mg/L)	Standard deviation
	1st	2nd	3rd	1st	2nd	3rd		
-30	355.1	355.1	327.1	5.198	5.198	4.789	5.062	0.237
0	350.2	352.7	333.7	5.126	5.163	4.884	5.058	0.151
15	168.9	226.9	157.1	2.472	3.321	2.299	2.697	0.547
30	64.3	106.1	72.3	0.941	1.553	1.058	1.184	0.325
60	17.7	11.4	2.8	0.259	0.167	0.041	0.156	0.109
120	0.0	0.0	0.0	0.000	0.000	0.000	0.000	0.000

Table E.22 Photocatalytic degradation of atrazine by 2.50 g of ZnO_550.

Time (min)	Peak area			Concentration (mg/L)			Average concentration (mg/L)	Standard deviation
	1st	2nd	3rd	1st	2nd	3rd		
-30	355.1	355.1	327.1	5.198	5.198	4.789	5.062	0.237
0	350.2	352.7	333.7	5.126	5.163	4.884	5.058	0.151
15	168.9	226.9	157.1	2.472	3.321	2.299	2.697	0.547
30	64.3	106.1	72.3	0.941	1.553	1.058	1.184	0.325
60	17.7	11.4	2.8	0.259	0.167	0.041	0.156	0.109
120	0.0	0.0	0.0	0.000	0.000	0.000	0.000	0.000

Table E.23 Photocatalytic degradation of atrazine by 5.00 g of ZnO_550.

Time (min)	Peak area			Concentration (mg/L)			Average concentration (mg/L)	Standard deviation
	1st	2nd	3rd	1st	2nd	3rd		
-30	355.1	355.1	327.1	5.198	5.198	4.789	5.062	0.237
0	350.2	352.7	333.7	5.126	5.163	4.884	5.058	0.151
15	168.9	226.9	157.1	2.472	3.321	2.299	2.697	0.547
30	64.3	106.1	72.3	0.941	1.553	1.058	1.184	0.325
60	17.7	11.4	2.8	0.259	0.167	0.041	0.156	0.109
120	0.0	0.0	0.0	0.000	0.000	0.000	0.000	0.000

Table E.24 Photocatalytic degradation of atrazine by 7.50 g of ZnO_550.

Time (min)	Peak area			Concentration (mg/L)			Average concentration (mg/L)	Standard deviation
	1st	2nd	3rd	1st	2nd	3rd		
-30	355.1	355.1	327.1	5.198	5.198	4.789	5.062	0.237
0	350.2	352.7	333.7	5.126	5.163	4.884	5.058	0.151
15	168.9	226.9	157.1	2.472	3.321	2.299	2.697	0.547
30	64.3	106.1	72.3	0.941	1.553	1.058	1.184	0.325
60	17.7	11.4	2.8	0.259	0.167	0.041	0.156	0.109
120	0.0	0.0	0.0	0.000	0.000	0.000	0.000	0.000

Table E.25 Photocatalytic degradation of atrazine by 0.10 g of 0.02Ce-ZnO (S) 5:1 powder.

Time (min)	Peak area			Concentration (mg/L)			Average concentration (mg/L)	Standard deviation
	1st	2nd	3rd	1st	2nd	3rd		
-30	309.1	309.1	309.1	4.525	4.525	4.525	4.525	0.000
0	342.6	316.9	309.8	5.015	4.638	4.535	4.729	0.253
15	302.6	292.4	308.9	4.429	4.281	4.521	4.410	0.122
30	287.7	261.2	271.1	4.212	3.824	3.968	4.001	0.196
60	231.0	229.3	221.6	3.381	3.356	3.244	3.327	0.073
120	176.7	155.1	161.2	2.587	2.271	2.359	2.405	0.163

Table E.26 Photocatalytic degradation of atrazine by 0.30 g of 0.02Ce-ZnO (S) 5:1 powder.

Time (min)	Peak area			Concentration (mg/L)			Average concentration (mg/L)	Standard deviation
	1st	2nd	3rd	1st	2nd	3rd		
-30	336.5	327.1	327.1	4.926	4.789	4.789	4.834	0.079
0	333.4	327.9	308.5	4.881	4.800	4.516	4.732	0.191
15	316.0	268.1	300.1	4.625	3.924	4.393	4.314	0.357
30	294.1	261.1	270.6	4.305	3.822	3.961	4.029	0.248
60	252.9	207.1	212.6	3.702	3.031	3.112	3.281	0.366
120	199.0	170.7	155.9	2.913	2.498	2.282	2.564	0.320

Table E.27 Photocatalytic degradation of atrazine by 0.50 g of 0.02Ce-ZnO (S) 5:1 powder.

Time (min)	Peak area			Concentration (mg/L)			Average concentration (mg/L)	Standard deviation
	1st	2nd	3rd	1st	2nd	3rd		
-30	309.1	309.1	309.1	4.525	4.525	4.525	4.525	0.000
0	316.2	320.4	299.6	4.628	4.690	4.385	4.568	0.161
15	283.2	283.8	286.8	4.146	4.155	4.198	4.166	0.028
30	259.6	262.2	260.2	3.800	3.838	3.809	3.816	0.020
60	197.3	199.3	199.4	2.888	2.917	2.918	2.908	0.017
120	114.9	150.3	127.6	1.681	2.200	1.868	1.917	0.263

Table E.28 Photocatalytic degradation of atrazine by 1.00 g of 0.02Ce-ZnO (S) 5:1 bead.

Time (min)	Peak area			Concentration (mg/L)			Average concentration (mg/L)	Standard deviation
	1st	2nd	3rd	1st	2nd	3rd		
-30	345.3	345.3	345.3	5.055	5.055	5.055	5.055	0.000
0	338.8	340.2	338.7	4.960	4.980	4.958	4.966	0.012
15	344.2	340.1	336.5	5.038	4.979	4.926	4.981	0.056
30	330.4	335.0	331.2	4.837	4.904	4.849	4.863	0.036
60	336.4	328.8	332.2	4.924	4.813	4.863	4.867	0.055
120	322.2	322.1	320.5	4.717	4.715	4.692	4.708	0.014

Table E.29 Photocatalytic degradation of atrazine by 2.50 g of 0.02Ce-ZnO (S) 5:1 bead.

Time (min)	Peak area			Concentration (mg/L)			Average concentration (mg/L)	Standard deviation
	1st	2nd	3rd	1st	2nd	3rd		
-30	345.3	345.3	345.3	5.055	5.055	5.055	5.055	0.000
0	330.2	337.8	320.1	4.833	4.945	4.686	4.821	0.130
15	341.1	319.5	322.4	4.993	4.677	4.720	4.797	0.172
30	341.4	317.5	319.9	4.998	4.648	4.683	4.776	0.193
60	328.3	313.6	315.7	4.806	4.591	4.622	4.673	0.116
120	317.1	311.8	308.8	4.641	4.564	4.521	4.575	0.061

Table E.30 Photocatalytic degradation of atrazine by 5.00 g of 0.02Ce-ZnO (S) 5:1 bead.

Time (min)	Peak area			Concentration (mg/L)			Average concentration (mg/L)	Standard deviation
	1st	2nd	3rd	1st	2nd	3rd		
-30	345.3	345.3	345.3	5.055	5.055	5.055	5.055	0.000
0	340.1	341.5	338.4	4.978	4.999	4.954	4.977	0.023
15	325.3	340.7	338.4	4.761	4.988	4.954	4.901	0.122
30	328.3	339.9	335.3	4.805	4.976	4.909	4.897	0.086
60	330.7	332.3	330.8	4.841	4.865	4.843	4.850	0.013
120	306.2	320.4	303.7	4.482	4.690	4.446	4.539	0.132

Table E.31 Photocatalytic degradation of atrazine by 0.10 g of 0.02Cu-ZnO (S) 5:1 powder.

Time (min)	Peak area			Concentration (mg/L)			Average concentration (mg/L)	Standard deviation
	1st	2nd	3rd	1st	2nd	3rd		
-30	309.1	309.1	309.1	4.525	4.525	4.525	4.525	0.000
0	313.9	320.6	303.0	4.595	4.693	4.436	4.575	0.130
15	316.8	308.1	300.8	4.638	4.510	4.404	4.517	0.117
30	317.6	295.6	308.3	4.649	4.327	4.513	4.496	0.162
60	312.5	316.9	304.4	4.574	4.638	4.455	4.556	0.093
120	300.8	297.0	300.1	4.404	4.348	4.393	4.381	0.029

Table E.32 Photocatalytic degradation of atrazine by 0.30 g of 0.02Cu-ZnO (S) 5:1 powder.

Time (min)	Peak area			Concentration (mg/L)			Average concentration (mg/L)	Standard deviation
	1st	2nd	3rd	1st	2nd	3rd		
-30	328.5	327.1	309.1	4.809	4.789	4.525	4.708	0.158
0	323.2	324.0	308.1	4.731	4.742	4.510	4.661	0.131
15	322.3	324.4	293.4	4.718	4.748	4.295	4.587	0.253
30	319.4	315.5	301.8	4.675	4.619	4.417	4.570	0.135
60	320.5	299.0	291.3	4.691	4.377	4.264	4.444	0.221
120	321.4	306.1	294.7	4.704	4.481	4.313	4.500	0.196

Table E.33 Photocatalytic degradation of atrazine by 0.50 g of 0.02Cu-ZnO (S) 5:1 powder.

Time (min)	Peak area			Concentration (mg/L)			Average concentration (mg/L)	Standard deviation
	1st	2nd	3rd	1st	2nd	3rd		
-30	309.1	309.1	309.1	4.525	4.525	4.525	4.525	0.000
0	310.3	326.3	314.8	4.543	4.777	4.608	4.643	0.121
15	301.8	303.8	302.1	4.418	4.447	4.423	4.429	0.015
30	302.4	307.9	300.0	4.427	4.507	4.391	4.442	0.059
60	307.4	307.3	303.9	4.499	4.498	4.448	4.482	0.029
120	302.3	299.5	299.7	4.425	4.384	4.387	4.399	0.022

Table E.34 Photocatalytic degradation of atrazine by 1.00 g of 0.02Cu-ZnO (S) 5:1 bead.

Time (min)	Peak area			Concentration (mg/L)			Average concentration (mg/L)	Standard deviation
	1st	2nd	3rd	1st	2nd	3rd		
-30	345.3	345.3	345.3	5.055	5.055	5.055	5.055	0.000
0	357.7	347.9	345.1	5.236	5.093	5.052	5.127	0.097
15	342.1	340.7	341.8	5.007	4.988	5.004	5.000	0.011
30	325.0	336.4	335.3	4.757	4.925	4.909	4.863	0.092
60	341.6	330.4	332.5	5.001	4.837	4.868	4.902	0.087
120	332.6	332.3	330.4	4.869	4.865	4.837	4.857	0.017

Table E.35 Photocatalytic degradation of atrazine by 2.50 g of 0.02Cu-ZnO (S) 5:1 bead.

Time (min)	Peak area			Concentration (mg/L)			Average concentration (mg/L)	Standard deviation
	1st	2nd	3rd	1st	2nd	3rd		
-30	345.3	345.3	345.3	5.055	5.055	5.055	5.055	0.000
0	353.8	341.6	342.7	5.179	5.001	5.017	5.065	0.098
15	342.9	349.3	343.2	5.020	5.113	5.024	5.052	0.052
30	346.6	332.9	340.9	5.074	4.873	4.991	4.979	0.101
60	349.2	342.1	338.7	5.111	5.008	4.958	5.026	0.078
120	340.5	357.6	332.1	4.985	5.235	4.862	5.027	0.190

Table E.36 Photocatalytic degradation of atrazine by 5.00 g of 0.02Cu-ZnO (S) 5:1 bead.

Time (min)	Peak area			Concentration (mg/L)			Average concentration (mg/L)	Standard deviation
	1st	2nd	3rd	1st	2nd	3rd		
-30	345.3	345.3	345.3	5.055	5.055	5.055	5.055	0.000
0	346.8	345.1	340.2	5.077	5.052	4.980	5.036	0.050
15	355.6	338.7	335.7	5.205	4.958	4.914	5.026	0.157
30	341.2	338.3	330.2	4.995	4.952	4.834	4.927	0.083
60	335.6	335.4	332.3	4.912	4.910	4.865	4.896	0.027
120	335.0	330.1	328.3	4.904	4.832	4.806	4.848	0.051

E.5 Effect of pH

Table E.37 Photocatalytic degradation of atrazine by ZnO powder at pH 3.99.

Time (min)	Peak area			Concentration (mg/L)			Average concentration (mg/L)	Standard deviation
	1st	2nd	3rd	1st	2nd	3rd		
-30	345.4	345.4	345.4	5.056	5.056	5.056	5.056	0.000
0	344.2	357.7	345.8	5.039	5.236	5.062	5.112	0.108
15	214.1	178.6	178.9	3.134	2.614	2.618	2.789	0.299
30	103.9	72.6	82.2	1.521	1.062	1.203	1.262	0.235
60	23.7	5.5	10.3	0.347	0.081	0.151	0.193	0.138
120	0.0	0.0	0.0	0.000	0.000	0.000	0.000	0.000

Table E.38 Photocatalytic degradation of atrazine by ZnO powder at pH 4.89.

Time (min)	Peak area			Concentration (mg/L)			Average concentration (mg/L)	Standard deviation
	1st	2nd	3rd	1st	2nd	3rd		
-30	328.5	335.8	335.8	4.809	4.916	4.916	4.880	0.062
0	331.8	333.3	332.9	4.857	4.879	4.873	4.870	0.012
15	176.0	216.9	208.1	2.576	3.175	3.046	2.932	0.315
30	85.5	117.0	100.8	1.251	1.712	1.475	1.479	0.231
60	23.8	45.3	37.1	0.348	0.662	0.542	0.518	0.158
120	0.0	7.0	0.0	0.000	0.102	0.000	0.034	0.059

Table E.39 Photocatalytic degradation of atrazine by ZnO powder at pH 6.92.

Time (min)	Peak area			Concentration (mg/L)			Average concentration (mg/L)	Standard deviation
	1st	2nd	3rd	1st	2nd	3rd		
-30	348.9	348.9	348.9	5.108	5.108	5.108	5.108	0.000
0	344.8	347.4	341.9	5.048	5.086	5.005	5.046	0.040
15	220.2	221.9	214.3	3.223	3.248	3.137	3.203	0.058
30	135.1	112.8	127.0	1.978	1.651	1.859	1.829	0.166
60	41.9	41.1	39.7	0.613	0.602	0.580	0.598	0.016
120	0.0	5.9	0.0	0.000	0.086	0.000	0.029	0.049

Table E.40 Photocatalytic degradation of atrazine by ZnO powder at pH 8.49.

Time (min)	Peak area			Concentration (mg/L)			Average concentration (mg/L)	Standard deviation
	1st	2nd	3rd	1st	2nd	3rd		
-30	352.1	352.1	352.1	5.155	5.155	5.155	5.155	0.000
0	342.7	342.2	329.1	5.017	5.010	4.817	4.948	0.113
15	222.0	220.4	195.0	3.249	3.226	2.855	3.110	0.221
30	129.7	109.7	115.2	1.899	1.605	1.686	1.730	0.152
60	41.3	38.0	26.6	0.604	0.556	0.389	0.517	0.113
120	0.0	7.2	0.0	0.000	0.105	0.000	0.035	0.060

Table E.41 Photocatalytic degradation of atrazine by ZnO₅₅₀ at pH 3.90.

Time (min)	Peak area			Concentration (mg/L)			Average concentration (mg/L)	Standard deviation
	1st	2nd	3rd	1st	2nd	3rd		
-30	338.9	338.9	338.9	4.961	4.961	4.961	4.961	0.000
0	328.9	334.9	335.7	4.815	4.903	4.914	4.877	0.054
15	304.4	319.8	302.9	4.456	4.681	4.434	4.524	0.137
30	300.8	293.7	291.6	4.404	4.299	4.269	4.324	0.071
60	267.3	266.7	272.7	3.913	3.904	3.991	3.936	0.048
120	207.0	212.6	221.1	3.030	3.112	3.236	3.126	0.104

Table E.42 Photocatalytic degradation of atrazine by ZnO_550 at pH 4.95.

Time (min)	Peak area			Concentration (mg/L)			Average concentration (mg/L)	Standard deviation
	1st	2nd	3rd	1st	2nd	3rd		
-30	355.1	340.6	340.6	5.198	4.986	4.986	5.057	0.123
0	360.7	332.7	328.3	5.280	4.871	4.805	4.985	0.258
15	338.3	314.7	317.4	4.952	4.606	4.647	4.735	0.189
30	334.1	298.9	306.0	4.891	4.375	4.480	4.582	0.273
60	320.8	267.1	263.5	4.696	3.909	3.857	4.154	0.470
120	280.5	222.5	216.4	4.106	3.257	3.167	3.510	0.518

Table E.43 Photocatalytic degradation of atrazine by ZnO_550 at pH 7.00.

Time (min)	Peak area			Concentration (mg/L)			Average concentration (mg/L)	Standard deviation
	1st	2nd	3rd	1st	2nd	3rd		
-30	339.2	339.2	339.2	4.966	4.966	4.966	4.966	0.000
0	325.0	308.8	334.9	4.757	4.520	4.903	4.727	0.193
15	313.5	319.9	324.5	4.589	4.682	4.750	4.674	0.081
30	296.0	296.7	302.5	4.333	4.343	4.428	4.368	0.052
60	259.0	263.2	267.6	3.792	3.853	3.917	3.854	0.063
120	193.0	213.7	222.4	2.825	3.128	3.255	3.069	0.221

Table E.44 Photocatalytic degradation of atrazine by ZnO_550 at pH 8.84.

Time (min)	Peak area			Concentration (mg/L)			Average concentration (mg/L)	Standard deviation
	1st	2nd	3rd	1st	2nd	3rd		
-30	343.2	343.2	343.2	5.024	5.024	5.024	5.024	0.000
0	341.4	332.0	345.6	4.997	4.860	5.059	4.972	0.102
15	298.5	313.8	312.0	4.370	4.593	4.567	4.510	0.122
30	297.1	298.0	301.6	4.349	4.362	4.414	4.375	0.035
60	261.5	258.9	261.6	3.827	3.789	3.830	3.816	0.023
120	197.5	199.5	214.9	2.891	2.920	3.145	2.985	0.139

E.6 Effect of atrazine initial concentration

Table E.45 Photocatalytic degradation of atrazine by ZnO powder using 1.0 mg/L of atrazine solution.

Time (min)	Peak area			Concentration (mg/L)			Average concentration (mg/L)	Standard deviation
	1st	2nd	3rd	1st	2nd	3rd		
-30	72.3	72.3	72.3	1.058	1.058	1.058	1.058	0.000
0	69.1	72.2	72.2	1.012	1.057	1.056	1.042	0.026
15	37.0	34.5	33.9	0.542	0.505	0.496	0.514	0.024
30	13.7	19.7	17.7	0.201	0.288	0.259	0.249	0.044
60	0.0	5.7	8.1	0.000	0.083	0.119	0.067	0.061
120	0.0	0.0	0.0	0.000	0.000	0.000	0.000	0.000

Table E.46 Photocatalytic degradation of atrazine by ZnO powder using 2.3 mg/L of atrazine solution.

Time (min)	Peak area			Concentration (mg/L)			Average concentration (mg/L)	Standard deviation
	1st	2nd	3rd	1st	2nd	3rd		
-30	156.3	156.3	156.3	2.288	2.288	2.288	2.288	0.000
0	161.8	157.1	152.1	2.368	2.300	2.226	2.298	0.071
15	86.0	95.5	105.3	1.259	1.398	1.542	1.400	0.141
30	50.3	50.0	56.7	0.736	0.732	0.830	0.766	0.056
60	12.7	17.7	18.1	0.186	0.258	0.265	0.236	0.044
120	0.0	0.0	0.0	0.000	0.000	0.000	0.000	0.000

Table E.47 Photocatalytic degradation of atrazine by ZnO powder using 4.9 mg/L of atrazine solution.

Time (min)	Peak area			Concentration (mg/L)			Average concentration (mg/L)	Standard deviation
	1st	2nd	3rd	1st	2nd	3rd		
-30	328.5	335.8	335.8	4.809	4.916	4.916	4.880	0.062
0	331.8	333.3	332.9	4.857	4.879	4.873	4.870	0.012
15	176.0	216.9	208.1	2.576	3.175	3.046	2.932	0.315
30	85.5	117.0	100.8	1.251	1.712	1.475	1.479	0.231
60	23.8	45.3	37.1	0.348	0.662	0.542	0.518	0.158
120	0.0	7.0	0.0	0.000	0.102	0.000	0.034	0.059

Table E.48 Photocatalytic degradation of atrazine by ZnO powder using 7.1 mg/L of atrazine solution.

Time (min)	Peak area			Concentration (mg/L)			Average concentration (mg/L)	Standard deviation
	1st	2nd	3rd	1st	2nd	3rd		
-30	487.6	487.6	487.6	7.138	7.138	7.138	7.138	0.000
0	488.6	485.3	486.3	7.153	7.104	7.119	7.125	0.025
15	337.1	340.8	291.7	4.934	4.988	4.270	4.731	0.400
30	198.8	196.6	164.7	2.910	2.877	2.411	2.733	0.279
60	76.3	73.1	63.7	1.116	1.070	0.932	1.039	0.096
120	8.6	11.2	9.4	0.125	0.163	0.138	0.142	0.019

Table E.49 Photocatalytic degradation of atrazine by ZnO powder using 9.9 mg/L of atrazine solution.

Time (min)	Peak area			Concentration (mg/L)			Average concentration (mg/L)	Standard deviation
	1st	2nd	3rd	1st	2nd	3rd		
-30	677.9	677.9	677.9	9.924	9.924	9.924	9.924	0.000
0	666.3	661.7	671.3	9.753	9.687	9.827	9.756	0.070
15	466.5	439.7	467.5	6.829	6.436	6.843	6.703	0.231
30	327.5	342.3	286.2	4.794	5.010	4.189	4.665	0.426
60	142.0	157.1	115.9	2.079	2.300	1.696	2.025	0.306
120	32.0	35.8	21.8	0.468	0.524	0.318	0.437	0.106

Table E.50 Photocatalytic degradation of atrazine by ZnO_550 using 1.0 mg/L of atrazine solution.

Time (min)	Peak area			Concentration (mg/L)			Average concentration (mg/L)	Standard deviation
	1st	2nd	3rd	1st	2nd	3rd		
-30	72.3	72.3	72.3	1.058	1.058	1.058	1.058	0.000
0	66.4	67.1	65.3	0.971	0.982	0.956	0.970	0.013
15	59.5	58.9	59.9	0.871	0.862	0.876	0.870	0.007
30	50.6	50.3	50.6	0.740	0.736	0.741	0.739	0.003
60	43.8	44.2	43.5	0.640	0.647	0.637	0.641	0.005
120	30.5	31.7	30.0	0.447	0.463	0.438	0.449	0.013

Table E.51 Photocatalytic degradation of atrazine by ZnO_550 using 2.3 mg/L of atrazine solution.

Time (min)	Peak area			Concentration (mg/L)			Average concentration (mg/L)	Standard deviation
	1st	2nd	3rd	1st	2nd	3rd		
-30	155.1	155.1	155.1	2.271	2.271	2.271	2.271	0.000
0	142.2	144.2	141.0	2.081	2.111	2.064	2.085	0.024
15	135.0	135.4	135.7	1.976	1.981	1.987	1.981	0.005
30	133.6	131.9	134.1	1.956	1.930	1.962	1.949	0.017
60	116.7	115.1	117.2	1.708	1.684	1.716	1.703	0.016
120	86.0	88.2	85.0	1.259	1.291	1.244	1.265	0.024

Table E.52 Photocatalytic degradation of atrazine by ZnO_550 using 4.8 mg/L of atrazine solution.

Time (min)	Peak area			Concentration (mg/L)			Average concentration (mg/L)	Standard deviation
	1st	2nd	3rd	1st	2nd	3rd		
-30	340.6	340.6	309.1	4.986	4.986	4.525	4.832	0.266
0	349.1	344.3	294.1	5.111	5.040	4.305	4.819	0.446
15	339.6	338.4	294.2	4.971	4.953	4.306	4.743	0.379
30	337.9	326.3	279.6	4.946	4.776	4.093	4.605	0.451
60	319.7	303.9	273.6	4.679	4.449	4.005	4.378	0.343
120	299.5	294.5	263.3	4.384	4.311	3.854	4.183	0.287

Table E.53 Photocatalytic degradation of atrazine by ZnO₅₅₀ using 7.1 mg/L of atrazine solution.

Time (min)	Peak area			Concentration (mg/L)			Average concentration (mg/L)	Standard deviation
	1st	2nd	3rd	1st	2nd	3rd		
-30	487.6	487.6	487.6	7.138	7.138	7.138	7.138	0.000
0	474.3	475.4	475.3	6.943	6.960	6.958	6.954	0.009
15	441.6	442.5	440.5	6.464	6.477	6.448	6.463	0.015
30	414.2	414.4	406.2	6.063	6.067	5.947	6.025	0.068
60	386.0	386.2	386.1	5.650	5.653	5.652	5.652	0.002
120	302.7	300.9	304.6	4.431	4.405	4.458	4.432	0.027

Table E.54 Photocatalytic degradation of atrazine by ZnO₅₅₀ using 9.9 mg/L of atrazine solution.

Time (min)	Peak area			Concentration (mg/L)			Average concentration (mg/L)	Standard deviation
	1st	2nd	3rd	1st	2nd	3rd		
-30	677.9	677.9	677.9	9.924	9.924	9.924	9.924	0.000
0	668.6	662.8	668.3	9.788	9.703	9.783	9.758	0.048
15	610.3	622.7	614.6	8.934	9.116	8.997	9.016	0.092
30	591.9	588.7	591.1	8.665	8.618	8.653	8.646	0.024
60	538.2	540.3	538.9	7.878	7.909	7.888	7.892	0.016
120	438.2	448.9	445.5	6.414	6.572	6.522	6.503	0.080

E.7 Surface passivation

Table E.55 Electrical conductivity of atrazine photocatalytic degradation by ZnO_550.

Time (min)	Electrical conductivity ($\mu\text{S}/\text{cm}$)			Average electrical conductivity ($\mu\text{S}/\text{cm}$)	Standard deviation
	1st	2nd	3rd		
-30	0	0	0	0	0
0	77	71	71	73	3
15	85	85	80	83	3
30	91	89	83	88	4
60	96	97	88	94	5
120	99	103	97	100	3

Table E.56 Zn element concentration of atrazine photocatalytic degradation by ZnO_550.

Time (min)	Zn concentration (mg/L)			Average Zn concentration (mg/L)	Standard deviation
	1st	2nd	3rd		
-30	0.0000	0.0000	0.0000	0.0000	0.0000
60	0.1814	0.3692	0.6703	0.4070	0.2466
120	1.5964	0.4334	1.4515	1.1605	0.6338

Table E.57 Electrical conductivity of atrazine photocatalytic degradation by 0.02Ce-ZnO (S) 5:1 bead.

Time (min)	Electrical conductivity ($\mu\text{S}/\text{cm}$)			Average electrical conductivity ($\mu\text{S}/\text{cm}$)	Standard deviation
	1st	2nd	3rd		
-30	0	0	0	0	0
0	131	129	118	126	7
15	151	134	128	138	12
30	161	137	130	143	16
60	162	140	145	149	12
120	166	141	149	152	13

Table E.58 Zn element concentrations of atrazine photocatalytic degradation by 0.02Ce-ZnO (S) 5:1 bead.

Time (min)	Zn concentration (mg/L)			Average Zn concentration (mg/L)	Standard deviation
	1st	2nd	3rd		
-30	0.0000	0.0000	0.0000	0.0000	0.0000
60	0.9592	1.0505	1.1220	1.0439	0.0816
120	2.1090	1.7774	2.2738	2.0534	0.2529

Table E.59 Electrical conductivity of atrazine photocatalytic degradation by 0.02Cu-ZnO (S) 5:1 bead.

Time (min)	Electrical conductivity ($\mu\text{S}/\text{cm}$)			Average electrical conductivity ($\mu\text{S}/\text{cm}$)	Standard deviation
	1st	2nd	3rd		
-30	0	0	0	0	0
0	175	177	194	182	10
15	184	183	200	189	10
30	188	188	202	193	8
60	191	192	205	196	8
120	193	196	207	199	7

Table E.60 Zn element concentrations of atrazine photocatalytic degradation by 0.02Cu-ZnO (S) 5:1 bead.

Time (min)	Zn concentration (mg/L)			Average Zn concentration (mg/L)	Standard deviation
	1st	2nd	3rd		
-30	0.0000	0.0000	0.0000	0.0000	0.0000
60	2.5414	1.4276	1.5221	1.8304	0.6176
120	2.1189	2.7683	2.8597	2.5823	0.4039

E.8 Effect of ionic strength

Table E.61 Ionic strength (I) of Na_2SO_4 in atrazine solution.

Na_2SO_4 concentration		Na_2SO_4 weight (g/0.1 kg atrazine solution)	Ionic strength (I) (mol/kg)
Molal (m) or mol/kg	mol/0.1 kg atrazine solution		
0.002	0.0002	0.0284	0.005
0.006	0.0006	0.0852	0.015
0.010	0.0010	0.1420	0.025

Table E.62 Electrical conductivity (σ) change before and after running reaction in the presence of Na_2SO_4 in atrazine solution.

Ionic strength (I) from Na_2SO_4 (mol/kg)	σ ($\mu\text{S}/\text{cm}$) before running reaction					σ ($\mu\text{S}/\text{cm}$) after running reaction				
	1st	2nd	3rd	σ	S.D.	1st	2nd	3rd	σ	S.D.
0.005	412	357	410	393	31	475	465	472	471	5
0.015	1070	1061	1068	1066	5	1133	1111	1118	1121	11
0.025	1555	1578	1577	1570	13	1667	1643	1643	1651	14

Table E.63 Atrazine photocatalytic degradation in the presence of Na_2SO_4 at different ionic strength values.

Time (min)	Ionic strength (I) from Na_2SO_4 (mol/kg)					
	0.005		0.015		0.025	
	C/C_0	S.D.	C/C_0	S.D.	C/C_0	S.D.
-30	1.000	0.000	1.000	0.000	1.000	0.000
0	0.902	0.005	0.903	0.011	0.951	0.008
15	0.856	0.005	0.845	0.013	0.856	0.007
30	0.796	0.014	0.778	0.057	0.802	0.023
60	0.736	0.003	0.705	0.019	0.662	0.005
120	0.587	0.017	0.588	0.006	0.497	0.003

Table E.64 Ionic strength (I) of NaCl in atrazine solution.

NaCl concentration		NaCl weight (g/0.1 kg atrazine solution)	Ionic strength (I) (mol/kg)
Molal (m) or mol/kg	mol/0.1 kg atrazine solution		
0.002	0.0002	0.0117	0.002
0.006	0.0006	0.0351	0.006
0.010	0.0010	0.0584	0.010

Table E.65 Electrical conductivity (σ) change before and after running reaction in the presence of NaCl in atrazine solution.

Ionic strength (I) from NaCl (mol/kg)	σ ($\mu\text{S}/\text{cm}$) before running reaction					σ ($\mu\text{S}/\text{cm}$) after running reaction				
	1st	2nd	3rd	σ	S.D.	1st	2nd	3rd	σ	S.D.
0.002	224	214	218	219	5	308	283	298	296	13
0.006	611	618	620	616	5	710	657	660	676	30
0.010	902	905	905	904	2	1077	1073	1070	1073	4

Table E.66 Atrazine photocatalytic degradation in the presence of NaCl at different ionic strength values.

Time (min)	Ionic strength (I) from NaCl (mol/kg)					
	0.002		0.006		0.010	
	C/C_0	S.D.	C/C_0	S.D.	C/C_0	S.D.
-30	1.000	0.000	1.000	0.000	1.000	0.000
0	0.918	0.004	0.872	0.023	0.929	0.037
15	0.856	0.001	0.825	0.031	0.838	0.007
30	0.797	0.008	0.780	0.019	0.749	0.004
60	0.748	0.005	0.705	0.010	0.708	0.026
120	0.584	0.010	0.585	0.051	0.537	0.023

Table E.67 Ionic strength (I) of Na_2CO_3 in atrazine solution.

Na_2CO_3 concentration		Na_2CO_3 weight (g/0.1 kg atrazine solution)	Ionic strength (I) (mol/kg)
Molal (m) or mol/kg	mol/0.1 kg atrazine solution		
0.002	0.0002	0.0212	0.005
0.006	0.0006	0.0636	0.015
0.010	0.0010	0.1060	0.025

Table E.68 Electrical conductivity (σ) change before and after running reaction in the presence of Na_2CO_3 in atrazine solution.

Ionic strength (I) from Na_2CO_3 (mol/kg)	σ ($\mu\text{S}/\text{cm}$) before running reaction					σ ($\mu\text{S}/\text{cm}$) after running reaction				
	1st	2nd	3rd	σ	S.D.	1st	2nd	3rd	σ	S.D.
0.005	448	440	440	443	5	427	397	442	422	23
0.015	1201	1185	1183	1190	10	1052	1044	1050	1049	4
0.025	1844	1840	1838	1841	3	1441	1583	1580	1535	81

Table E.69 Atrazine photocatalytic degradation in the presence of Na_2CO_3 at different ionic strength values.

Time (min)	Ionic strength (I) from Na_2CO_3 (mol/kg)					
	0.005		0.015		0.025	
	C/C_0	S.D.	C/C_0	S.D.	C/C_0	S.D.
-30	1.000	0.000	1.000	0.000	1.000	0.000
0	0.890	0.029	0.917	0.050	0.949	0.013
15	0.858	0.025	0.895	0.007	0.950	0.029
30	0.850	0.006	0.878	0.051	0.903	0.021
60	0.796	0.037	0.843	0.019	0.888	0.038
120	0.736	0.024	0.839	0.021	0.881	0.016

Table E.70 Ionic strength (I) of NaHCO_3 in atrazine solution.

NaHCO_3 concentration		NaHCO_3 weight (g/0.1 kg atrazine solution)	Ionic strength (I) (mol/kg)
Molal (m) or mol/kg	mol/0.1 kg atrazine solution		
0.002	0.0002	0.0168	0.002
0.006	0.0006	0.0504	0.006
0.010	0.0010	0.0840	0.010

Table E.71 Electrical conductivity (σ) change before and after running reaction in the presence of NaHCO_3 in atrazine solution.

Ionic strength (I) from NaHCO_3 (mol/kg)	σ ($\mu\text{S}/\text{cm}$) before running reaction					σ ($\mu\text{S}/\text{cm}$) after running reaction				
	1st	2nd	3rd	σ	S.D.	1st	2nd	3rd	σ	S.D.
0.002	188	194	185	189	5	222	224	223	223	1
0.006	516	513	518	516	3	565	558	552	558	7
0.010	820	824	825	823	3	911	924	909	915	8

Table E.72 Atrazine photocatalytic degradation in the presence of NaHCO_3 at different ionic strength values.

Time (min)	Ionic strength (I) from NaHCO_3 (mol/kg)					
	0.002		0.006		0.010	
	C/C_0	S.D.	C/C_0	S.D.	C/C_0	S.D.
-30	1.000	0.000	1.000	0.000	1.000	0.000
0	0.939	0.044	0.990	0.004	0.991	0.002
15	0.972	0.018	0.967	0.017	0.996	0.011
30	0.907	0.016	0.884	0.064	0.970	0.000
60	0.889	0.006	0.860	0.050	0.966	0.006
120	0.833	0.006	0.879	0.012	0.920	0.007

Table E.73 Ionic strength (I) of Na_2HPO_4 in atrazine solution.

Na_2HPO_4 concentration		Na_2HPO_4 weight (g/0.1 kg atrazine solution)	Ionic strength (I) (mol/kg)
Molal (m) or mol/kg	mol/0.1 kg atrazine solution		
0.002	0.0002	0.0284	0.002
0.006	0.0006	0.0852	0.006
0.010	0.0010	0.1420	0.010

Table E.74 Electrical conductivity (σ) change before and after running reaction in the presence of Na_2HPO_4 in atrazine solution.

Ionic strength (I) from Na_2HPO_4 (mol/kg)	σ ($\mu\text{S}/\text{cm}$) before running reaction					σ ($\mu\text{S}/\text{cm}$) after running reaction				
	1st	2nd	3rd	σ	S.D.	1st	2nd	3rd	σ	S.D.
0.002	323	300	320	314	13	350	339	369	353	15
0.006	921	930	923	925	5	845	850	852	849	4
0.010	1413	1408	1410	1410	3	1399	1390	1385	1391	7

Table E.75 Atrazine photocatalytic degradation in the presence of Na_2HPO_4 at different ionic strength values.

Time (min)	Ionic strength (I) from Na_2HPO_4 (mol/kg)					
	0.002		0.006		0.010	
	C/C_0	S.D.	C/C_0	S.D.	C/C_0	S.D.
-30	1.000	0.000	1.000	0.000	1.000	0.000
0	1.009	0.019	1.019	0.030	1.035	0.032
15	0.986	0.016	1.002	0.003	1.010	0.026
30	0.923	0.049	0.983	0.008	0.983	0.008
60	0.904	0.029	0.944	0.027	0.943	0.039
120	0.841	0.034	0.893	0.005	0.890	0.037

E.9 Effect of anions

Table E.76 Photocatalytic degradation of atrazine using ZnO_550 and 0.02Ce-ZnO (S) 5:1 bead with free anions.

Time (min)	ZnO_550		0.02Ce-ZnO (S) 5:1 bead	
	C/C ₀	S.D.	C/C ₀	S.D.
-30	1.000	0.000	1.000	0.000
0	0.985	0.027	0.954	0.026
15	0.936	0.015	0.949	0.034
30	0.906	0.032	0.945	0.038
60	0.820	0.072	0.924	0.023
120	0.693	0.085	0.905	0.012

Table E.77 Photocatalytic degradation of atrazine using ZnO_550 in the presence of anions from sodium salts.

Time (min)	Na ₂ SO ₄ <i>I</i> = 0.025 m		NaCl <i>I</i> = 0.010 m		Na ₂ CO ₃ <i>I</i> = 0.025 m		NaHCO ₃ <i>I</i> = 0.010 m		Na ₂ HPO ₄ <i>I</i> = 0.010 m	
	C/C ₀	S.D.	C/C ₀	S.D.	C/C ₀	S.D.	C/C ₀	S.D.	C/C ₀	S.D.
-30	1.000	0.000	1.000	0.000	1.000	0.000	1.000	0.000	1.000	0.000
0	0.951	0.008	0.929	0.037	0.949	0.013	0.991	0.002	1.035	0.032
15	0.856	0.007	0.838	0.007	0.950	0.029	0.996	0.011	1.010	0.026
30	0.802	0.023	0.749	0.004	0.903	0.021	0.970	0.000	0.983	0.008
60	0.662	0.005	0.708	0.026	0.888	0.038	0.966	0.006	0.943	0.039
120	0.497	0.003	0.537	0.023	0.881	0.016	0.920	0.007	0.890	0.037

Table E.78 Photocatalytic degradation of atrazine using 0.02Ce-ZnO (S) 5:1 bead in the presence of anions from sodium salts.

Time (min)	Na ₂ SO ₄ <i>I</i> = 0.025 m		NaCl <i>I</i> = 0.010 m		Na ₂ CO ₃ <i>I</i> = 0.025 m		NaHCO ₃ <i>I</i> = 0.010 m		Na ₂ HPO ₄ <i>I</i> = 0.010 m	
	C/C ₀	S.D.	C/C ₀	S.D.	C/C ₀	S.D.	C/C ₀	S.D.	C/C ₀	S.D.
-60	1.000	0.000	1.000	0.000	1.000	0.000	1.000	0.000	1.000	0.000
-50	0.963	0.011	0.975	0.013	0.959	0.037	0.926	0.028	0.935	0.059
-40	0.991	0.013	0.987	0.011	0.985	0.008	0.966	0.005	0.928	0.039
-30	0.929	0.052	0.972	0.025	0.990	0.018	0.957	0.011	0.953	0.031
-15	0.970	0.015	1.008	0.042	0.974	0.022	0.964	0.030	0.936	0.017
0	0.970	0.007	0.975	0.014	0.993	0.035	0.886	0.022	0.946	0.029
15	0.918	0.064	0.977	0.005	0.967	0.016	0.957	0.005	0.926	0.012
30	0.873	0.064	0.954	0.007	0.946	0.025	0.959	0.021	0.938	0.037
45	0.886	0.018	0.938	0.005	0.931	0.053	0.905	0.016	0.922	0.040
60	0.887	0.079	0.936	0.012	0.963	0.027	0.948	0.019	0.863	0.067
120	0.885	0.025	0.934	0.009	0.928	0.028	0.947	0.005	0.891	0.052

E.10 Other metal dopants on ZnO

Table E.79 Photocatalytic degradation of atrazine using 0.005Cu-0.005Ce-ZnO (S) powder.

Time (min)	Peak area			Concentration (mg/L)			Average concentration (mg/L)	Standard deviation
	1st	2nd	3rd	1st	2nd	3rd		
-60	303.5	303.5	303.5	4.443	4.443	4.443	4.443	0.000
-50	297.0	301.1	304.5	4.348	4.408	4.458	4.404	0.055
-40	309.5	304.4	308.5	4.531	4.456	4.516	4.501	0.040
-30	304.0	298.8	303.5	4.450	4.374	4.443	4.423	0.042
-15	307.7	298.7	291.8	4.505	4.373	4.272	4.383	0.117
0	304.3	274.3	289.7	4.455	4.016	4.241	4.237	0.220
15	308.8	297.1	292.6	4.521	4.349	4.283	4.384	0.122
30	279.7	294.6	301.1	4.095	4.313	4.408	4.272	0.161
45	301.9	299.9	298.1	4.420	4.390	4.364	4.391	0.028
60	305.9	294.8	289.9	4.478	4.316	4.244	4.346	0.120
120	305.6	293.7	308.9	4.474	4.300	4.522	4.432	0.117

Table E.80 Photocatalytic degradation of atrazine using 0.005Fe-0.005Ce-ZnO (S) powder.

Time (min)	Peak area			Concentration (mg/L)			Average concentration (mg/L)	Standard deviation
	1st	2nd	3rd	1st	2nd	3rd		
-60	303.5	303.5	303.5	4.443	4.443	4.443	4.443	0.000
-50	301.0	311.1	265.0	4.406	4.554	3.879	4.280	0.355
-40	277.6	307.9	292.6	4.064	4.507	4.283	4.285	0.222
-30	299.9	300.5	290.2	4.390	4.399	4.248	4.346	0.085
-15	300.2	304.4	290.4	4.395	4.456	4.251	4.367	0.105
0	295.2	298.6	294.2	4.322	4.371	4.307	4.333	0.034
15	296.1	269.9	287.7	4.335	3.951	4.212	4.166	0.196
30	297.2	280.8	277.1	4.351	4.111	4.057	4.173	0.157
45	278.7	268.3	272.0	4.080	3.928	3.982	3.997	0.077
60	279.8	288.7	246.8	4.096	4.226	3.613	3.978	0.323
120	237.1	235.1	218.9	3.471	3.442	3.205	3.372	0.146

Table E.81 Photocatalytic degradation of atrazine using 0.005Ag-0.005Ce-ZnO (S) powder.

Time (min)	Peak area			Concentration (mg/L)			Average concentration (mg/L)	Standard deviation
	1st	2nd	3rd	1st	2nd	3rd		
-60	303.5	303.5	303.5	4.443	4.443	4.443	4.443	0.000
-50	303.9	307.4	295.6	4.449	4.500	4.327	4.425	0.089
-40	303.5	301.1	282.5	4.443	4.408	4.136	4.329	0.168
-30	298.0	296.8	298.4	4.363	4.345	4.368	4.359	0.012
-15	297.7	300.4	301.6	4.358	4.398	4.415	4.390	0.029
0	307.6	278.6	284.2	4.503	4.079	4.161	4.247	0.225
15	246.2	260.4	224.1	3.604	3.812	3.281	3.566	0.268
30	207.9	219.4	231.1	3.044	3.212	3.383	3.213	0.170
45	166.5	192.4	181.2	2.437	2.817	2.653	2.636	0.190
60	144.5	147.0	137.2	2.115	2.152	2.009	2.092	0.075
120	44.5	92.2	57.4	0.651	1.350	0.840	0.947	0.361

Table E.82 Photocatalytic degradation of atrazine by 0.005Ag-0.005Ce-ZnO (S) powder using 0.9 mg/L of atrazine solution.

Time (min)	Peak area			Concentration (mg/L)			Average concentration (mg/L)	Standard deviation
	1st	2nd	3rd	1st	2nd	3rd		
-60	63.1	63.1	63.1	0.924	0.924	0.924	0.924	0.000
-50	66.2	61	70.8	0.969	0.893	1.036	0.966	0.072
-40	65.9	59.1	65.2	0.965	0.865	0.954	0.928	0.055
-30	67.2	60.1	62.3	0.984	0.880	0.912	0.925	0.053
-15	54.3	61.3	51.9	0.795	0.897	0.760	0.817	0.071
0	63.1	62.8	51.9	0.924	0.919	0.760	0.868	0.093
15	50.8	55.2	67.7	0.744	0.808	0.991	0.848	0.128
30	44	44.7	58.5	0.644	0.654	0.856	0.718	0.120
45	35.6	38.9	47.4	0.521	0.569	0.694	0.595	0.089
60	29.7	29.1	41.1	0.435	0.426	0.602	0.487	0.099
120	8.9	12.2	7.4	0.130	0.179	0.108	0.139	0.036

Table E.83 Photocatalytic degradation of atrazine by 0.005Ag-0.005Ce-ZnO (S) powder using 2.8 mg/L of atrazine solution.

Time (min)	Peak area			Concentration (mg/L)			Average concentration (mg/L)	Standard deviation
	1st	2nd	3rd	1st	2nd	3rd		
-60	190.2	190.2	190.2	2.784	2.784	2.784	2.784	0.000
-50	178	178	192.6	2.606	2.606	2.820	2.677	0.123
-40	171.1	182.6	188.9	2.505	2.673	2.765	2.648	0.132
-30	174.9	176.7	185.5	2.560	2.587	2.716	2.621	0.083
-15	179.2	172.2	180.3	2.623	2.521	2.639	2.595	0.064
0	152.6	177	180	2.234	2.591	2.635	2.487	0.220
15	149.2	141	136.5	2.184	2.064	1.998	2.082	0.094
30	127.5	128	116.4	1.867	1.874	1.704	1.815	0.096
45	98.3	95.2	84.9	1.439	1.394	1.243	1.359	0.103
60	80.7	82.7	65.7	1.181	1.211	0.962	1.118	0.136
120	28.9	42.7	24.7	0.423	0.625	0.362	0.470	0.138

Table E.84 Photocatalytic degradation of atrazine by 0.005Ag-0.005Ce-ZnO (S) powder using 4.4 mg/L of atrazine solution.

Time (min)	Peak area			Concentration (mg/L)			Average concentration (mg/L)	Standard deviation
	1st	2nd	3rd	1st	2nd	3rd		
-60	303.5	303.5	303.5	4.443	4.443	4.443	4.443	0.000
-50	301	311.1	265	4.406	4.554	3.879	4.280	0.355
-40	277.6	307.9	292.6	4.064	4.507	4.283	4.285	0.222
-30	299.9	300.5	290.2	4.390	4.399	4.248	4.346	0.085
-15	300.2	304.4	290.4	4.395	4.456	4.251	4.367	0.105
0	295.2	298.6	294.2	4.322	4.371	4.307	4.333	0.034
15	296.1	269.9	287.7	4.335	3.951	4.212	4.166	0.196
30	297.2	280.8	277.1	4.351	4.111	4.057	4.173	0.157
45	278.7	268.3	272	4.080	3.928	3.982	3.997	0.077
60	279.8	288.7	246.8	4.096	4.226	3.613	3.978	0.323
120	237.1	235.1	218.9	3.471	3.442	3.205	3.372	0.146

Table E.85 Photocatalytic degradation of atrazine by 0.005Ag-0.005Ce-ZnO (S) powder using 6.0 mg/L of atrazine solution.

Time (min)	Peak area			Concentration (mg/L)			Average concentration (mg/L)	Standard deviation
	1st	2nd	3rd	1st	2nd	3rd		
-60	407.0	407.0	407.0	5.958	5.958	5.958	5.958	0.000
-50	407.5	405.7	399.0	5.966	5.939	5.841	5.915	0.066
-40	409.5	403.3	406.7	5.995	5.904	5.954	5.951	0.045
-30	382.8	393.8	364.4	5.604	5.765	5.335	5.568	0.217
-15	368.3	434.0	389.8	5.392	6.353	5.706	5.817	0.490
0	387.7	397.2	399.7	5.676	5.815	5.851	5.781	0.093
15	353.5	345.8	325.4	5.175	5.062	4.764	5.000	0.213
30	305.2	294.4	313.1	4.468	4.310	4.584	4.454	0.137
45	284.9	244.2	244.4	4.171	3.575	3.578	3.775	0.343
60	243.6	234.2	204.1	3.566	3.429	2.988	3.328	0.302
120	127.7	129.9	97.3	1.869	1.902	1.424	1.732	0.267

Table E.86 Photocatalytic degradation of atrazine by 0.005Ag-0.005Ce-ZnO (S) powder using 9.5 mg/L of atrazine solution.

Time (min)	Peak area			Concentration (mg/L)			Average concentration (mg/L)	Standard deviation
	1st	2nd	3rd	1st	2nd	3rd		
-60	647.9	647.9	647.9	9.485	9.485	9.485	9.485	0.000
-50	640.1	641.9	633.3	9.371	9.397	9.271	9.346	0.066
-40	637.5	628.4	636.2	9.333	9.199	9.314	9.282	0.072
-30	653	594.9	624.4	9.560	8.709	9.141	9.136	0.425
-15	643.5	637.7	657.5	9.420	9.336	9.625	9.460	0.149
0	633.5	648.7	627.1	9.274	9.497	9.180	9.317	0.162
15	575	551.9	527.1	8.418	8.079	7.716	8.071	0.351
30	450.3	471.1	461.3	6.592	6.897	6.753	6.747	0.152
45	431.8	416.5	411.4	6.321	6.097	6.023	6.147	0.155
60	367.4	341.1	370	5.379	4.993	5.417	5.263	0.234
120	197	202.2	223	2.884	2.960	3.265	3.036	0.201

E.11 Competitive effects from natural organic matter

Table E.87 Photocatalytic degradation of atrazine by 0.02Ce-ZnO (S) bead with free humic acid.

Time (min)	Peak area			Concentration (mg/L)			Average concentration (mg/L)	Standard deviation
	1st	2nd	3rd	1st	2nd	3rd		
0	330.2	337.8	320.1	4.833	4.945	4.686	4.821	0.130
15	341.1	319.5	322.4	4.993	4.677	4.720	4.797	0.172
30	341.4	317.5	319.9	4.998	4.648	4.683	4.776	0.193
60	328.3	313.6	315.7	4.806	4.591	4.622	4.673	0.116
120	317.1	311.8	308.8	4.641	4.564	4.521	4.575	0.061

Table E.88 Photocatalytic degradation of atrazine by 0.02Ce-ZnO (S) bead in the presence of 1.0 mg/L humic acid.

Time (min)	Peak area			Concentration (mg/L)			Average concentration (mg/L)	Standard deviation
	1st	2nd	3rd	1st	2nd	3rd		
0	327.8	314.8	326.2	4.799	4.608	4.775	4.728	0.104
15	328.4	331.6	322.2	4.808	4.854	4.717	4.793	0.070
30	316.4	318.5	315.9	4.632	4.663	4.625	4.640	0.020
45	315.9	324.2	311.0	4.625	4.746	4.553	4.641	0.098
60	303.3	314.5	307.1	4.440	4.604	4.496	4.513	0.083
120	305.0	300.7	307.0	4.465	4.402	4.494	4.454	0.047

Table E.89 Photocatalytic degradation of atrazine by 0.02Ce-ZnO (S) bead in the presence of 3.0 mg/L humic acid.

Time (min)	Peak area			Concentration (mg/L)			Average concentration (mg/L)	Standard deviation
	1st	2nd	3rd	1st	2nd	3rd		
0	334.4	337.6	320.9	4.895	4.942	4.698	4.845	0.130
15	303.8	329.9	317.8	4.447	4.830	4.652	4.643	0.191
30	322.7	317.8	315.0	4.724	4.652	4.611	4.663	0.057
45	324.2	328.1	319.9	4.746	4.803	4.683	4.744	0.060
60	312.6	314.0	311.2	4.576	4.597	4.556	4.576	0.020
120	313.5	307.0	310.3	4.589	4.494	4.543	4.542	0.048

Table E.90 Photocatalytic degradation of atrazine by 0.02Ce-ZnO (S) bead in the presence of 5.0 mg/L humic acid.

Time (min)	Peak area			Concentration (mg/L)			Average concentration (mg/L)	Standard deviation
	1st	2nd	3rd	1st	2nd	3rd		
0	302.0	332.6	318.7	4.421	4.869	4.666	4.652	0.224
15	323.1	306.7	318.6	4.730	4.490	4.664	4.628	0.124
30	322.8	309.2	311.2	4.726	4.526	4.556	4.603	0.107
45	297.8	314.9	305.7	4.360	4.610	4.475	4.482	0.125
60	308.0	313.9	301.7	4.509	4.595	4.417	4.507	0.089
120	153.3	274.2	266.9	2.244	4.014	3.907	3.389	0.992

Table E.91 Photocatalytic degradation of atrazine by 0.005Ag-0.005Ce-ZnO (S) powder with free humic acid.

Time (min)	Peak area			Concentration (mg/L)			Average concentration (mg/L)	Standard deviation
	1st	2nd	3rd	1st	2nd	3rd		
0	307.6	278.6	284.2	4.503	4.079	4.161	4.247	0.225
15	246.2	260.4	224.1	3.604	3.812	3.281	3.566	0.268
30	207.9	219.4	231.1	3.044	3.212	3.383	3.213	0.170
45	166.5	192.4	181.2	2.437	2.817	2.653	2.636	0.190
60	144.5	147.0	137.2	2.115	2.152	2.009	2.092	0.075
120	44.5	92.2	57.4	0.651	1.350	0.840	0.947	0.361

Table E.92 Photocatalytic degradation of atrazine by 0.005Ag-0.005Ce-ZnO (S) powder in the presence of 50.0 mg/L humic acid.

Time (min)	Peak area			Concentration (mg/L)			Average concentration (mg/L)	Standard deviation
	1st	2nd	3rd	1st	2nd	3rd		
0	412.9	356.3	412.8	6.045	5.216	6.043	5.768	0.478
15	411.4	353.4	339.8	6.023	5.174	4.974	5.390	0.557
30	313	343.6	333.2	4.582	5.030	4.878	4.830	0.228
45	316.1	291.7	330.2	4.628	4.270	4.834	4.577	0.285
60	263.8	254.3	320.3	3.862	3.723	4.689	4.091	0.522
120	170.2	163.7	252.5	2.492	2.396	3.696	2.862	0.725

E.12 Langmuir-Hinshelwood-Hougen and Watson (LHHW) kinetics

Table E.93 Initial rate of atrazine photocatalytic degradation by catalyst powders and catalyst bead.

ZnO powder		0.005Ag-0.005Ce-ZnO (S) powder		ZnO_550	
C_0	r_0	C_0	r_0	C_0	r_0
1.042	9.882	0.868	-0.520	0.970	1.268
2.298	15.461	2.487	7.096	2.085	2.106
4.870	32.692	4.247	12.692	4.985	4.491
7.125	38.891	5.781	13.457	6.954	7.757
9.756	53.408	9.180	18.102	9.758	13.929

Table E.94 Atrazine photocatalytic degradation by catalyst powders and catalyst bead for LHHW linear plotting.

ZnO powder		0.005Ag-0.005Ce-ZnO (S) powder		ZnO_550	
$1/C_0$	$1/r_0$	$1/C_0$	$1/r_0$	$1/C_0$	$1/r_0$
0.960	0.101	1.152	-1.924	1.031	0.789
0.435	0.065	0.402	0.141	0.480	0.475
0.205	0.031	0.235	0.079	0.201	0.223
0.140	0.026	0.173	0.074	0.144	0.129
0.103	0.019	0.109	0.055	0.102	0.072

E.13 Catalyst reliability

Table E.95 Reliability test of atrazine photocatalytic degradation by ZnO_550 at 120 min.

Cycle	Atrazine removal at 120 min (%)				
	1st	2nd	3rd	Average atrazine removal	Standard deviation
1	22.235	33.123	34.090	29.816	6.583
2	18.908	30.117	29.916	26.314	6.415
3	16.496	24.707	24.387	21.863	4.651
4	13.321	19.507	18.005	16.944	3.226
5	11.699	18.726	17.106	15.844	3.679

E.14 Evaluation of photocatalytic degradation pathway of atrazine

Table E.96 C/C_0 and TOC/TOC_0 of atrazine photocatalytic degradation using ZnO and 0.005Ag-0.005Ce-ZnO (S) powders.

Time (min)	ZnO powder		0.005Ag-0.005Ce-ZnO (S) powder	
	C/C_0	TOC/TOC_0	C/C_0	TOC/TOC_0
0	1.000	1.000	1.000	1.000
15	0.602	0.868	0.841	0.790
30	0.304	0.703	0.759	0.718
45	-	0.505	0.623	0.594
60	0.106	0.498	0.493	0.558
90	-	0.465	-	0.505
120	0.007	0.382	0.226	0.430
150	-	0.369	-	0.382
180	0.000	0.355	0.133	0.371

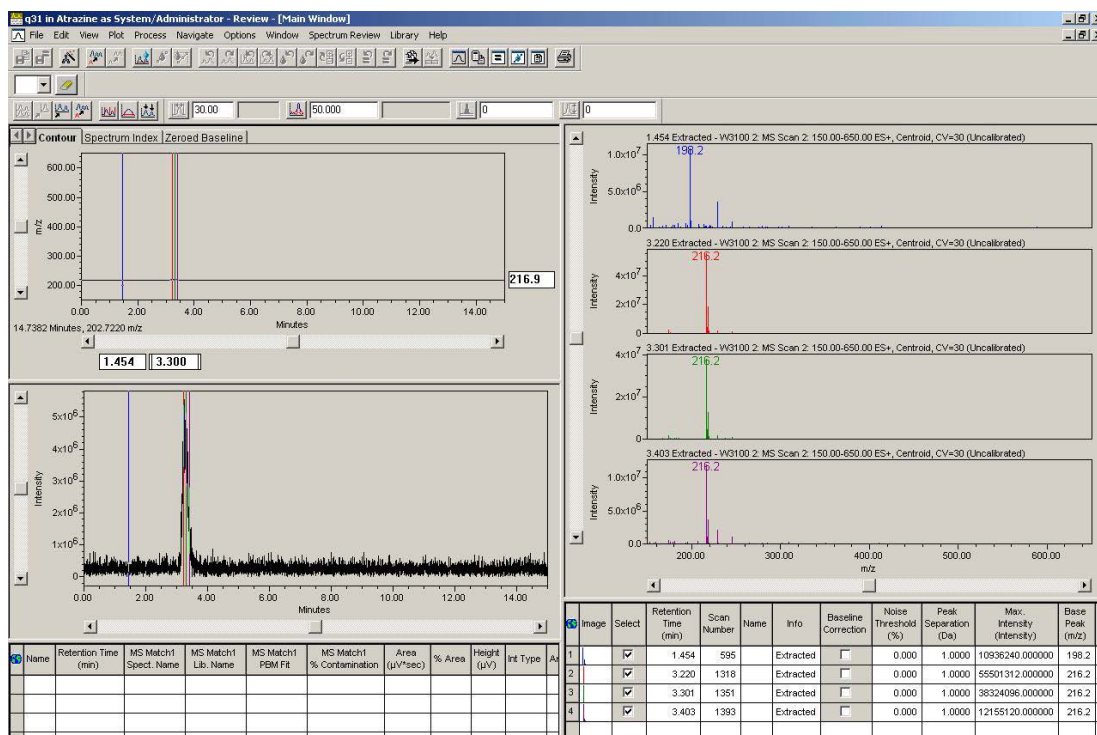


Figure E.2 LC-MS spectra of atrazine photocatalytic degradation using ZnO powder at 0 min.

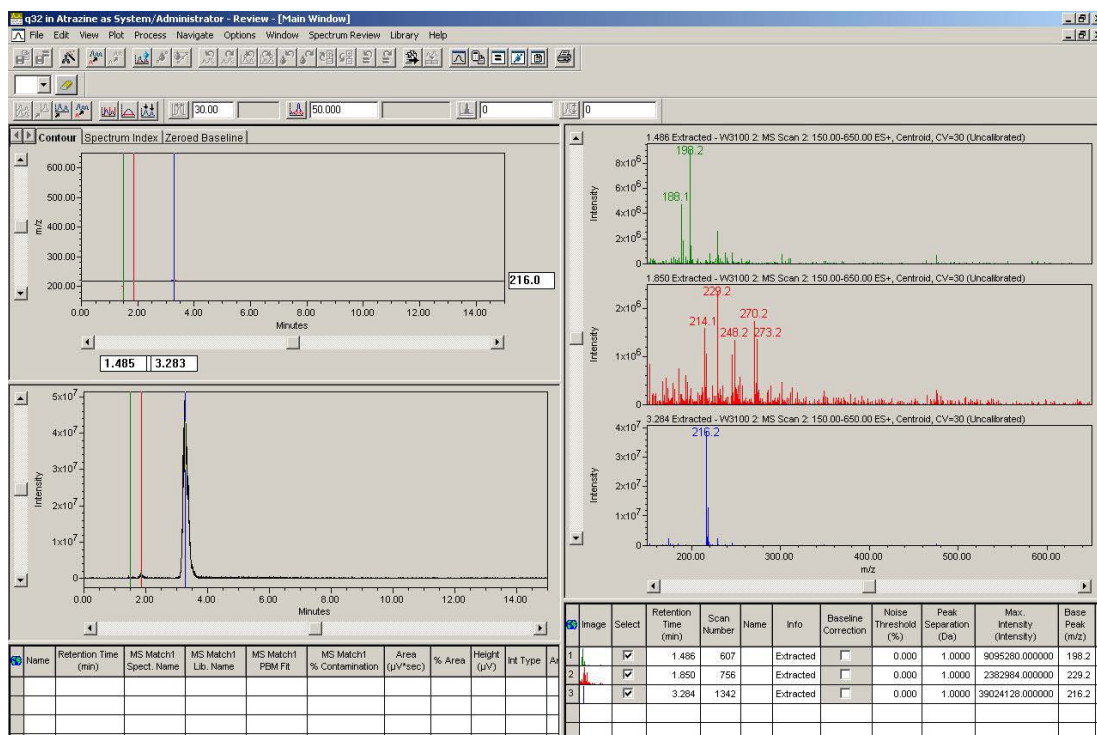


Figure E.3 LC-MS spectra of atrazine photocatalytic degradation using ZnO powder at 15 min.

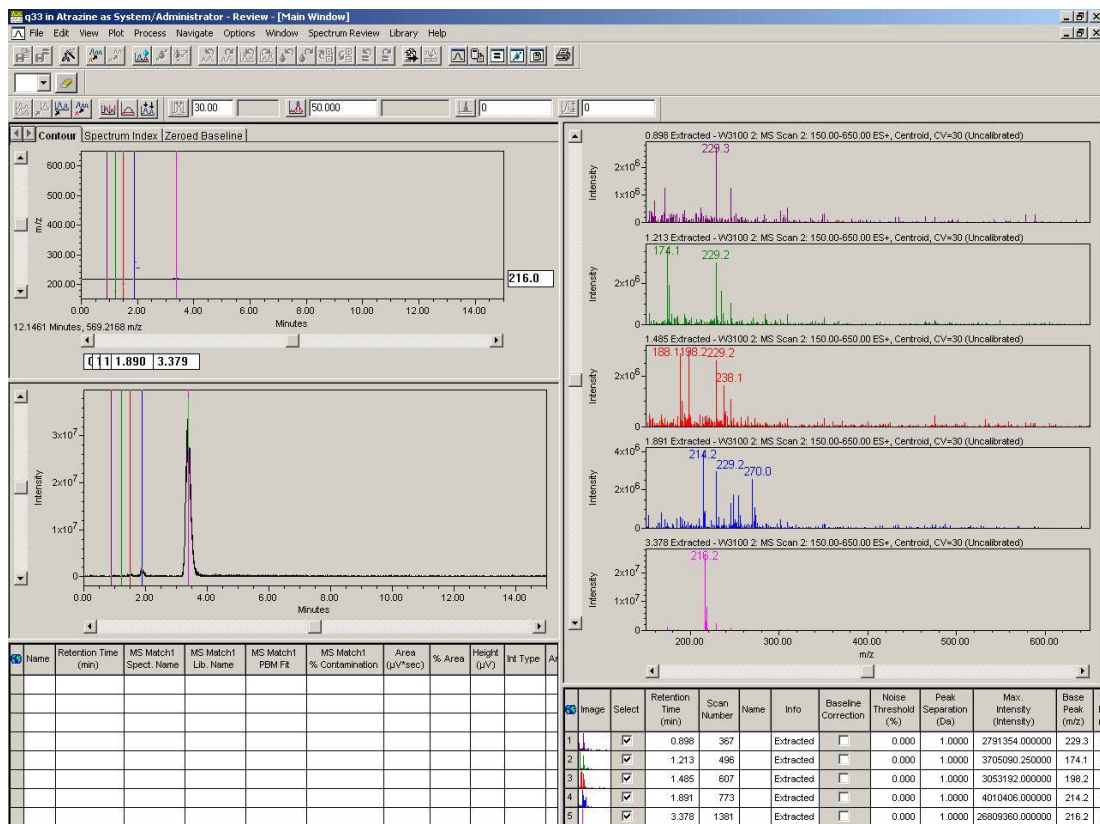


Figure E.4 LC-MS spectra of atrazine photocatalytic degradation using ZnO powder at 30 min.

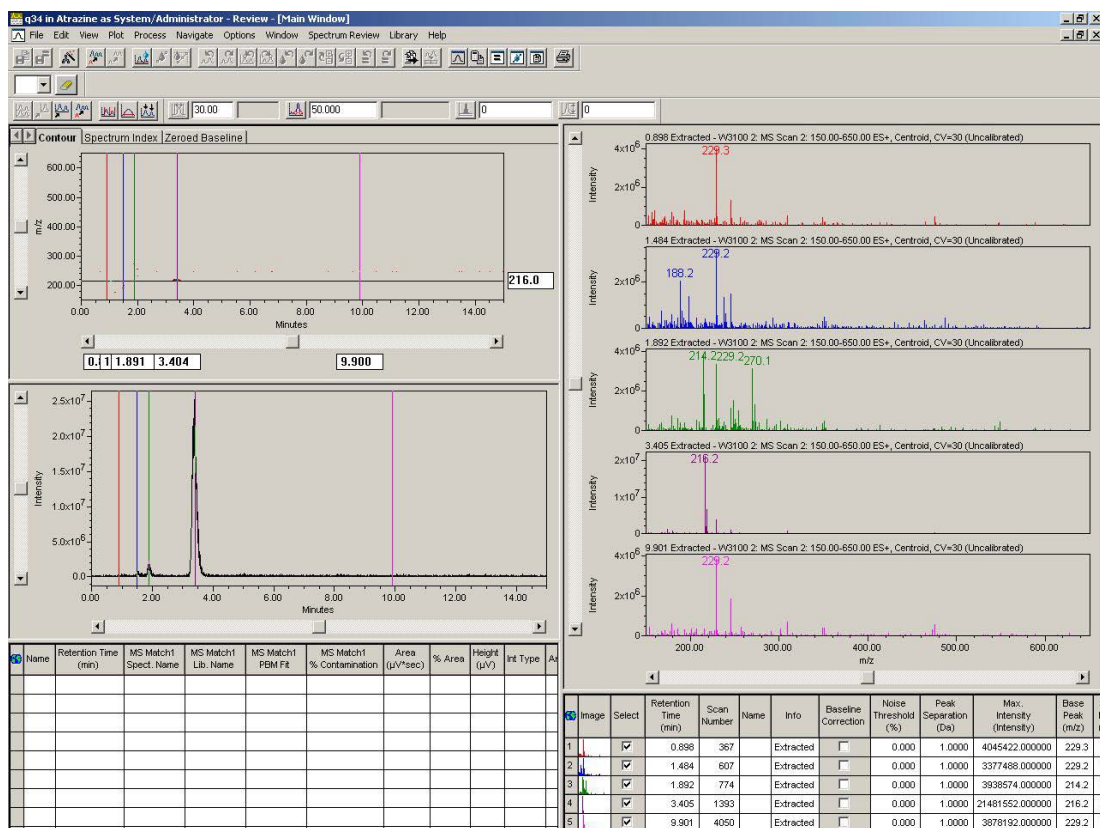


Figure E.5 LC-MS spectra of atrazine photocatalytic degradation using ZnO powder at 45 min.

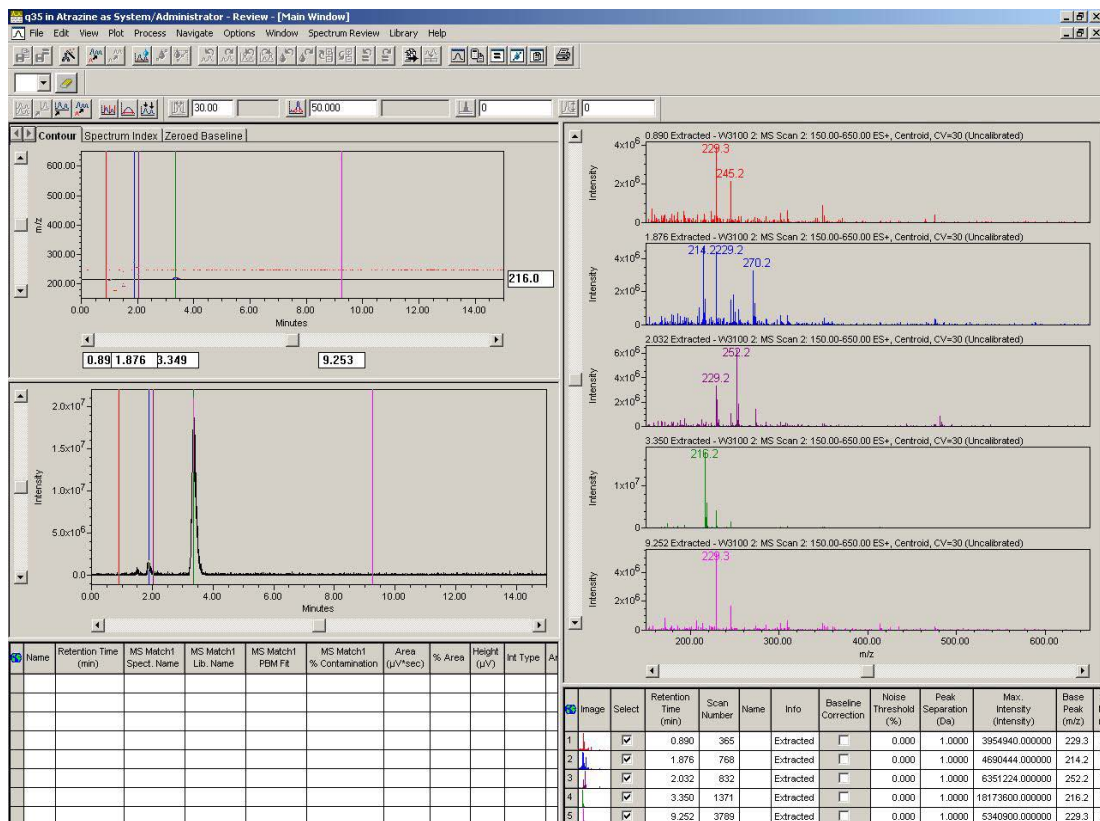


Figure E.6 LC-MS spectra of atrazine photocatalytic degradation using ZnO powder at 60 min.

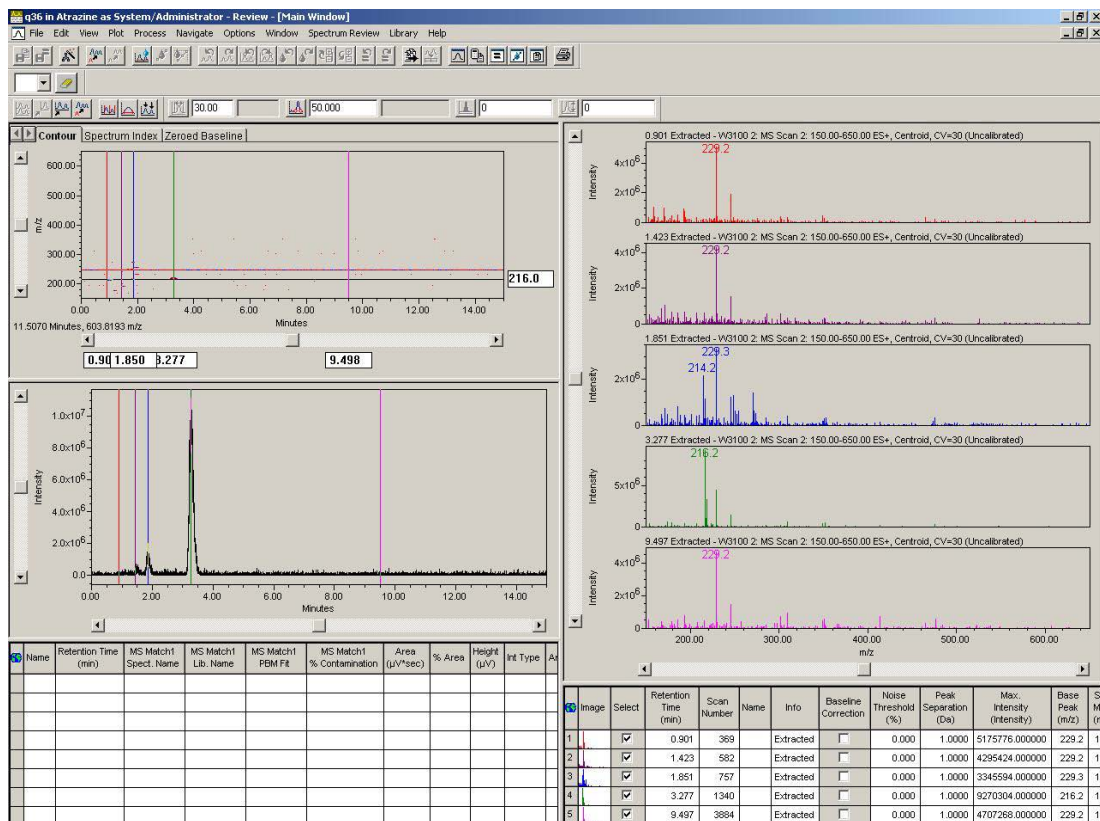


Figure E.7 LC-MS spectra of atrazine photocatalytic degradation using ZnO powder at 90 min.

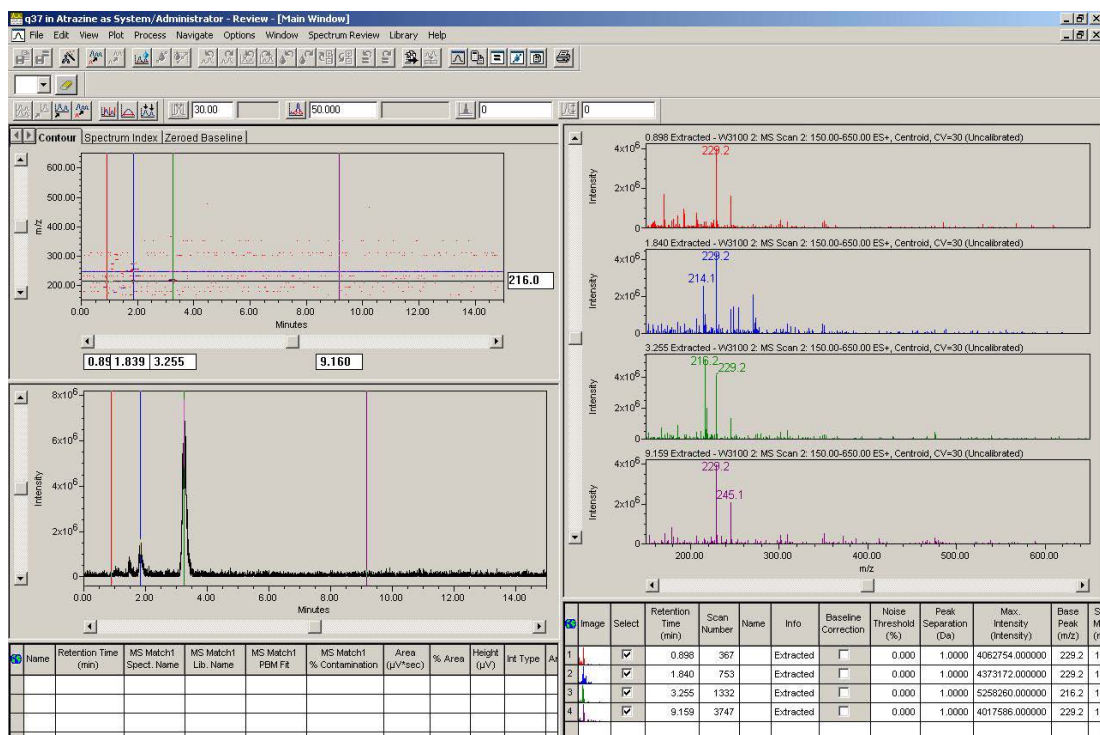


Figure E.8 LC-MS spectra of atrazine photocatalytic degradation using ZnO powder at 120 min.

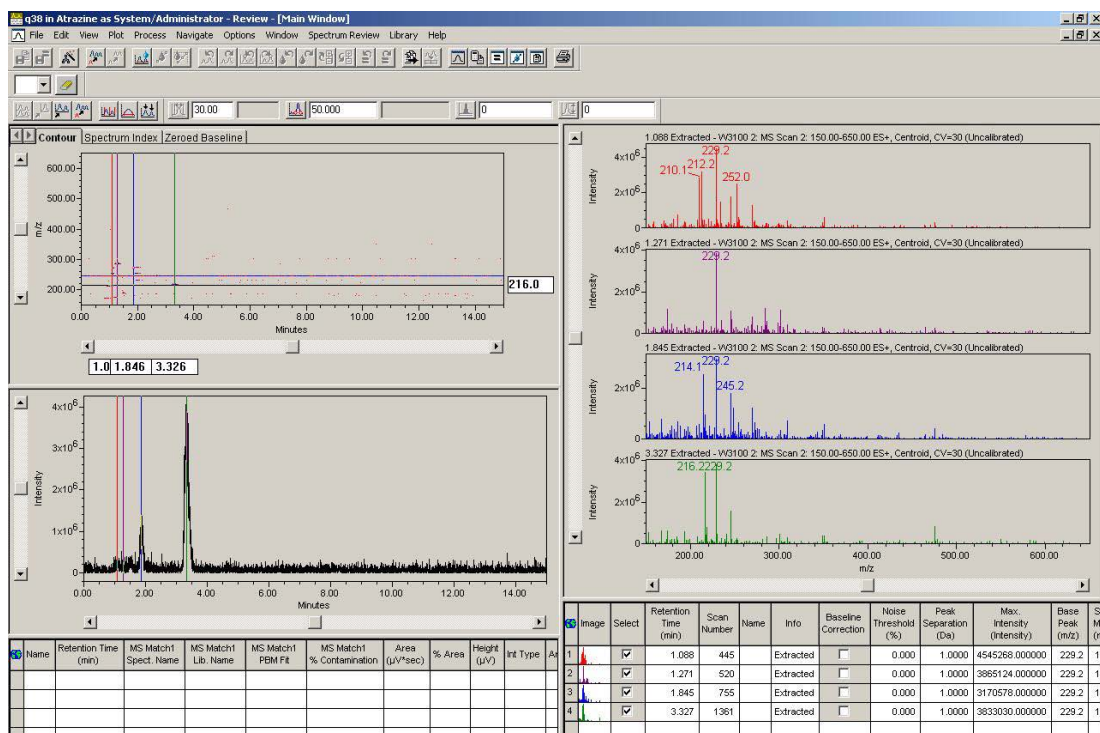


Figure E.9 LC-MS spectra of atrazine photocatalytic degradation using ZnO powder at 150 min.

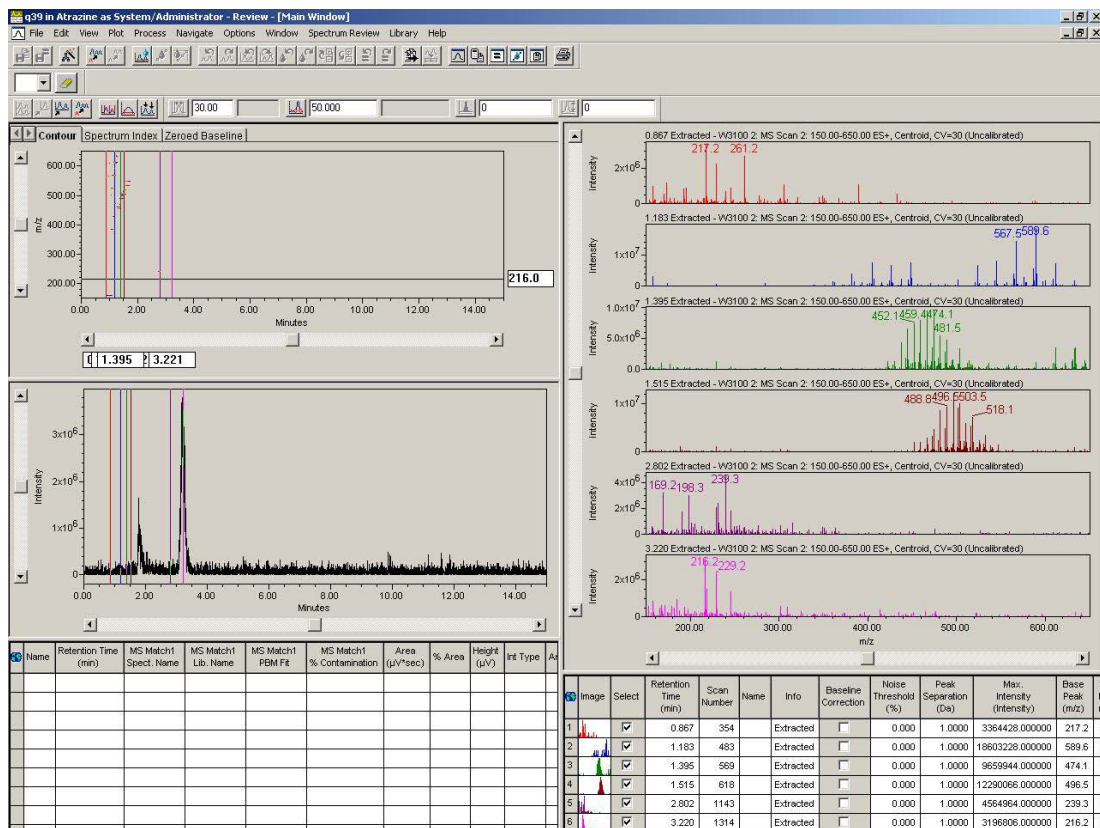


Figure E.10 LC-MS spectra of atrazine photocatalytic degradation using ZnO powder at 180 min.

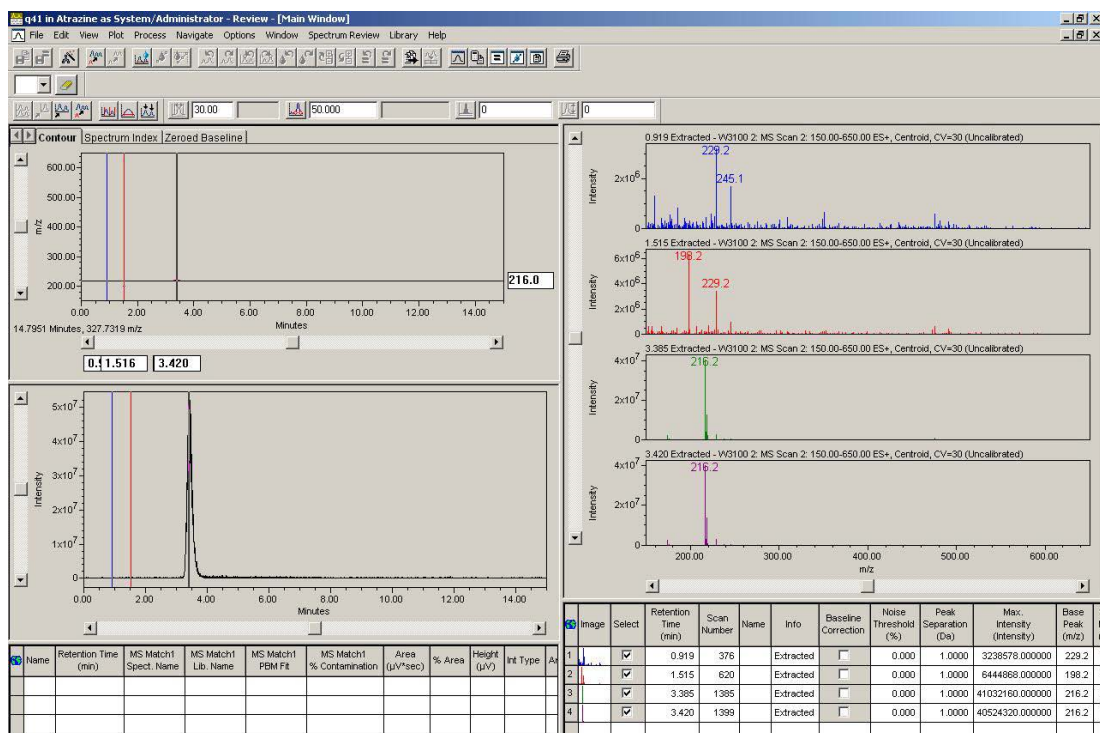


Figure E.11 LC-MS spectra of atrazine photocatalytic degradation using 0.005Ag-0.005Ce-ZnO powder at 0 min.

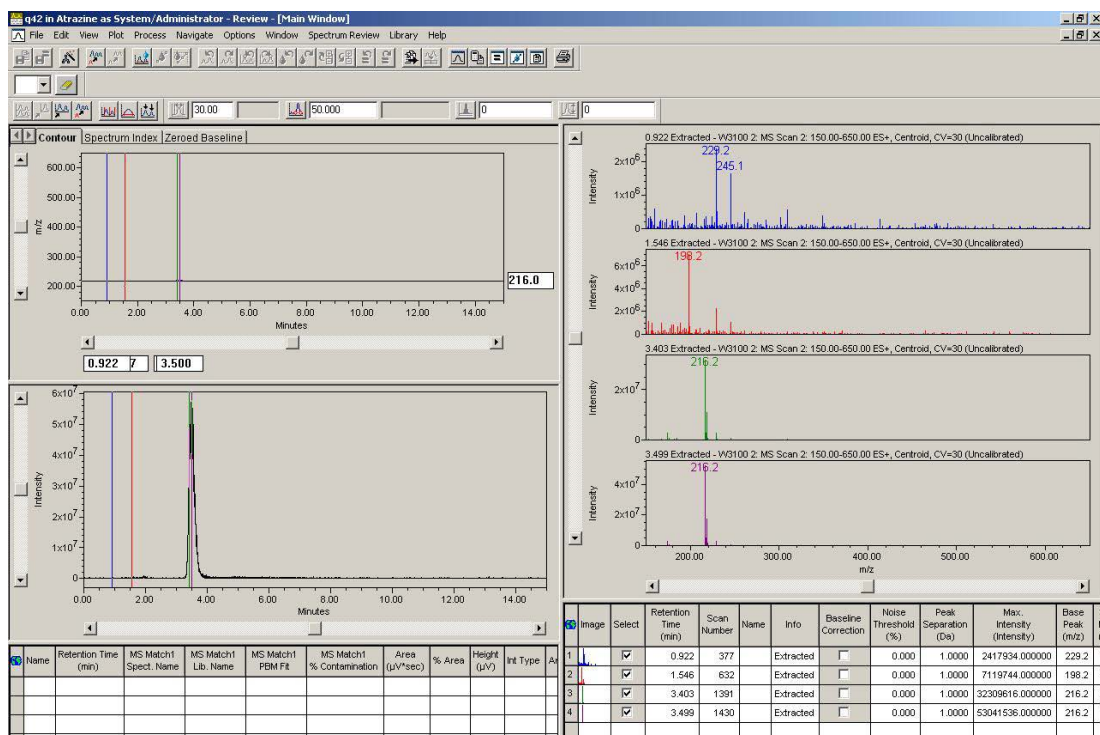


Figure E.12 LC-MS spectra of atrazine photocatalytic degradation using 0.005Ag-0.005Ce-ZnO powder at 15 min.

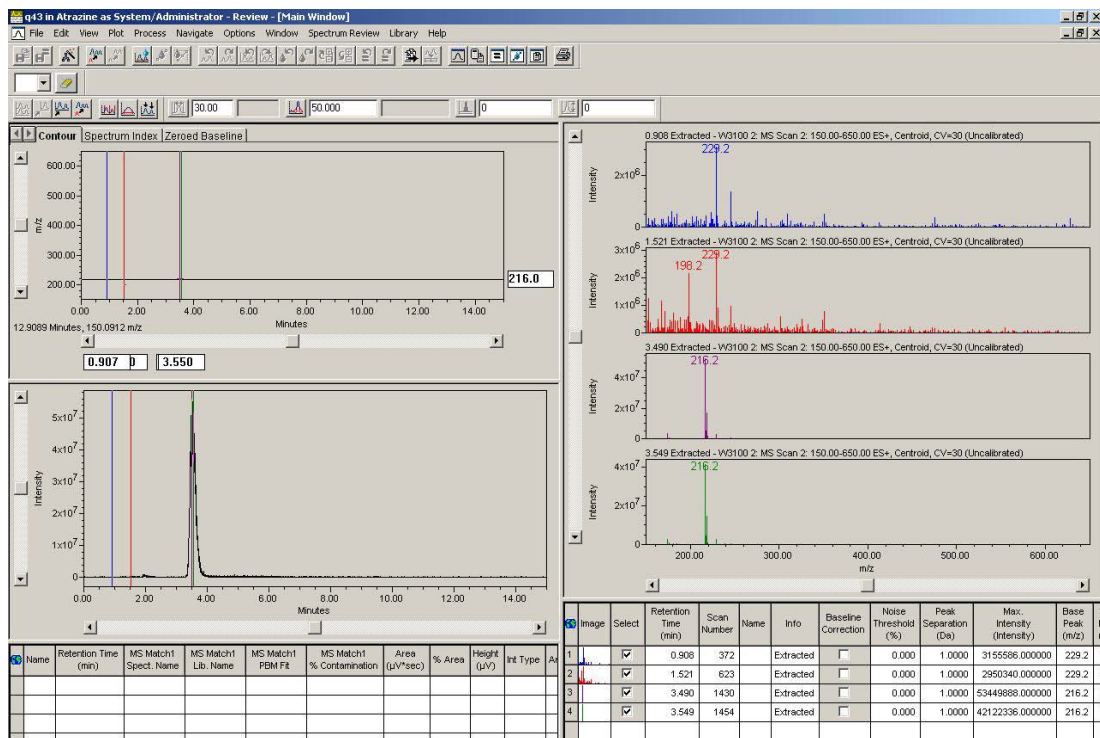


Figure E.13 LC-MS spectra of atrazine photocatalytic degradation using 0.005Ag-0.005Ce-ZnO powder at 30 min.

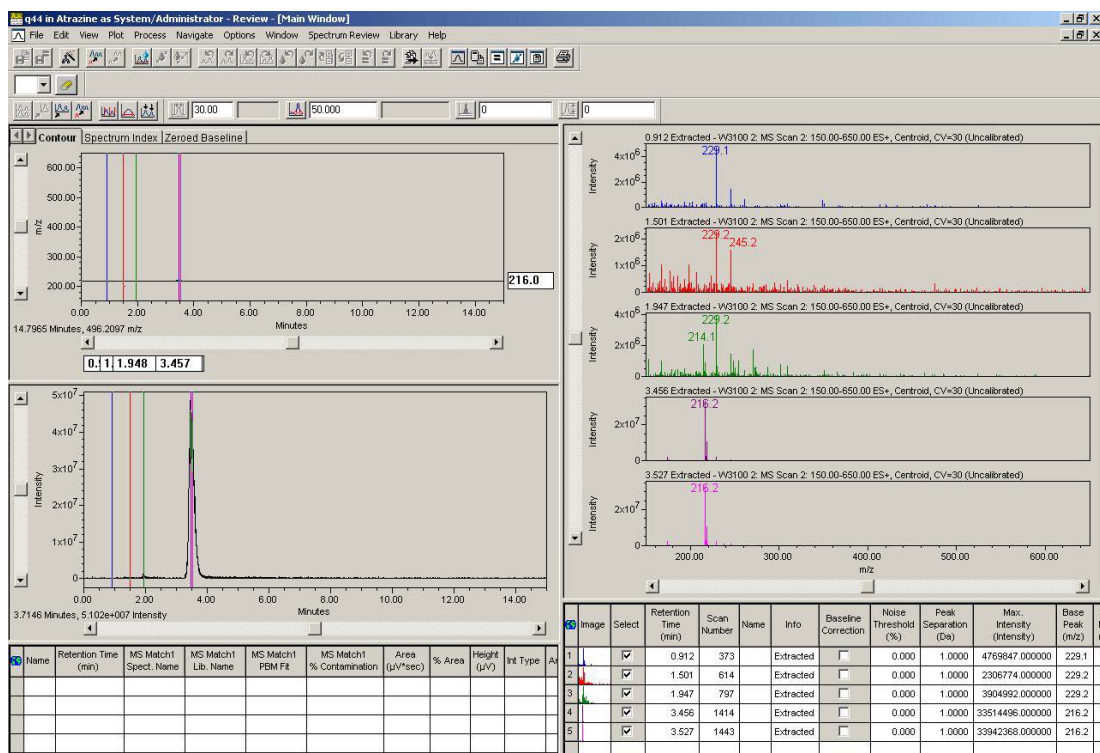


Figure E.14 LC-MS spectra of atrazine photocatalytic degradation using 0.005Ag-0.005Ce-ZnO powder at 45 min.

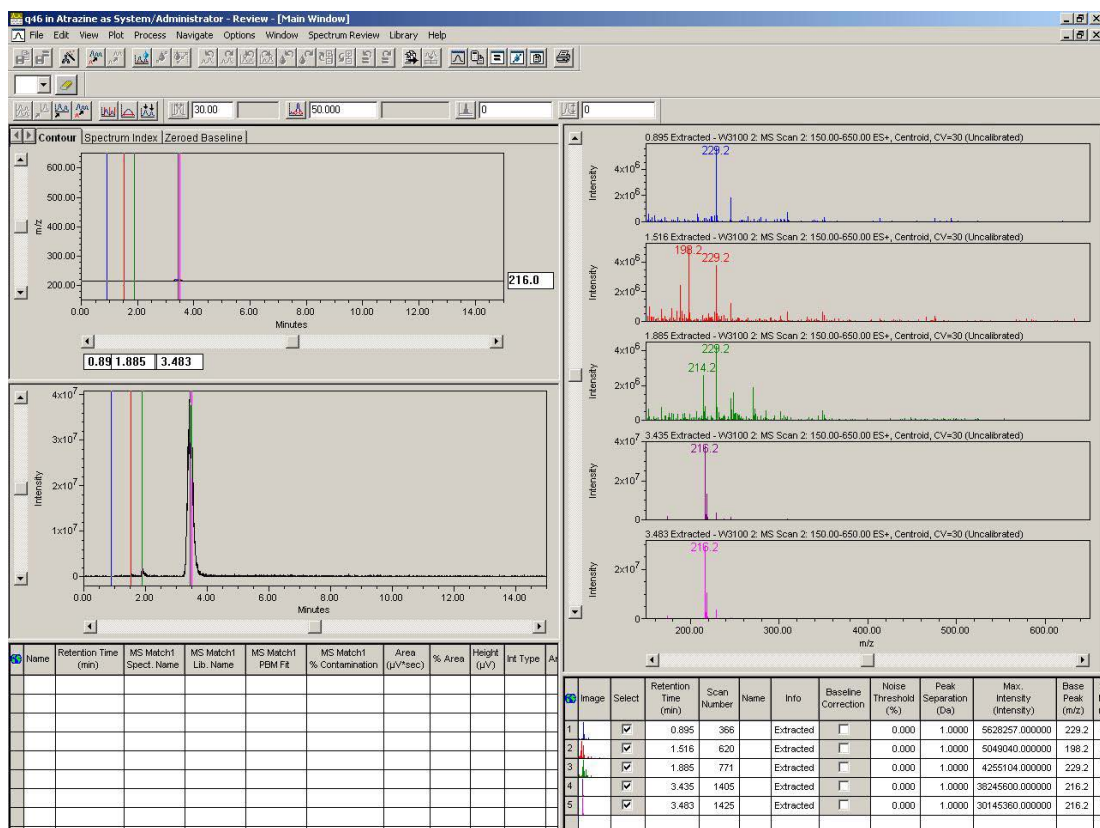


Figure E.16 LC-MS spectra of atrazine photocatalytic degradation using 0.005Ag-0.005Ce-ZnO powder at 90 min.

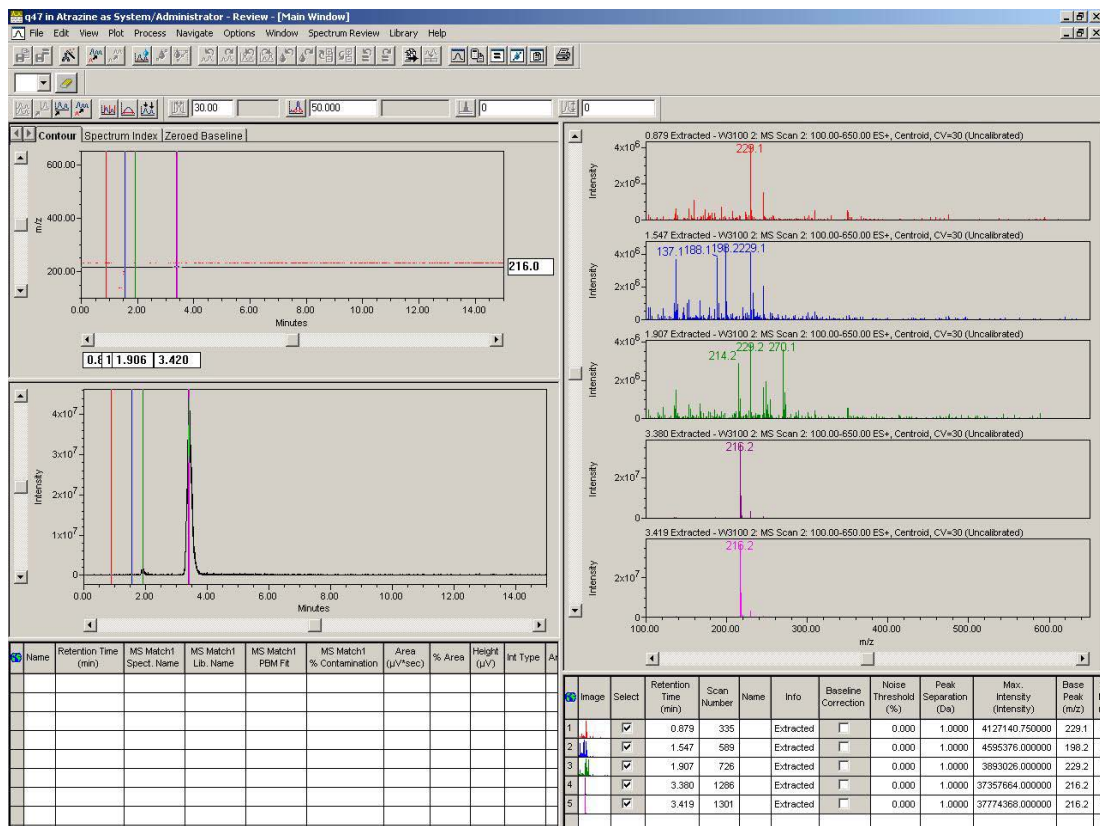


Figure E.17 LC-MS spectra of atrazine photocatalytic degradation using 0.005Ag-0.005Ce-ZnO powder at 120 min.

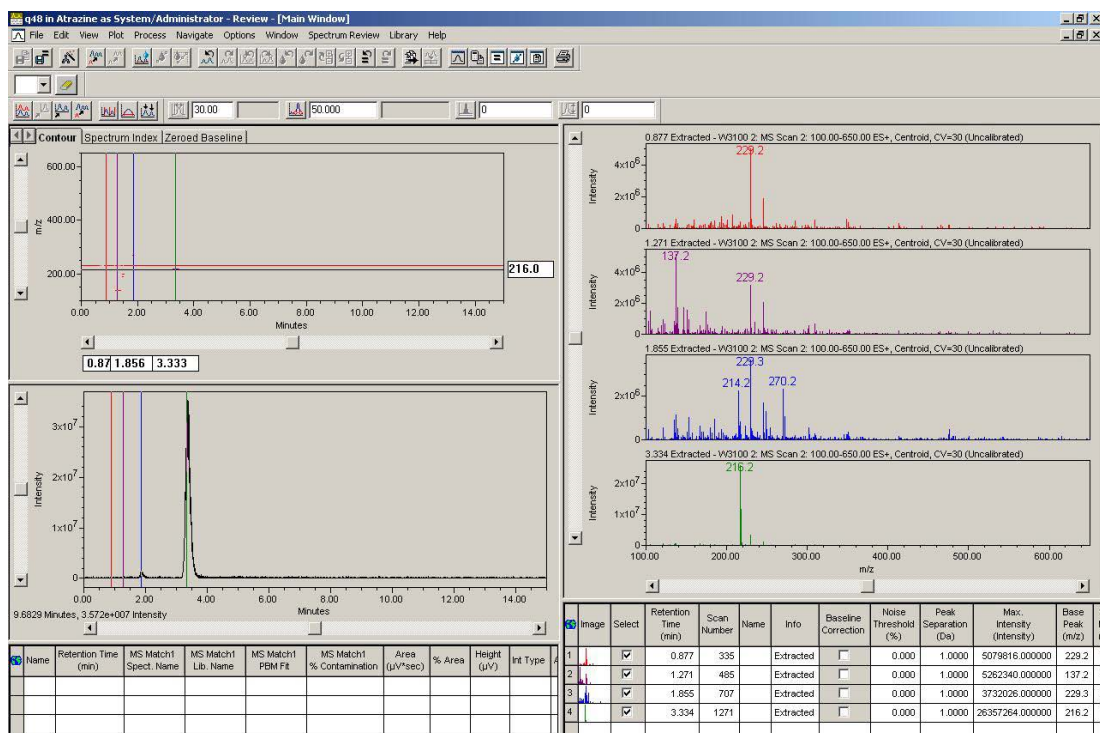


Figure E.18 LC-MS spectra of atrazine photocatalytic degradation using 0.005Ag-0.005Ce-ZnO powder at 150 min.

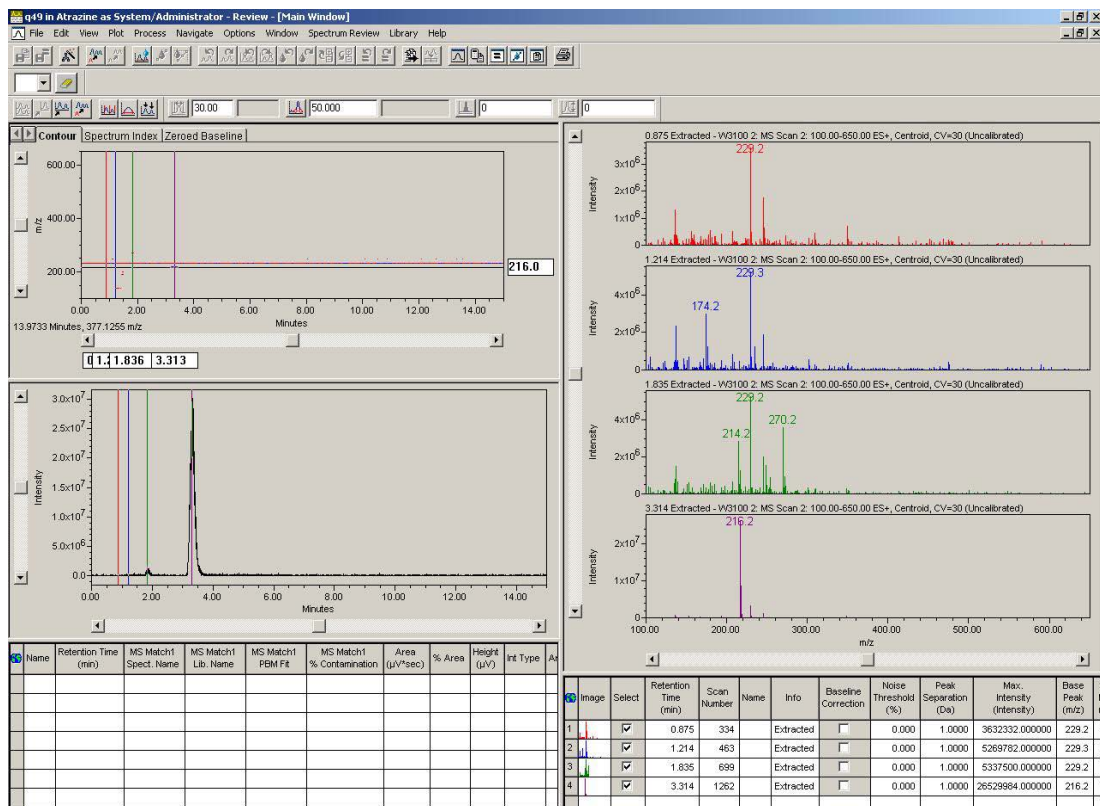


Figure E.19 LC-MS spectra of atrazine photocatalytic degradation using 0.005Ag-0.005Ce-ZnO powder at 180 min.

BIOGRAPHY

Born in 1981 in a province in Thailand, Pummarin Khamdahsag has grown up as an only child of Raungrit and Aurai Khamdahsag. She finished her primary school at Chumchonbanmaetun School, Li district, Lamphun, where she first discovered her passion for science-astronomy after being inspired by a book in biography of scientists. Consequently, she pursued her secondary education focusing in science at Teerakarnbanhong School, Banhong district, Lamphun where she eventually shifted her interest towards biology and chemistry. She then continued her higher education at Chiangmai University in Faculty of Education, Major of Science-Chemistry. She had done great works in teaching and studying in chemistry specializing in inorganic chemistry and environmental chemistry. However, she was undecided on what career path to pursue after she graduated in three and a half years. She had several questions on her mind that could not be answered. After deep soul searching, she finally took her chances by going to the United States as an exchange student called Aupair for a year. Thru the program, she gained valuable life skills and experiences, and most importantly friendship. However, some questions on her back of her mind still remained unanswered. After again resorting to profound soul searching, in the end she decided to return home to Thailand and work as an academic services officer at Sirindhorn International Institute of Technology (SIIT), Thammasat University. During that time, she pursued a master's degree in the Faculty of Engineering, Thammasat University, under the Energy and Environmental Management Technology program. She continued her passion in environmental chemistry and specialized in hazardous materials treatment. Although she enjoyed her work and co-workers at SIIT, she was felt unfulfilled primarily because her field of specialization was different. Eventually after two years and four months, she resigned from SIIT to pursue her doctoral study at Chulalongkorn University.